IOWA STATE UNIVERSITY
Digital Repository

2010

Evaluation of mechanistic-based compaction measurements for earthwork QC/QA

Jiake Zhang
Iowa State University

Evaluation of mechanistic-based compaction measurements for earthwork QC/QA

by

Jiake Zhang

A thesis submitted to the graduate faculty

in partial fulfillment of the requirements for the degree of

MASTER OF SCIENCE

Major: Civil Engineering (Geotechnical Engineering)

Program of Study Committee:
David White, Major Professor
Vernon Schaefer
Max Morris

Iowa State University

Ames, Iowa

2010

TABLE OF CONTENTS

LIST OF FIGURES

LIST OF TABLES

LIST OF SYMBOLS

Symbol	Description	Units
a	Radius of loading plate	mm
A	Sample cross-section area	m^2
B	Width of footing	m
B_1	Diameter of plate used in plate load test	m
c_c	Coefficient of curvature	-
c_u	Coefficient of uniformity	-
d_o	Measured settlement	mm
$d_{o(ri)}$	Deflection measured at the ith sensor	mm
D_{10}	Diameter corresponding to 10% finer	mm
D_{30}	Diameter corresponding to 30% finer	mm
D_{60}	Diameter corresponding to 60% finer	mm
D_i	Radial distance from the center of the plate to i^{th} sensor	mm
e	Eccentricity	mm
E_{BCD}	BCD modulus	MPa
E_{LWD}	Elastic modulus	MPa
E_{LWD-P3}	Elastic modulus determined using 300 mm diameter plate Prima LWD	MPa
E_{LWD-T3}	Elastic modulus determined using 300 mm diameter plate TFT LWD	MPa
$E_{equivalent}$	Equivalent modulus estimated from DCP	MPa
E_{v1}	Initial elastic modulus	MPa
E_{v2}	Reloading elastic modulus	MPa
f	Shape factor for LWD	-
G_s	Specific gravity	-
H	Sample height at any gyration cycle	m
I_z	Influence factor at z depth	-
k_s	Modulus of subgrade reaction	kPa/m
k_1	Stiffness estimated from a static plate load test	kPa/m
k_1, k_2, k_3	Regression coefficients	-

Symbol	Description	Units
M_r	Resilient modulus	MPa
P	Applied load at surface	N
P_a	Atmospheric pressure	MPa
R	Resultant force	N
z	Depth from the surface	mm
τ_G	Shear resistance from gyratory compactor PDA	kPa
θ	Sum of principle stress or bulk stress	MPa
σ_d	Deviator stress	MPa
ν	Poisson's ratio	-
σ_o	Applied stress	MPa
r	Radius of loading plate	mm
ε	Hoop strain on BCD plate	-
γ_{dmax}	Maximum dry unit weight	kN/m^3
w_{opt}	Optimum moisture content	%
s_u	Undrained shear strength	kPa
σ_z	Stress at depth of z	kPa

ABSTRACT

Compaction control for subgrade and base materials used in highway construction is typically based on field tests in comparison to laboratory Proctor tests that determine the relationship between dry unit weight and moisture content. The "optimum" moisture content and maximum dry unit weight are established and then a minimum relative compaction value and moisture content range is specified for acceptance during construction. This approach, although widely accepted, does not directly determine the mechanistic properties of the compacted material (i.e., strength or stiffness). The premise for adopting QA/QC tests that determine mechanistic properties is that the QA/QC operations would more directly relate to the design and also provide perhaps more value for ensuring quality as a final product. A further limitation of standard QA/QC practices is that generally not enough information is collected due to limited test frequency to ensure adequate reliability in quality over large areas. Non-homogeneous vertical soil profiles are one aspect of in-situ testing that has largely been ignored.

This study addressed these problems by evaluating five mechanistic-based devices in the field and in the laboratory. Field studies were conducted at sites in West Virginia, Iowa, Ohio, New York, and Michigan, to investigate the performance of five mechanistic-based compaction control measurement devices. Laboratory tests were also performed to evaluate relationship between moisture content, density, shear strength, and elastic/resilient modulus. A unique aspect of this research in addition to the field studies is that gyratory compaction samples were used to assess engineering properties of several soils and provided information on moisture content, density, and shear resistance relationships during the compaction process and a sample to test using other methods. Based on the comparison of the five mechanistic-based devices conducted for this study, trends were observed between devices and tradition density measurements, and the results provide data to evaluate the in situ variability of compacted materials. The results of the laboratory study showed that gyratory compacted samples provide useful information to determine mechanistic-based target values for QC/QA practices.

CHAPTER 1. INTRODUCTION

The traditional approach for evaluating compaction quality of earth materials consists of determining the moisture content (w) and dry unit weight (γ_d). Quality control (QC) specifications typically require that the w and γ_d be within certain limits, and quality assurance (QA) specifications require that w and γ_d be above some minimum value. However, the w and γ_d are only surrogates to mechanistic properties which are used in design. Design parameter values for pavements, slopes, foundations retaining structures, etc. typically rely on strength or modulus/compressibility parameters. The study described here focused on evaluating measurement technologies that link w and γ_d to mechanistic-based parameters both in the laboratory and in the field.

Five mechanistic stiffness/strength measurement devices were evaluated in this study: light weight deflectometer (LWD), falling weight deflectometer (FWD), plate load test (PLT), Briaud compaction device (BCD), and dynamic cone penetrometer (DCP). The LWD and FWD are dynamic tests, PLT is a static test, BCD is a small-strain test, and DCP is an intrusive test. FWD and PLT have limitations that prevent wide spread implementation. For example, the FWD needs a tow truck, which creates accessibility issues for the site, and PLT needs a heavy load truck or frame to jack against. To make use of these devices, it is important to have a better understanding for how these devices are related to each other, what the factors that affect the measurements are and how target quality assurance values can be developed. Further, variation in elastic modulus with depth surely affects the surface measurement, but the impact of such condition has not been incorporated into practice.

To address these issues, both laboratory and field studies were covered in this research. A series of LWD tests were performed in the field with different sizes of loading plates and drop heights at the same applied stress to investigate the relationships between E_{LWD} measurements. Further, different in situ stiffness/strength measurement devices were applied in the field to investigate their correlations for different field conditions. The correlation study between DCP measurements and LWD measurements was conducted to evaluate the

influence of different layered soil conditions on the surface modulus. Based on the findings, a standard protocol for developing E_{LWD} target values is discussed in this research.

Multiple regression analysis was applied during the target value determination study. Relationships between w, γ_d and E_{LWD} were developed based on LWD measurements performed on laboratory gyratory compacted samples. Statistical significance of each variable was assessed based on p- and t- values.

Goals

The ultimate goals of this research were to investigate relationships between different in situ stiffness/strength measurement devices (e.g., LWD, FWD, PLT, BCD, and DCP), to improve the understanding of factors that affect the device measurements. Although several devices were studied, the primary effort focused on LWD measurements.

Objectives

To effectively implement use of mechanistic in situ measurement devices for compaction control and to establish target values for QC/QA, the following research objectives were established for this study:

- obtain LWD measurements with different device configurations (i.e., diameter of plate and surface contact stresses),
- correlate the LWD measurements with other in situ stiffness/strength measurements (e.g., FWD, PLT, and BCD),
- investigate the effects of layered soil profiles on surface measurements,
- evaluate the relationship between E_{LWD}, w and γ_d for gyratory compacted specimens under rigid and flexible boundary conditions,
- link LWD laboratory measurements to field measurements and establish LWD target values.

Significance

The results of this research will demonstrate the relationships between different in situ stiffness/strength measurement devices and accelerate the implementation of these devices in field compaction control. Further, the results from this research will document factors that affect E_{LWD} measurements and apply this new information to field practice for choosing selecting suitable LWD configuration for compaction control. At last, a standard protocol for E_{LWD} target value determination for quality assurance was developed using gyratory laboratory compacted specimens. The advantage of laboratory determination of target values is that this work can be done prior to construction.

Thesis Organization

In addition to this introductory chapter, Chapter 2 discusses previous research that investigated the factors that affect the E_{LWD} measurement and reviews the literature of some commonly used mechanistic-based compaction control devices. Chapter 3 describes the laboratory and field test methods, and Chapter 4 summarizes the index properties of the materials involved in this research. Chapter 5 presents field case studies of each of the six test sites, provides tests results, and discusses these results as they relate to the study's objectives. The last chapter summarizes the conclusions from this research and offers suggestions for future research.

CHAPTER 2. BACKGROUND

This chapter reviews previous studies of some commonly used in situ mechanistic-based compaction control measurement devices. Seven soil compaction measurement devices were involved in this study, a light weight deflectometer (LWD), a falling weight deflectometer (FWD), a plate load test (PLT), a Briaud compaction device (BCD), a dynamic cone penetrometer (DCP), and a gyratory compactor with pressure distribution analyzer (PDA).

Light Weight Deflectometer (LWD)

The LWD was developed to rapidly determine the in situ elastic modulus (E_{LWD}) of compacted fill materials. LWDs typically consist of a 100- to 300-mm diameter loading plate with a drop weight of 10 kg; an accelerometer or geophones determine deflection; and a load cell or calibration factor. In the field, the height of the drop weight is calibrated to determine plate contact stress. The elastic modulus of the tested material can be determined by using the deflection reading and the impact load of the drop weight.

The LWD measurements are affect by several factors, such as type and location of deflection transducer, plate rigidity, loading rate, buffer stiffness, and measurement of load versus assumption of load based on laboratory calibration from a standardized drop height, but this study focused on two major factors, the size of the loading plate, and plate contact stress.

Size of LWD loading plate

Terzaghi (1955) developed two equations (Equations 1 and Equation 2) to estimate the modulus of subgrade reactions (k) for different footing sizes from plate load tests. According to these equations, the modulus of subgrade reaction is proportional to the ratio of the diameter of loading plate.

$$k_s = k_1 \left[\frac{B_1}{B}\right] \qquad \text{for footing on clay} \qquad (1)$$

$$k_s = k_1 \left[\frac{B+B_1}{2B}\right] \qquad \text{for footing on sand} \qquad (2)$$

where:

  B_1 = side dimension of a square plate used in load test (m),

  B = width of footing (m),

  k_s = modulus of subgrade reaction (kPa/m), and

  k_1 = stiffness estimated from a static plate load test (kPa/m).

Lin et al. (2006) found that E_{LWD} for a 100-mm diameter loading plate was approximately 1.5 to 1.6 times higher than for a 300-mm diameter plate at similar applied loads on a natural sandy soil deposit (ASSHTO classification: A-1-b). The manufacturer of Prima LWD suggests selecting plate sizes based on the material stiffness. When E_{LWD} is less than 125 MPa, the 300-mm diameter loading plate is recommended. The 100-mm and 200-mm diameter loading plate is recommended for E_{LWD} is between 125 MPa and 170 MPa and $E_{LWD} > 170$ MPa. By reducing the size of the loading plate, the contact stress will increase and therefore increase deflections to within a measurable range. However, using a larger plate for less stiff material reduces the possibility of excessive deflection and bearing capacity failure.

Vennapusa and White (2009) compared the influence of plate diameter with experimental data presented by several researchers (Stratton 1994, Chaddock and Brown 1995, Lin et al. 2006) using static plate load tests and LWDs to Terzaghi's theoretical relationships (Eqs 1 and 2), as shown in Figure 1.
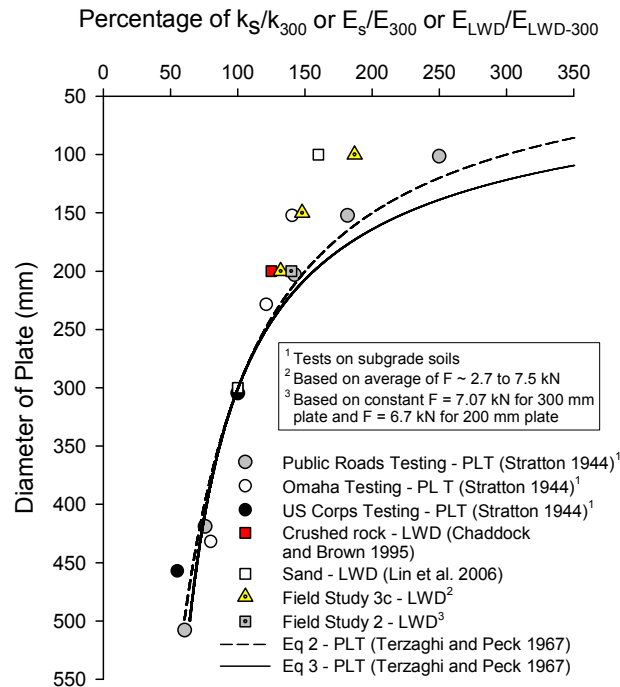
Figure 1. Relationship between material stiffness and diameter of bearing plate (from Vennapusa and White 2009)

Plate contact stress

Previous research indicates that the measured deflection will increase with higher applied contact stress. For example, Fleming et al. (2000) found that by increasing plate contact stress from 35 kPa to 120 kPa the measured E_{LWD-P3} increased by 1.15 times, while E_{LWD-T3} increased by 1.3 times. Van Gurp et al. (2000) did similar research on very stiff crushed aggregate and stabilized aggregate material, and for plate contact stress that varied from 140 kPa to 200 kPa no significant difference (< 3%) was observed.

Vennapusa and White (2009) conclude that for dense and compacted granular materials, E_{LWD} values tend to increase as the applied contact stress increase, except where the values are influenced by underlying softer subgrade materials. For cementitious materials, the measured E_{LWD} was not sensitive to changes in contact stress.

Falling Weight Deflectometer (FWD)

FWDs have been in use since the 1980s and over time have become the predominant pavement system evaluation device. As pavement design moves towards mechanistic-based practice, the number of FWDs in use is expected to rise. FWD equipment is manufactured and marketed by four companies, Carl Bro, Dynatest, Foundation Mechanics, Inc., and KUAB. This study used an FWD with a 300-mm diameter loading plate made by KUAB. This FWD is a trailer-mounted dynamic impulse loading device which can be towed by any suitable towing vehicle.

The major components of a typical FWD unit include: a control system, a loading system, a hydraulic system, and geophones. The FWD loading system applies the impulse load to the surface, and vertical responses are measured at various distances from the loading plate by a serious of geophone sensors. Deflection profiles under different impulse loads are measured and analyzed with different theoretical models of distinct constitutive behaviors to determine the modulus of the pavement system. The modulus obtained from FWD tests represents the composite modulus of the layers within the influence depth rather than the true modulus of the tested layer. To estimate the modulus of the tested layer, a multi-layered system solution needs to be considered to back-calculate the modulus of each layer. The Odemark's (1949) method, which is referred as the Method of Equivalent Thickness (MET), can be used to back-calculate the layer's modulus on multi-layer systems. Modulus values of the underlying layers were calculated using Equation 3, where v is the Poisons ratio, σ_o is the applied stress, r is the radius of the loading plate, D_i is the radial distance from the center of the plate to the ith sensor, $d_{o(ri)}$ is the deflection measured at the ith sensor.

$$E_{FWDi} = \frac{(1-v^2)\cdot\sigma_o \cdot r^2}{D_i d_{o(ri)}} \tag{3}$$

Several agencies correlated the FWD modulus with the resilient modulus, but the majority of the agencies characterized the level of reliability of these correlations as fair (NCHRP 2008). George (2003) reported a similar conclusion based on the tests conducted in Mississippi. Ten

subgrade test sections were built and evaluated with both in situ FWD test and laboratory M_r test, and the correlation was not robust enough nor could be justified on a theoretical basis.

Plate Load Test (PLT)

PLT is a common in situ method for estimating modulus of subgrade reaction and soil bearing capacity that has been used for many years. The major components of a typical plate load test device are a 300 mm diameter rigid bearing plate, a 90-kN load cell, and three 50 mm linear voltage displacement transducers (LVDTs). PLT is conducted by loading the bearing plate which is in contact with the surface and measuring the corresponding deflections under load increments. The load is usually transmitted to the plate by a hydraulic jack acting against heavy mobile equipment or a frame. The corresponding deflection is measured by LVDTs which are arranged in triangle shape above the bearing plate and the average of three readings are used in the calculation.

A typical PLT consists of initial and reload procedures, and the load and deformation readings are continuously recorded during the test. The major drawbacks of PLTs are that they are relatively slow, and they need a loaded truck or a frame, which introduces accessibility issues for some project sites. In those cases, small-scale stiffness/strength measurement devices, such as LWD, BCD are considered as the better options.

Briaud Compaction Device (BCD)

The BCD is a simple, small-strain, nondestructive testing apparatus for evaluating the modulus of compacted soils, and it can be applied both in the laboratory and in the field as a quality control testing tool (Weidinger and Ge 2009). BCD measurements are taken by loading a thin, steel plate in contact with the compacted material and measuring the bending strain of the plate, then relating that strain to the modulus of the compacted material. The main components of the BCD are the acquisition processing and readout display unit, a load cell, and a 2 mm thick strain-gage instrumented steel plate as shown in Figure 2.
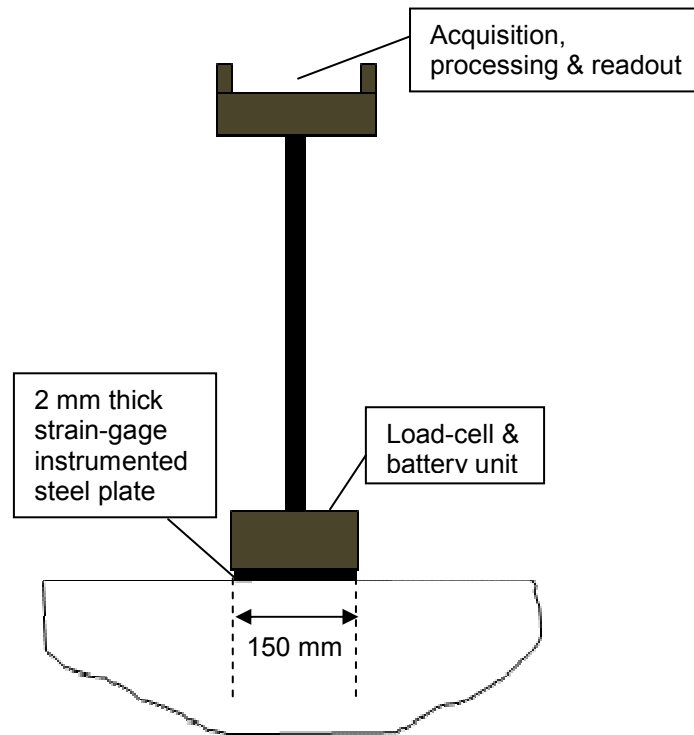
Figure 2. Conceptual sketch of BCD unit

The measured bending strain depends on the stiffness of the tested material. For instance, the measured bending strain is greater when the tested material is soft than stiff material. According to the BCD user manual (BCD 2009), the typical BCD measurement range is 5 MPa to 150 MPa. The measurement depths for the BCD device are 240 mm and 150 mm for modulus values of 10 MPa and 100 MPa respectively (BCD 2009). Li (2004) reported that as the modulus increases from 3 MPa to 300 MPa under large loads the influence depth of the BCD modulus decreases from 311 mm to 121 mm. However, Weidinger and Ge (2009) concluded that the influence depth of BCD under the testing loads (220 N) is much smaller based on numerical simulations.

Several researchers have found that BCD modulus correlated very well with other modulus tests such as PLTs and the resilient modulus tests (Li, 2004; Rhee, 2008). Weidinger and Ge (2009) concluded that BCD modulus correlated well with the ultrasonic pulse velocity results where the R^2 value was 0.8 or better on the same compacted silt samples. Briaud et al. (2006)

recommended a compaction control procedure that to perform BCD tests on the Proctor test specimens confined in the mold in order to obtain the maximum BCD modulus and the optimum water content for the material, which can be used to specify a percentage of the maximum BCD modulus as the target value in the field.

Dynamic Cone Penetrometer (DCP)

DCPs are low cost, in situ strength measurement devices that are increasingly being considered in geotechnical and foundation engineering for site investigation and quality control and quality assurance testing. The DCP unit consists of a fixed 575 mm travel rod with 8 kg dropping hammer, a lower rod containing a drive anvil; and a replaceable cone at the end of the rod. A schematic of the DCP is shown in Figure 3. DCP tests are conducted by dropping the hammer at the fixed drop height (575 mm) and recording the number of blows versus depth. The test result is interpreted in terms of DCP index (DCPI) or penetration rate (PR) with the unit of mm per blow.

The DCP is a simple test that characterizes the properties of pavement layers without digging test pits or collecting soil samples. DCP tests can verify both the level and uniformity of compaction (Burnham 1996; Siekmeier et al. 2000). Further, DCP tests results show the thickness of the layer of soil of various profiles.

Several studies have been conducted to correlate DCPI with California Bearing Ratio (CBR) based on empirical relationships. Kelyn (1975) developed Equation 4 based on 2,000 measurements.

$$Log\ CBR = 2.62 - 1.27\ logDCPI \tag{4}$$

Smith and Pratt (1983) and Riley et al. (1984) recommended Equation 5 based on field study.

$$Log\ CBR = 2.56 - 1.15\ logDCPI \tag{5}$$
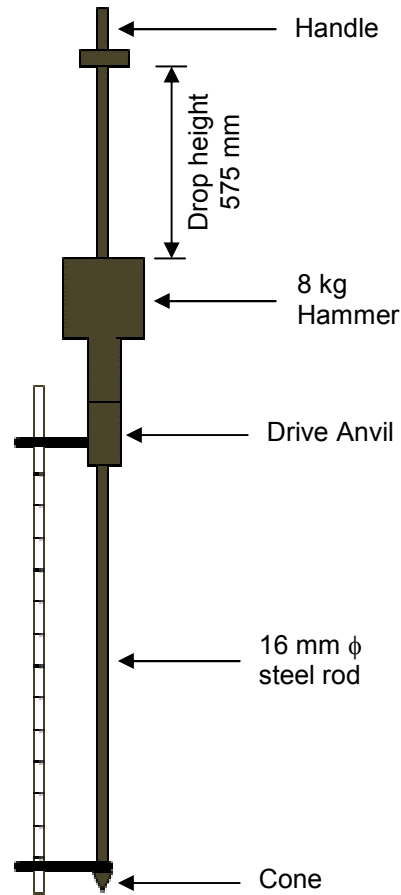
Figure 3. Conceptual sketch of DCP unit

Livneh and Ishia (1987) studied the correlation between DCP values and CBR values. Both CBR and DCP tests were performed on a wide range of undisturbed and compacted fine-grained soil samples. This study resulted in the following quantitative correlation relationship between the CBR values and DCP values.

$$Log\ CBR = 2.2 - 0.71\ (logDCPI)^{1.5} \tag{6}$$

Further, Livneh (1991) conducted tests on 76 samples to revalidate the CBR-DCP relationships and indicated that the correlation relationship is reasonable acceptable .Harrison (1986) suggested the following correlations relationships for different soils:

$$Log\ CBR = 2.56 - 1.16 \log DCPI \quad \text{for clayey soil of DCPI} > 10 \text{ mm/blow} \qquad (7)$$

$$Log\ CBR = 2.70 - 1.12 \log DCPI \quad \text{for granular soil of DCPI} < 10 \text{ mm/blow} \qquad (8)$$

The empirical relationship that was developed by the U.S. Army Corps of Engineers is accepted by most researchers (Livneh 1995; Webster et al. 1992; Siekmeier et al. 2000; Chen et al., 2001), and the equation for that relationship is shown as Equation 9:

$$Log\ CBR = 2.47 - 1.12 \log DCPI \quad \text{or} \quad CBR = 292/DCPI^{1.12} \qquad (9)$$

Current study of correlating the DCPI and CBR are based on empirical relationship and the correlation relationships are different for different field cases.

White et al. (2009) conducted the correlation study between DPI and s_u based on UC tests performed on samples obtained from different depths at the DCP test locations. Good correlation was obtained with $R^2 = 0.6$ for non-linear log relationship. Similar relationship was published by McElvanet and Djatnika (1991) for testing lime-stabilized materials as shown in Figure 4.
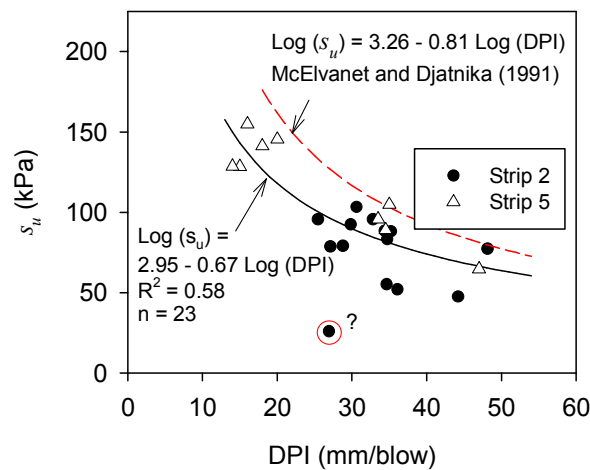
Figure 4. Relationship between DPI and s_u (from White et al. 2009)

Influence of Soil Layering

Sridharan (1990) compared two methods for estimating the equivalent spring constant of a layered system, which are the weighted average method and Odemark's method. Tests were conducted in two series: two-layer and three-layer systems using different materials. These tests showed that the weighted average method more accurately predicts the equivalent spring constant than Odemark's method.

Poulos and Davis (1974) developed an approach for estimating the stress distribution under a circular area (Equation 10), which can be explained as the applied load at the surface multiplied by the influence factor. In this study, influence factor was also used to correlate the surface reaction with different layers underneath.

$$\sigma_z = P\left[1 - \left\{\frac{1}{1+(\frac{a}{z})^2}\right\}^{3/2}\right] \tag{10}$$

where:

P = applied load at the surface,

a = radius of loading plate, and

z = depth from the surface.

Correlations between LWD and Other In Situ Point Measurements

Nazzal et al. (2004) conducted a study that correlated the Prima 100 model – LFWD with other standard tests including the falling weight deflectometer (FWD) and the plate load test (PLT). Good correlation was observed between E_{LWD} and E_{FWD} with a correlation coefficient of 0.97, and a similar relationship was also obtained by Fleming (2001).

Vennapusa and White (2009) compared the Zorn LWD and PLT, and concluded that E_{LWD} had better correlation between the initial modulus (E_{V1}) than reload modulus (E_{V2}). Good

correlation between Zorn LWD and PLT was also obtained from Nazzal et al (2004), with the correlation coefficient (R^2) equal to 0.92 and 0.94 for E_{V1} and E_{V2}, respectively.

Fleming et al. (2002) found that Zorn LWD consistently gave lower modulus than the other devices, such as FWD and Prima LWD and perhaps because the accelerometer is mounted within the bearing plate for Zorn LWD.

Target Value Determination for Quality Assurance

The target value determination study consisted of performing laboratory tests on gyratory compacted specimens. The benefits of using the gyratory compactor include: (1) gyratory compacted specimens are larger (150 mm diameter × 150 mm high) compared to Proctor specimens (102 mm diameter × 116 mm high) and (2) measurements provide complete density and shear resistance curves versus number of gyrations for each specimens. The gyratory compactor provided the density curves versus the number of gyrations, and the pressure distribution analyzer (PDA) determined the shear resistance for each gyration.

Gyratory Compactor

With developments in compaction equipment technology and increasing use of heavy rollers, researchers have introduced concerns over laboratory Proctor and vibratory compaction methods in developing moisture-density relationships that simulate field conditions. The Army Corps of Engineers (Coyle and West 1956, McRae 1965) introduced the gyratory compaction test procedure for soils based on extensive testing on silty sand material in Mississippi and demonstrated that gyratory compaction can simulate field compaction characteristics better than impact compaction with standard Proctor energy. Recent work by Kim and Labuz (2006) and Gupta et al. (2009) on recycled granular materials in Minnesota provided similar conclusions. Based on testing fine sand and silty sand materials, Ping et al. (2003) found that the optimum moisture and maximum densities achieved in the field were closer to gyratory compaction results than both impact (modified Proctor) and vibratory

compaction. According to Browne (2006), the gyratory compaction method produced maximum dry unit weights greater than the modified Proctor method for three different types of soils (A-1-a, A-3, and A-7-6), but the results depended on the number of gyrations and compaction pressure.

The gyratory compaction method was standardized by ASTM (ASTM D-3387 *Standard Test Method for Compaction and Shear Properties of Bituminous Mixtures by Means of the U.S. Corps of Engineers Gyratory Testing Machine (GTM)*) based on the work by McRae (1965) for its use for subgrade, base and asphalt mixtures. This method, however, has not been widely implemented for compaction of subgrade and base materials. One reason for slow implementation may be that no standard gyratory variables (e.g. gyration angle, number of gyrations, normal stress, or rate of gyrations) have been developed for subgrade and subbase materials.

Pressure Distribution Analyzer (PDA)

Guler et al. (2000) developed the PDA to evaluate the stability of asphalt mixtures during compaction in a gyratory mold. The main components of the PDA are three 9-kN load cells; two hardened steel plates that can fit into the gyratory mold; and a computer that is used to download data from the PDA. The three load cells are distributed at the same radial distance 120 degrees apart on the upper plate of the assembly as seen in Figure 5 and Figure 6. The resultant ram force (R) and the average eccentricity (e) are obtained from the PDA output data, which can be used to calculate the shear resistance of the compacted samples. According to Gular et al (2000), 50 readings were taken per gyration from each load cell during the compaction process.

Bahia et al. (2004) conducted a study of PDA using asphalt mixtures, and concluded that the shear resistance (τ_G) is sensitive to asphalt content, aggregate gradation, and air voids. The more important finding is that no direct relationship was detected between density and shear resistance. However, it is believed that shear resistance provides a good indication of stability

of the compacted materials.
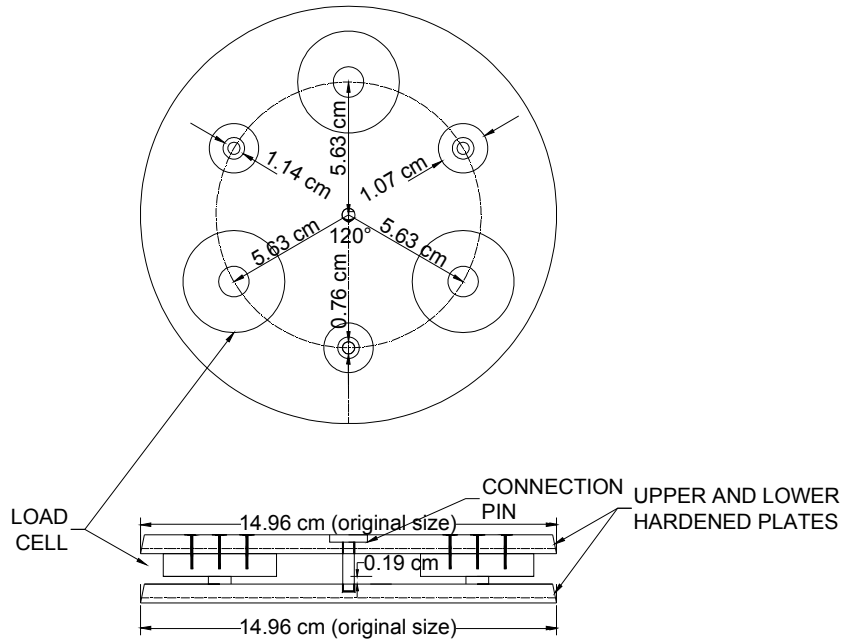
Figure 5. Pressure distribution analyzer (PDA)
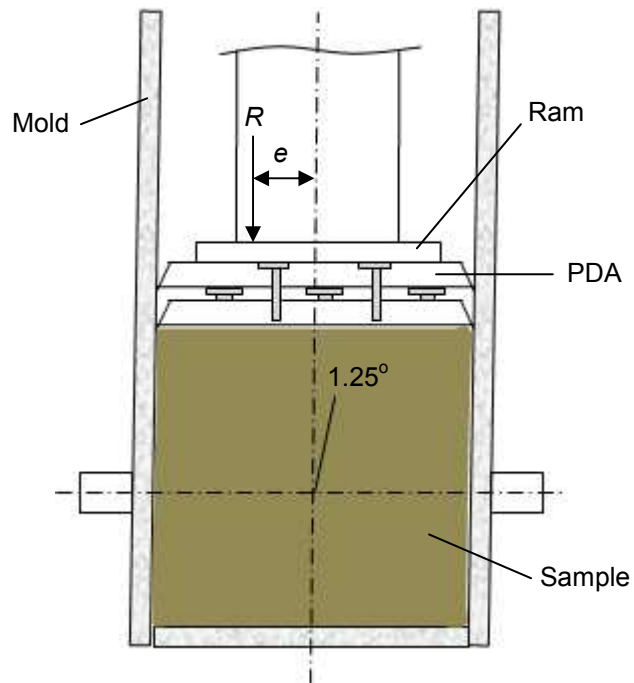
Figure 6. PDA in the gyratory mold during gyration

CHAPTER 3. TEST METHODS

This section summarizes the field and laboratory tests methods employed in the research and the test standards followed. The descriptions of the standards for field and laboratory tests were adopted from White et al. (2009).

Field Test Methods

Six field measurements devices are used in this research and the standard followed to perform the field tests are summarized in Table 1.

Table 1. Summary of devices utilized in this research

Devices	Standard followed
Nuclear gauge (NG)	ASTM D2922-05
Light weight deflectometer (LWD)	LWD Operation Manual (2000)
Falling weight deflectometer (FWD)	KUAB 2m-FWD 150 Operation and Technical Reference Manual (2009)
Plate load test (PLT)	ASTM D1195-93
Briaud compaction device (BCD)	BCD Instruction Manual (2009)
Dynamic cone penetrometer (DCP)	ASTM D6951-03

A calibrated nuclear moisture-density gauge (NG) device (Figure 7) was used to provide rapid measurements of soil dry unit weight and moisture content. Tests were performed following ASTM D2922-05 *Test Method for Density of Soil and Soil Aggregate Inplace by Nuclear Methods (Shallow Depth)*. Generally, two measurements of moisture and dry unit weight were obtained at a particular location with the average value being reported. Probe penetration depths were selected base on the compaction layer thickness.

Figure 7. Nuclear moisture-density gauge

LWD tests (Figure 8) with different device configurations were used to determine the dynamic modulus at the surface. LWD tests were conducted in accordance with the manufacture recommendations (Zorn 2003) for this research. The LWD modulus can be determined using equation (11):

$$E_{LWD} = \frac{(1-v^2)\sigma_o r}{d_o} \times F \tag{11}$$

where, E_{LWD} = elastic modulus (MPa), d_o = measured settlement (mm), v = Poisson's ratio (assumed to be 0.4 for this research), σ_o = applied stress (MPa), r = radius of the plate (mm) and f = shape factor that depends on the stress. Vennapusa and White (2009) provide a detailed description of the test methods for the equipment used in this study.

During this study, LWD tests were performed in the laboratory on the gyratory compacted specimens. The compacted specimens were extruded from the gyratory mold and tested with four different boundary conditions as shown in Figure 9: (a) no confinement, (b) confinement with a soft polyurethane (Durometer = 20 A) sleeve, (c) confinement with a stiff polyurethane (durometer = 50 A) sleeve, and (d) rigid confinement in the gyratory mold to

investigate the influence of boundary conditions. According to Vennapusa and White (2009), the measuring range of the deflection transducer for Zorn LWD is 0.2 mm to 30 mm. The measured deflections during laboratory target value determination study were ranging from 0.47 mm to 10.47 mm, which within the Zorn LWD measurement range.

Figure 8. Light weight deflectometer test with 200-mm diameter plate
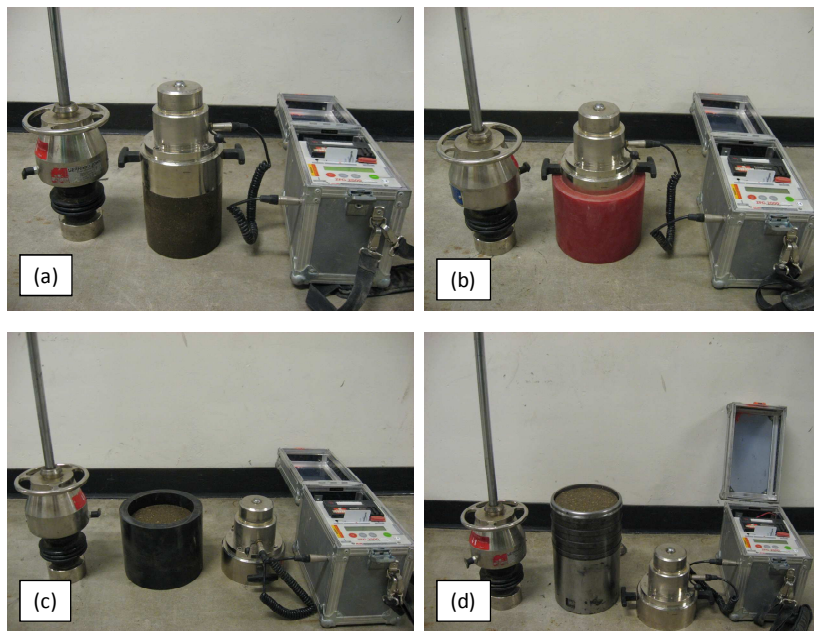
Figure 9. LWD testing with four different boundary conditions: (a) no boundary, (b) soft polyurethane (Durometer = 20 A), (c) stiff polyurethane (Durometer = 50 A), and (d) rigid gyratory compaction mold

Falling weight deflectometer (FWD) test (Figure 10) is non-destructive field test and it is widely used for evaluating the pavement layer moduli. KUAB 2m-FWD 150 was employed in this study, and FWD tests were conducted in accordance with the operation and technical reference manual (KUAB 2009). Three measurements were taken for each testing location with the applied normal forces of 26.7 kN, 40.0 kN and 53.4 kN which were recorded by a load cell. The responses were measured using deflection sensors placed at the center of the plate and at 0.2, 0.3, 0.5, 0.6, 0.8, 0.9, 1.2, 1.52, and 1.8 m offsets from the center of the plate. The surface modulus measured from FWD test was calculated by using Equation 11 which is the same formula to calculate LWD modulus.

Figure 10. Falling weight deflectometer test with 300-mm diameter plate

Stress-controlled static plate load test (PLT) (ASTM D 1195 *Standard Test Method for Repetitive Static Plate Load Tests of Soils and Flexible Pavement Components, for Use in Evaluation and Design of Airport and Highway Pavements*) (shown in Figure 11) was conducted by applying a static load on a 300 mm diameter plate against a 62 kN capacity reaction force. The applied load was measured using a 90-kN load cell and deformations were measured using three 50-mm linear voltage displacement transducers (LVDTs). The average of the three deflection measurements was used in the calculation. The load and deformation readings were continuously recorded during the test using a data logger. Initial (E_{V1}) and re-load (E_{V2}) modulus were determined using Equation (6) by using stress and deformation readings taken from 0.2 to 0.4 MPa for granular materials and 0.1 to 0.2 MPa for

non-granular subgrade soils (see Figure 12).

Figure 11. Static plate load test setup with 300-mm diameter plate
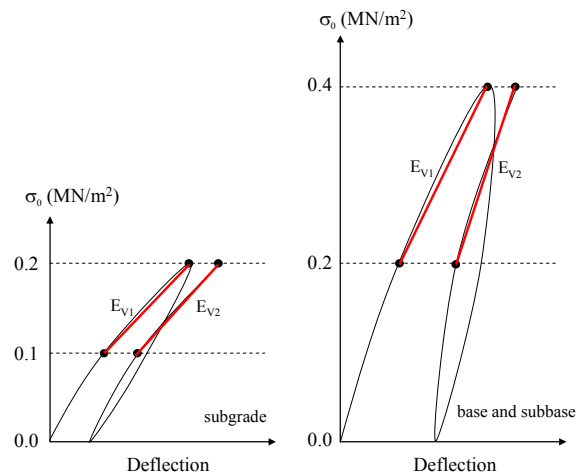
Figure 12. Static plate load test data modulus scheme for subgrade, subbase, and base materials (from White et al. 2009)

The Briaud compaction device (BCD), developed at Texas A&M University (BCD 2009), was used to determine the BCD modulus of compacted soils. The device consists of the following components: a 150-mm diameter flexible plate, a load cell, and the display unit as shown in Figure 13. BCD instruction manual (BCD 2009) was followed to conduct the tests. A thin moist sand cushion was placed on the testing location to ensure a good contact

between the BCD plate and the uneven soil surface. The bending strain of the plate was automatically recorded when the operator applied a load larger than 223 N (50 lb). With the recorded strain and applied pressure, the BCD modulus can be calculated using Equation 12 (BCD instruction manual). Three measurements were taken at the same location and the averaged BCD test results were taken as the BCD field modulus.

$$\text{BCD modulus} = \frac{P}{\varepsilon},\tag{12}$$

where, P is the measured pressure under the plate when the applied load exceed 223 N, ε is the hoop strain on the plate. The BCD field tests were conducted by Deeyvid Saez at Texas A&M University and the results shared for comparison to other measurements at the same locations.
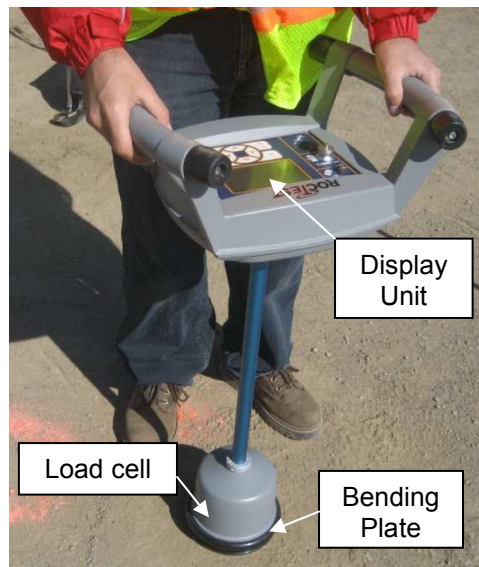
Figure 13. BCD test on embankment material

Dynamic cone penetrometer (DCP) tests (Figure 14) were performed following ASTM D6951-03 *Standard Test Method for Use of the Dynamic Cone Peneterometer in Shallow Pavement Applications*. The device consists of an 8-kg hammer dropped at 575 mm height. Dynamic penetration index (DPI) is reported from the tests with units of mm/blow, which

relates to the soil strength. The following empirical equations have been proposed in ASTM D 6951-03 for calculating California bearing ratio (CBR) from DPI:

$$CBR = \frac{292}{(DCPI)^{1.12}}, \text{ for all soils except for CH soils or CL soil with CBR} < 10 \tag{13}$$

$$CBR = \frac{1}{(0.017019 \cdot DCPI)^2}, \text{ CL soils with CBR} < 10 \tag{14}$$

$$CBR = \frac{1}{0.002871 \cdot DCPI}, \text{ CH soils} \tag{15}$$

Figure 14. Dynamic cone penetration test

Laboratory Test Methods

Laboratory tests were conducted on the materials sampled from various project sites to find the material index properties of the investigated soils.

Soil Index Properties Tests

ASTM D422-63(2002) *Standard Test Method for Particle-Size Analysis of Soils* was followed to conduct grain-size distribution test. The prepared samples were divided into two

portions by the No.10 sieve. Sieve analysis was performed on the portion washed and retained on No. 10 sieve and hydrometer analysis was conducted on the portion passing the No. 10 sieve using a 152 H hydrometer. After finishing the hydrometer test, the suspended material was washed through the No. 200 sieve, oven dried, and then sieved through the No. 40 and No. 100 sieves.

Atterberg limits tests were performed in accordance with ASTM D4318-05 *Standard Test Methods for Liquid Limit, Plastic Limit, and Plasticity Index of Soils*. The dry preparation method was adopted and involved oven drying at a temperature below 60°C. Samples were sieved through the No. 40 sieve before testing. Atterberg limits were used to classify the material according to American Association of State Highway and Transportation Officials (AASHTO) classification and Unified Soil Classification System (USCS).

ASTM D854-05 *Standard Test Methods for Specific Gravity of Soil Solids by Water Pycnometer* was followed to conduct specific gravity tests. Method B – procedure for oven-dried specimens was adopted for all the materials.

Laboratory Compaction Tests

The moisture content and dry density relationship for the investigated materials were developed by performing standard and modified Proctor compaction tests. ASTM D698-00 and ASTM D1557-02 were followed for standard and modified Proctor tests, respectively. Test method A was followed, and materials were air dried, sieved through the No.4 sieve, and then moisture conditioned. The materials were stored in a moist condition for at least 16 hours prior to testing.

Relative density tests were performed on granular materials using a vibratory table. ASTM D4253 *Standard Test Methods for Maximum Index Density of Soils Using a Vibratory Table* and ASTM D 4254 *Standard Test Methods for Minimum Index Density of Soils and Calculation of Relative Density* were followed to perform the compaction test to obtain the

maximum and minimum dry unit weights.

Gyratory compacted specimens were prepared using a AFGB1A Brovold gyratory compactor (manufactured by Pine Instrument Company) and pressure distribution analyzer (PDA) shown in Figure 15. ASTM D3387-83 *Standard Test Method for Compaction and Shear Properties of Bituminous Mixtures by Means of the U.S. Corps of Engineers Gyratory Testing Machine (GTM)* was followed to produce the compacted specimens. Materials were compacted with selected vertical stresses (σ_o) ranging from 100 to 900 kPa at a constant rate of 30 gyrations per minute with the gyration angle set at 1.25 degrees. The PDA is a device that can be placed above or below the sample in the gyratory compaction mold to capture the pressure distribution across the sample during compaction. It provides the resultant force (R) and the eccentricity (e) where the resultant force was acting during the compaction process. With measured R and e, the frictional resistance or shear resistance (τ_G) of the compacted materials can be calculated using Equation (16) (Guler et al. 1996):

$$\tau_G = \frac{R.e}{A.H} \tag{16}$$

where, R = resultant force, e = eccentricity, A = sample cross-sectional area, and H = sample height at any gyration cycle. The relationships between τ_G and M_r, s_u, and E_{LWD} are explored in this research.

Figure 15. AFGB1A gyratory compactor (left) and pressure distribution analyzer (right)

Laboratory Strength Tests

Unconfined compressive (UC) tests (see Figure 16) were performed on the gyratory compacted specimens in accordance with ASTM D2166 *Standard Test Method for Unconfined Compressive Strength of Cohesive Soil*. In contrast with the ASTM standard, the height-to-diameter ratio of the gyratory compacted specimens was approximately equal to one instead of between 2 and 2.5. The strain rate for the UC tests was 1 %/min and loading continued until 15 % strain was reached. Western Iowa loess (USCS: SL) was used in the research to investigate the correlation between undrained shear strength (s_u) and shear resistance (τ_G) from the gyratory compacted specimens.

Figure 16. Unconfined compressive test on gyratory compacted specimen

Resilient modulus (M_r) tests and unconsolidated-undrained triaxial compression (UU) tests were performed on the gyratory compacted specimens in accordance with AASHTO T 307-99 *Standard Method of Test for Determining the Resilient Modulus of Soils and Aggregate Materials* and ASTM D 2850 *Standard Test Method for Unconsolidated-Undrained Triaxial Compression Test on Cohesive Soils*. Specimens were prepared with the height to diameter ratio H/D = 1:1 and H/D =2:1 to investigate the influence of the sample size on the resilient modulus. The H/D=1:1 specimens (see Figure 17) were made using the gyratory compactor,

and the H/D=2:1 specimens were trimmed from the gyrator samples using a tube sample to reduce the diameter as shown in Figure 18. TH 60 non-granular material was prepared at the optimum moisture content from the standard Proctor test (w_{opt}=18%). The mean M_r value was calculated from fifteen different loading sequences. The Witczak and Uzan (1988) model that combines deviator and bulk stress affects (Equation 17), was used in the interpretation of results.

$$M_r = k_1 P_a \left(\frac{\theta}{P_a}\right)^{k_2} \left(\frac{\sigma_d}{P_a}\right)^{k_3} \tag{17}$$

where, k_1, k_2, k_3 = regression coefficients, with $k_1 > 0$, $k_2 \geq 0$, and $k_3 \leq 0$, θ = sum of principle stresses or bulk stress ($\sigma_1 + \sigma_2 + \sigma_3$), P_a = atmospheric pressure, same units as M_r and θ, σ_d = deviator stress, same units as M_r and θ.
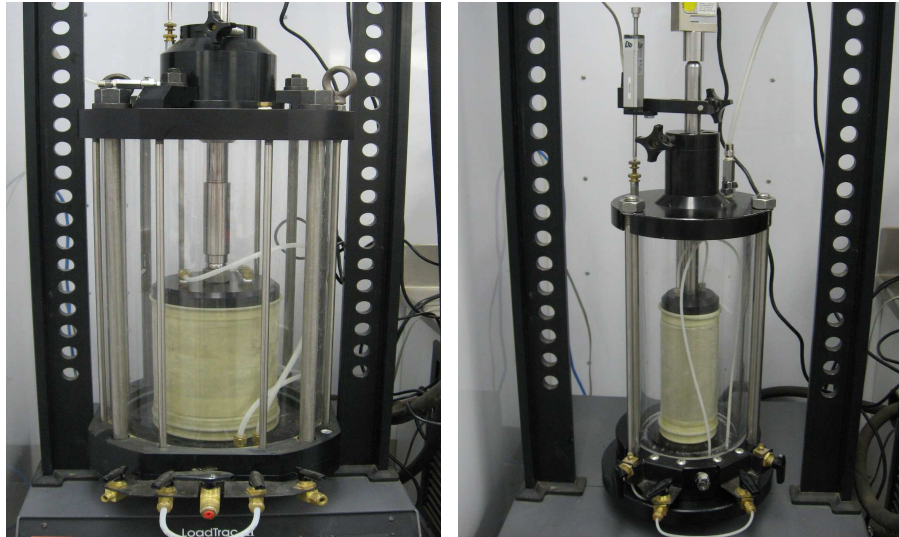
Figure 17. Resilient modulus testing on 1:1 (left) and 2:1 (right) gyratory compacted specimens

Figure 18. Procedure for inserting Shelby tube into gyratory compacted specimen to generate 2:1 height to diameter ratio specimens

CHAPTER 4. MATERIALS

This chapter summarizes the index properties of the materials collected from six project sites. The material index properties include gradation, Atterberg limits, w and γ_d compaction relationship, and classifications. Table 2 provides the summary of the tested materials.

Table 2. Summary of investigated materials

Projects	Material ID	Locations	USCS (AASHTO) classification	Laboratory testing	In situ testing
Mn/DOT IC	TH 60	Bigelow Minnesota	CL (A-6(11))	Gradation, Proctor, Gyratory compaction, PDA, M_r	LWD
	US 10	Staples Minnesota	SP-SM (A-3)	Gradation, Gyratory compaction, PDA	LWD
	Iowa Loess	Turin Iowa	ML (A-4)	Gradation, Proctor, Gyratory compaction, PDA, UCS	—
Geosynthetics Reinforcement Study	Subgrade	Weirton West Virginia	CL (A-7-6)	Gradation, Proctor	LWD, DCP
	Base	Weirton West Virginia	GP-GM (A-1-a)	Gradation, Relative density,	LWD, DCP
Hormel PCC	Silt	Dubuque Iowa	GW-GM (A-1-a)	Gradation	LWD, DCP
Ohio Bridge Approach	Bridge #1	Westchester Ohio	SP (A-1-b)	Gradation, Relative density	DCP, NG
	Bridge #2	Wilmington Ohio	SW-SM (A-1-b)	Gradation, Relative density	DCP
	Bridge #3	Dayton Ohio	SW-SM (A-1-b) / GP (A-1-a) / GW (A-1-a)	Gradation, Relative density	DCP, LWD
	Bridge #4	Columbus Ohio	GP (A-1-a) / GM (A-1-a)	Gradation, Relative density	DCP, LWD
	Bridge #5	Licking County Ohio	SM (A-4) / GM (A-2-4)	—	DCP, LWD, NG
	Bridge #6	Medina County Ohio	GP-GM (A-1-a)	Gradation, Relative density	DCP, LWD, PLT
	Bridge #7	Medina County Ohio	—	—	DCP, LWD
FHWA IC	Embankment	Springville New York	SM (A-1-b)	Gradation	LWD, BCD, DCP
	Aggregate	Springville New York	GW (A-1-a)	Gradation	LWD, DCP
Pavement Foundation Study	Untrimmed Base	I-94 Michigan	GW (A-1-a)	Gradation, Relative density	LWD, DCP, FWD
	TB 2	I-94 Michigan	SP-SM (A-2-4)	Gradation, Relative density	LWD, DCP, FWD

Notes: IC – Intelligent compaction; PDA – Pressure distribution analyzer; M_r – Resilient modulus test; LWD – Light weight deflectometer; DCP – Dynamic cone penetrometer; NG – Nuclear gauge; PLT – Static plate load test.

TH 60 – Bigelow

TH 60 subgrade material was sampled from Bigelow, Minnesota. The performed laboratory tests include: grain-size distribution analysis, Atterberg limits tests, standard and modified Proctor tests and gyratory compaction tests with the pressure distribution analyzer (PDA).

The material was classified as CL (lean clay sand) based on USCS classification and A-6(11) from AASHTO classification (Figure 19). The Atterberg limits test results shown that the liquid limit of the material is 39, plastic limit is 20 and plasticity index is 19. The maximum dry unit weight and optimum moisture content for the modified Proctor test is 19.3 kN/m^3 and 12.8% respectively; the maximum dry unit weight and optimum moisture content for the standard Proctor test is 17.2 kN/m^3 and 17.7 % respectively as shown in Figure 20. Table 3 summarizes the material index properties for this soil.

Gyratory compaction tests produced specimens for laboratory LWD tests with different boundary conditions and resilient modulus tests with different sample sizes. PDA was placed on the top of the gyratory compaction mold to capture the pressure distribution of the sample during compaction process. Gyratory compaction tests were performed with 300 kPa applied vertical pressure and 100 gyrations when producing the resilient modulus test specimens and applied vertical pressures from 100 kPa to 600 kPa with 100 gyrations when producing the LWD tests specimens. Figure 21 and Figure 22 provide the dry unit weight and shear resistance versus number of gyrations and also the shear resistance versus degree of saturation for this material. Based on τ_G versus degree of saturation curves, over-compaction starts around 90% saturation for the samples with moisture content more than 16%.
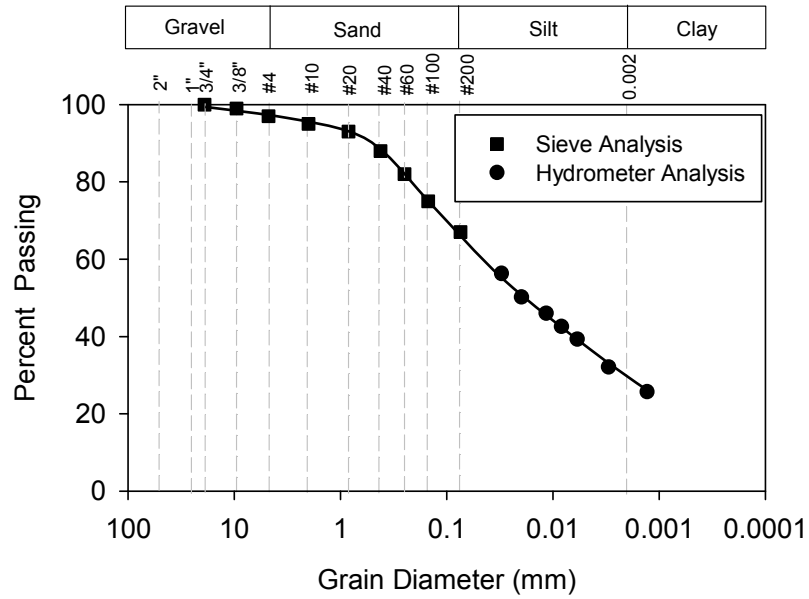
Figure 19. Grain-size distribution curve of TH 60 sugrade clay sample
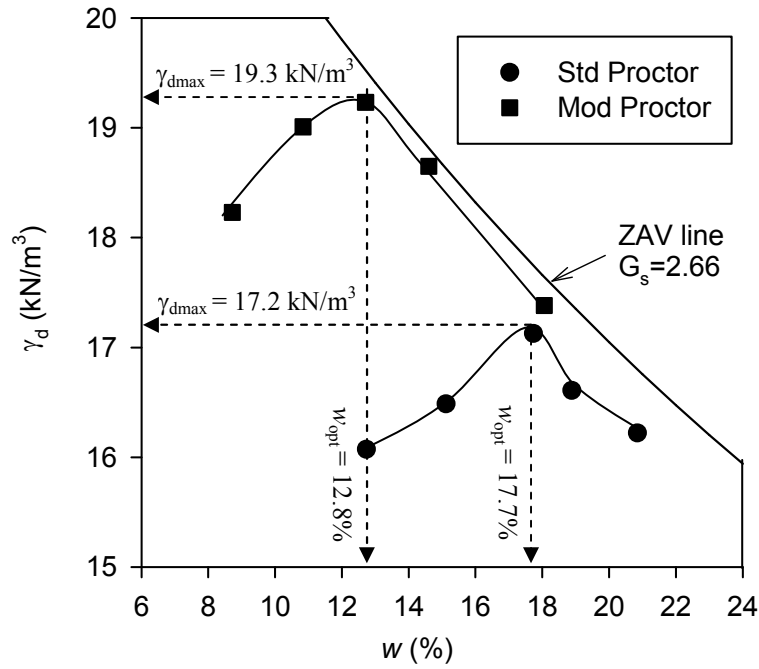
Figure 20. Standard and modified Proctor test results

Table 3. Summary of the material properties for TH 60 non-granular soil

Parameter/Material	TH 60 subgrade clay
Material Description	Sandy lean clay
Maximum dry unit weight (kN/m^3) and optimum moisture content (%)	
Standard Proctor	17.2 (17.7)
Modified Proctor	19.3 (12.8)
Gravel Content (%) (> 4.75mm)	3
Sand Content (%) (4.75mm – 75μm)	30
Silt Content (%) (75μm – 2μm)	38
Clay Content (%) (< 2μm)	29
Coefficient of Uniformity (c_u)	—
Coefficient of Curvature (c_c)	—
Liquid Limit, LL (%)	39
Plasticity Index, PI	19
AASHTO	A-6(11)
USCS	CL
Specific Gravity, G_s (Assumed)	2.66
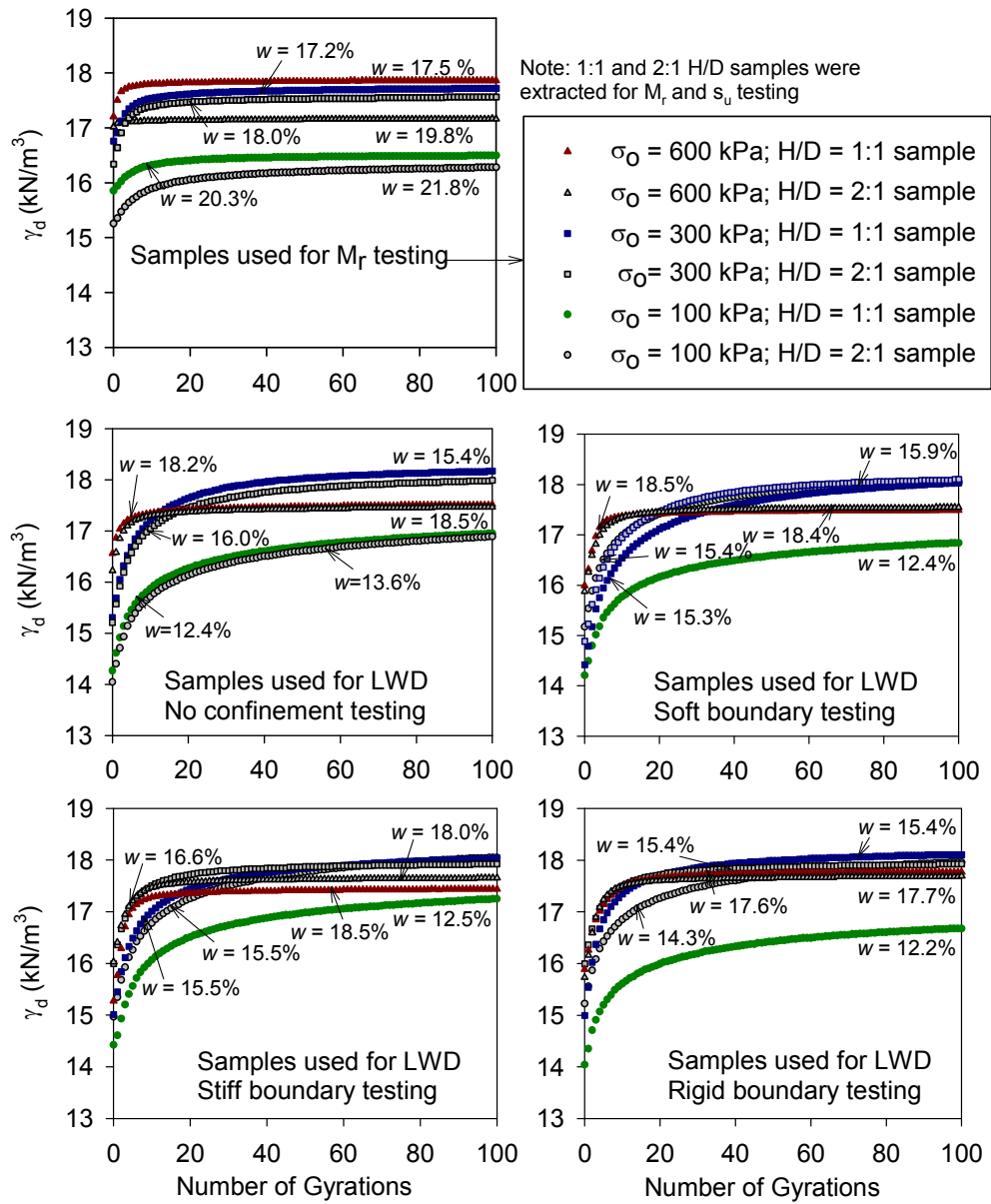
Figure 21. Dry unit weight versus number of gyrations for TH 60 soil (USCS: CL)
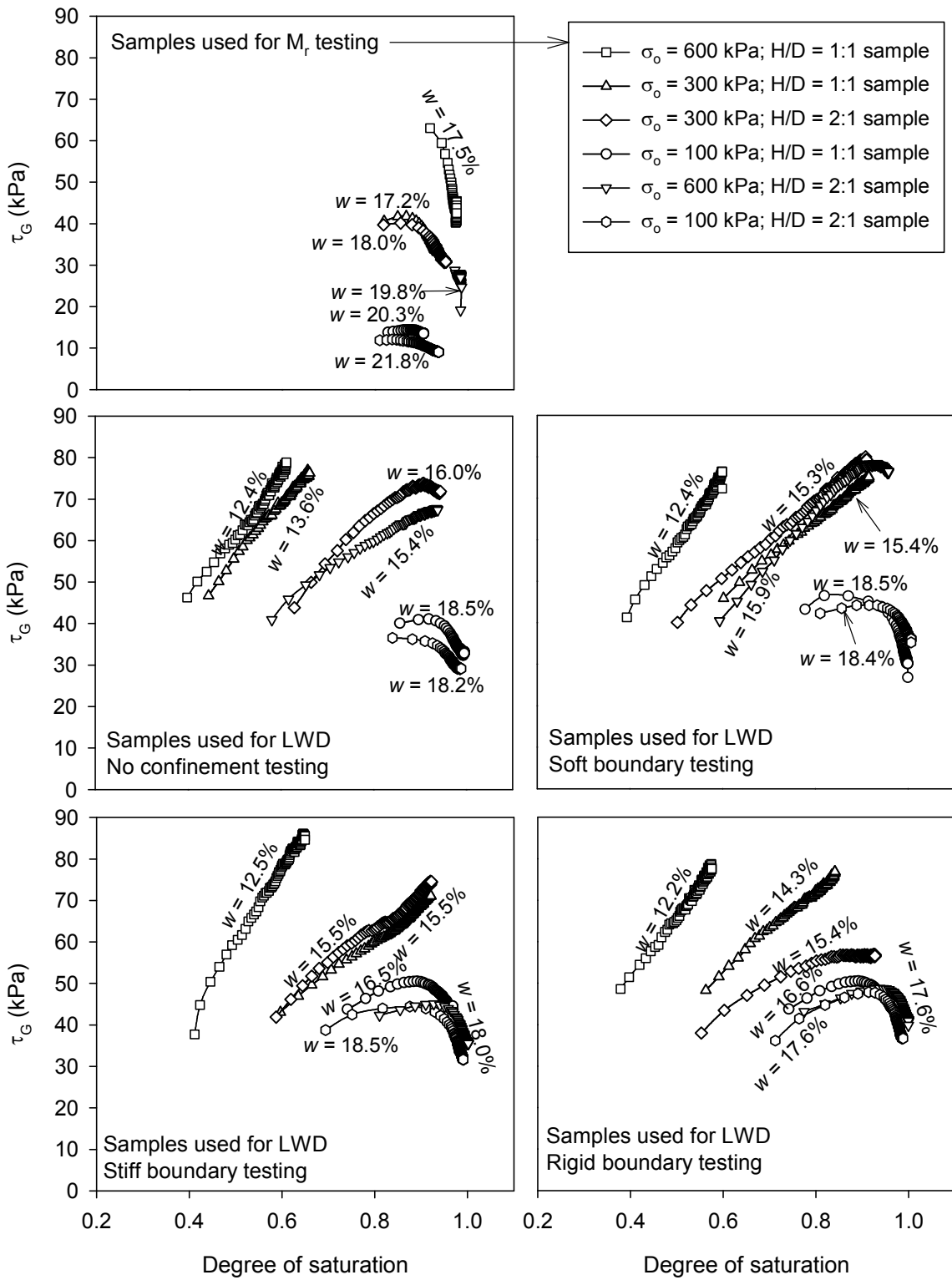
Figure 22. Shear resistance versus degree of saturation during gyratory compaction (TH60 soil USCS: CL)

US 10 – Staples

US 10 soil was sampled from Staples, Minnesota. The preformed laboratory tests for this material consist of grain-size distribution test, standard and modified Proctor tests and gyratory compaction tests with PDA installed.

The material was classified as A-3 per AASHTO and SP-SM (poorly graded sand with silt) per USCS classification. The grain-size distribution curve is shown in Figure 23. The optimum moisture content and maximum dry unit weight for the standard Proctor test is 12.2% and 17.5 kN/m^3 respectively; the optimum moisture content and maximum dry unit weight for the modified Proctor test is 10.0% and 18.1 kN/m^3 respectively. Table 4 summarizes the material index properties obtained from the laboratory tests.

Gyratory compaction tests were performed on this material to produce compacted specimens for laboratory LWD tests with different boundary conditions. Samples were prepared at moisture content ranging from 6% to 12% at increments of 2%. The gyratory compactor was setup with 300 kPa applied vertical pressure at 100 gyrations when producing the compacted specimens. The dry unit weight versus number of gyrations is shown in Figure 25.
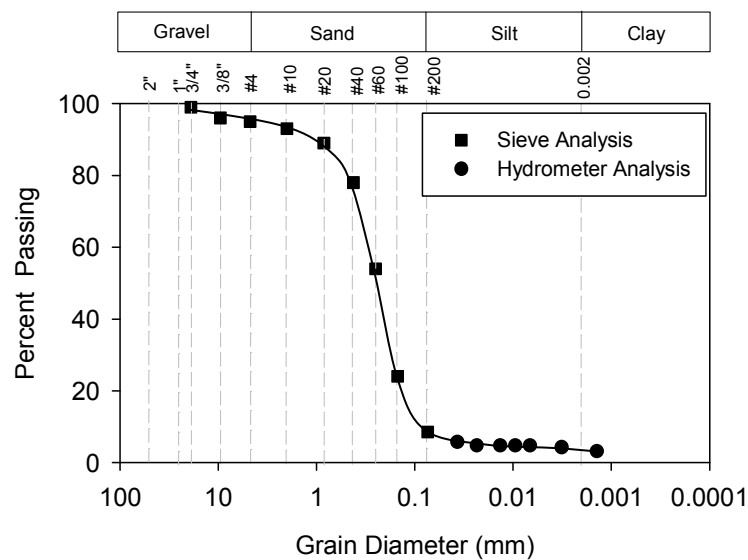
Figure 23. Grain-size distribution curve of US 10 granular material
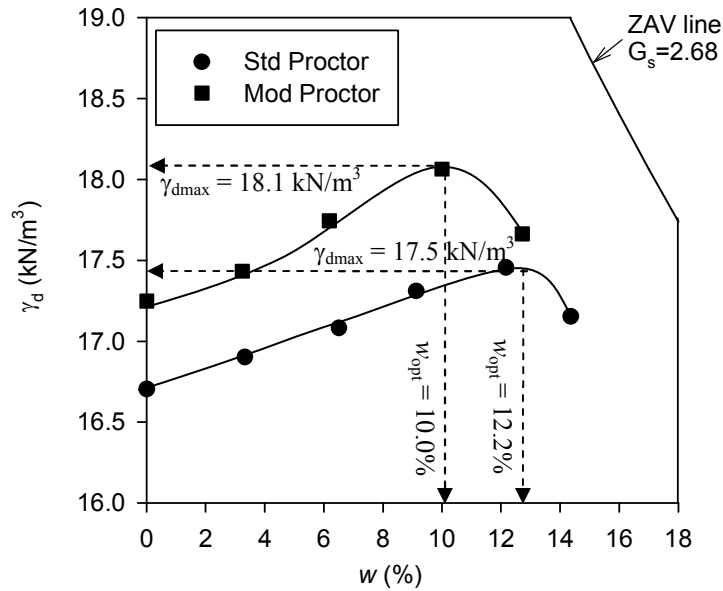
Figure 24. Standard and modified Proctor test results for US 10 material

Table 4. Summary of the material properties for US 10 granular material

Parameter/Material	US 10 granular material
Material Description	Poorly graded sand with silt
Maximum dry unit weight (kN/m^3) and optimum moisture content (%)	
Standard Proctor	17.5 (12.2)
Modified Proctor	18.1 (10.0)
Gravel Content (%) (> 4.75mm)	4
Sand Content (%) (4.75mm – 75μm)	87
Silt Content (%) (75μm – 2μm)	4
Clay Content (%) (< 2μm)	4
Coefficient of Uniformity (c_u)	3.15
Coefficient of Curvature (c_c)	1.15
Liquid Limit, LL (%)	—
Plasticity Index, PI	—
AASHTO	A-3
USCS	SP-SM
Specific Gravity, G$_s$ (Assumed)	2.68
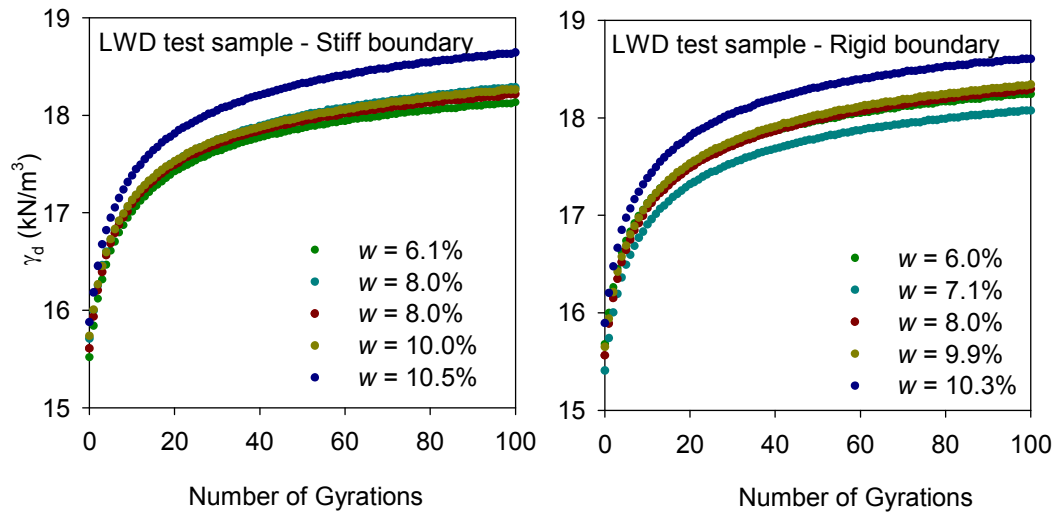
Figure 25. Dry unit weight versus number of gyrations for US10 granular material (USCS: SP-SM)

Western Iowa loess

Western Iowa loess was used to investigate the relationship between undrained shear strength (s_u) and shear resistance (τ_G) on gyratory compacted specimens. The loess material used in predominately silt (about 90%) with some clay size particles and it was classified as ML based on USCS classification. Atterberg limits test results shown that the liquid limit of the material is 29, plastic limit is 23 and plasticity index is 6. The optimum moisture content and the maximum dry unit weight for standard Proctor test is 18.6% and 15.9 kN/m^3 respectively; the optimum moisture content and maximum dry unit weight for modified Proctor is 15.1% and 17.4 kN/m^3 respectively. Figure 26 shows the relationship between moisture content and dry unit weight from standard and modified Proctor compaction tests and Table 5 summarizes the material index properties of the Western Iowa loess.

The material was prepared at six different moisture contents in general following the standard Proctor test, which ware -9%, -6%, -3%, 0%, +3% and +6% of optimum moisture content , to perform gyratory compaction tests. Material was compacted using vertical pressure $\sigma_o = 100$ kPa, 300 kPa and 600 kPa with 100 gyrations. Dry unit weight versus

number of gyrations for this material is shown in Figure 27.
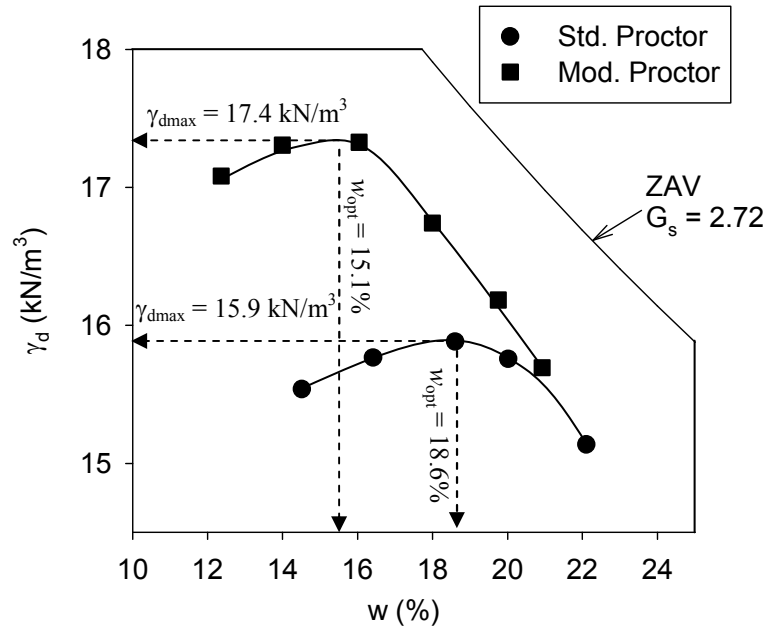
Figure 26. Standard and modified Proctor test results for Western Iowa loess (USCS: ML)

Table 5. Summary of the material properties for Western Iowa loess

Parameter/Material	Western Iowa loess
Material Description	Silt
Maximum dry unit weight (kN/m^3) and optimum moisture content (%)	
Standard Proctor	15.9 (18.6)
Modified Proctor	17.4 (15.1)
Gravel Content (%) (> 4.75mm)	0
Sand Content (%) (4.75mm – 75μm)	2.9
Silt Content (%) (75μm – 2μm)	90.6
Clay Content (%) (< 2μm)	6.5
Coefficient of Uniformity (c_u)	—
Coefficient of Curvature (c_c)	—
Liquid Limit, LL (%)	29
Plasticity Index, PI	6
AASHTO	A-4
USCS	ML
Specific Gravity, G_s (Assumed)	2.72
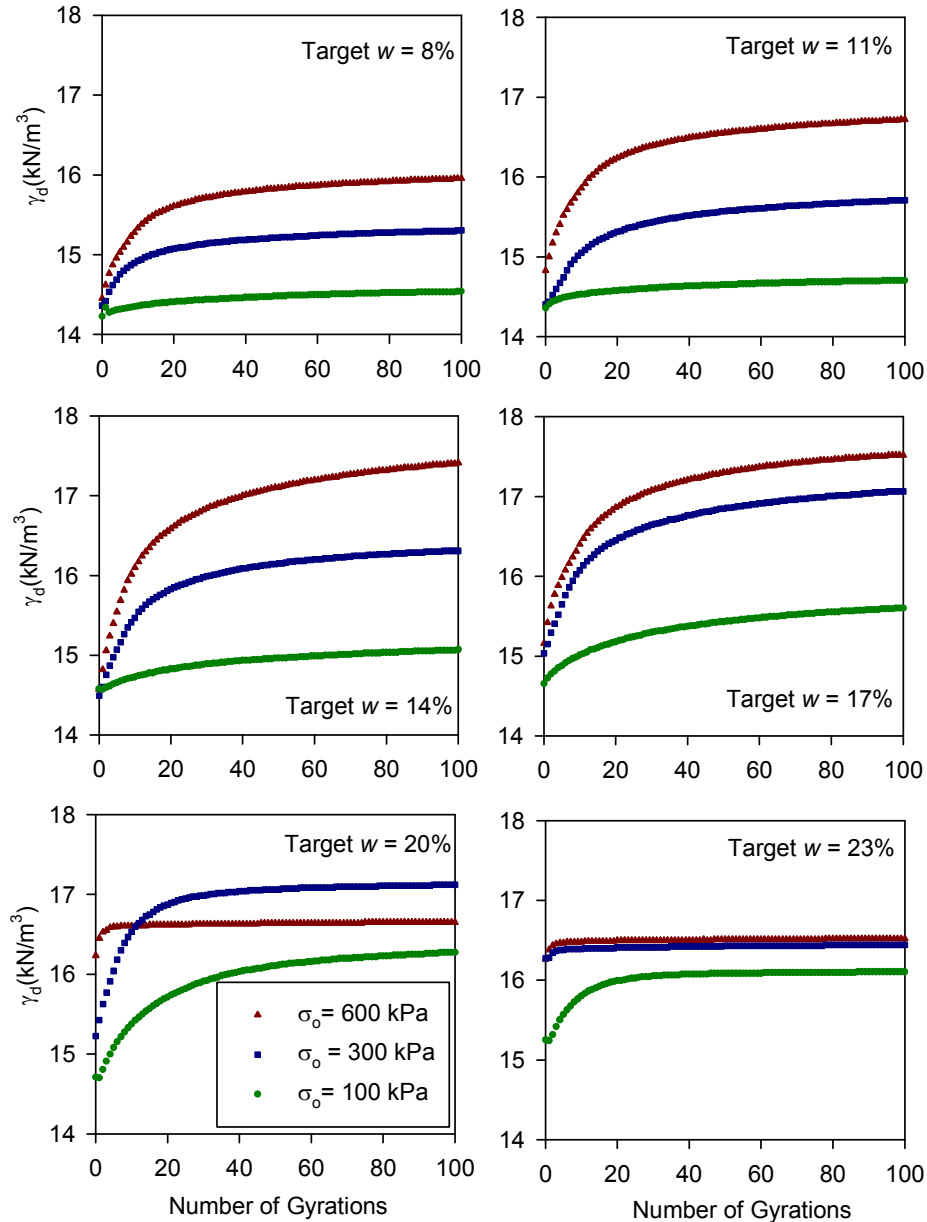
Figure 27. Dry unit weight versus number of gyrations for Iowa loess (USCS: ML)

Geosynthetic Reinforcement Study

Two types of materials were involved in the geosynthetic reinforcement study, which were subgrade and base materials. The performed laboratory tests include grain-size distribution tests on both subgrade and base materials, standard Proctor test on the subgrade material and

relative density test on the base material. Figure 28 and Figure 29 are the grain-size distribution curves for the subgrade and base materials. The subgrade material was classified as CL and the base material was classified as GP-GM per USCS classification. The optimum moisture content of the subgrade material is 17.2% and the maximum dry unit weight is 17.4 kN/m^3 based on standard Proctor test (Figure 30). The base material had the maximum dry unit weight of 22.2 kN/m^3 and the minimum dry unit weight is 16.7 kN/m^3 based on relative density test as shown in Figure 31. The field relative density is going to align the curve which connecting the maximum and minimum dry unit weight of the material. Table 6 summarizes the material index properties for these two soils.

Figure 28. Grain-size distribution curve of subgrade material from West Virginia site

Figure 29. Grain-size distribution curve of base material from West Virginia site
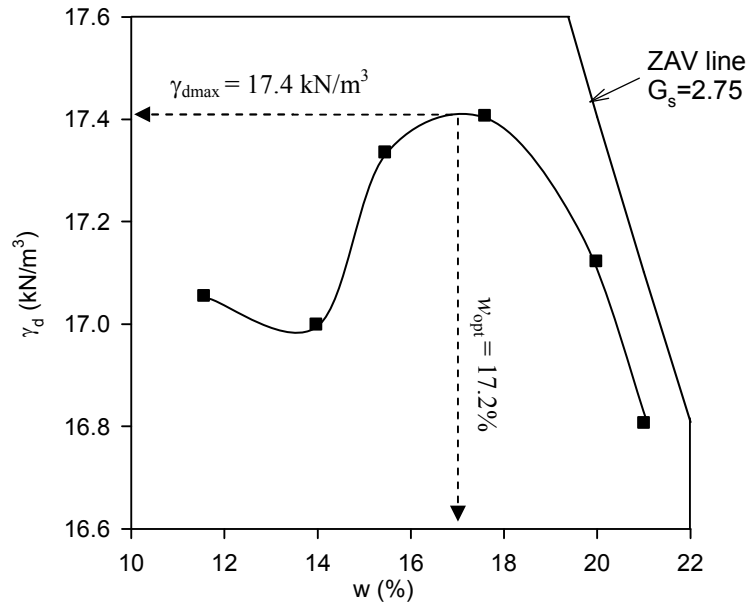
Figure 30. Standard Proctor test result for subgrade from West Virginia (USCS: CL)
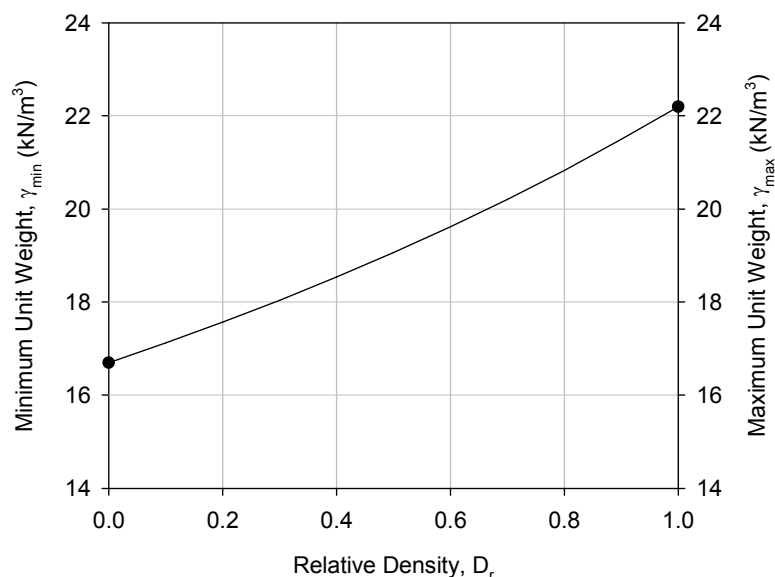
Figure 31. Relative density curve with maximum and minimum dry unit weight for base material from West Virginia (USCS: GP-GM)

Table 6. Summary of the material index properties for West Virginia site

Parameter	West Virginia site	
Layer	Subgrade	Base
Material Description	Clay	Poorly graded gravel with silt
Maximum dry unit weight (kN/m³) and optimum moisture content (%)		
Standard Proctor	17.4 (17.2)	—
Maximum Dry Unit Weight (kN/m³)	—	22.2
Minimum Dry Unit Weight (kN/m³)	—	16.7
Gravel Content (%) (> 4.75mm)	6	55
Sand Content (%) (4.75mm – 75µm)	16	37
Silt Content (%) (75µm – 2µm)	41	6
Clay Content (%) (< 2µm)	37	2
Coefficient of Uniformity (c_u)	—	29.2
Coefficient of Curvature (c_c)	—	3.2
Liquid Limit, LL (%)	45	NP
Plasticity Index, PI	21	NP
AASHTO	A-7-6	A-1-a
USCS	CL	GP-GM
Specific Gravity, G_s (Assumed)	2.75	2.75

Hormel PCC

This field study was to evaluate the PCC pavement foundation for Hormel Facility in Dubuque, Iowa. The material involved in this research was classified as GW-GM, and the performed laboratory test on this material was grain-size distribution test. Table 7 summarizes the material index properties and the grain-size distribution curve is shown in Figure 32.
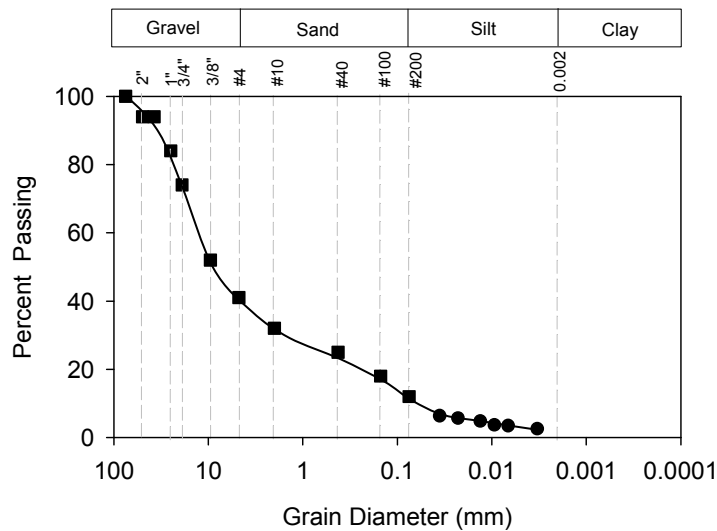
Figure 32. Grain-size distribution curve of gravel subbase material

Table 7. Summary of the material properties for the gravel subbase material

Parameter	Dubuque, IA site
Material Description	Well-graded gravel with silt
Gravel Content (%) (> 4.75mm)	59
Sand Content (%) (4.75mm – 75μm)	29
Silt Content (%) (75μm – 2μm)	10
Clay Content (%) (< 2μm)	2
D_{10}	0.06
D_{30}	1.5
D_{60}	12.6
Coefficient of Uniformity (c_u)	200.4
Coefficient of Curvature (c_c)	2.8
AASHTO	A-1-a
USCS	GW-GM

Ohio Bridge Approach

The soil index properties of a total of 15 backfill material samples from bridge approaches at seven project sites in Ohio were determined. Five of the samples were collected by the Ohio Department of Transportation (ODOT), and 10 samples were collected by researchers from Iowa State University (ISU). The ODOT samples were tested for grain-size distribution (Table 8), and the ISU samples were tested for grain-size distribution, relative density, w and γ_d, and laboratory collapse potential (Table 9).

Table 8. Summary of soil index properties for backfill materials (sampled by ODOT)

Description	Location				
	Marzane at Perryville			Shelly at Newark	West Mill Grove
Material ID	Natural Sand type 1	Natural Sand type 2	Crushed Gravel	Natural Sand	MF Sand
Gravel Content (%) (>4.75mm)	0.1	—	49.4	—	2.9
Sand Content (%) (4.75mm - 75 μm)	95.9	94.6	33.6	91.7	93.3
Fine Content (%) (< 75 μm)	4.0	5.4	17.0	8.3	3.8
Coefficient of Uniformity (C_u)	5.47	5.40	—	6.09	8.31
Coefficient of Curvature (C_c)	0.77	0.90	—	1.19	1.31
AASHTO	A-1-b	A-1-b	A-1-b	A-1-b	A-1-b
USCS	SP	SP-SM	GM	SW-SM	SW

Table 9. Summary of soil index properties for backfill materials (sampled by ISU)

Description	Bridge ID				
	BUT-75-0660	CL1-73-0985		MOT-75-1393	
Material ID	BUT Select Fill	CL1 Sand	MOT Sand	MOT Pea Gravel	MOT Subbase
Gravel Content (%) (>4.75mm)	—	—	3	97	68
Sand Content (%) (4.75mm - 75 μm)	99	95	88	—	32
Fine Content (%) (< 75 μm)	1	5	9	3	—
Coefficient of Uniformity (c_u)	3.15	7.09	6.83	1.76	23.06
Coefficient of Curvature (c_c)	0.96	1.18	1.74	1.14	2.52
Maximum Dry Density (kg/m^3)	1903.3	1914.8	1822.3	1652.3	2147.2
Minimum Dry Density (kg/m^3)	1592.6	1475.5	1397.6	1499.6	1663.7
AASHTO	A-1-b	A-1-b	A-1-b	A-1-a	A-1-a
USCS	SP	SW-SM	SW-SM	GP	GW

Description	Bridge ID				
	FRA-670-0904B		LIC-37-1225L		MED-71-0729
Material ID	FRA Porous Backfill	FRA Subbase	LIC EB- Till	LIC WB-Till	MED SB Gravel
Gravel Content (%) (>4.75mm)	95	43	24	39	49
Sand Content (%) (4.75mm - 75 μm)	1	33	35	34	44
Fine Content (%) (< 75 μm)	4	14	41	27	7
Coefficient of Uniformity (c_u)	1.82	—	—	—	36.74
Coefficient of Curvature (c_c)	1.16	—	—	—	0.84
Maximum Dry Density (kg/m^3)	1609.8	1854.3	—	—	2120.9
Minimum Dry Density (kg/m^3)	1444.3	1535.3	—	—	1670.4
Liquid Limit, LL (%)	NP	NP	23	24	NP
Plasticity Index, PI	NP	NP	8	7	NP
AASHTO	A-1-a	A-1-a	A-4	A-2-4	A-1-a
USCS	GP	GM	SM	GM	GP-GM

Note: No material collected from MED-71-075

FHWA Intelligent Compaction (IC)

The project site is located at Springville, New York. Two materials were tested both in situ and in laboratory, which were base material and embankment material. The grain-size distribution curves for the base material and the embankment material are shown in Figure 33 and Figure 34. Standard Proctor tests were conducted on both embankment material and aggregate base material to develop the relationship between moisture content and dry unit weight, and the tests results are shown in Figure 35 and Figure 36. Table 10 summarizes the laboratory tests results for both base material and embankment material.
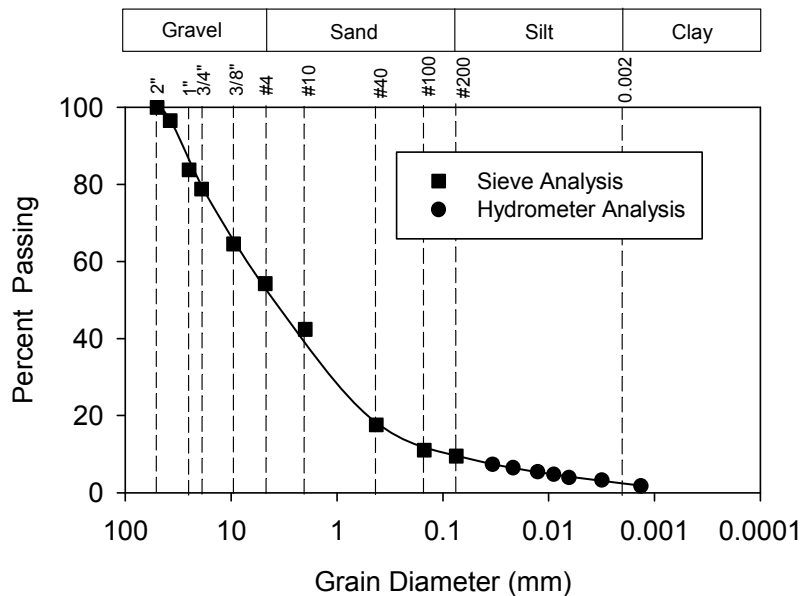
Figure 33. Grain-size distribution curve for the base material

Figure 34. Grain-size distribution for the embankment material

Figure 35. Standard Proctor test result for embankment material
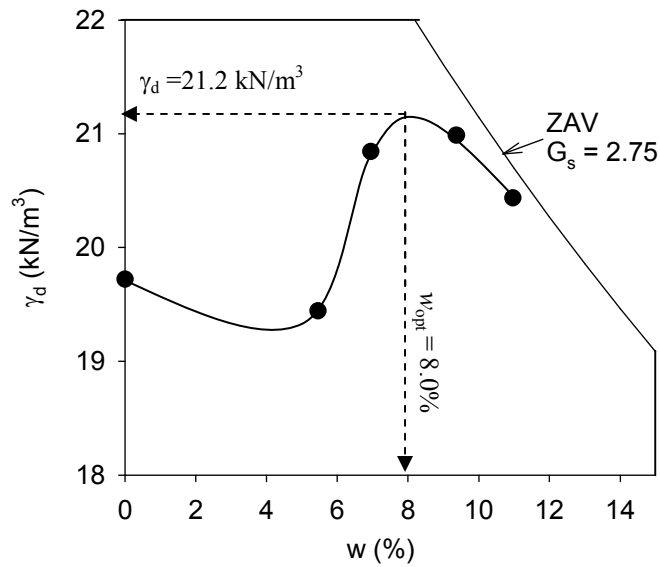
Figure 36. Standard Proctor test result for aggregate base material

Table 10. Summary of material index properties from New York project site

Parameter	Embankment Material	Aggregate Base
Maximum dry unit weight (kN/m^3) and optimum moisture content (%)		
Standard Proctor	20.5 (8.6)	21.2 (8.0)
Relative Density Test Results (oven-dry material)		
γ_{dmin} (kN/m^3)	Not	15.95
γ_{dmax} (kN/m^3)	Performed	20.01
Gravel Content (%) (> 4.75mm)	24	46
Sand Content (%) (4.75mm – 75μm)	55	44
Silt Content (%) (75μm – 2μm)	15	7
Clay Content (%) (< 2μm)	6	3
Coefficient of Uniformity, c_u	185.5	93.1
Coefficient of Curvature, c_c	2.9	2.3
Liquid Limit, LL (%)	16	15
Plastic Limit, PL (%)	Non-Plastic	
AASHTO Classification	A-1-b	A-1-a
USCS Classification	SM	GW
Specific Gravity, G$_s$ (Assumed)	2.65	2.75

Pavement Foundation Study

Three test beds were tested from the Michigan pavement foundation study. Test bed #1 consists of 40.6 cm of compacted and trimmed open-graded aggregate subbase over a recompacted mixture of sand and silty clays. Test bed #2 was a section of 22.9 cm thick, jointed concrete pavement constructed 40 years ago, and the material under the concrete panel was sampled and transported to the laboratory to determine the grain-size distribution and perform a standard Proctor test. Test bed #3 had the same material as test bed #1, which is open-graded aggregate subbase material. The laboratory tests performed for the material sampled from test bed #1 and #3 include grain-size distribution analysis and relative density tests. The material sampled from test bed #1 was classified as GW and material sampled from test bed #2 was classified as SP-SM per USCS classification. The grain-size distribution curves for materials sampled from test bed #1 and #3 are shown in Figure 37 and Figure 38, respectively. The standard Proctor test result for material sampled from test bed #2 is shown in Figure 39 and the relative density test results for material from test bed #1 is shown in Figure 40. Table 11 summarizes the laboratory tests results for both materials.
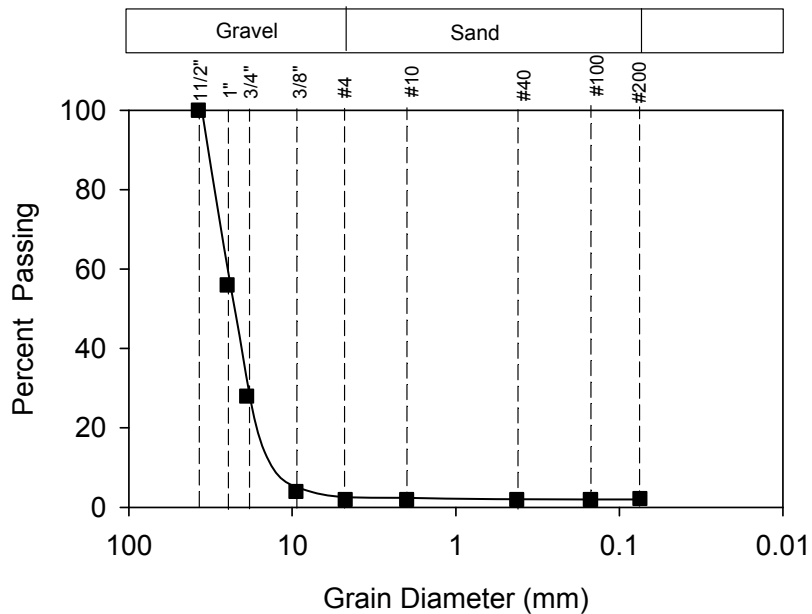
Figure 37. Grain-size distribution curve for the untrimmed base material (TB1&3)
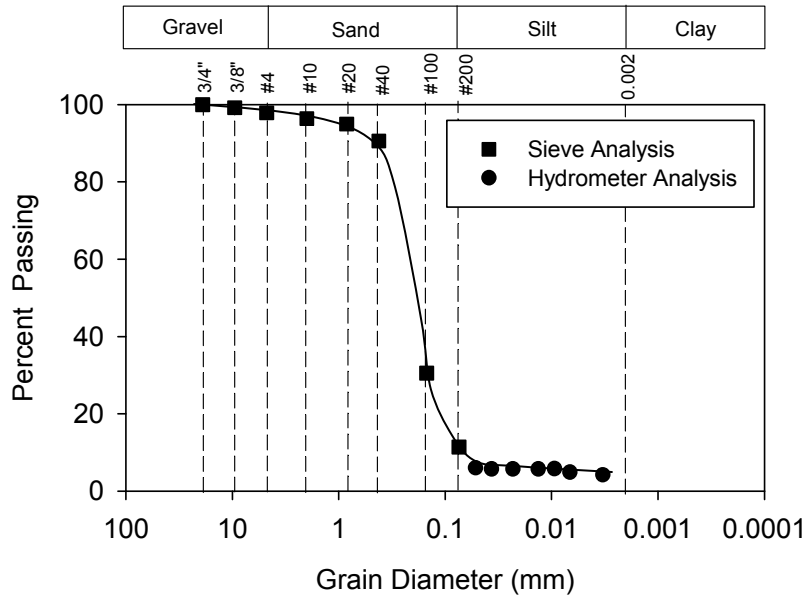
Figure 38. Grain-size distribution curve for material from test bed #2
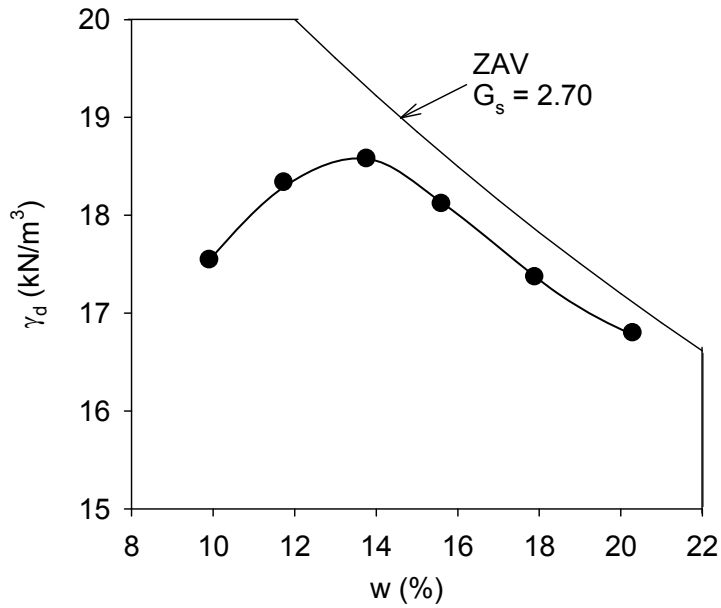
Figure 39. Standard Proctor test result for material from test bed #2
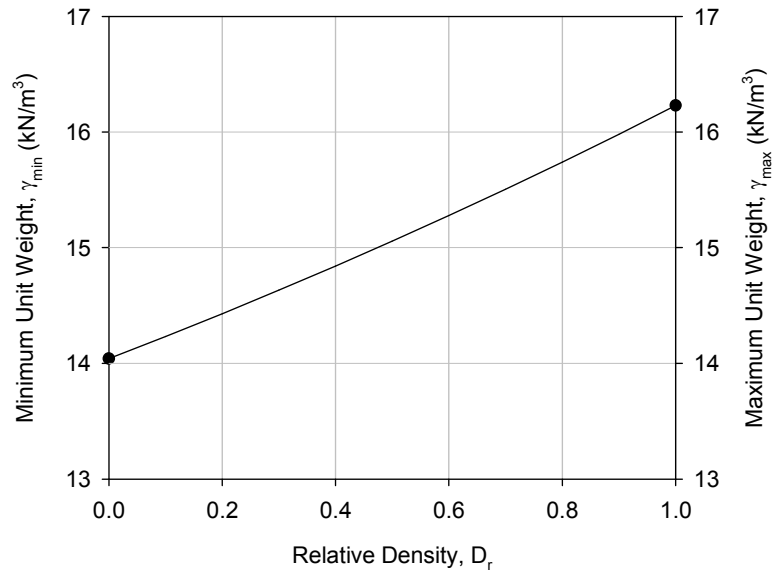
Figure 40. Relative density curve with maximum and minimum dry unit weight for material from test bed #1

Table 11. Summary of soil index properties for the tested materials

Parameter	Untrimmed Base	TB2
Standard Proctor γ_{dmax} (kN/m^3), w_{opt} (%)	—	18.6 (13.8)
Maximum and minimum index density (kN/m^3)	16.23 (14.04)	—
Gravel Content (%) (> 4.75mm)	98	2.1
Sand Content (%) (4.75mm – 75µm)	—	86.5
Silt Content (%) (75µm – 2µm)	2	7.5
Clay Content (%) (< 2µm)	—	3.9
D_{10} (mm)	13.44	0.069
D_{30} (mm)	19.57	0.149
D_{60} (mm)	26.18	0.243
Coefficient of Uniformity, c_u	1.95	3.50
Coefficient of Curvature, c_c	1.09	1.31
AASHTO Classification	A-1-a	A-2-4
USCS Classification	GW	SP-SM
Specific Gravity, G_s (Assumed)	2.75	2.65

CHAPTER 5. TEST RESULTS AND DISCUSSION

This chapter presents and discusses the test results from both field and laboratory studies in this order:

- case studies of field projects,
- the influence of LWD device configuration,
- correlations between LWD and other in situ point measurements,
- the influence of soil layering profiles on surface modulus,
- laboratory test results, and
- target value determination study for quality assurance.

Case Studies of Field Projects

Field studies were conducted at sites in West Virginia, Iowa, Ohio, New York, and Michigan, to investigate the performance of five mechanistic-based compaction control measurement devices and to use the devices to develop standard protocols for earthwork QC/QA practices.

Geosynthetic Reinforcement Study

This field study was conducted at Weirton, West Virginia from March 17 to 20, 2009. The goal for the field study was to evaluate the performance of three different geogrid reinforcement materials. These materials were placed over relatively weak subgrade soils and covered by aggregate base material. Four 18.3 m long sections each with 5 test points were constructed, a control section and three sections labeled according to the geogrid material used in each section (Figure 41 and Figure 42). Caterpillar and Case smooth drum rollers (Figure 43) were used to compact the test beds. Nuclear gauge (NC), dynamic cone penetrometer (DCP), light weight deflectometer (LWD) and plate load test (PLT) were performed to determine the density, strength, and stiffness of the compacted materials. Two

aggregate base layers were built on top of the compacted subgrade with the geogrid in between the aggregate base and subgrade. The in situ measurements were taken at 2 roller passes for subgrade, 0, 2, 4, and 10 roller passes for the first lift of subbase and 0, 2, 4, 10, and 21 roller passes for the second lift aggregate base. The thickness of the first lifts for W-PP-FT and Tensar BX1200 sections was 246.5 mm, and the thickness of the first lifts for control and Tensar TX160 sections was 289.5 mm. The thickness for the second lifts for sections W-PP-FT and Tensar BX1200 was 176.7 mm and 151.5 mm for control and Tensar TX160 sections.

Two tests were performed, LWD and DCP tests. The LWD tests were done to limit the possibility of disturbance. The LWD tests measured the surface modulus of the compacted material, and DCP tests were conducted to obtain the strength change with depth. LWD measurements were expressed in terms of E_{LWD-Z2} with the number of roller passes as shown in Figure 44, Figure 45, and Figure 46. DCP index was converted into CBR using formula $CBR = 292 / DCPI^{1.12}$. Because CBR can more directly represent the strength of each layer. The DCP-CBR plots for all the tested points are provided in Appendix.
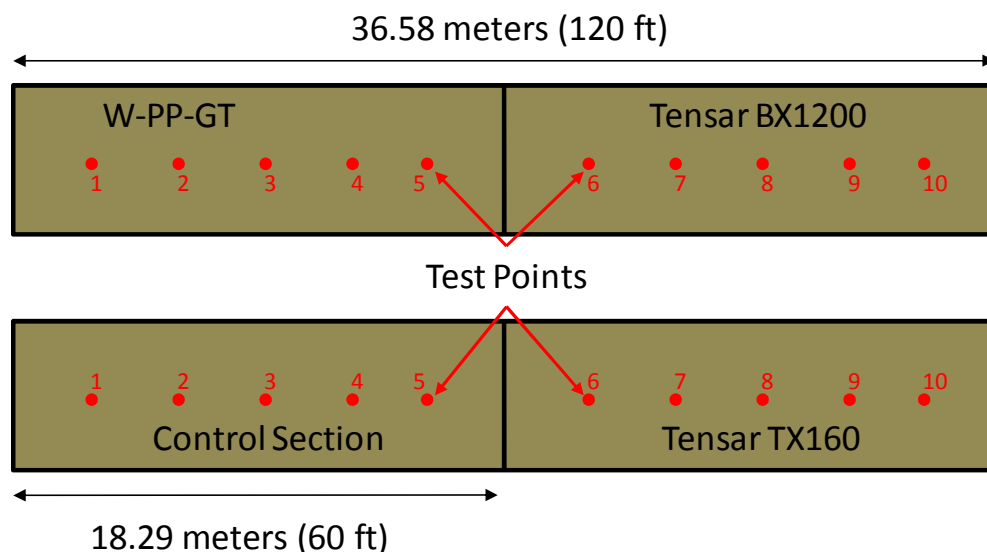
Figure 41. Test bed layout for West Virginia field study
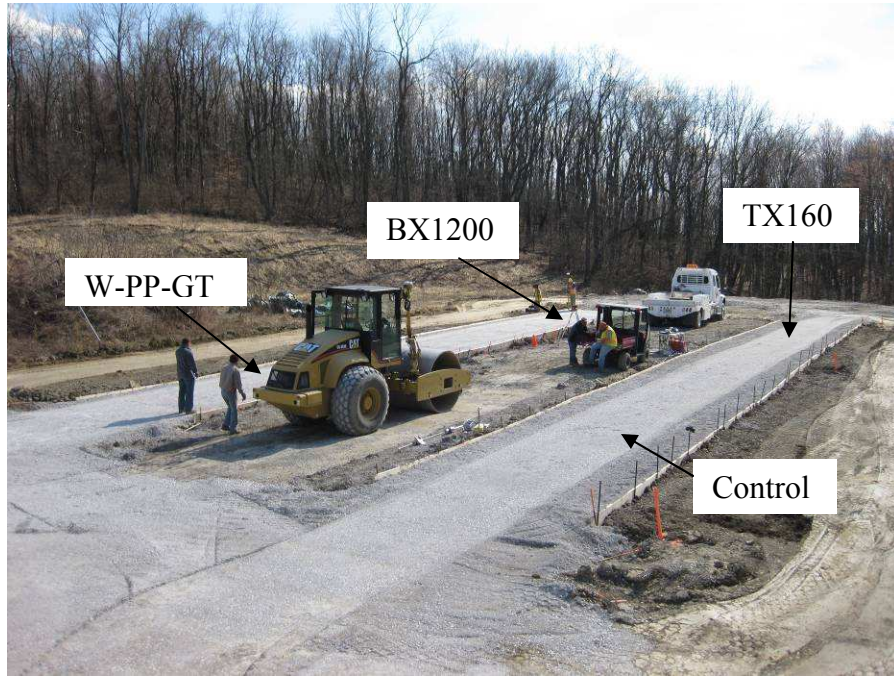
Figure 42. Overview of the site

Figure 43. Caterpillar (left) and Case (right) smooth drum rollers used in the West Virginia site
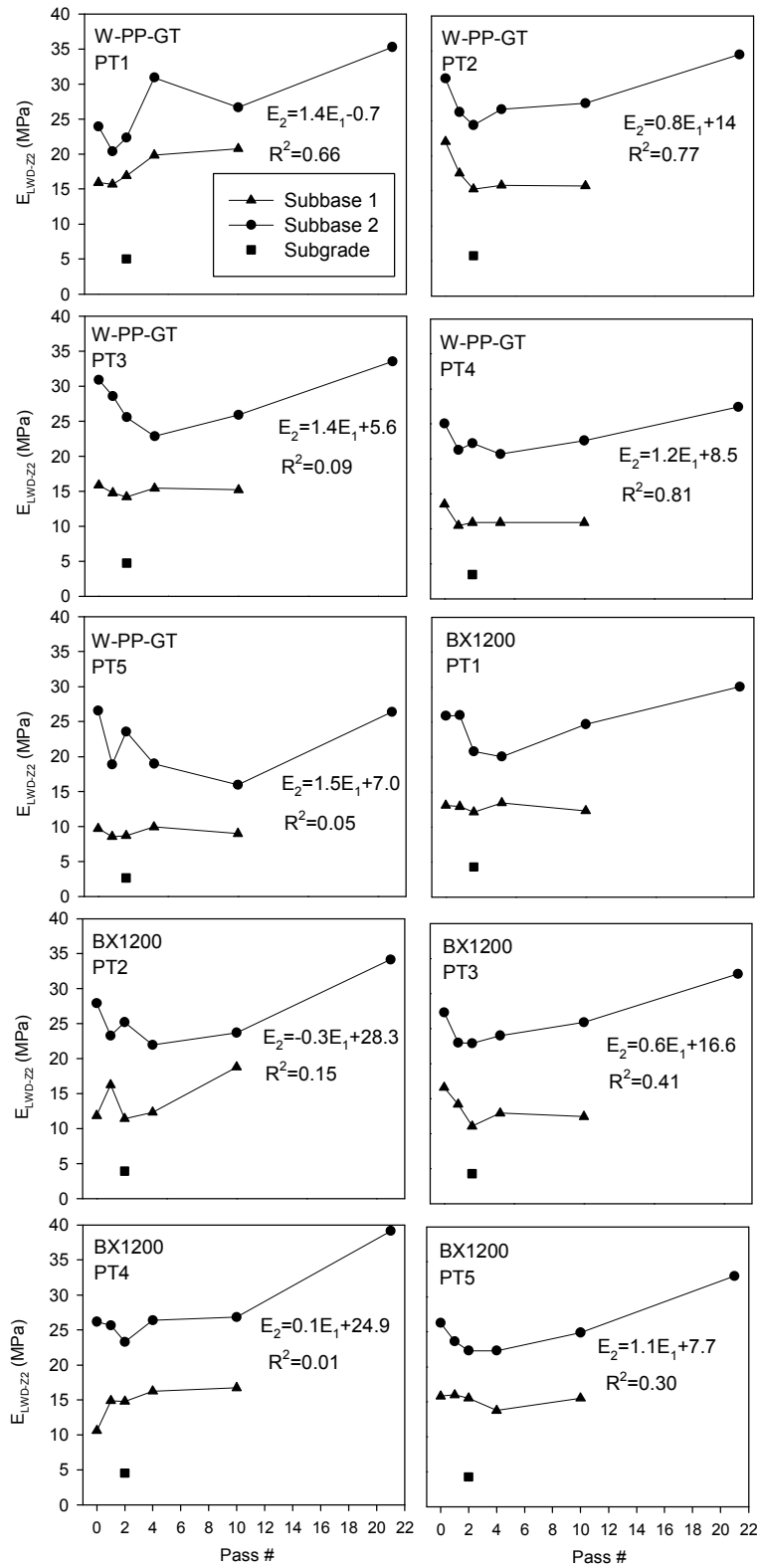
Figure 44. E_{LWD} compaction curves for W-PP-GT and BX1200 sections
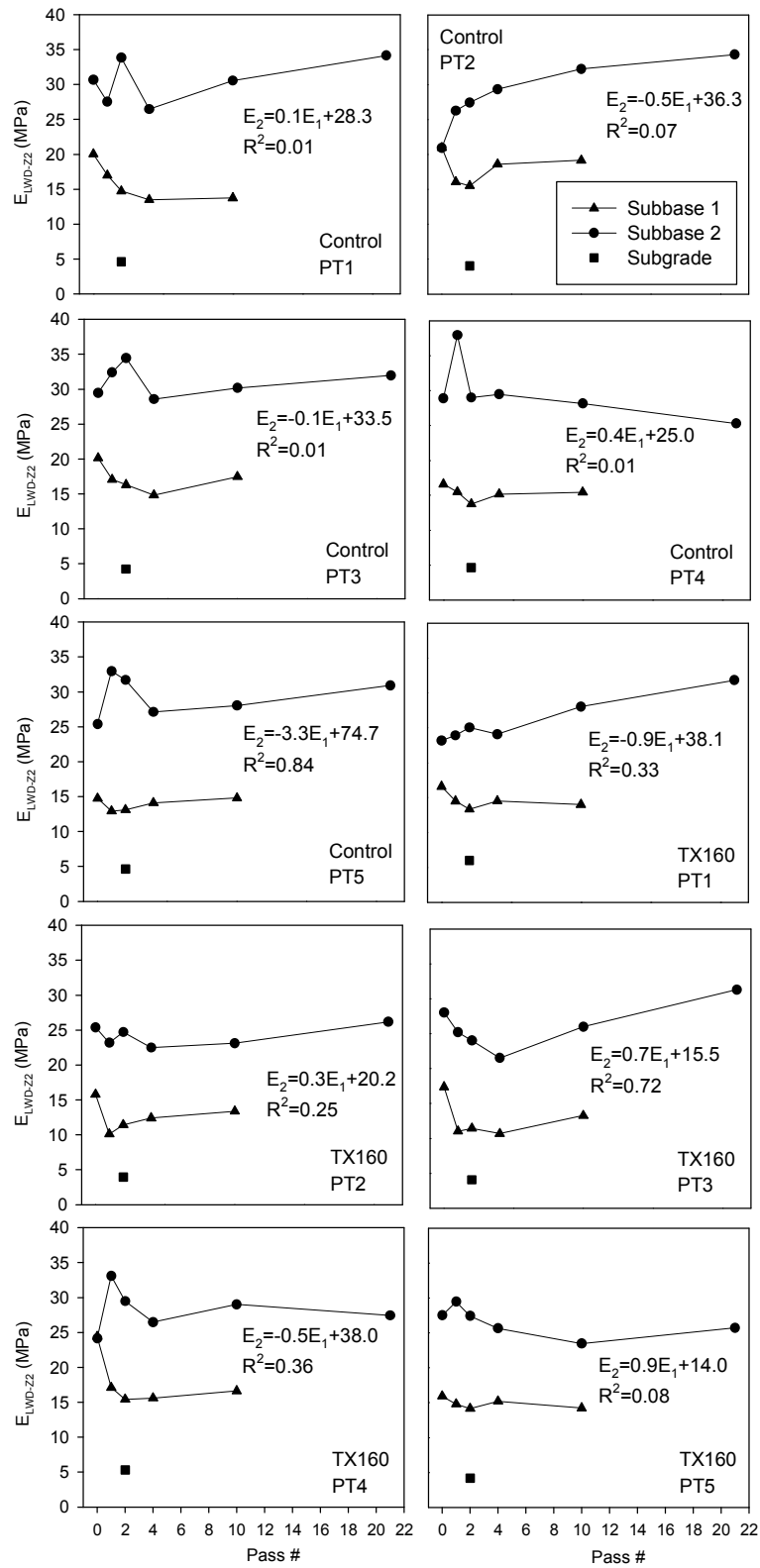
Figure 45. E_{LWD} compaction curves for control and TX160 section
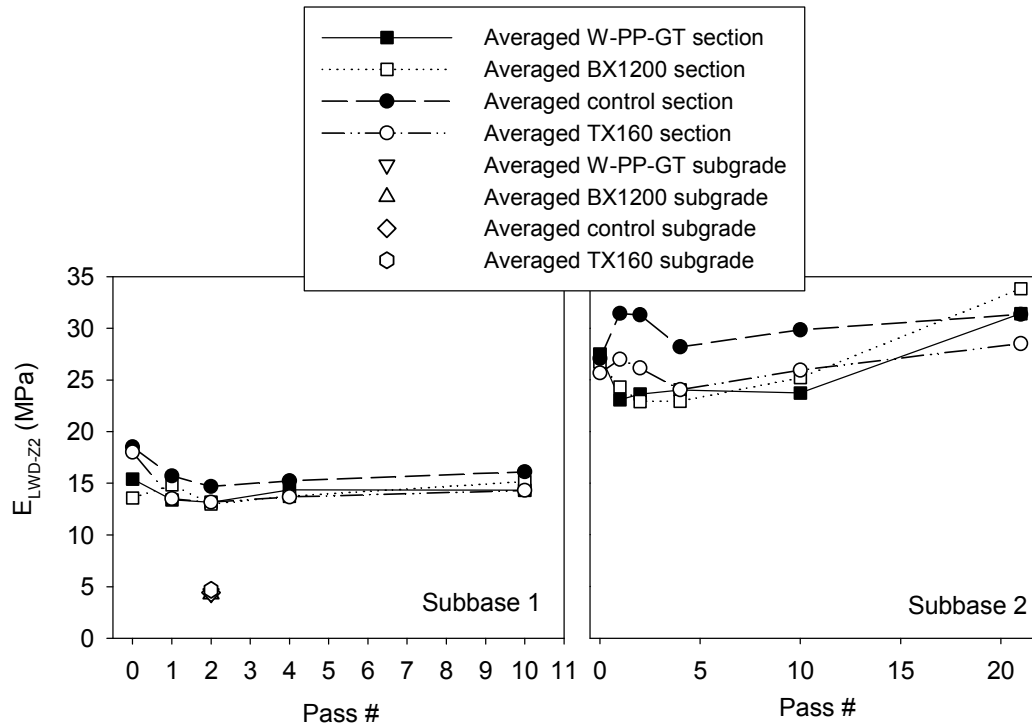
Figure 46. Averaged E_{LWD} compaction curves for each section

The following key findings are withdrawn from this field case study:

- No significant improvement of LWD modulus for all sections when the roller passes change from one to four, and the modulus of the base layer was clearly increased after roller pass 21 times.

- The stiffness of the second base layer was significantly increased and no clear evidence to prove the difference of using these geosynthetics.

Hormel PCC

A new Hormel facility with adjacent parking areas and driveways was under construction in Dubuque, Iowa. Cracks had developed in sections of the recently completed pavement. Two test sections were located, one in the paved driveway where the cracks had appeared and a second in the unpaved loading dock area. The plan view in Figure 47 shows the in situ test locations. FWD tests were performed on the paved driveway, and DCP and LWD tests were

conducted in the unpaved loading dock.
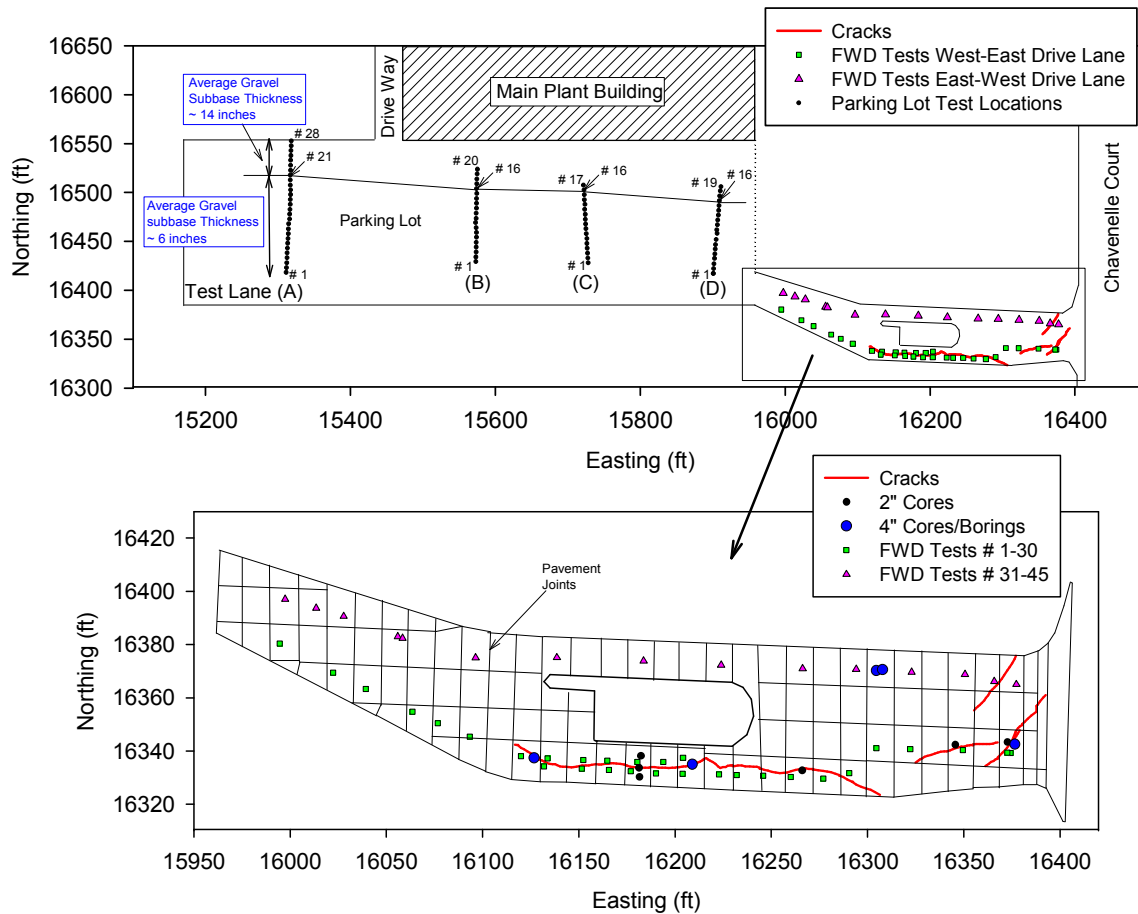
Figure 47. Plan view of in situ test locations, results of crack survey using GPS and cracks on the paved drive way (from White et al. 2009)

Before FWD data was collected from points on the paved driveway, three setting drops were made to ensure that the loading plate was in good contact with the surface at each of the 45 points where the FWD tests were conducted to show the E_{FWD} variance: these results are shown in Figure 48.
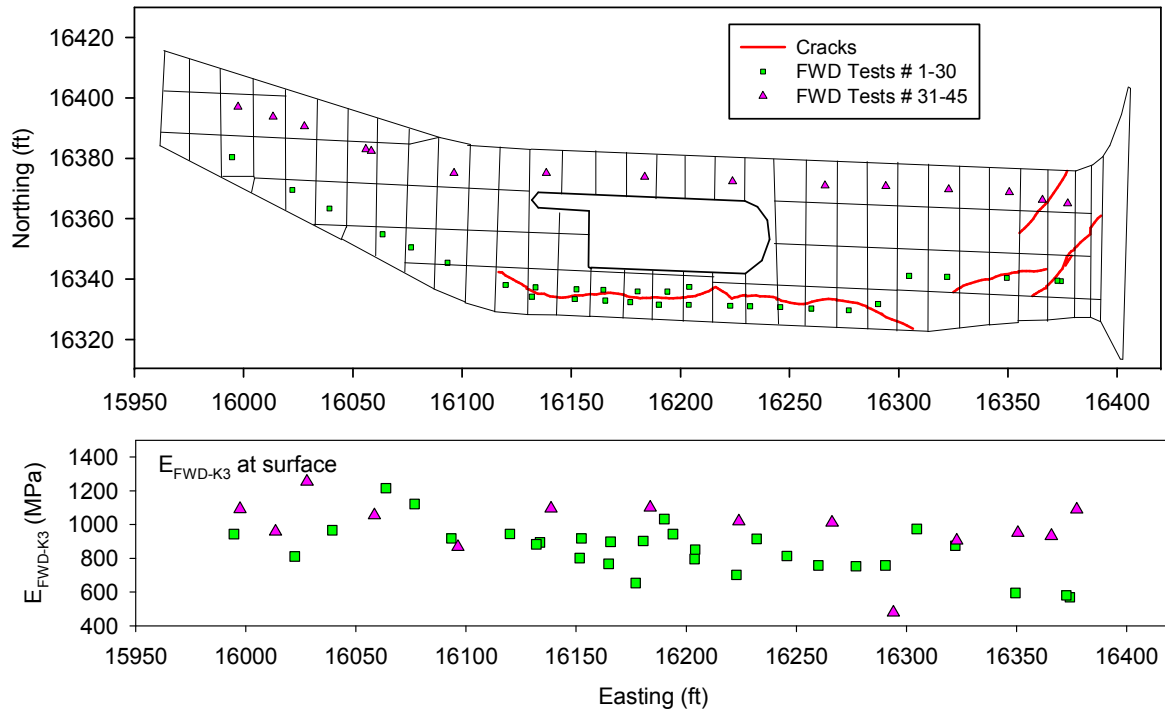
Figure 48. FWD test results – paved drive way (from White et al. 2009)

LWD tests consist of 200 mm diameter loading plate with 50 cm drop height. Three setting drops were conducted before taking deflection measurements. Four testing lanes (lane A, B, C, and D) were constructed on the unpaved loading dock area, and the measurement points for each lane vary from 17 to 28. The LWD tests results for each testing lane are shown from Figure 49 to Figure 52. For testing lane D, moisture content and dry unit weight were measured using nuclear gauge.
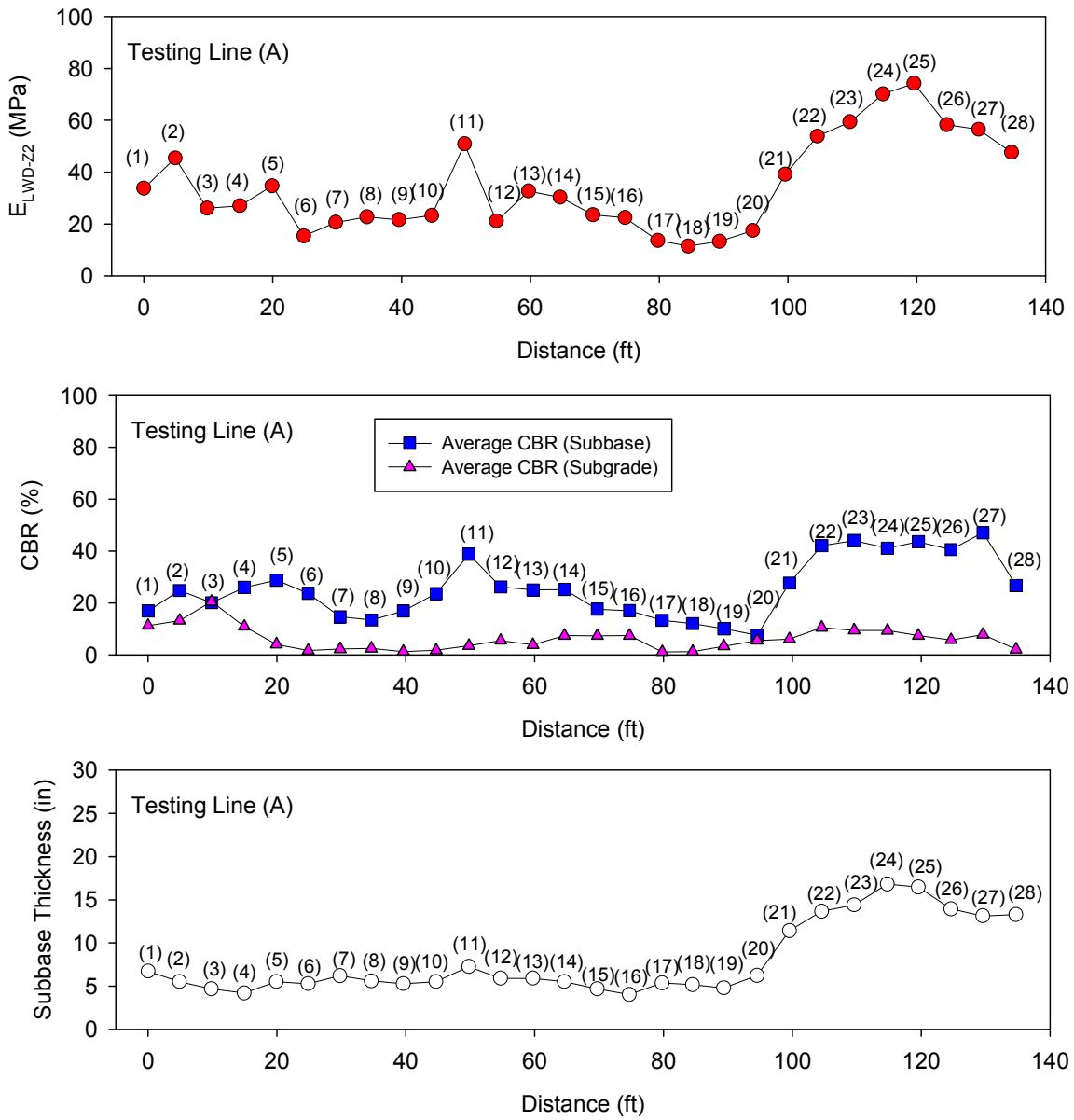
Figure 49. LWD, CBR, and subbase thickness (interpreted from DCP-CBR profiles) measurements on testing lane A (tests on unpaved area granular subbase) (from White et al. 2009)
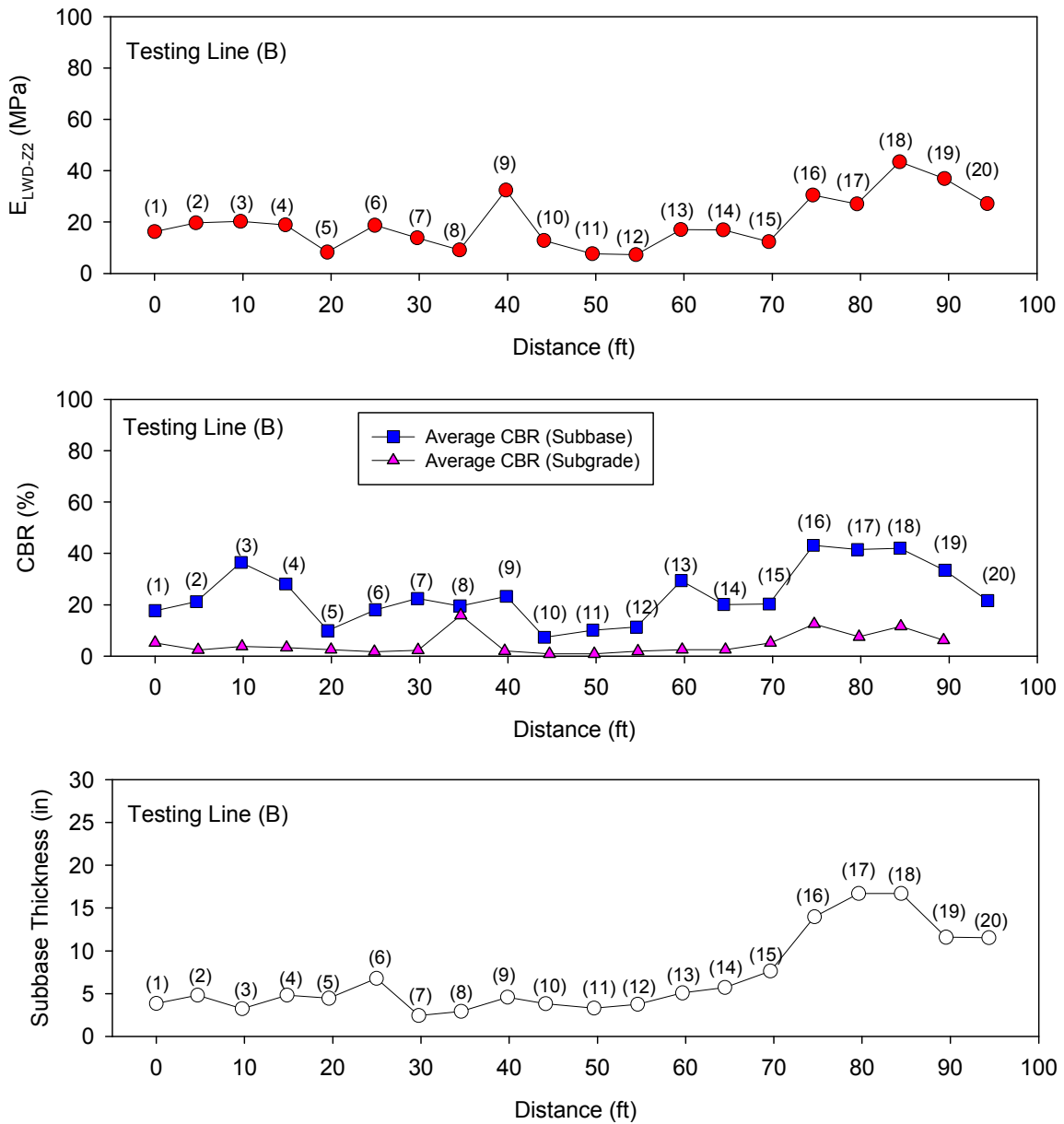
Figure 50. LWD, CBR, and subbase thickness (interpreted from DCP-CBR profiles) measurements on testing lane B (tests on unpaved area granular subbase) (from White et al. 2009)
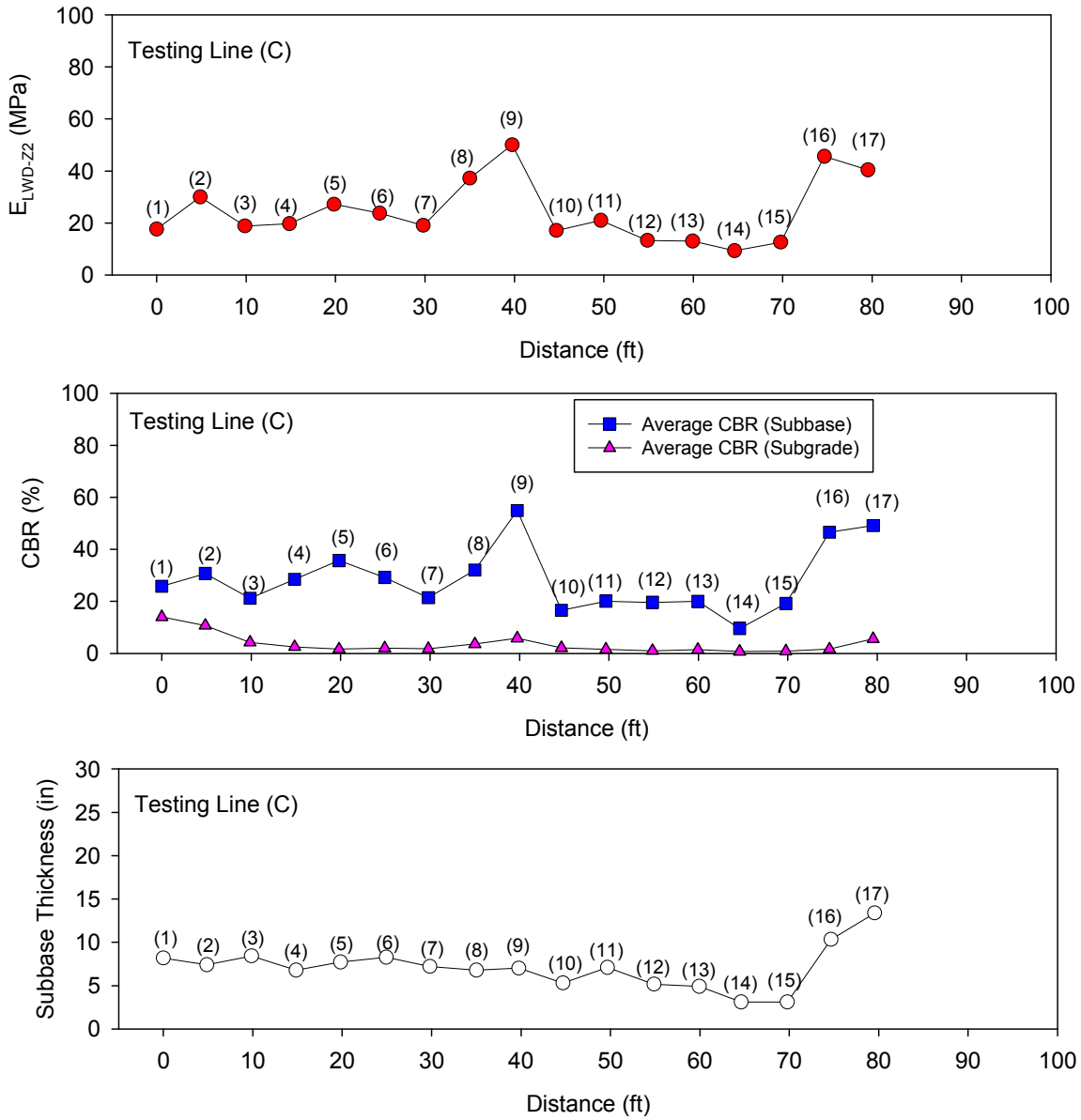
Figure 51. LWD, CBR, and subbase thickness (interpreted from DCP-CBR profiles) measurements on testing lane C (tests on unpaved area granular subbase) (from White et al. 2009)
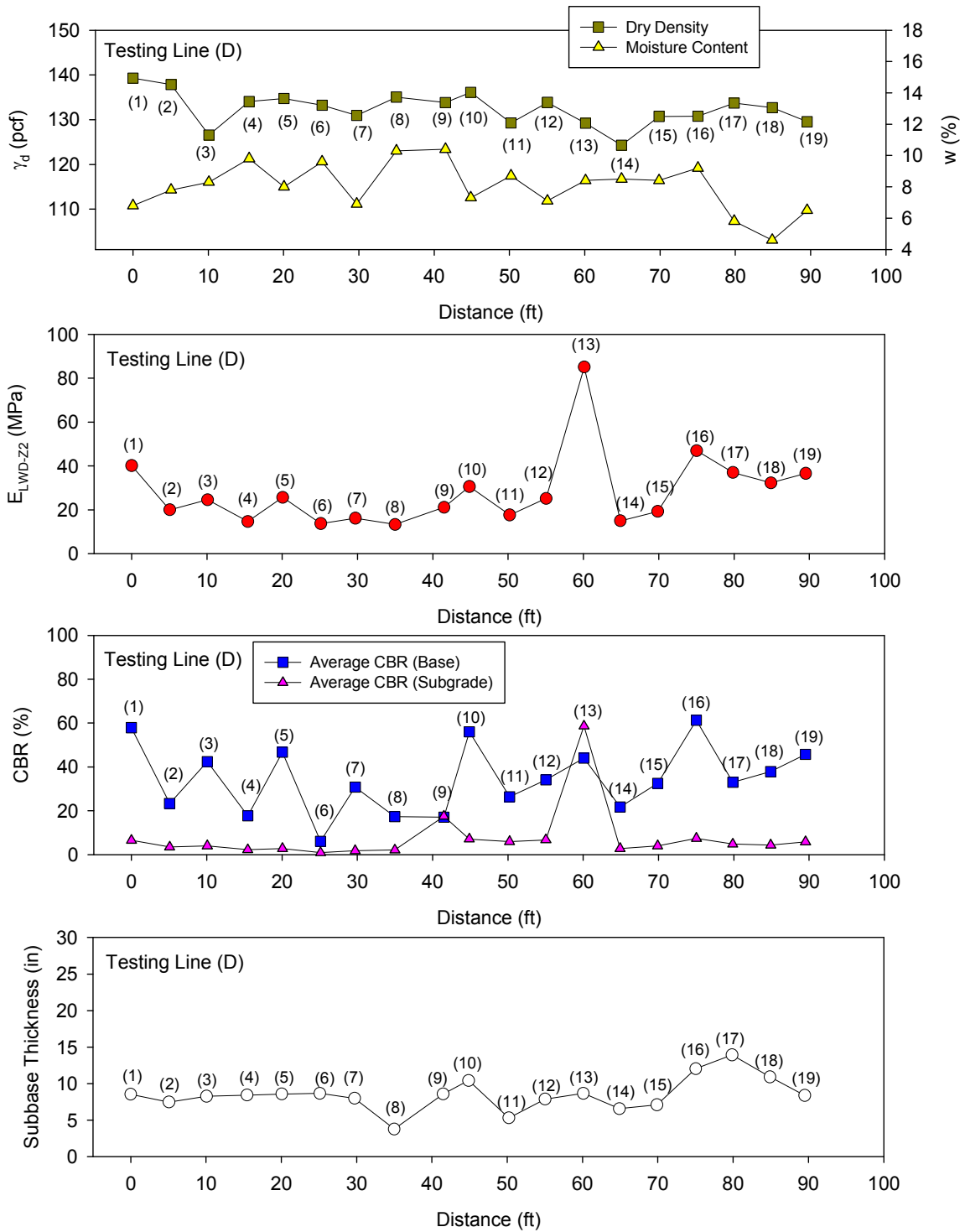
Figure 52. LWD, CBR, and subbase thickness (interpreted from DCP-CBR profiles) measurements on testing lane D (tests on unpaved area granular subbase) (from White et al. 2009)

DCP tests were performed after LWD test to avoid the disturbance caused by previous tests for the testing points. The DCP tests results were interpreted in terms of CBR which can present the strength of the tested soil more directly. The DCP-CBR tests results are shown from Figure 53 to Figure 56.
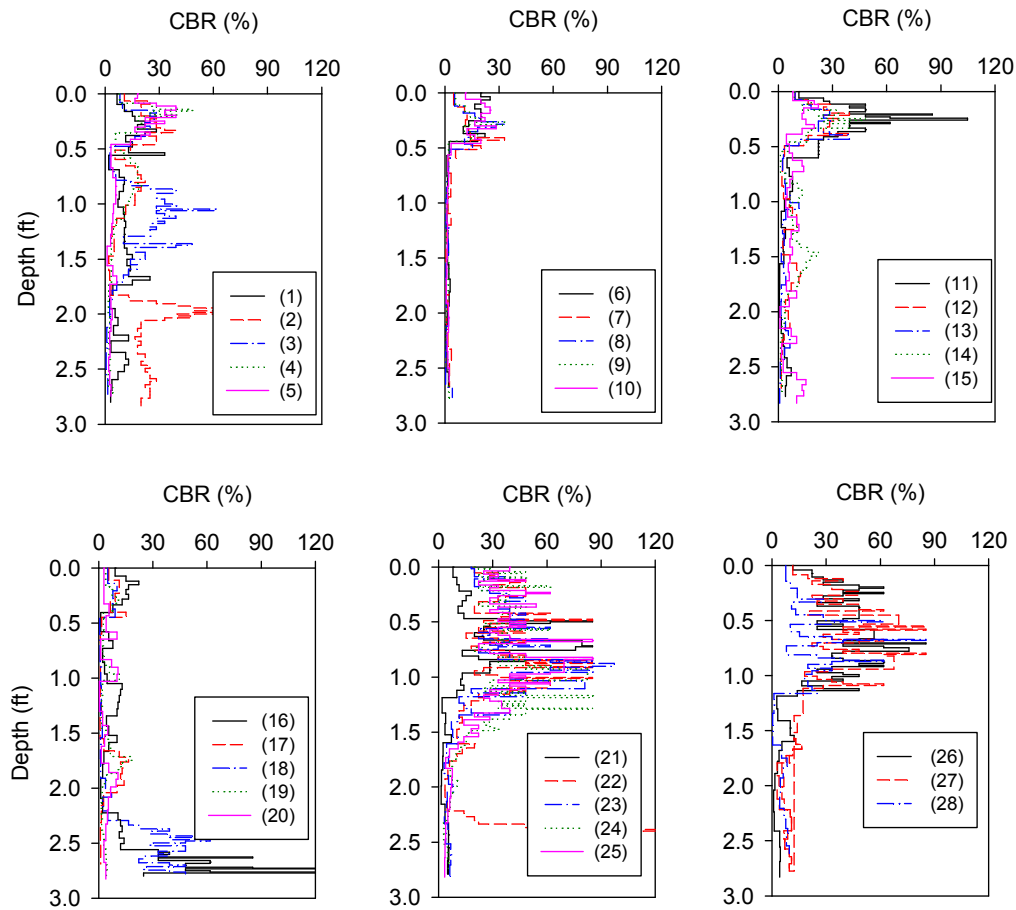
Figure 53. DCP-CBR profiles on testing lane A – unpaved area granular subbase (from White et al. 2009)
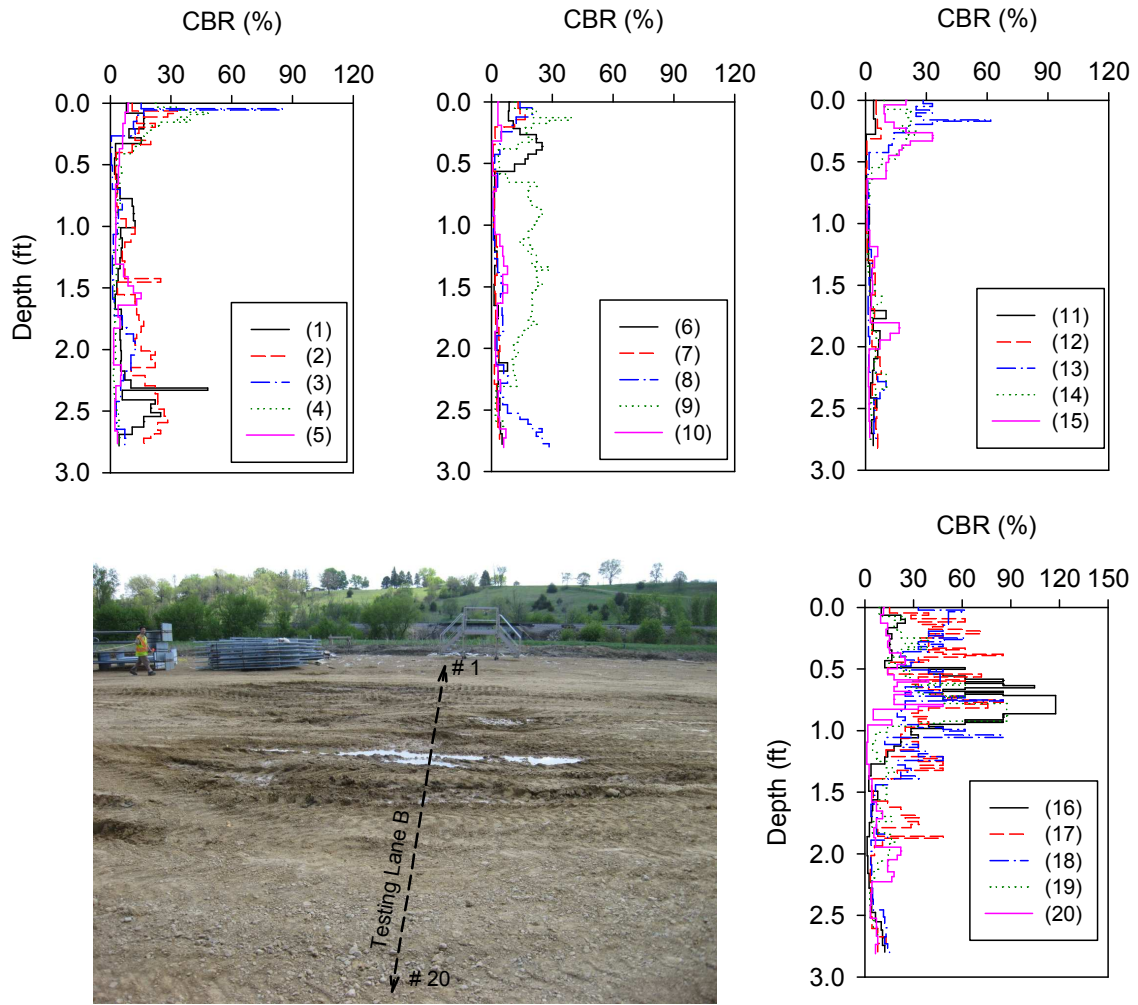
Figure 54. DCP-CBR profiles on testing lane B – unpaved area granular subbase (from White et al. 2009)
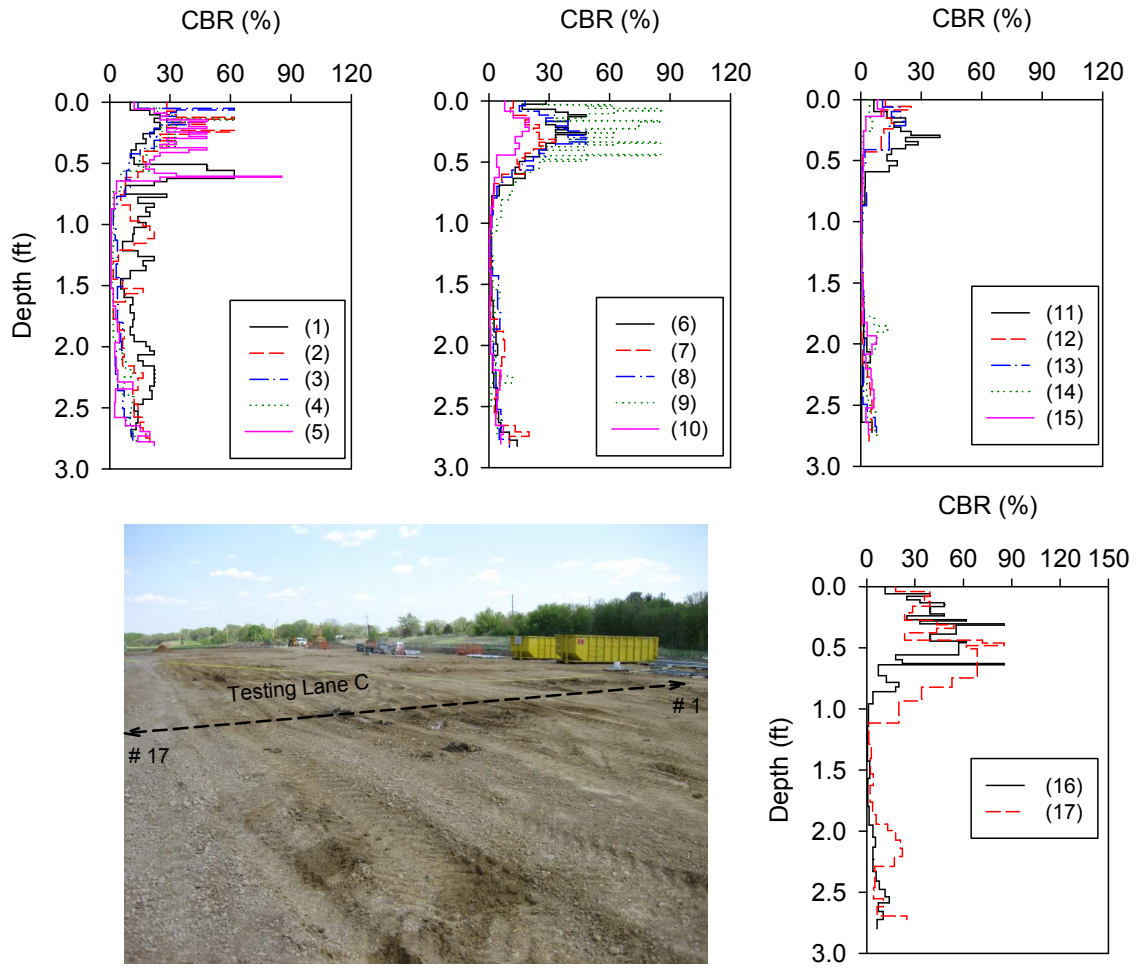
Figure 55. DCP-CBR profiles on testing lane C – unpaved area granular subbase (from White et al. 2009)
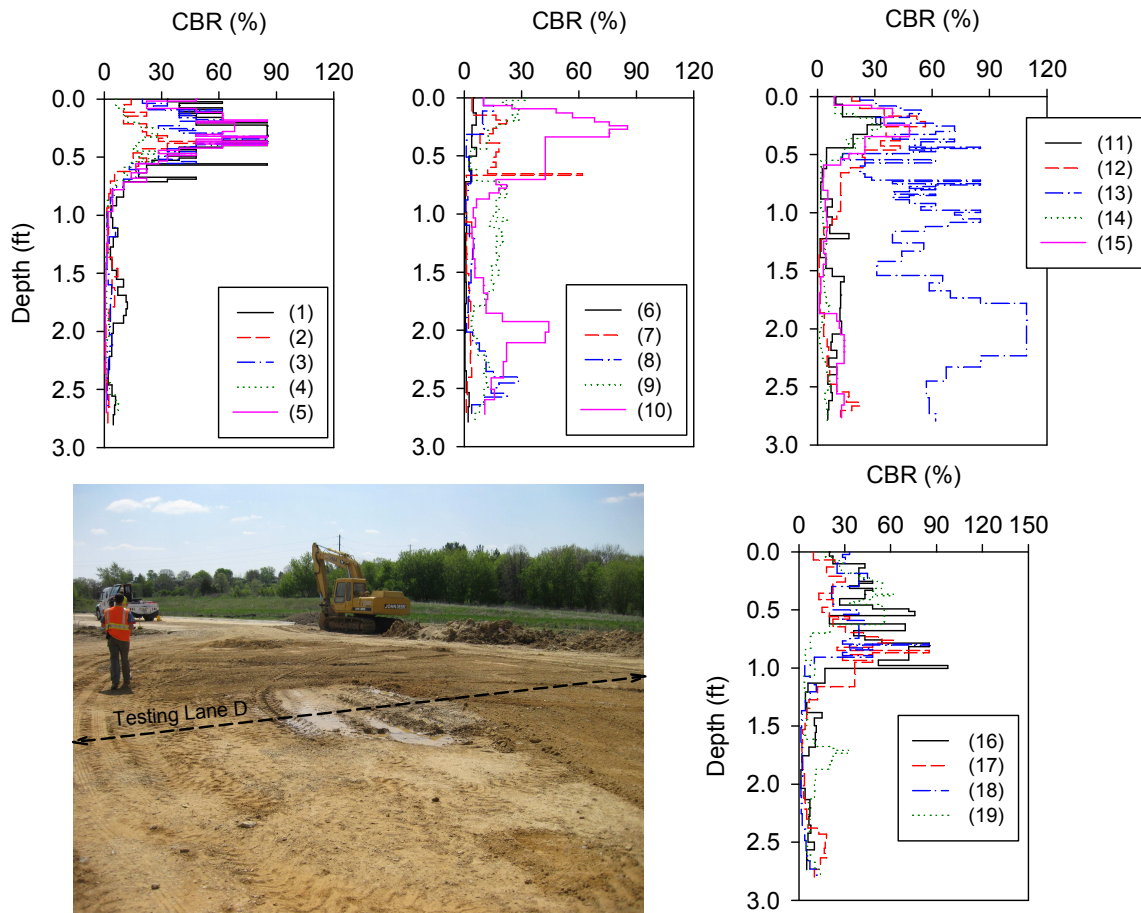
Figure 56. DCP-CBR profiles on testing lane D – unpaved area granular subbase (from White et al. 2009)

Some key findings can be obtained from this field case study include:

- The FWD measurements indicate that no clear surface modulus variance on the paved driveway.

- There were significant variances of LWD modulus on testing lane A to testing lane D, and for each testing lane the LWD modulus on the side closer to the main plant building is higher than the LWD modulus from the other side.

- DCP-CBR tests results provide the same trend as the LWD measurements, and the moisture and dry unit weight measurements on testing lane D indicate that no significant changes of moisture and dry density on that testing lane.

Ohio Bridge Approach

The purpose of this field study was to characterize the backfill materials of the new bridge approach in Ohio area. Seven new bridges were investigated during this field study and the summary of the project locations is provided in Table 12. The geotechnical investigations for this project consist of field testing and laboratory testing. The field testing including: density/moisture measurement using nuclear gauge, elastic modulus measurement by performing LWD tests and PLTs, and strength measurement by conducting DCP tests. Laboratory tests were performed on the representative samples which were transported to the laboratory from the field, and the laboratory tests include grain-size distribution tests, relative density tests, standard Proctor test, and collapse potential test.

Table 12. Summary of in situ testing at different bridge locations

Bridge number	Date	Bridge ID (SFN)	Location	In situ testing
#1	5/14/2009	BUT-75-0660 (0901822)	Westchester, Ohio	DCP, NG
#2	5/14/2009	CL1-73-0985 (1402293)	Wilmington, Ohio	DCP
#3	5/14/2009	MOT-75-1393 (5708443)	Dayton, Ohio	DCP, LWD
#4	5/15/2009	FRA-670-0904B (2517949)	Columbus, Ohio	DCP, LWD
#5	5/15/2009	LIC-37-1225L (4501691L)	Licking County, Ohio	DCP, LWD, NG
#6	5/16/2009	MED-71-0729 (5202809)	Medina County, Ohio	DCP, LWD, PLT
#7	5/16/2009	MED-71-0750 (5204275)	Medina County, Ohio	DCP, LWD

Note: SFN – Structural file number; DCP – Dynamic cone penetrometer; NG – Nuclear moisture – density gauge; LWD – 200-mm plate diameter zorn light weight deflectometer, PLT – 300-mm diameter static plate load test

Bridge # 1 is located at the I-75 & SR 129 interchange in West Chester, Ohio. Mechanically Stabilized Earth (MSE) walls were built on spread footing foundations on the North-East

(NE) and South-West (SW) sides of the interchange (Figure 57) to support the completed bridge, which will be a 35.4 m single-span bridge constructed of prestressed concrete I-beams with semi-integral abutments. Select granular material (USCS classification: SP) was used as backfill material for the MSE walls, and it was loosely placed, watered, and compacted using a hand-operated vibratory plate compactor within 1.8 m of the MSE wall. The moisture content of the backfill material was reported to be about 4% before watering, about 8% to 11% after watering, and about 5% at about 10 min after watering.

In situ testing was conducted at four test locations as showm in Figure 57. In situ testing included DCPs to depth of up to 2 m from the ground surface, and NG tests with a probe penetration depth of about 0.2 m. DCP tests were performed at distances of 0.15 m, 0.45 m, 0.91 m, and 1.83 m away from the SE and NW MSE walls. NG tests were performed at distances of about 0.45 m, 1.83 m, 3.66 m, and 5.49 m away from the SE and NW walls. The CBR values ranged from 0% to 10% at 0.15 m to 0.91 m away from the MSE walls for the upper 2.0 m of the backfill, which indicates variability and relatively low strength of the backfill material (Figure 58). The tests performed at 1.83 m away from the MSE showed higher CBR values at depths greater than about 1.5 m. Because the DCP tests were conducted at the fill stage, no compaction had occurred in the upper 0.5 m of loose lift. Figure 59 shows CBR value with distance from the MSE for selected depth. Results show an increase in CBR value with distance from the MSE with depth.

The dry density measurements of the backfill material at the SW wall and NE wall ranged from 14.9 kN/m^3 to 16.5 kN/m^3. The moisture content measurements were relatively constant for the measured locations except for the tests conducted at 0.46 m away the NE wall, which could be the result of that location having been watered just before the measurements were taken. Figure 60 shows the moisture content, which ranged from 5% to 10% for the test locations.

Figure 57. Bridge #1(BUT-75-0660) at I-75 &SR 129 interchange: (a) location of south and north MSE walls; (b) DCP test locations; (c) watering of backfill prior to compaction; (d) compaction of backfill next to the wall
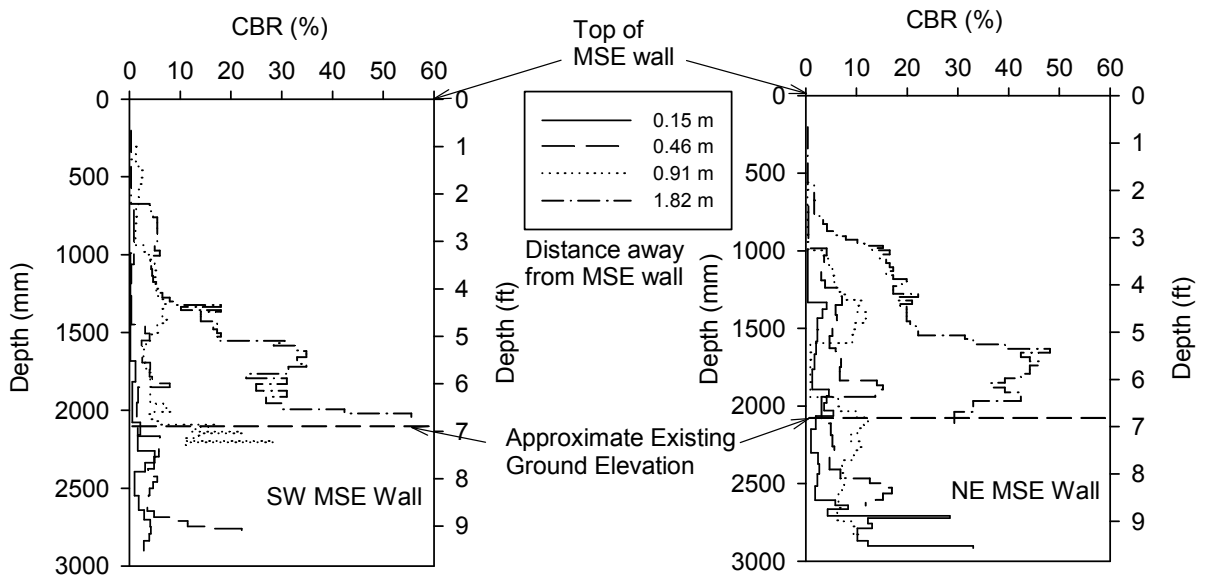
Figure 58. DCP-CBR profiles at location away from the NE and SW MSE walls – Bridge #1
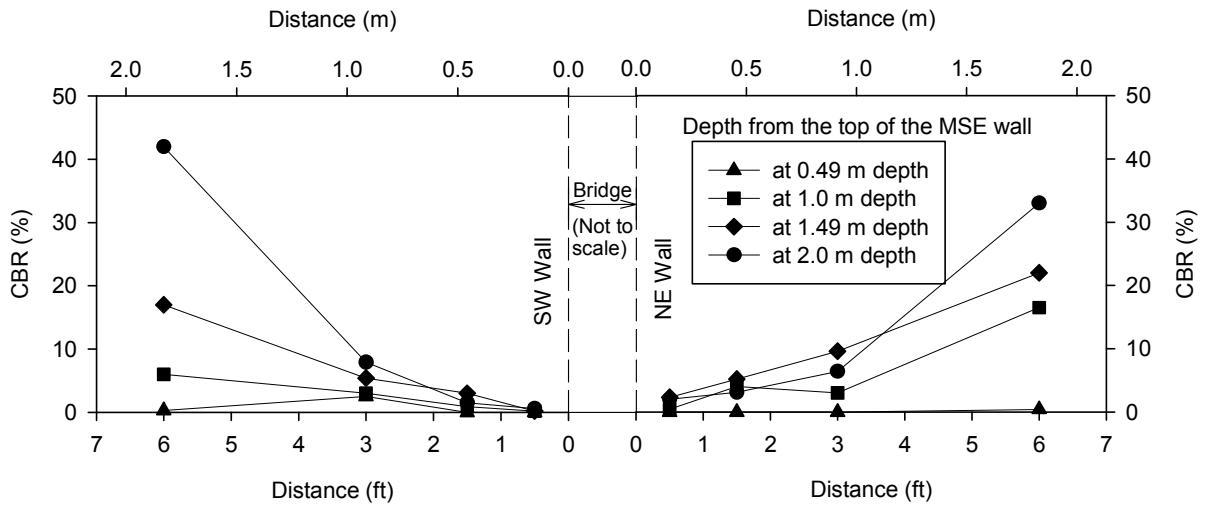
Figure 59. CBR at different depths from the top of the MSE wall at locations away from the walls – Bridge #1
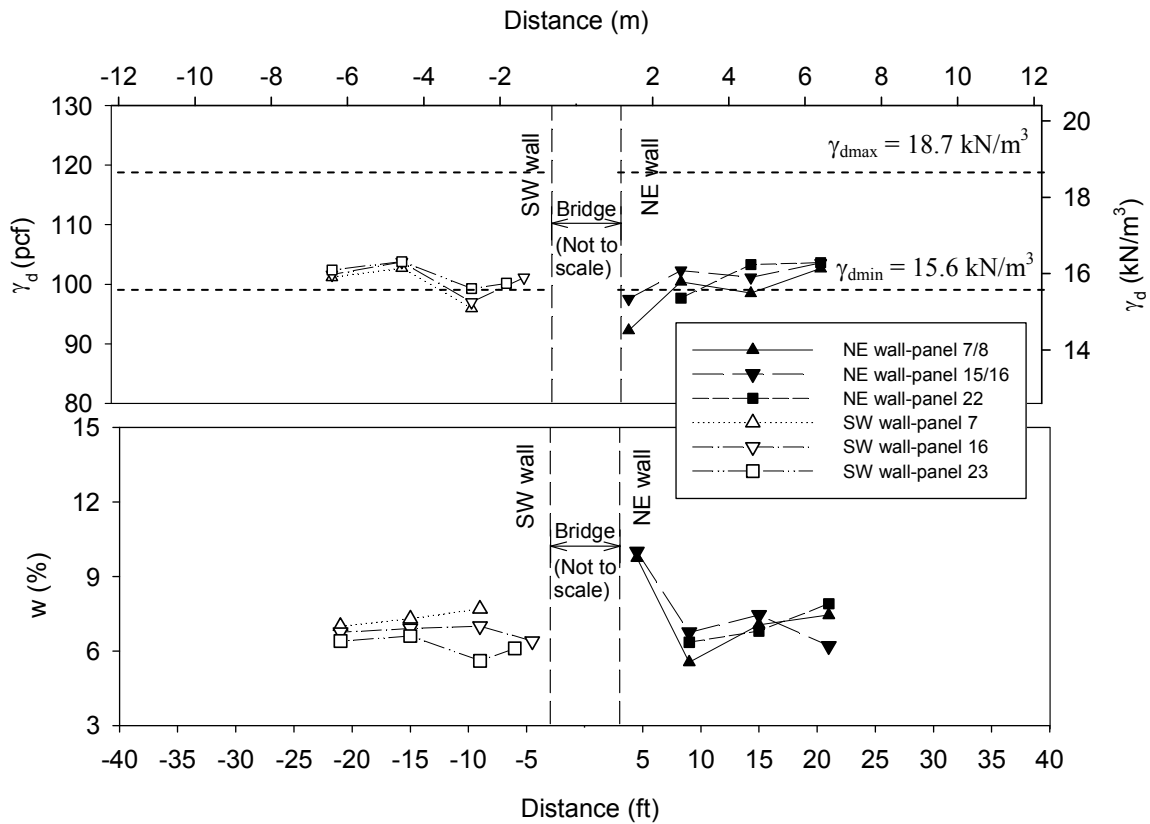
Figure 60. Moisture and dry density measurements at locations away from the MSE walls – Bridge #1

Bridge # 2 is located in Wilmington, Ohio. The bridge structures are two semi-integral stub abutments, MSE wall with cap, column piers, and a 9.1 m long approach slab. The abutments will support a 27.7 m long span constructed of continuous precast prestressed concrete I-beam with a reinforced concrete deck. Because of the construction stage, only the south abutment was investigated. A CAT 5636 compactor was used to compact the area away from piles, and a vibrating plate sled compactor was used within 1.8 m around the piles. The backfill material used in this bridge was classified as SW-SM on the unified soil classification system (USCS). Figure 61 shows an overview of the site, the in situ testing locations, and compaction device used around piles for this bridge site.

DCP tests were performed at distances of 0.3 m, 0.9 m, and 3.7 m away from the MSE wall. Between 0.3 m to 0.9 m away from the MSE wall the CBR values did not change significantly; the test conducted at 3.7 m away from the MSE wall showed a higher CBR value. The CBR values for the tests conducted at 0.3 m and 0.9 m away from the MSE wall ranged from 0.7% to 23% from the surface to 2 m below the ground, and the DCP test conducted at 3.7 m away from the MSE wall shown the CBR value ranged from 1.7% to 50% which indicates a significant increase. DCP tests results are presented in Figure 62.

Figure 61. Bridge #2 at Wilmington: (a) overview of the south MSE wall; (b) DCP test locations; (c) vibratory plate compactor used to compaction of wall backfill
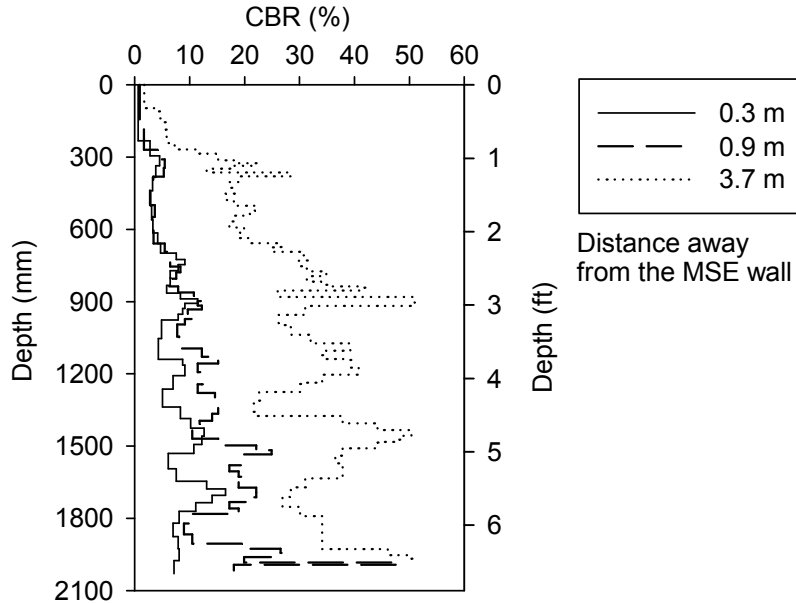
Figure 62. DCP-CBR profiles at locations away from the MSE wall – Bridge #2 (USCS: SW-SM)

Bridge # 3, which is located in Downtown Dayton, Ohio, is a curved girder bridge with a 9.1 m by 13.7 m approach slab. The bridge structures will consist of four span composite welded curved steel plate girders on a cap and column pier, single column piers, and stub abutments behind MSE walls. A 0.6 m thick layer of porous backfill (USCS: GP) was used behind the abutment underneath the approach slab. A 0.3 m thick layer of subbase (GW) was placed on top of the selected granular backfill (SW-SM).

In situ testing was conducted along the paving notch and the south wall (Figure 63). DCP tests were conducted at distances of 0.5 m, 0.9 m, and 1.8 m away from the paving notch and 0.2 m, 0.5 m, 0.9 m, and 1.8 m away from south wall. LWD tests were conducted at the same locations as the DCP tests and at three points behind the east end of the approach slab.

CBR values generally increased with distance away from the paving notch and the south wall (Figure 64). There is a soft layer at about 1 m below the surface along the tested lane perpendicular to the paving notch. The CBR values near the paving notch ranged from 1% to 15% at the distance from 0.5 m to 0.9 m away from the paving notch, and at 1.8 m away

from the paving notch the CBR values ranged from 9% to 48%. The tests conducted along the lane perpendicular to the south wall returned CBR values that range from 0.2% to 20% within 0.9 m of the wall, and the CBR values for the test at 1.8 m away the wall ranged from 5% to 35%.

Figure 65 shows the LWD modulus change at test locations away from the paving notch and the south wall. LWD tests were conducted at the same location as DCP tests in general, and three tests were conducted at the location behind the end of approach slab. For these test locations, the individual LWD modulus values ranged from 33 MPa to 72 MPa, and there was no significant difference between the test locations with subbase or those without subbase material. Figure 65 shows the modulus values with distance from the paving notch.
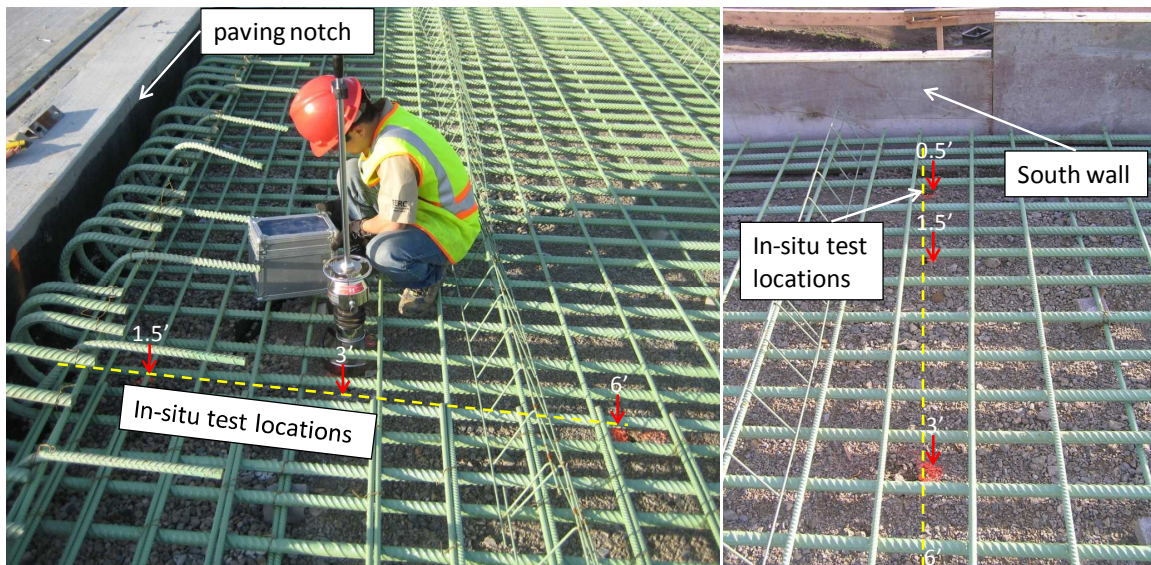
Figure 63. Bridge #3 (MOT-75-1393) at downtown Dayton
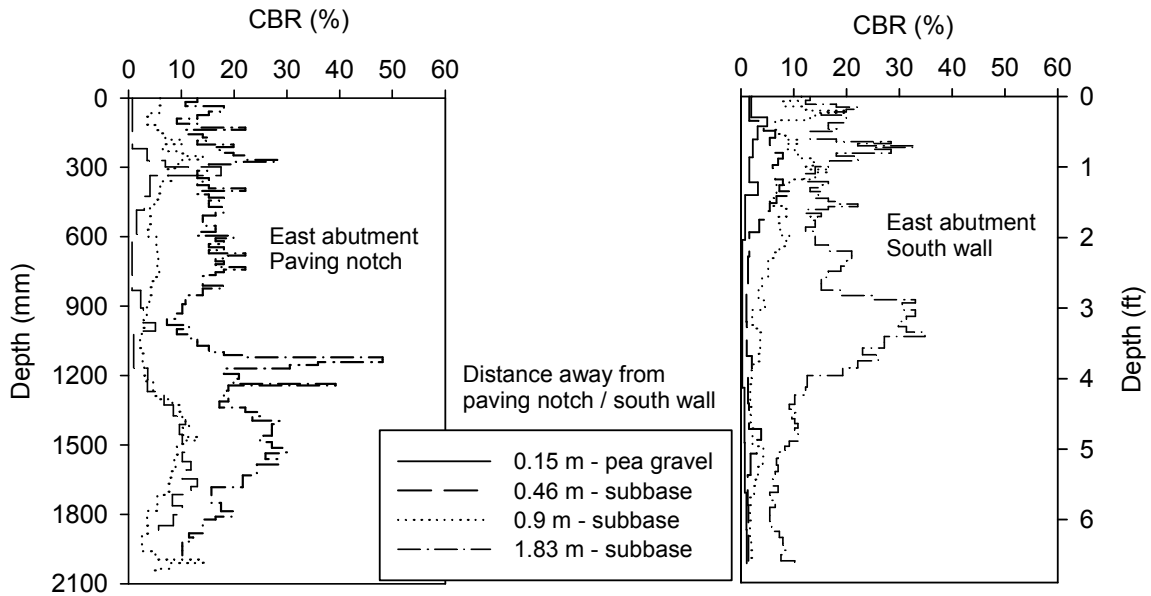
Figure 64. DCP-CBR profiles at locations away from south wall and paving notch at east abutment – Bridge #3
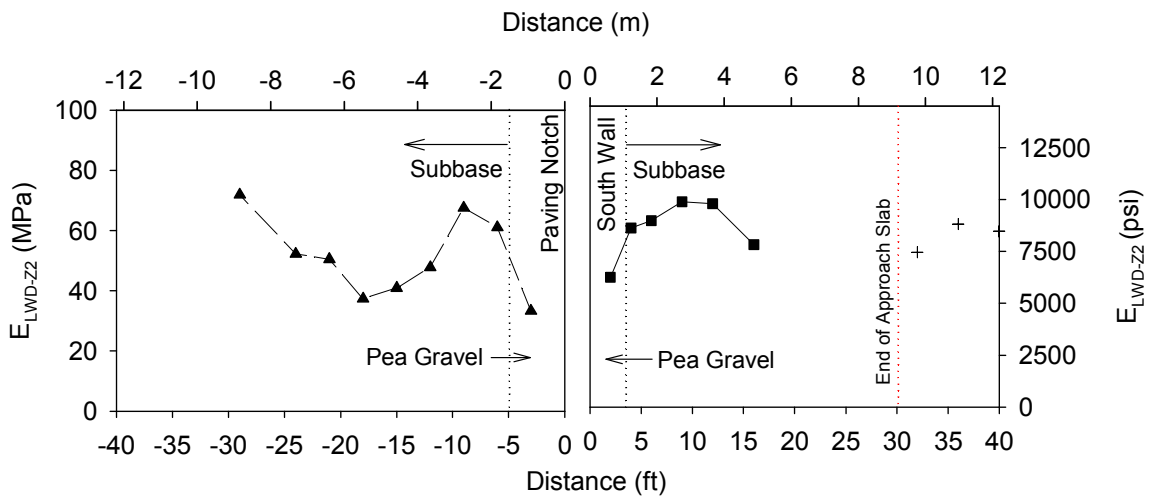
Figure 65. E$_{LWD-Z2}$ measurements at locations away from paving notch and south wall on the east abutment – Bridge #3

Bridge # 4 is located at the Columbus, Ohio airport, near Johnstown Road. The bridge structure is 18.8 m long, single span prestressed concrete I-beams with reinforced composite deck on semi-integral abutments, which is supported by piles behind MSE walls. The approach slabs were modified 9.1 m long section. Aggregate base (USCS: GP) was the

backfill material for the MSE wall.

DCP tests were conducted at four locations inside the approach slab, at 0.3 m, 0.9 m, 1.8 m, and 8.5 m away from the paving notch, and one test was conducted at 0.6 m behind the end of the approach slab (Figure 66), the CBR value generally increases with distance away from wall, and there is a stiff layer at the depth of 1.2 m to 1.5 m for the test location within 0.9 m away from the wall (Figure 67). The test conducted at 1.8 m away from the paving notch indicates that the backfill started getting stiff from 300 m below the surface, and no significant changes of strength for the location near the end of the approach slab.

Because of the construction stage at bridge #4, LWD tests were not conducted inside of the approach slab region. Five points LWD tests were conducted behind the end of the approach slab, and the tests results indicate modulus values from 50 MPa to 65 MPa (Figure 68).
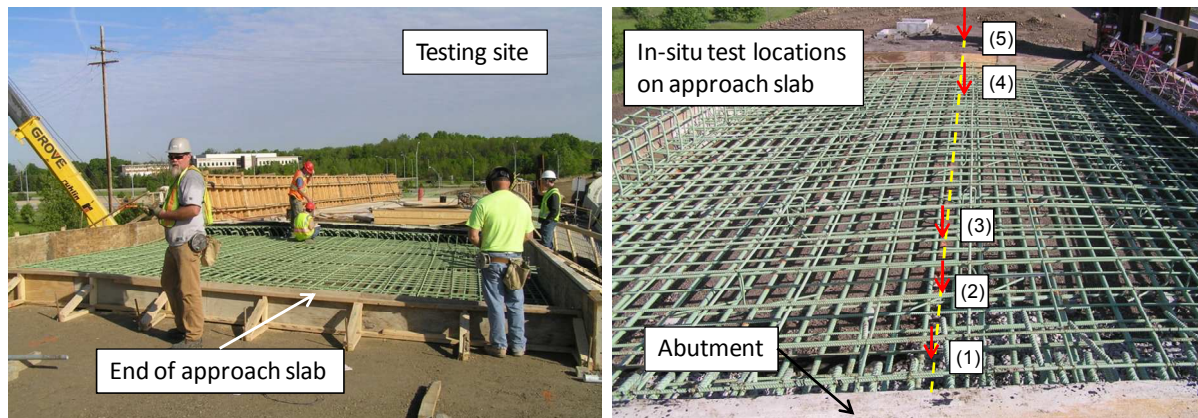
Figure 66. Bridge #4 (FRA-670-0904B) near Columbus airport

Figure 67. DCP-CBR profiles at locations away from the abutment – Bridge #4
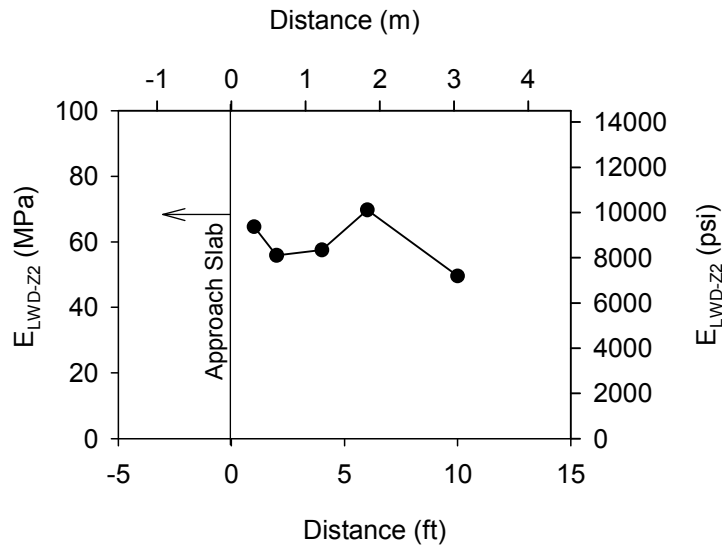
Figure 68. E_{LWD-Z2} at locations away from the approach slab – Bridge #4

Bridge # 5 is located at Licking 161 over Moot Creek. The bridge structure consisted of three-span composite prestressed concrete I-beams with cap, column piers and semi-integral abutments with 7.6 m long approach slabs. The backfill material used in the east abutment and west abutment were silty sand with gravel and silty gravel with sand, respectively. A

layer of pea gravel was placed next to the abutment with the thickness of 1.5 m to 1.8 m. The west abutment rests on hard rock shale and the east abutment rests on alluvium soils. Figure 69 provides the test location, site overview and location of bridge #5.

Standard Proctor tests were conducted on the material sampled from both the east and west abutments. The maximum dry unit weights for the materials sampled from east abutment and west abutment are 19.7 kN/m^3 and 19.5 kN/m^3, respectively. The optimum moisture content for the material sampled from east abutment is 11.2% and 10.6% for the material sampled from west abutment. By comparing the in situ moisture-dry unit weight measurements and the standard Proctor test results, the moisture content of the backfill material in the field was close to the optimum moisture content. However, the dry unit weight was lower than the maximum dry unit weight from the standard Proctor test. Figure 70 provides the standard Proctor test results and the in situ moisture-dry unit weight measurement for the backfill material.

DCP tests were conducted at distances of 0.3 m, 0.6 m away from the abutment for the east bound lane and then 1.5 m interval to 10.7 m away for the west bound center lane on the west abutment. For the east abutment, DCP test were conducted at 0.3 m away and then at interval of 1.5 m to 9.1 m from the abutment. Figure 71 shows the DCP-CBR profiles for the tested locations. LWD tests were performed at the same locations as DCP tests except for the tested points at 1.5 m away west abutment and at 0.3 m from the east abutment. Moisture and dry density measurements were obtained using nuclear gauge at the same locations as LWD test. Figure 72 and Figure 73 provide the LWD tests and nuclear gauge tests results respectively.

For the tests performed at the distance of 0.3 m and 0.6 m away the abutment provide similar CBR profiles along the west abutment east bound lane. The CBR profiles for both west abutment and east abutment indicate that the lowest strength occurred at 0.3 m away the abutment and then increases with distance away the abutment. LWD tests results show that the modulus generally increases with distance away from wall, and dry unit weight measurements also show a similar trend.

The moisture content measurements near the west abutment indicate that the lowest moisture content was next to the abutment and at further distances away from the abutment the moisture content ranged from 9 % to 12 %. The results from the east abutment indicated that the moisture content decrease with distance away from the abutment from 1.5 m to 6.1 m and within the range of 9 % to 12%.

Figure 69. Bridge #5 (LIC-37-1225L) at Licking 161 over Moot Creek
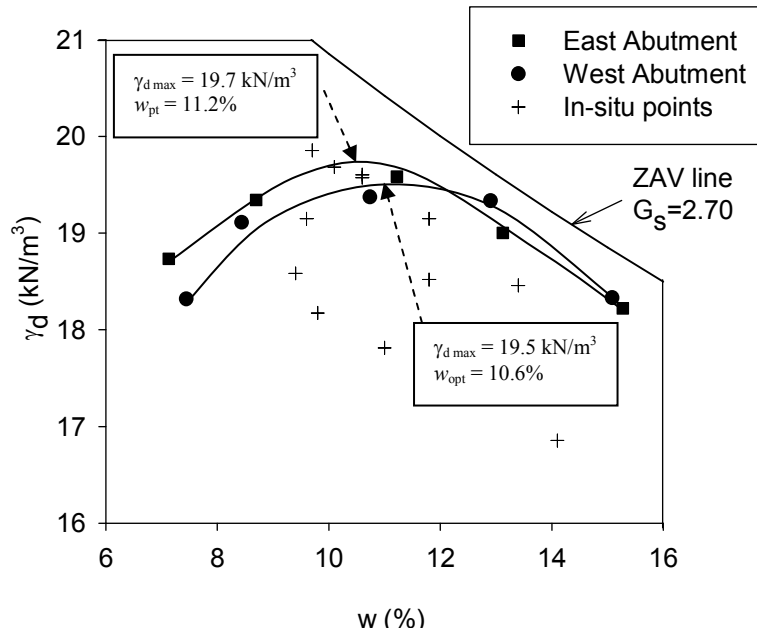
Figure 70. Proctor curve and field moisture and dry density measurement – Bridge #5
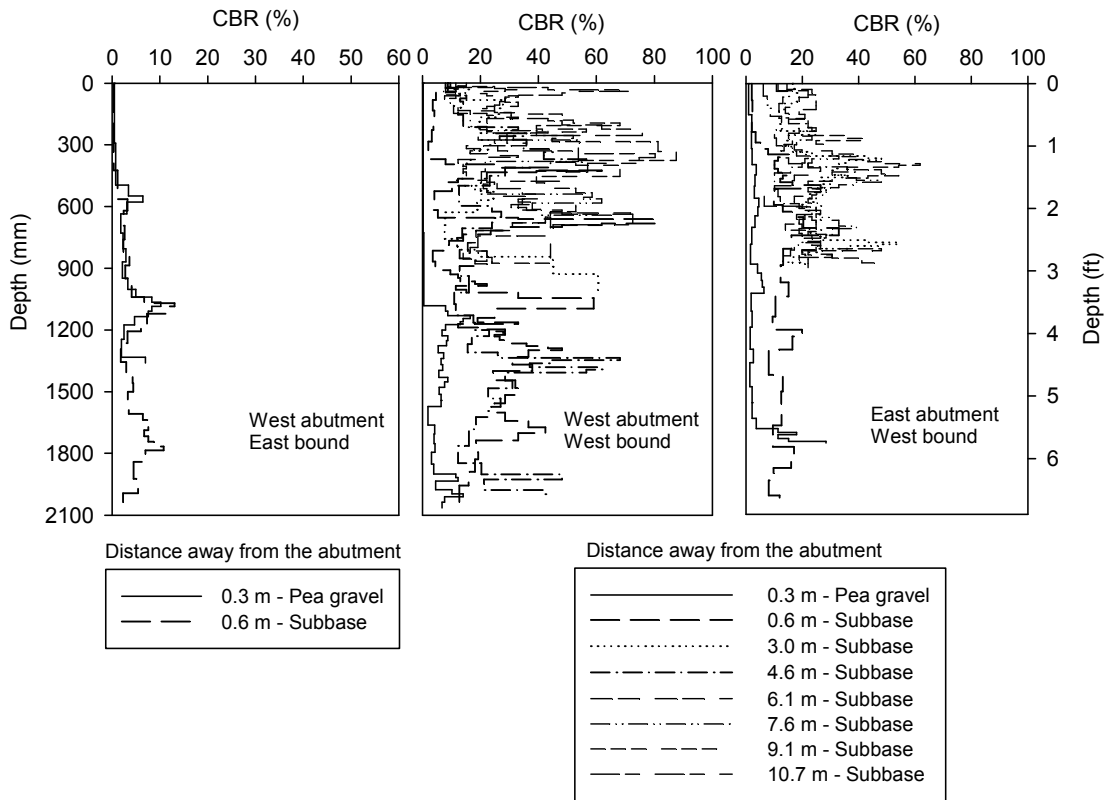
Figure 71. DCP-CBR profiles at locations away from the east and west abutments – Bridge #5
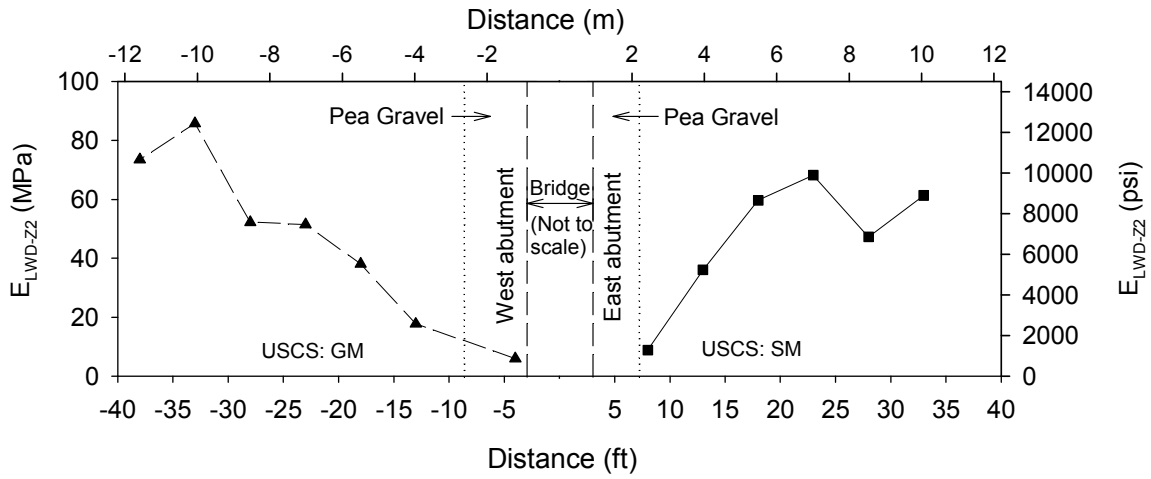
Figure 72. E_{LWD-Z2} measurements at locations away from the east and west abutments – Bridge #5
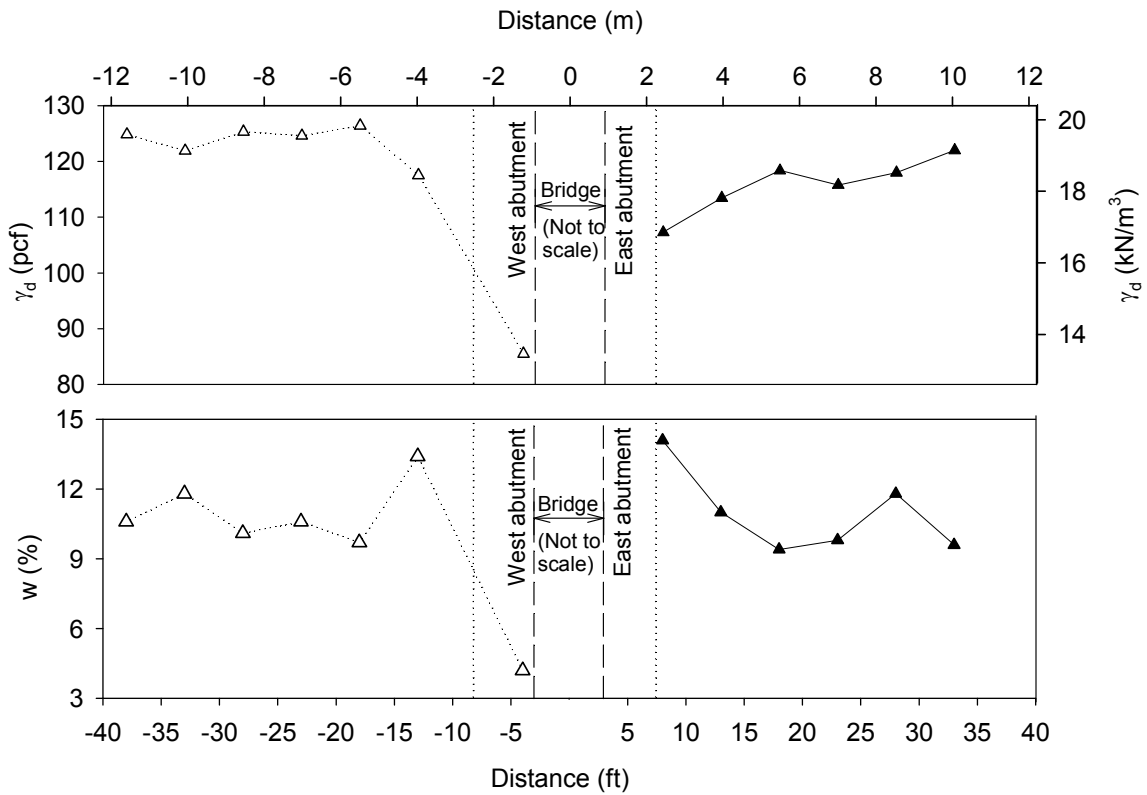
Figure 73. Moisture and dry density measurements at locations away from the east and west abutments – Bridge #5

Bridge # 6 located at the interchange of I-71 & I-76 on the section of I-71 over Greenwich Road at Medina County, Ohio. The structures for this project site was a single span steel girder bridge with reinforced concrete deck and semi-integral wall type abutments with a 9.1 m long modified approach slab. There was an existing wall about 9.1 m away from the new wall. A gap between the existing slab and the exposed fill material can be seen from the existing wall. Figure 74 shows the project site conditions and in situ tests locations for this bridge study and the conducted in situ tests include DCP, LWD and PLT along two testing lanes. The material from the site is classified as poorly graded gravel to silty gravel with sand per USCS.

DCP tests were conducted on two testing lanes which were west lane and east lane at 0.3 m away from the abutment and then at 1.5 m interval to 9.1 m from the abutment. Figure 75 provides the DCP tests results in terms of CBR values for both west and east lanes. The CBR profiles from the west lane shows that at the same depth CBR values increase with distance away from wall, but with the distance of 7.6 m to 9.1 m away from the wall the CBR values start to decrease. That may caused by the existing wall near the end of the west lane. The DCP tests conducted on the east lane also gives the similar conclusion.

LWD tests were performed on both east and west testing lanes along south abutment. Nine testing points were constructed on east testing lane and thirteen points were tested along west lane on south abutment. Figure 76 shows the E_{LWD-Z2} varies with distance away from the south abutment for both testing lanes. The LWD tests results indicated that the modulus values at the middle part of the two testing lanes are higher than the E_{LWD} measured at the ends, and the modulus values from the two testing lanes show similar trend and the typical E_{LWD-Z2} range was 5 MPa to 30 MPa.

PLTs were conducted at three locations that parallel the new abutment within a distance of 4.9 m away from the abutment. At the third testing point, water was introduced at the surface of the soil while maintaining a static stress of 0.4 MPa to evaluate the collapse potential of the backfill material. Figure 77 provides the PLTs results and the test setup. The PLT

indicates minimal in situ collapse potential, because only 8 mm additional settlement was shown up when the material was saturated and that was less than the settlement during the loading stage.
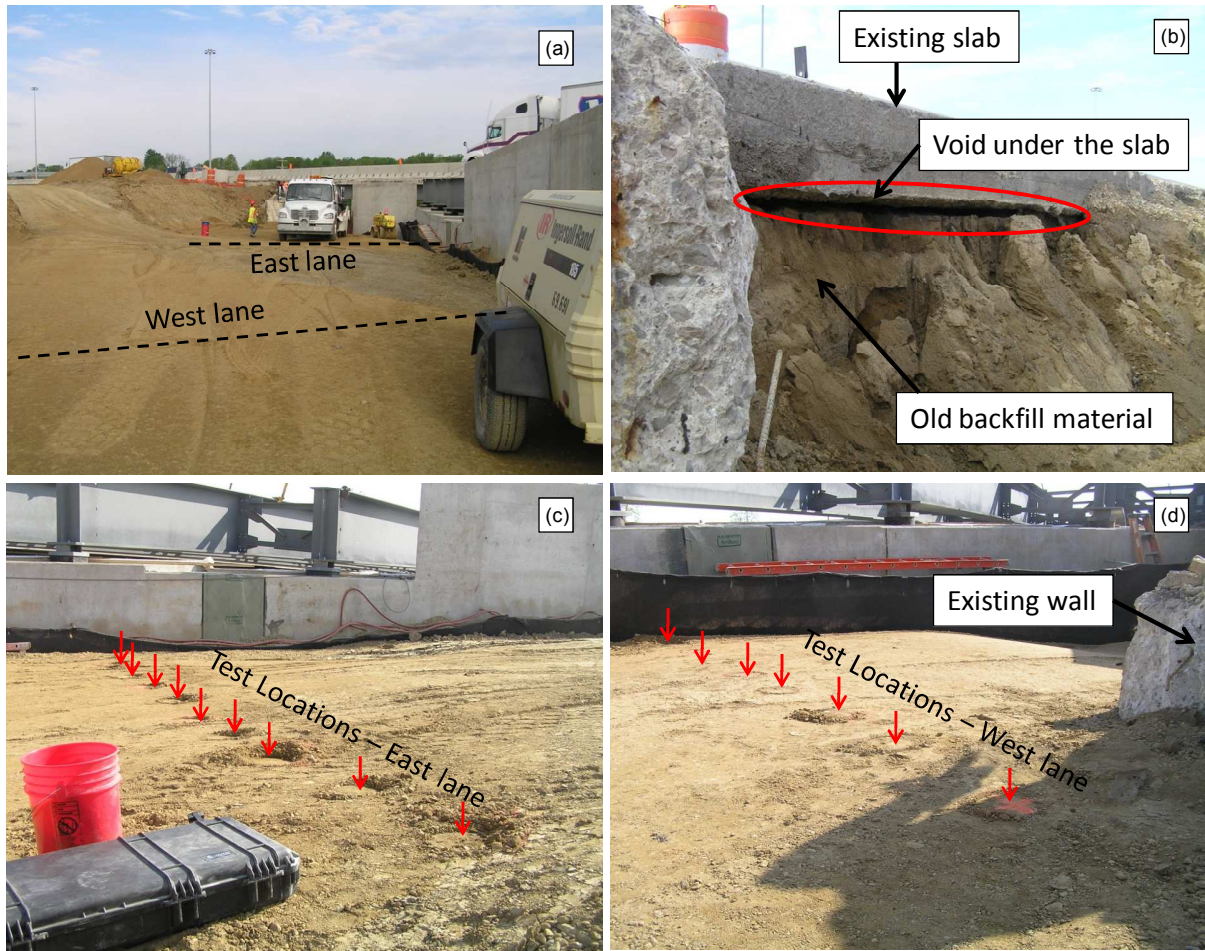
Figure 74. Bridge #6 (MED-71-0729) at I-71 and I-76 interchange: (a) location of test site; (b) void under the existing slab and old backfill material (c) in situ test locations – east lane (d) in situ test locations – west lane
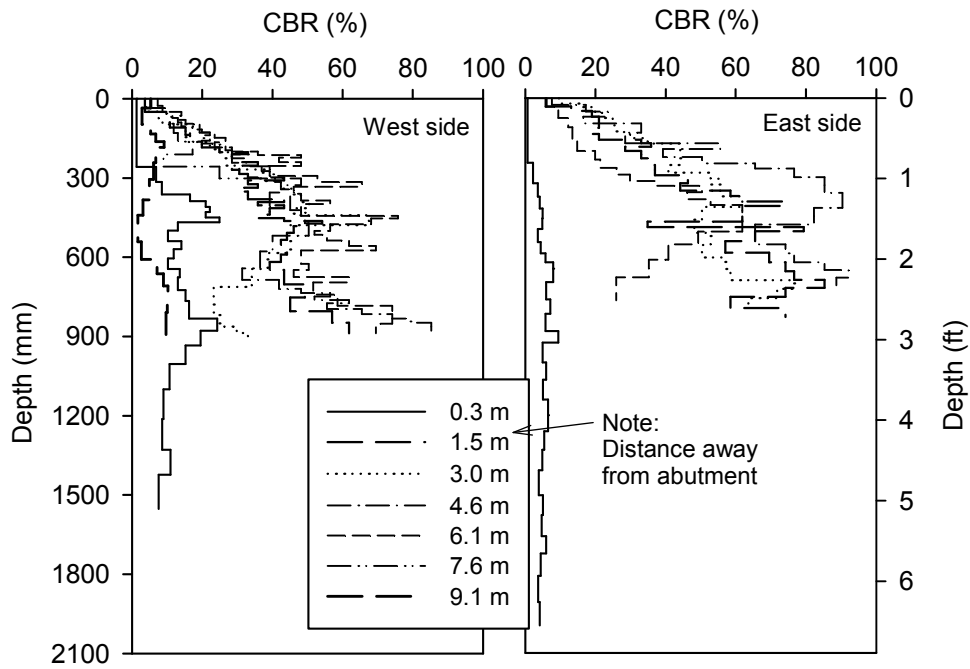
Figure 75. DCP-CBR profiles at locations away from the south abutment for west and east lanes – Bridge #6 (USCS: GP-GM)
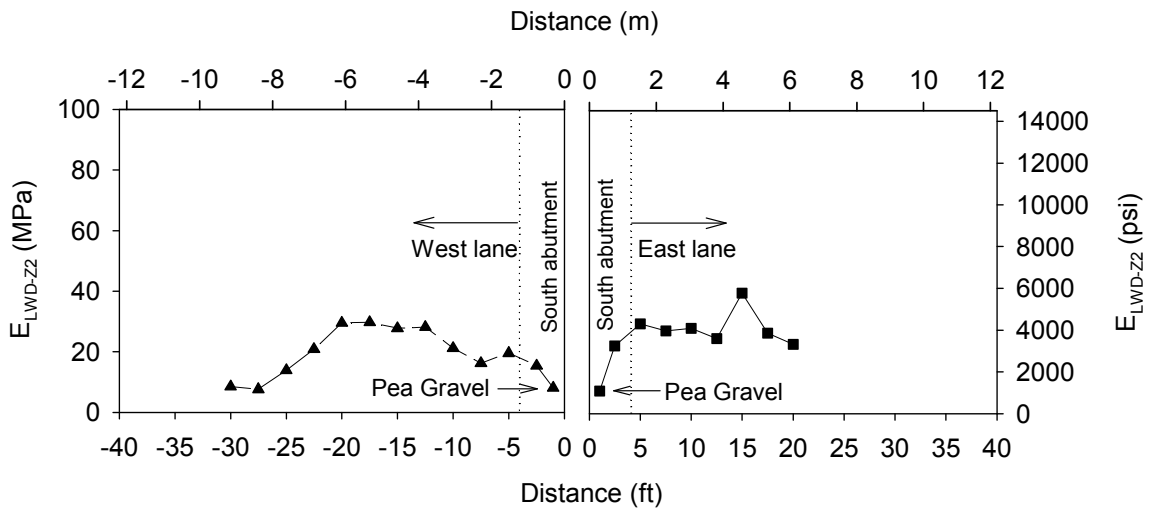
Figure 76. E_{LWD-Z2} at locations away from the south abutment on east and west lanes – Bridge #6
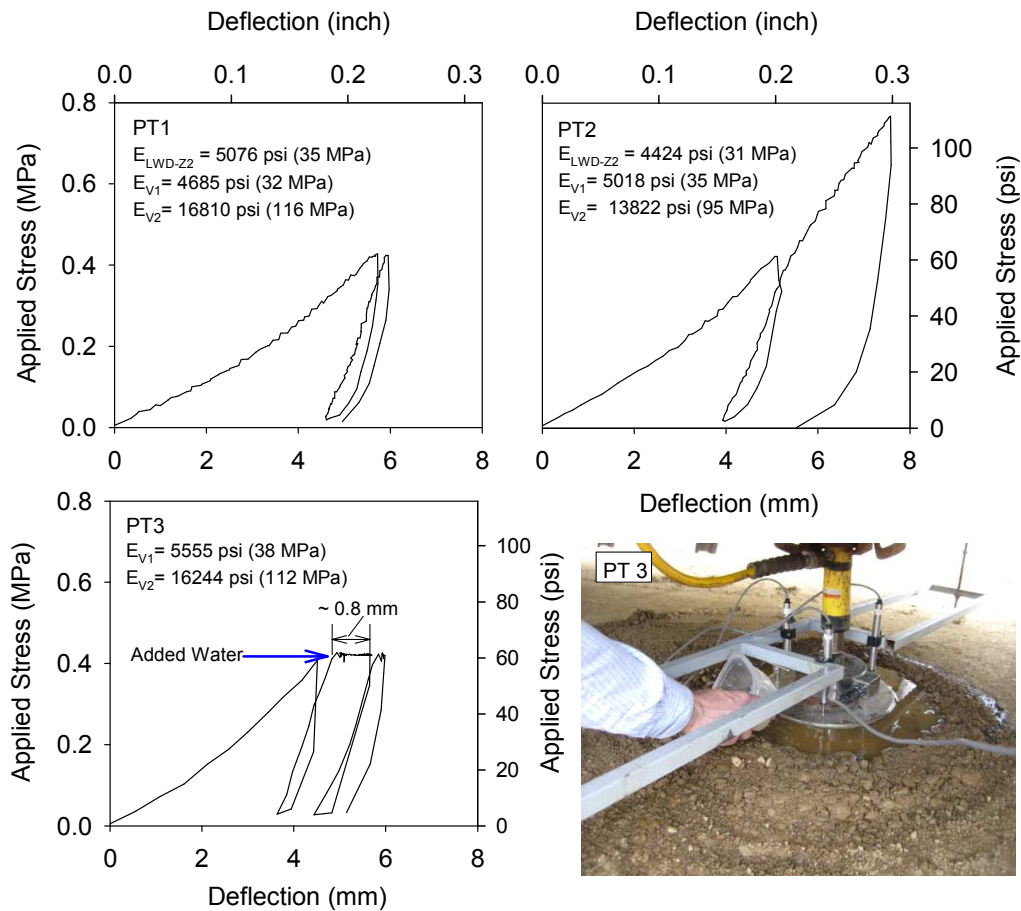
Figure 77. Stress-strain curves for static plate load tests – Bridge #6

Bridge # 7 is located at the interchange of I-71 & I-76 over I-71 at Medina County, Ohio. The structure is a continuous steel girder bridge with a reinforced concrete deck on semi-integral abutments and cap and column piers. 9.1 m modified approach slabs were specified for this bridge. Figure 78 shows the in situ testing locations.

DCP tests were performed at 0.2 m, 0.3 m and then at 1.5 m intervals to 6 m away from the abutment and the tests results are provided in Figure 79 in terms of CBR. LWD tests were conducted near the DCP test locations; LWD test results are shown in Figure 80.

Based on the DCP-CBR profile, the measurements at 0.3 m away from the wall indicated the lowest strength profile. The LWD tests results indicate that modulus values for the backfill

ranged from 5 MPa to 35 MPa.
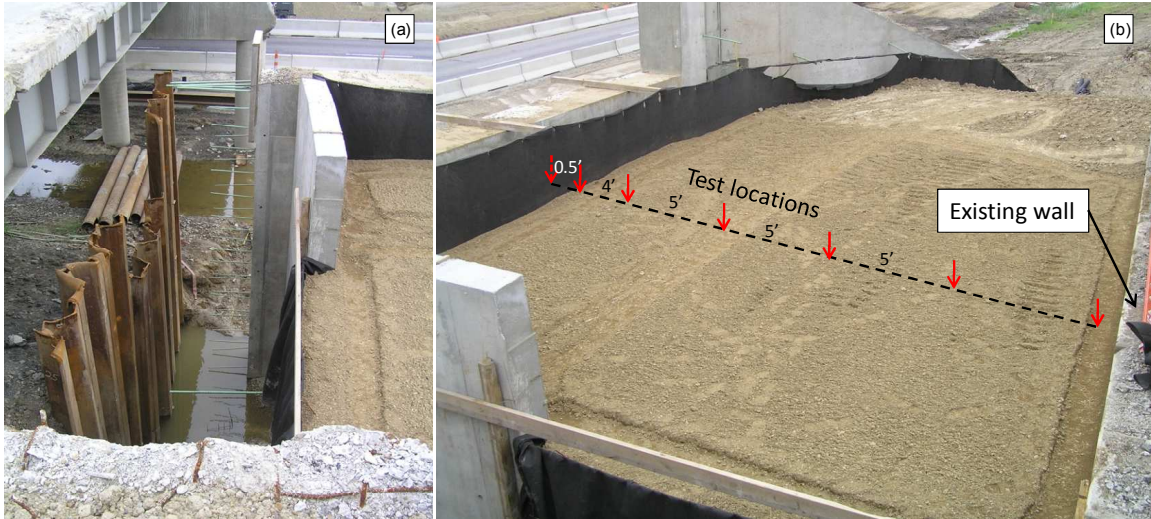
Figure 78. Bridge #7 (MED-71-0750) at I-71 and I-76 interchange: (a) site location; (b) in situ test locations

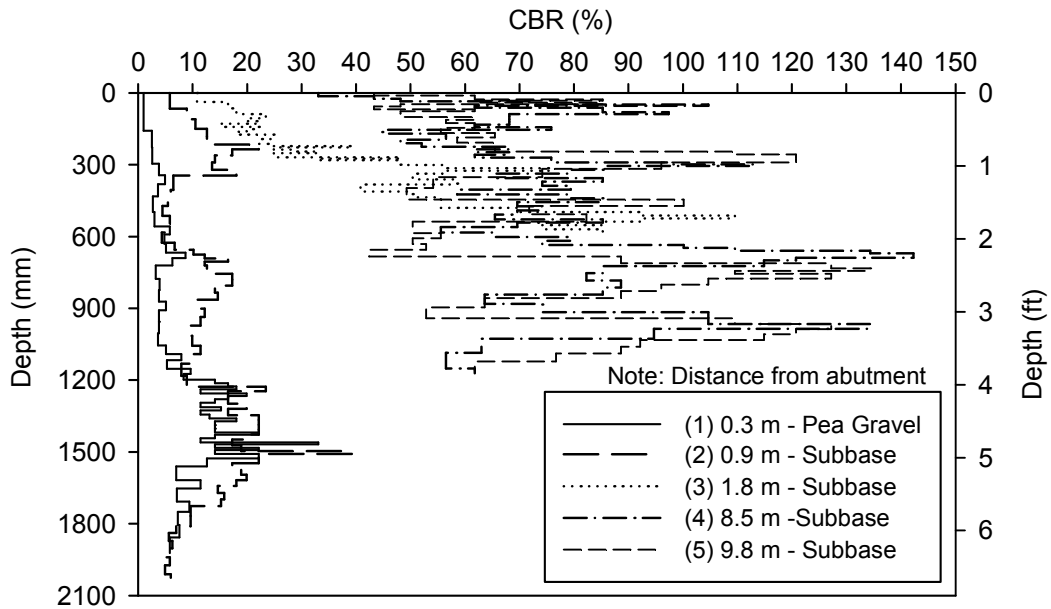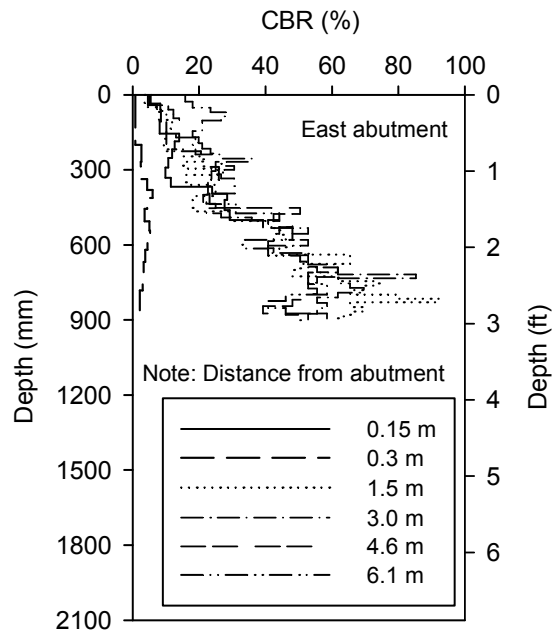**Figure 79. DCP-CBR profiles at locations away from east abutment – Bridge #7**
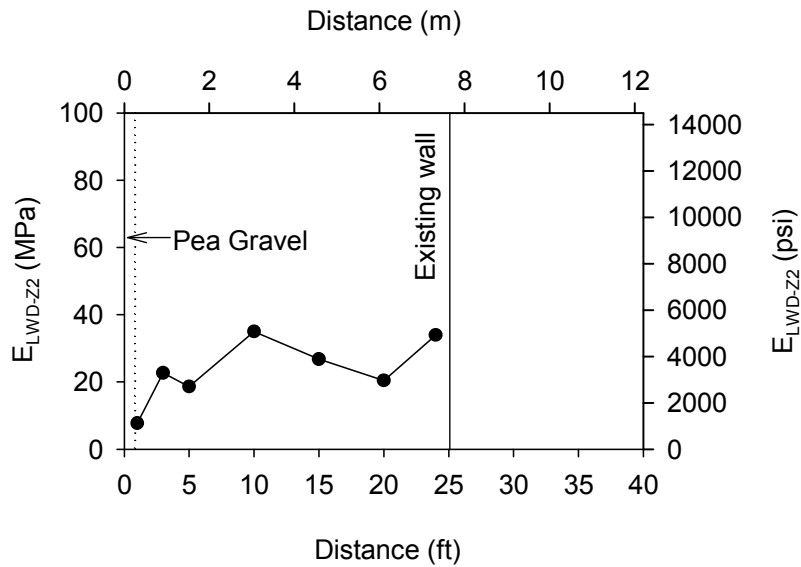
Figure 80. E$_{LWD-Z2}$ at locations away from east abutment – Bridge #7

The laboratory and in situ studies conducted for this project yielded these key findings:

- Laboratory tests demonstrated that sandy granular backfill is susceptible to collapse upon wetting and saturation if the material is compacted with moisture content near the bulking moisture content (about 3 to 6%). Collapse potential can be as high as 14%.

- In general, at each of the seven bridges in this study, the LWD tests results and DCP-CBR profiles showed that the backfill materials with about 1.5 m of the abutment or MSE wall were poorly compacted. Poorly compacted backfill materials in this region will provide less support to the approach slab.

FHWA Intelligent Compaction (IC)

This field study was conducted in Springville, New York. The goals of this study were to develop correlations between LWD and other in situ point measurements devices such as BCD and FWD, and to investigate the relationships between the measured surface E$_{LWD}$ values with different LWD device configurations. Ten test beds were constructed on this project site. Table 13 summarizes the test beds information and the performed in situ tests for

each test bed.

Table 13. Summary of test beds and performed in situ testing

TB	Material	Test bed Structure	Test bed Size	In situ Test
1	Embankment	A section of rubber tire fill at < 1 m below the grade	18 m × 200 m	DCP, LWD
2	Embankment	A section of rubber tire fill at < 1 m below the grade	18 m × 71 m	DCP, LWD
3	Embankment	Compacted embankment granular subgrade material	10 m × 105 m	LWD
4	Gravel Subbase	2 m to 2.5 m thick loosely placed aggregate subbase material over geofabric placed on top of TBs 1 and 2	—*	BCD, LWD
5			—*	BCD, DCP, LWD
6	Gravel Subbase	Aggregate subbase material placed over geofabric on top of TB1 embankment material	—*	DCP, LWD, BCD
7			—*	
8	Embankment	Compacted embankment granular subgrade material	10 m × 100 m	FWD, PLT
9	Gravel Subbase	Aggregate subbase material placed over geofabric on top of a compacted embankment layer	—*	BCD, LWD, DCP
10	Embankment	Compacted embankment granular subgrade material	—*	BCD, DCP, LWD, PLT

Note: * not measured

To avoid the relative influence and sensitivity of soil disturbance on test results, the tests were performed in the following order: FWD, LWD, BCD, and DCP. The LWD drop height of the LWD apparatus was adjusted to obtain the same applied contact stress for each of the 200 mm, 150 mm and 100 mm diameter plates. The measured E_{LWD} values on test bed 2 are provided in Table 14.

The key findings from this field case study are provided in the correlation evaluation sections.

Table 14. Field LWD measurements from FHWA New York site

Applied stress	Device configuration	Point #	1	2	3	4	5	6
σ_o= 190 N/m^2	D=200 mm h=50 cm	E_{LWD}, MPa	92.42	146.60	69.32	37.51	177.14	67.84
	D=150 mm h=16 cm	E_{LWD}, MPa	37.07	116.60	47.50	19.61	54.81	32.39
	D=100 mm h=3.1 cm	E_{LWD}, MPa	43.21	176.43	66.86	26.91	94.80	23.01
σ_o= 230 N/m^2	D=200 mm h=72 cm	E_{LWD}, MPa	126.49	263.88	103.41	38.45	168.18	66.25
	D=150 mm h=22.8 cm	E_{LWD}, MPa	75.05	197.99	85.70	32.90	73.14	52.92
	D=100 mm h=4.5 cm	E_{LWD}, MPa	57.11	231.89	85.98	28.66	115.95	30.13
σ_o= 340 N/m^2	D=150 mm h=50 cm	E_{LWD}, MPa	91.43	327.03	85.89	35.58	85.03	61.61
	D=100 mm h=9.9 cm	E_{LWD}, MPa	65.17	246.50	90.71	34.78	87.90	49.95
σ_o= 400 N/m^2	D=150 mm h=72 cm	E_{LWD}, MPa	61.46	329.13	97.17	42.25	87.21	56.84
	D=100 mm h=14.2 cm	E_{LWD}, MPa	70.07	256.48	82.89	33.07	97.10	42.09

Pavement Foundation Study

The pavement foundation study was conducted on two sections along I-94 in St. Clair and Macomb Counties, Michigan. The two goals of this study were to obtain typical elastic modulus values for different field conditions by performing LWD tests, and to obtain the correlations between LWD measurements and FWD measurements. Three test beds were identified for this study. Test bed 1 consisted of 40.6 cm of compacted and trimmed open-graded aggregate subbase material over a recompacted mixture of sand and silty clays soils. A 6.1 m by 6.1 m grid was built on this test bed to perform LWD, DCP, and NG tests and the test points were set on 0.61 m centers Figure 81.

Test bed 2 was a 23 cm thick existing concrete pavement which was built 40 years ago as shown in Figure 82. FWD tests were performed before the panels were removed, then the

LWD and DCP tests were conducted on the existing subgrade after the pavement panels were removed to determine the elastic modulus and CBR of the subgrage soils.

Test bed 3 (Figure 83) had similar material type as test bed 1 which was compacted open-graded aggregate subbase material prior to trimming. On test bed 3, the LWD and DCP tests were conducted at test points every 15.2 m along a centerline and along parallel lines that were 3.1 m to the left and right of the centerline. In situ testing involved determination of (a) in situ moisture and density using nuclear density gauge, (b) dynamic cone penetration index (DCPI), (c) light weight deflectometer modulus (E_{LWD}), (d) following weight deflectometer modulus (E_{FWD}), and (e) plate load tests (PLT). The in situ test results obtained from this field case study are used to perform the correlation evaluation between these different field measurement devices in the following section.

Figure 81. Overview for test bed 1

Figure 82. Overview for test bed 2
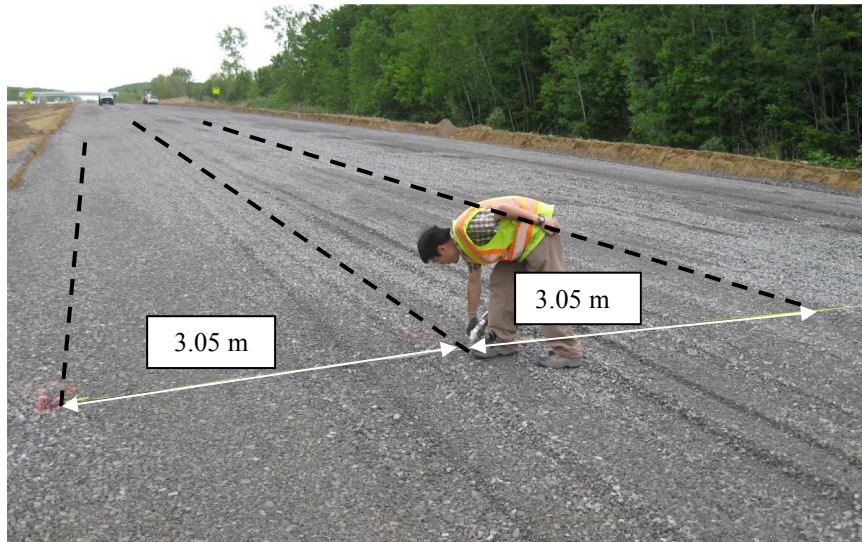
Figure 83. Overview for test bed 3

Influence of Device Configuration

LWD device configurations study was performed on the data obtained from FHWA IC project site in Springville, New York. Table 15 summarizes the correlation relationships for LWD measurements with different sizes of loading plate at certain drop height. Six points were repeatedly tested during this project site with the applied stress vary from 190 N/m^2 to

400 N/m^2. For these different sizes of load plate, the drop height was adjusted to obtain the same applied contact stress. The linear relationships between the measured surfaces LWD modulus with different device configurations are shown in Figure 84. The simplified relationships between E_{LWD} with different loading plate sizes, which developed based on Terzaghi and Peck (1967) and field study results are shown in Figure 85 for 200 mm diameter loading plate and Figure 86 for 150 mm diameter loading plate.

These tests revealed variance between the correlation relationships found in the field and theoretical relationships expressed in the literature. In general, the ratios between E_{LWD} with different sizes of loading plates from field measurements are higher than the theoretical ratios expressed by Terzaghi and Peck (1967). Further, these tests indicate that better correlation coefficients were obtained with higher applied contact stresses.

Table 15. Summary of measured E_{LWD} with different sizes of loading plates

Applied stresses	Device configuration	Field study relationship	R^2	Terzaghi and Peck equation
σ_o= 190 N/m^2	D=200 mm h=50 cm / D=100 mm h=16 cm	$\dfrac{E_{LWD-Z2}}{E_{LWD-Z1}} = 1.1$	0.19	$\dfrac{E_{LWD-Z2}}{E_{LWD-Z1}} = 0.56$
	D=200 mm h=50 cm / D=150 mm h=3.1 cm	$\dfrac{E_{LWD-Z2}}{E_{LWD-Z1.5}} = 1.7$	0.23	$\dfrac{E_{LWD-Z2}}{E_{LWD-Z1.5}} = 0.77$
	D=150 mm h=16 cm / D=100 mm h=3.1 cm	$\dfrac{E_{LWD-Z1.5}}{E_{LWD-Z1}} = 0.7$	0.92	$\dfrac{E_{LWD-Z1.5}}{E_{LWD-Z1}} = 0.69$
σ_o= 230 N/m^2	D=200 mm h=72 cm / D=150 mm h=22.8 cm	$\dfrac{E_{LWD-Z2}}{E_{LWD-Z1.5}} = 1.4$	0.84	$\dfrac{E_{LWD-Z2}}{E_{LWD-Z1.5}} = 0.77$
	D=200 mm h=72 cm / D=100 mm h=4.5 cm	$\dfrac{E_{LWD-Z2}}{E_{LWD-Z1}} = 1.3$	0.84	$\dfrac{E_{LWD-Z2}}{E_{LWD-Z1}} = 0.56$
	D=150 mm h=22.8 cm / D=100 mm h=4.5 cm	$\dfrac{E_{LWD-Z1.5}}{E_{LWD-Z1}} = 0.9$	0.86	$\dfrac{E_{LWD-Z1.5}}{E_{LWD-Z1}} = 0.69$
σ_o= 340 N/m^2	D=150 mm h=50 cm / D=100 mm h=9.9 cm	$\dfrac{E_{LWD-Z1.5}}{E_{LWD-Z1}} = 1.3$	0.97	$\dfrac{E_{LWD-Z1.5}}{E_{LWD-Z1}} = 0.69$
σ_o= 400 N/m^2	D=150 mm h=72 cm / D=100 mm h=14.2 cm	$\dfrac{E_{LWD-Z1.5}}{E_{LWD-Z1}} = 1.2$	0.97	$\dfrac{E_{LWD-Z1.5}}{E_{LWD-Z1}} = 0.69$
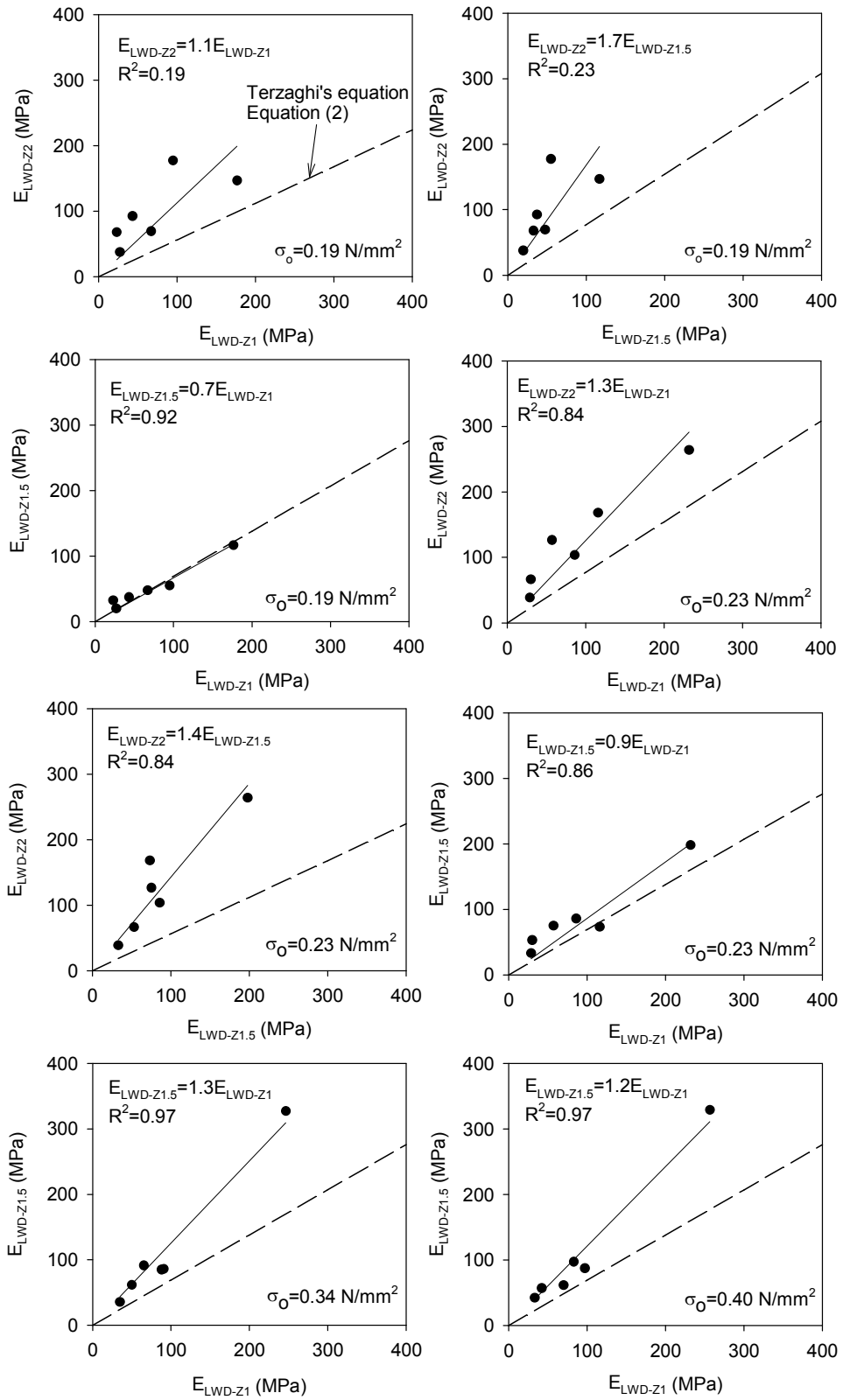
Figure 84. Correlations between E_{LWD} with different sizes of loading plate

Percentage of $E_{LWD}/E_{LWD-Z200}$
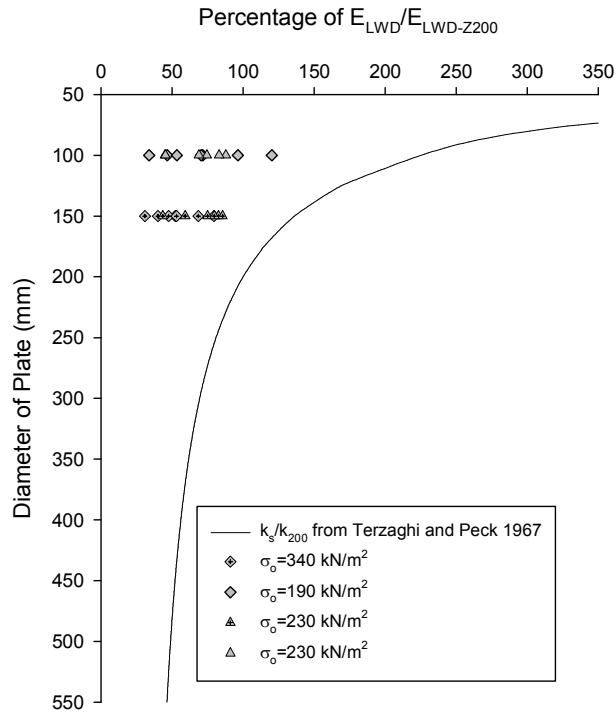
Figure 85. Relationship between E_{LWD} and E_{LWD-Z2} with different bearing plate

Percentage of $E_{LWD}/E_{LWD-Z150}$
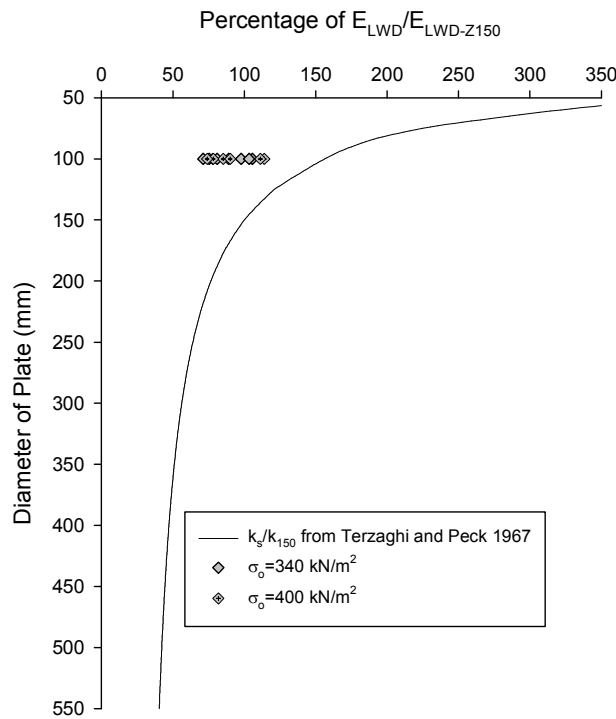
Figure 86. Relationship between E_{LWD} and $E_{LWD-Z1.5}$ with different bearing plate

Correlations between LWD and Other in situ Point Measurements

Due to the limitation of some large modulus measurement devices, such as the accessibility of FWD and PLT needs load truck or frame to jack against, it is beneficial to use the correlation relationships between LWD and these devices to estimate the modulus with different terms. Since LWD tests are easy and rapid to conduct, the in situ testing period can be significantly shortened.

The regression analysis between E_{LWD} and E_{FWD} was performed on the data collected from the FHWA IC project site in New York and the pavement foundation study at Michigan site. LWD tests were performed using 300 mm diameter loading plate with 72 cm drop height and KUAB FWD was employed to obtain FWD modulus with 300 mm diameter loading plate. Six drops which including three setting drops and three measurements were applied at each testing point for both LWD and FWD tests. The lowest applied stress and the deflection measurement at the surface were used in the correlation analysis for FWD tests. For the New York site, LWD tests and FWD tests data collected from test bed four and test bed five were used to conduct the correlation analysis and the material from these test beds consist of embankment granular material. For the Michigan project site, LWD and FWD measurements from test bed three were used to conduct the correlation analysis, and the material from this test bed consist of open-graded aggregate subbase. The results of regression analysis between E_{LWD} and E_{FWD} for the two project sites are shown in Figure 87. The correlation coefficients (R^2) indicate that poor correlations between LWD and FWD were obtained. In general, the FWD modulus from New York site is higher than the LWD modulus, and the FWD modulus from the Michigan site is lower than the LWD modulus.

The correlation study between LWD and BCD was conducted from the FHWA IC project site in New York. LWD consists of 300 mm diameter loading plate with 72 cm drop height and BCD consists of 150 mm diameter bending plate with recorded applied stress on the testing locations. The LWD and BCD data collected from three test beds, which consist of subbase material and one test bed consist of embankment material, was used to conduct the

regression analysis. The linear relationship between E_{BCD} and E_{LWD-Z3} is shown in Figure 88. Poor correlation between LWD and BCD was obtained with the correlation coefficient (R^2) equal to 0.11, and the LWD modulus is about three times higher than the BCD modulus.

Three project sites were involved in the correlation analysis between LWD tests and PLTs tests, which were geosynthetic reinforcement study in West Virginia, FHWA IC in New York, and pavement foundation study in Michigan. Zorn LWD with 200 mm diameter loading plate at 50 cm drop height was used for this project site and PLTs were performed after LWD tests for all the testing locations. The regression analysis result between E_{LWD-Z2} and E_{V1}, E_{V2} is presented in Figure 89. For the FHWA IC project site, PLT and LWD data collected from test bed 10 was used for the correlation analysis and the material from this test bed consists of embankment granular subgrade (USCS: GW). Three testing lanes were constructed on this test bed and each testing lane includes 22 testing points. The regression analysis between E_{LWD-Z3} and E_{V1}, E_{V2} are shown in Figure 90. For the Michigan project site, LWD data and PLT data collected from test bed 3 was used to conducting the regression analysis and the material in this test bed was compacted open-graded aggregate subbase. PLT test data was collected at various points along the test bed and 300 mm diameter loading plate Zorn LWD tests were performed before PLTs. The regression analysis result from this project site is shown in Figure 91. Table 16 summarizes all the regression analysis results for all the in situ measurement involved in this study.

Table 16. Summary of relationships between E_{LWD} and other in situ point measurements

	Project site	LWD	R^2	n
FWD	New York	$E_{FWD} = 0.3\ E_{LWD-Z3}+51.3$	0.07	38
	Michigan	$E_{FWD} = 0.4\ E_{LWD-Z3}+8.1$	0.30	50
BCD	New York	$E_{BCD} = 0.3\ E_{LWD-Z3}+29$	0.11	141
PLT	West Virginia	$E_{V1} = 1.8\ E_{LWD-Z2}-10.6$ $E_{V2} = 3.2\ E_{LWD-Z2}+1.2$	0.69 0.70	31
	New York	$E_{V1} = 1.5\ E_{LWD-Z3}+36.5$ $E_{V2} = 5.1\ E_{LWD-Z3}+78.1$	0.40 0.82	32
	Michigan	$E_{V1} = 1.2\ E_{LWD-Z3}+13.3$ $E_{V2} = 4.6\ E_{LWD-Z2}-8.3$	0.39 0.36	10
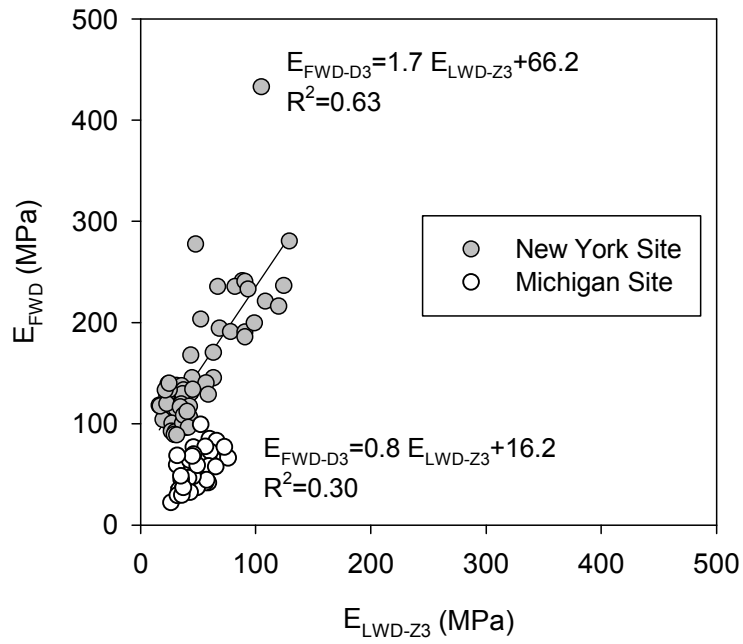
Figure 87. Correlations between E_{LWD} and E_{FWD} with 300 mm diameter loading plate
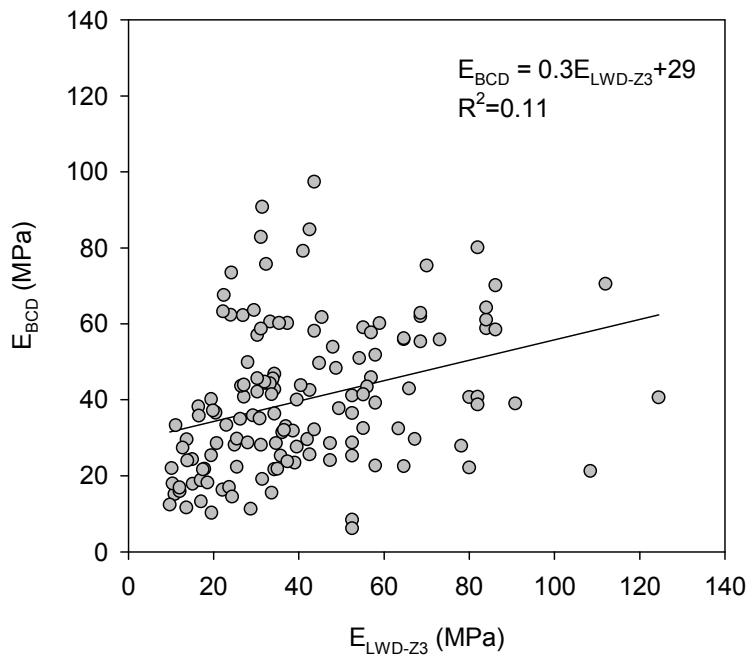
Figure 88. Correlation between LWD measurement and BCD measurements
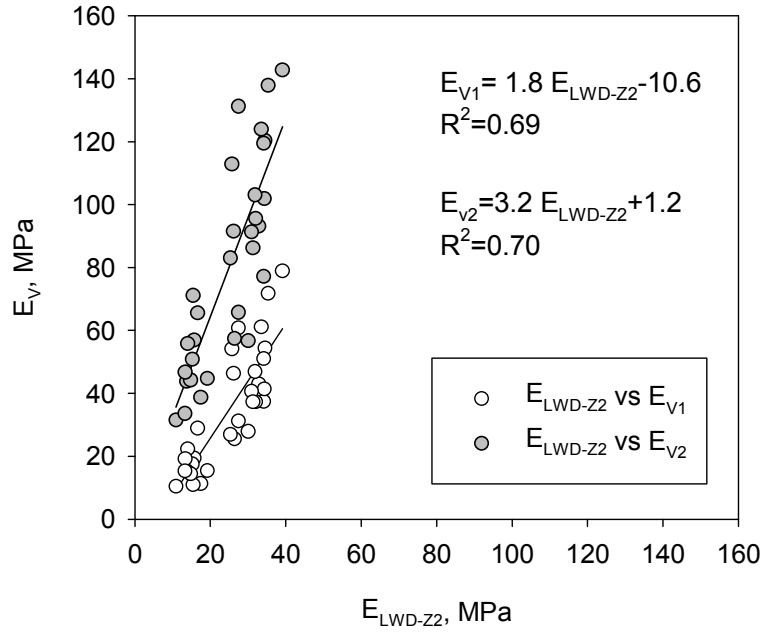
Figure 89. Correlation between LWD measurements and PLT measurements for West Virginia site
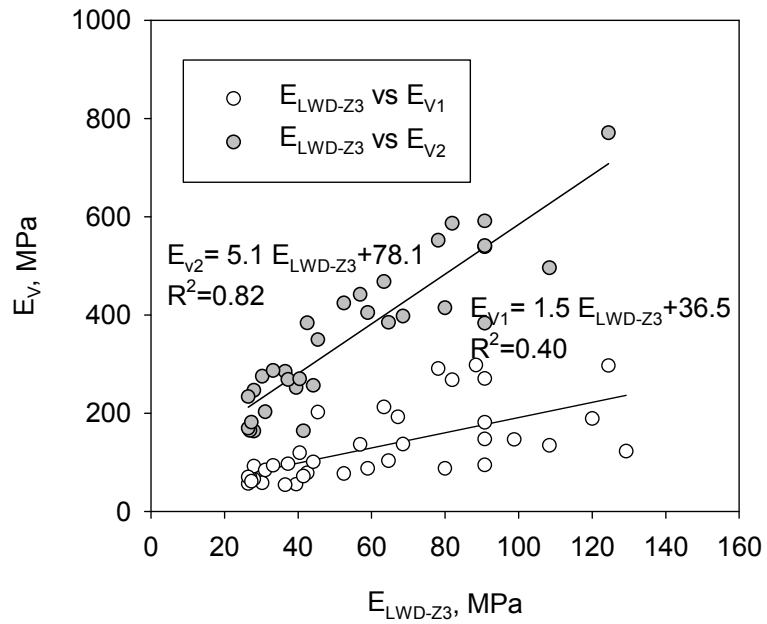
Figure 90. Correlation between E_{LWD-Z3} and PLT measurements for New York project site
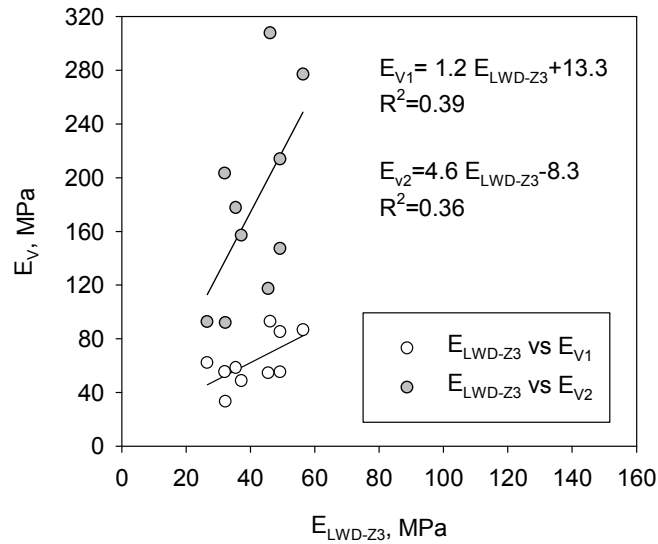
Figure 91. Correlation between E$_{LWD-Z3}$ and PLT measurements for Michigan site

Influence of Layered Soil Profiles on Surface Modulus

Three soil layering profiles will be covered in this section: soft soil over stiff soil; stiff soil over soft soil; and the intermediate case in which the stiffness of the soil changed from soft soil over stiff soil to stiff soil over stiff soil after multiple number of roller passes. For each of these profiles, the layered soil profiles were characterized by DCP measurements and the surface modulus was obtained by taking LWD measurements. The equivalent modulus (E$_{equivalent}$) was then calculated in three steps. First the influence factor of each layer with circular loading case was estimated using the equation proposed by Poulos and Davis (1974) (Equation 18). The DCP-CBR value for each layer was multiplied by the influence factor, and the sum of the CBR multiplied by the influence factor was divided by the sum of the influence factor to obtain the equivalent CBR for the composite the layer which from the surface up to two times of the diameter of the LWD loading plate (Equation 19). The equivalent modulus was estimated using the equation proposed by Powell et al. (1984) (Equation 20).

$$I_z = 1 - \{\frac{1}{1+(a/z)^2}\}^{3/2} \tag{18}$$

$$CBR_{equi.} = \frac{\sum CBR \times I_z}{\sum I_z} \tag{19}$$

$$E_{equivalent}(MPa) = 17.58 \times \text{CBR}_{equi.}^{0.64} \tag{20}$$

A sample calculation for estimating the equivalent modulus using DCP measurements is shown in Figure 92.

The first set of data was collected from Ohio bridge approach project site and 31 testing points were evaluated. The data can be separated into two groups, which collected further than 6 m away the abutment and collected within 6 m from abutment. Data collected from 6 m away the abutment was the case of stiff soil over soft soil and data collected within 6 m away the abutment was the case of soft soil over stiff soil. Good correlation coefficients (R^2 = 0.72) were obtained from both cases as shown in Figure 93 and the calculations for all data points are provided in Appendix.

PT #	Depth (mm)	CBR	I_z	CBR×I_z
1	0	12.6	1.0	23.1
2	33	12.6	1.0	12.3
3	183	17.3	0.3	5.6
4	277	23.7	0.2	4.0
5	395	14.3	0.1	1.3

Sum (CBR×I_z): 23.1

Sum (I_z): 1.6

CBR$_{equi.}$ = Sum (CBR×I_z)/sum(I_z)   14.9

$E_{equi.}$ =   17.6×CBR$_{equi.}^{0.64}$ 99.1
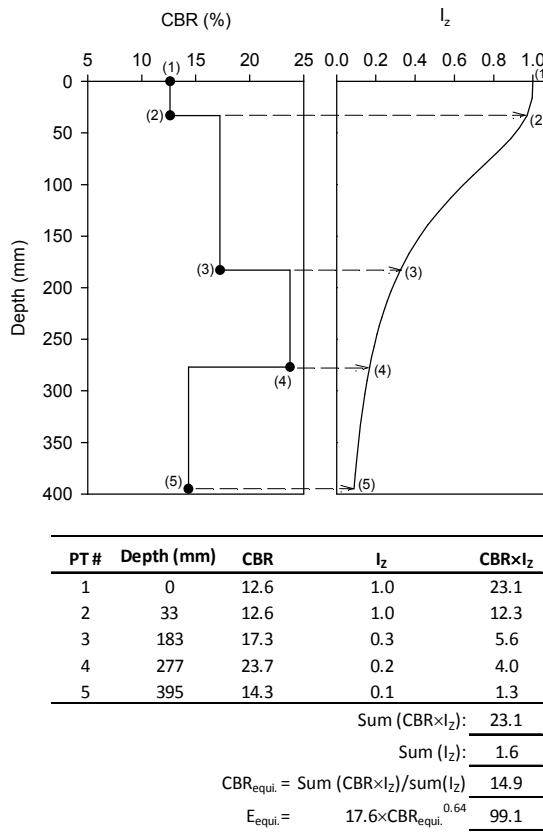
Figure 92. Sample calculation for estimating the equivalent modulus using DCP measurements
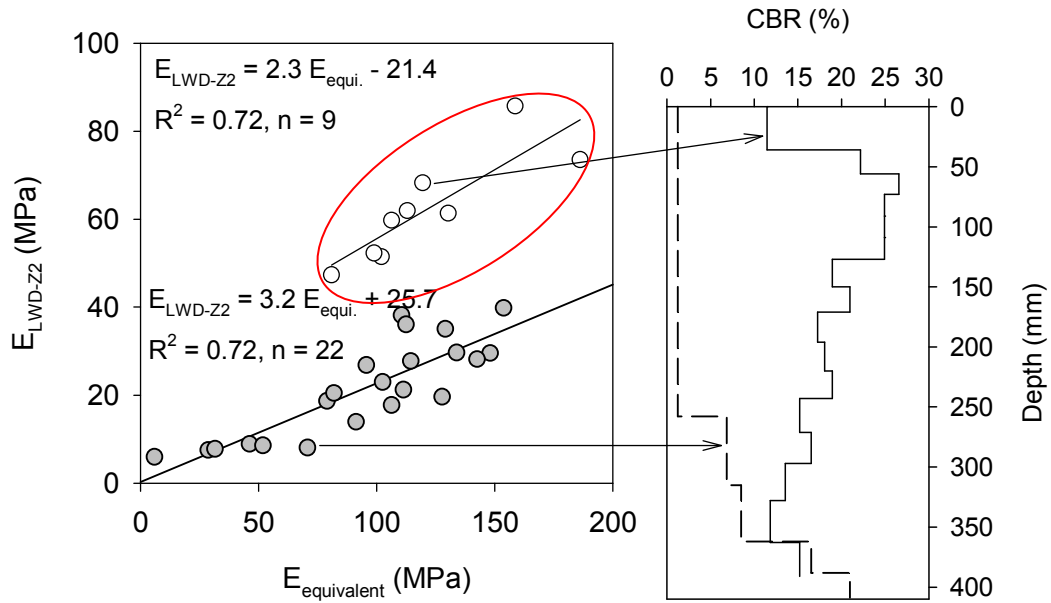
Figure 93. Correlation between $E_{equivalent}$ and E_{LWD-Z2} for Ohio project site

The second profile, stiff soil over soft soil, was found at the Hormel PCC project site, and 84 points were tested. The regression analysis result ($R^2 = 0.54$) from this project site provides a better correlation than the case of soft soil over stiff soil (Figure 94), and the calculations for all data points are provided in Appendix.
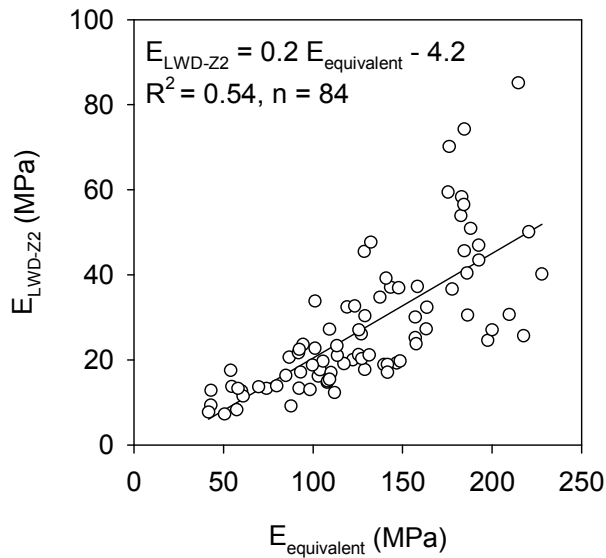
Figure 94. Correlation between $E_{equivalent}$ and E_{LWD-Z2} for Hormel PCC project site

The third project site conducted this topic of study was the West Virginia project site for the geosynthetic reinforcement study, and it was an intermediate case between soft soil over stiff soil and stiff soil over soft soil. The stiffness of the soil was changing from soft to stiff with the number of roller passes. The regression analysis result indicates that this case had $R^2 =$ 0.64 with 220 measurements as shown in Figure 95 and the calculations for all data points are provides in Appendix.

The plot shows:

$E_{LWD-Z2} = 0.3\ E_{equivalent} - 1.1$
$R^2 = 0.64,\ n = 220$

with y-axis labeled E_{LWD-Z2} (MPa) and x-axis labeled $E_{equivalent}$ (MPa).
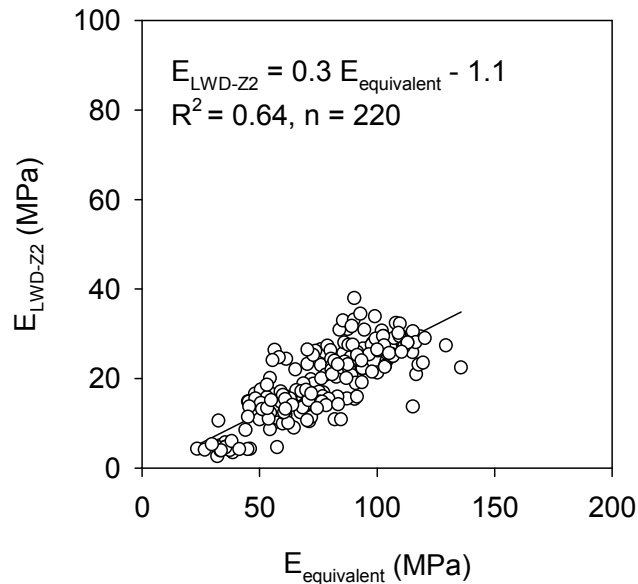
Figure 95. Correlation between $E_{equivalent}$ and E_{LWD-Z2} for West Virginia project site

There are some limitations with this approach. First, the influence factor equation adopted in this study only considering the isotropic and homogenous soil profile; second, the modulus for each layer was estimated based on empirical relationship which introduces accuracy issues to this approach; besides that, LWD measures larger area (the same size as loading plate) than DCP measurements (2 mm).

Laboratory Test Results

The laboratory tests evaluated compacted soils for w-γ_d-E_{LWD}- DPI/s_u Relationships from gyratory samples under two conditions, rigid boundary conditions that did not reflect field

conditions and flexible boundary conditions that more closely matched field conditions.

Results from rigid boundary conditions

Three types of materials were tested in this topic of research, which were US 10 granular materials, TH 36 silty clay, and TH 60 non-granular material. DPI, s_u, and E_{LWD} measurements obtained on gyratory compacted specimens confined with the rigid boundary condition. Multiple regression analysis was performed to determine the relationships between E_{LWD}, w and γ_d. Statistical significance of each variable was assessed based on p- and t-values. The selected criteria for identifying the significance of a parameter include: p- value < 0.05 = significant, < 0.10 = possibly significant, > 0.10 = not significant, and t- value < -2 or $> +2$ = significant. The p- value indicates the significance of a parameter and the t- ratio value indicates the relative importance. The multiple regression relationships obtained are presented as contour plots in relationship with Proctor w and γ_d relationships for all the three types of materials as shown from Figure 96 to Figure 101. The regression relationships are summarized in Table 17 including R^2 vlues which range from 0.7 to 0.9. An advantage of presenting the results in contour format is that the E_{LWD} or DPI "target" values with respect to acceptable w and γ_d can be graphically determined and the influence of moisture content is clearly evident. The statistical model output figures are provided in Appendix.

$$E_{LWD} = -6568.48 + 27.60\,w + 693.28\,\gamma_d - 2.79\,w^2 - 18.09\,\gamma_d^2$$
$$R^2 = 0.85, n = 24$$
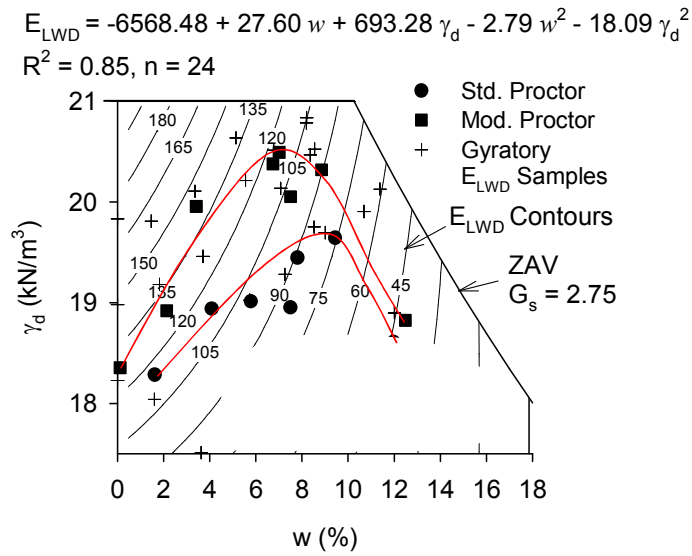
Figure 96. $E_{LWD\text{-}Z1}$ contours in relationship with moisture and dry unit weight – US 10 granular material (USCS: SP-SM) ($d_{LWD\text{-}Z1} = 85/E_{LWD\text{-}Z1}$)

$$E_{LWD\text{-}z1} = -388.05 + 27.01w + 27.84\gamma_d - 1.84w\gamma_d$$
$$R^2 = 0.93, n = 17$$
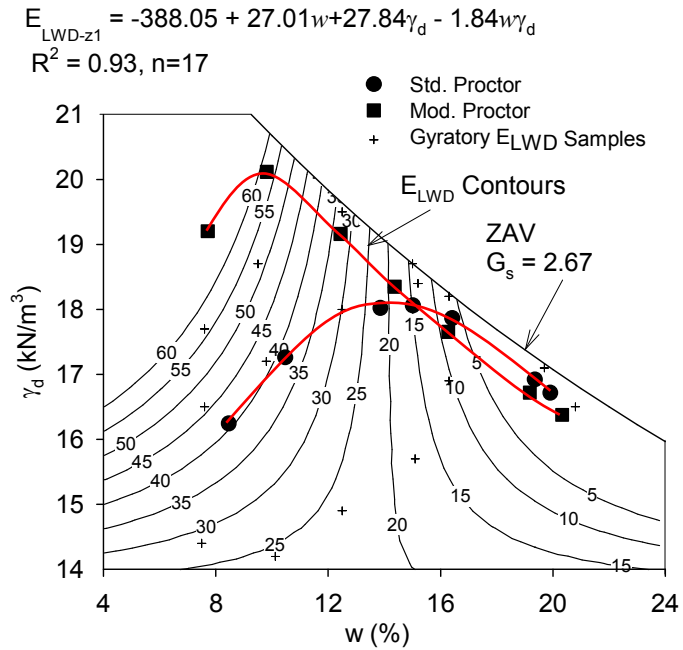
Figure 97. $E_{LWD\text{-}Z1}$ contours in relationship with moisture and dry unit weight – TH36 silty clay material (USCS: ML) ($d_{LWD\text{-}Z1} = 59.4/E_{LWD\text{-}Z1}$)

E_{LWD-z1} = 43.67 - 6.09 w + 3.86 γ_d - 1.87 (γ_d - 17.82)(w - 13.93)
R^2 = 0.88, n = 28
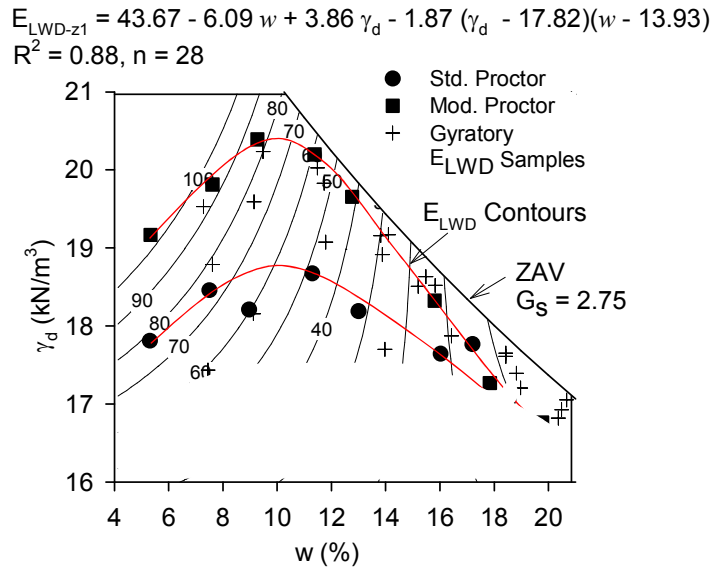
Figure 98. E_{LWD-Z1} contours in relationship with moisture and dry unit weight – TH60 soil 301 material (USCS: CL) (d_{LWD-Z1} = 49.8/E_{LWD-Z1})

E_{LWD-z1} = -288.58+13.68w+24.11γ_d-1.43$w\gamma_d$+0.24w^2
R^2 = 0.84, n = 88
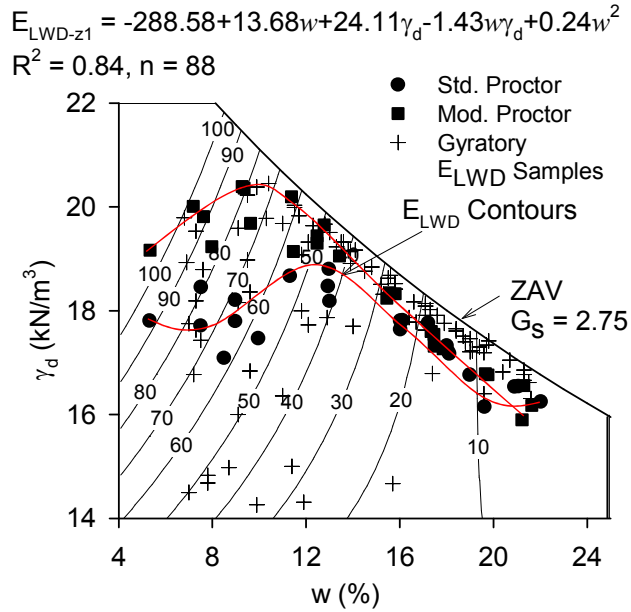
Figure 99. E_{LWD-Z1} contours in relationship with moisture and dry unit weight – TH60 (301, 303, and 305 combined) non-granular material (USCS: CL) (d_{LWD-Z1} = 49.8/E_{LWD-Z1})

$$DPI = 284.09 - 32.28w - 13.32\gamma_d + 1.17w\gamma_d + 0.77w^2$$

$$R^2 = 0.79, n = 70$$
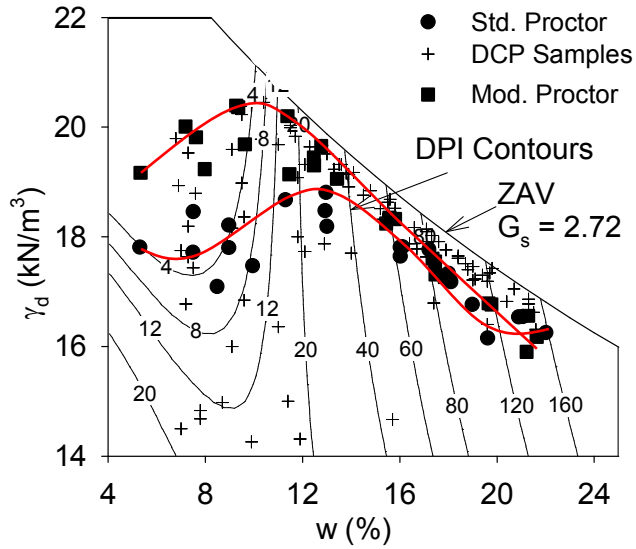
Figure 100. DPI contours in relationship with moisture and dry unit weight – TH60 non-granular material (301, 303, and 305 combined) (USCS: CL)

$$s_u = -9565.44 + 289.5w + 972.9\gamma_d - 19.44w\gamma_d - 21.31\gamma_d^2$$

$$R^2 = 0.71, n = 70$$
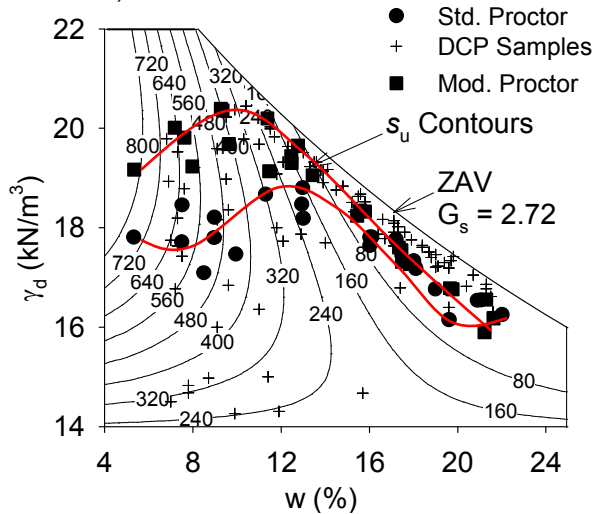
Figure 101. s_u contours in relationship with moisture and dry unit weight – TH60 non-granular material (301, 303, and 305 combined) (USCS: CL) (s_u determined from empirical relationship with DPI)

Table 17. Summary of laboratory determined w-γ_d-DPI/s_u/E_{LWD} relationships

Soil ID	USCS	Project location	Relationship	n	R^2
US10	SP-SM	Staples, MN	$E_{LWD\text{-}Z1}=-6568.48+27.60w+693.28\gamma_d-2.79w^2-18.09\gamma_d^2$	24	0.85
TH36 silty clay	ML	North St. Paul, MN	$E_{LWD\text{-}z1}=-388.05+27.01w+27.84\gamma_d-1.84w\gamma_d$	17	0.93
TH60 soil 301	CL	Bigelow, MN	$E_{LWD\text{-}z1}=43.67-6.09w+3.86\gamma_d-1.87(\gamma_d-17.82)(w-13.93)$	28	0.88
			$DPI=146.74-27.70w-0.20w\gamma_d+1.71w^2$	18	0.95
			$s_u=-1964.84+163.09w+140.90\gamma_d-10.95w\gamma_d$	18	0.97
TH60 soil 303			$E_{LWD\text{-}z1}=-56.2-4.69w+8\gamma_d$	28	0.74
			$DPI=125.2-18.03w-2.89\gamma_d+1.22w^2$	20	0.98
			$s_u=-1825.04+167.39w+131.44\gamma_d-11.05w\gamma_d$	20	0.89
TH60 soil 305			$E_{LWD\text{-}z1}=-298.49+17.90w+22.44\gamma_d-1.27w\gamma_d$	32	0.82
			$DPI=0.27+7.71w-4.07\gamma_d$	32	0.79
			$s_u=-4922.31+383.82w+344.98\gamma_d-25.48w\gamma_d$	32	0.79
TH60 subgrade clay (combining 301, 303 and 305 soils)			$E_{LWD\text{-}z1}=-288.58+13.68w+24.11\gamma_d-1.43w\gamma_d+0.24w^2$	88	0.84
			$DPI=284.09-32.28w-13.32\gamma_d+1.17w\gamma_d+0.77w^2$	70	0.79
			$s_u=-9565.44+289.5w+972.9\gamma_d-19.44w\gamma_d-21.31\gamma_d^2$	70	0.71

Results from flexible boundary conditions

TH 60 non granular and US 10 granular materials were used to evaluate the boundary conditions. Samples were compacted using gyratory compactor with PDA installed, and the gyratory compactor was setup with 300 kPa applied vertical stress at 100 gyrations. The PDA continuously recorded τ_G measurements during the compaction process. Figure 102 and Figure 103 provide the shear resistance change with the number of gyrations for both TH 60 non granular and US 10 granular materials. Figure 104 interpret the shear resistance varies with moisture content for both granular and non granular materials. Both the averaged shear resistance from the last 10 gyration and the peak shear resistance were used to represent the shear resistance of the compacted specimens for the non granular material. It is indicated from the figure that the non granular material is highly sensitive to moisture content which causing significant reduction in τ_G with increasing moisture content and also indicate that

over-compaction contributes to low τ_G with increasing number of gyrations, for samples at high moisture contents ($w > 16\%$ for this material). Test results from the US 10 granular material provide relative less sensitive to moisture content compared with TH 60 non granular material.

Figure 105 and Figure 106 show relationships between LWD measurement and moisture content with four different boundary conditions (i.e., no confinement, "stiff", "soft" and rigid). The results indicate that E_{LWD} values for the rigid boundary conditions are relatively higher than the other boundary conditions for both 150 mm diameter and 100 mm diameter LWD loading plates. The LWD measurements with "stiff", "soft" and no confinement conditions were grouped within a similar range. Relationship between E_{LWD} and shear resistance provide good correlations for the TH 60 non-granular material with R^2 values > 0.7.

The influence of the boundary condition for the US 10 granular material is shown in Figure 107, which is more significant than the non-granular material as expected. Results indicate that the polyurethane "stiff" and "soft" mold does not provide significant confinement and the measured E_{LWD} values were quite low. Figure 108 provide the relationship between E_{LWD} values and the averaged shear resistance from the last 10 gyrations, and no clear correlations were provided from this test sequence.
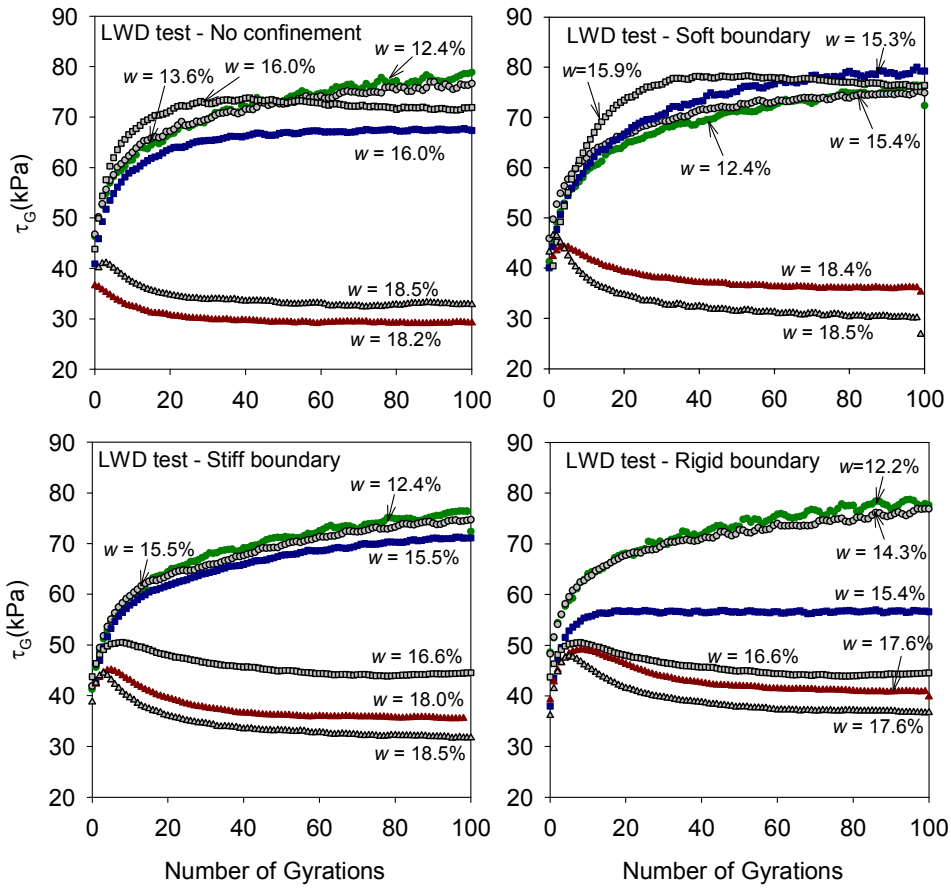
Figure 102. Shear resistance versus number of gyrations (σ_o = 300 kPa) for TH 60 soil 306 (USCS: CL)
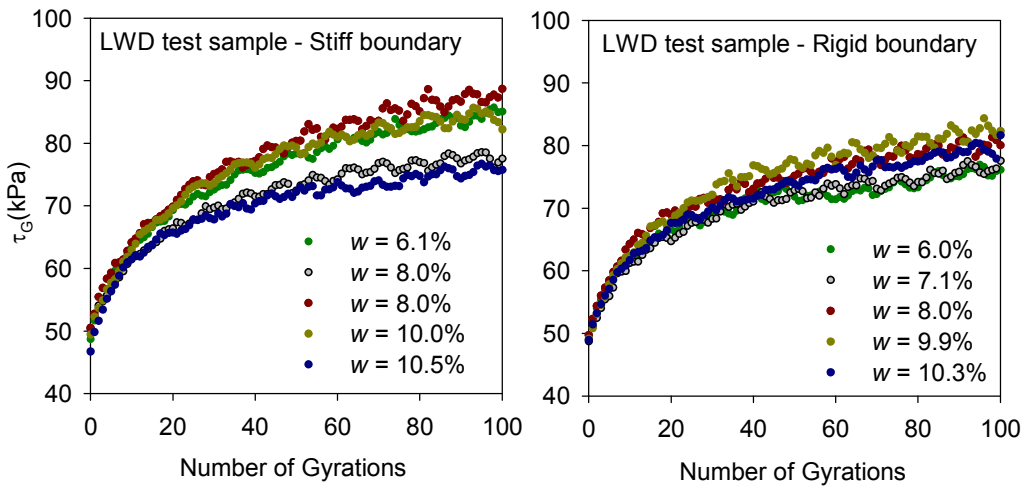
Figure 103. Shear resistance versus number of gyrations for US10 granular material (USCS: SP-SM) (σ_o = 300 kPa)
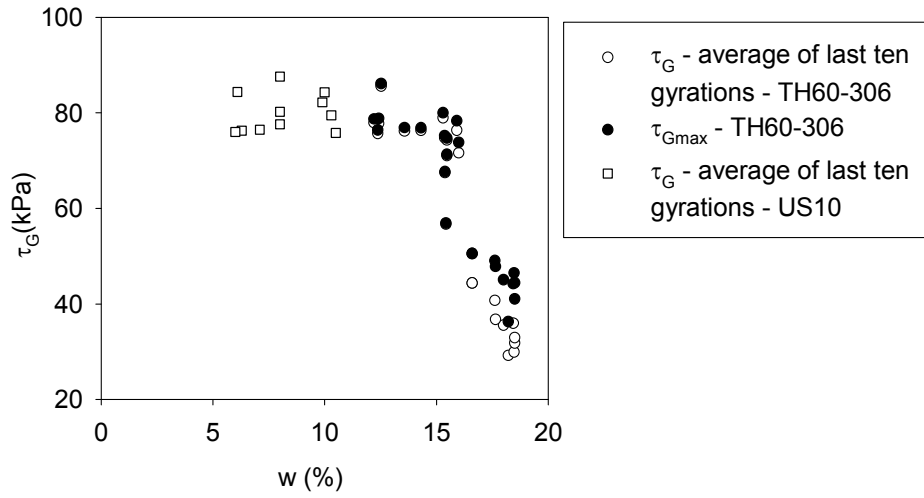
Figure 104. Influence of moisture content on τ_G for TH60 – soil 306 non-granular (USCS: CL) and US 10 granular (USCS: SP-SM) materials
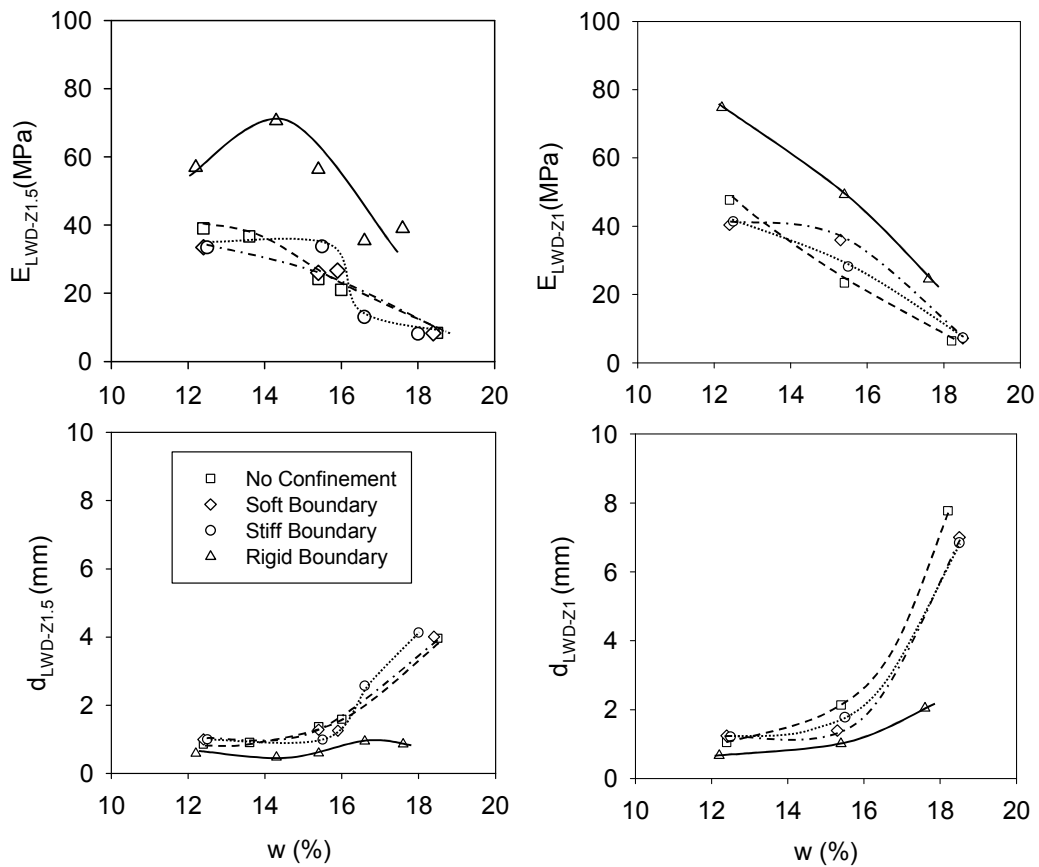
Figure 105. Influence of boundary conditions on LWD measurements on gyratory compacted specimens at different moisture contents – TH 60 soil 306 (USCS: CL)
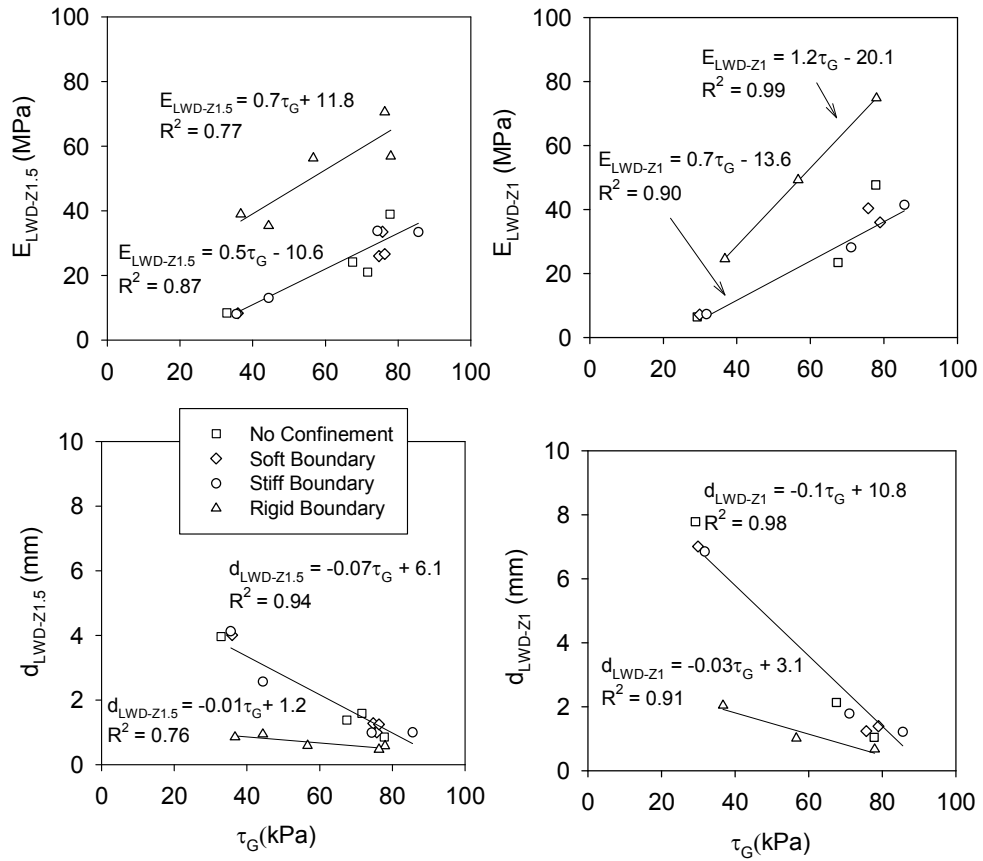
Figure 106. Relationships between LWD measurements and τ_G for different boundary conditions – TH 60 soil 306 (USCS: CL)
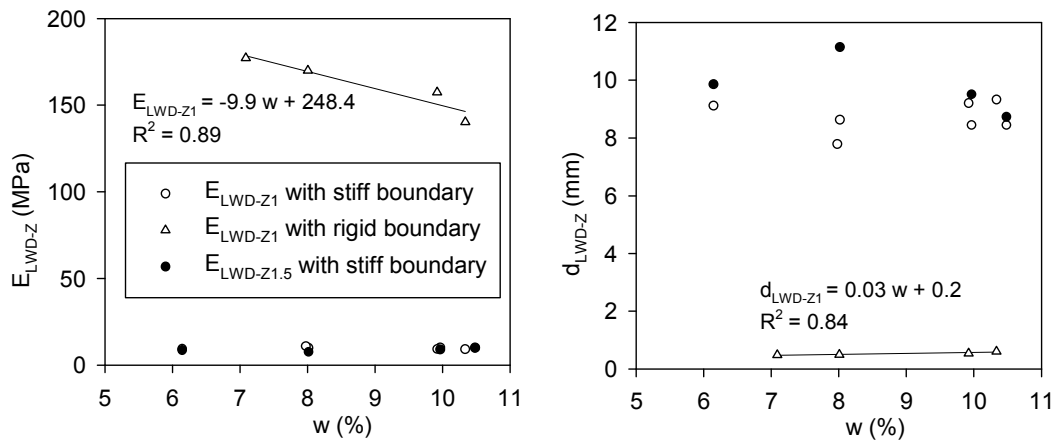
Figure 107. Influence of boundary conditions on LWD measurements on gyratory compacted specimens at different moisture contents – US10 granular material (USCS: SP-SM)
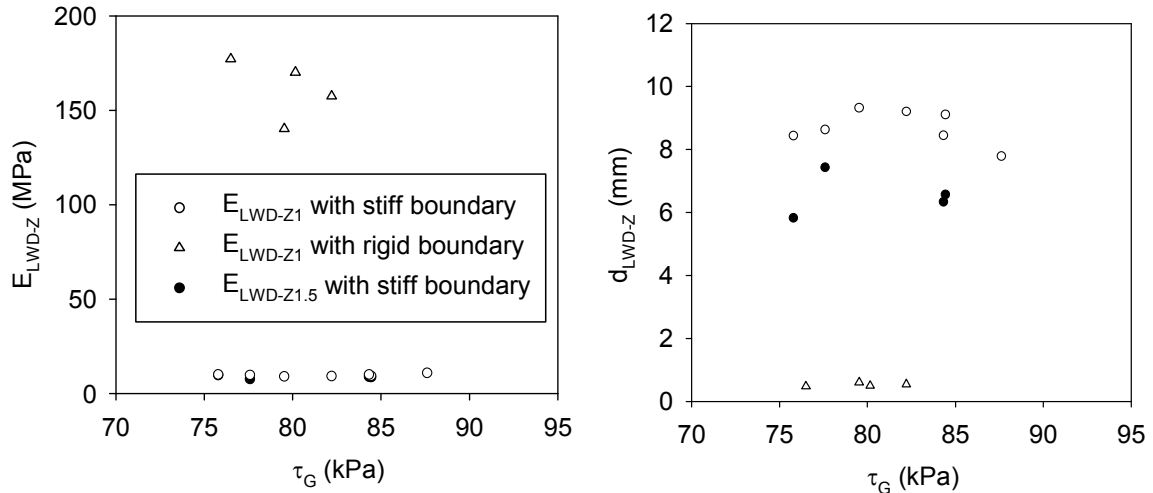
Figure 108. Relationship between LWD measurements and τ_G for different boundary conditions – US10 granular material (USCS: SP-SM)

Relationship between PDA Shear Resistance and Undrained Shear Strength

Unconfined compression (UC) tests were performed on gyratory compacted specimens to investigate the relationship between τ_G and s_u. Due to the large amount of soil involved, western Iowa loess (USCS: ML) was used for this topic of study. Samples were prepared at six different moisture contents, which were -9%, -6%, -3%, 0%, +3% and +6% of optimum moisture content from standard Proctor test. Samples were compacted with applied stress of 100 kPa, 300 kPa and 600 kPa at 100 gyrations. τ_G versus number of gyrations is presented in Figure 109 for all specimens. Results show increasing shear resistance with increasing number of gyrations up to about 15 gyrations and then no significant increase up to 100 gyrations for samples with $w < 17\%$. Shear softening was observed at high moisture contents ($w > 18\%$) with number of gyration increase. Figure 110 shown the τ_G and s_u change with moisture content for all the tested specimens, and it is clear shown from the figure that the τ_G and s_u increase with the applied stress increase. Figure 111 provide strong correlation between τ_G and s_u measured from the same specimen with $R^2 = 0.94$. On average, the s_u is about 1.6 times τ_G.
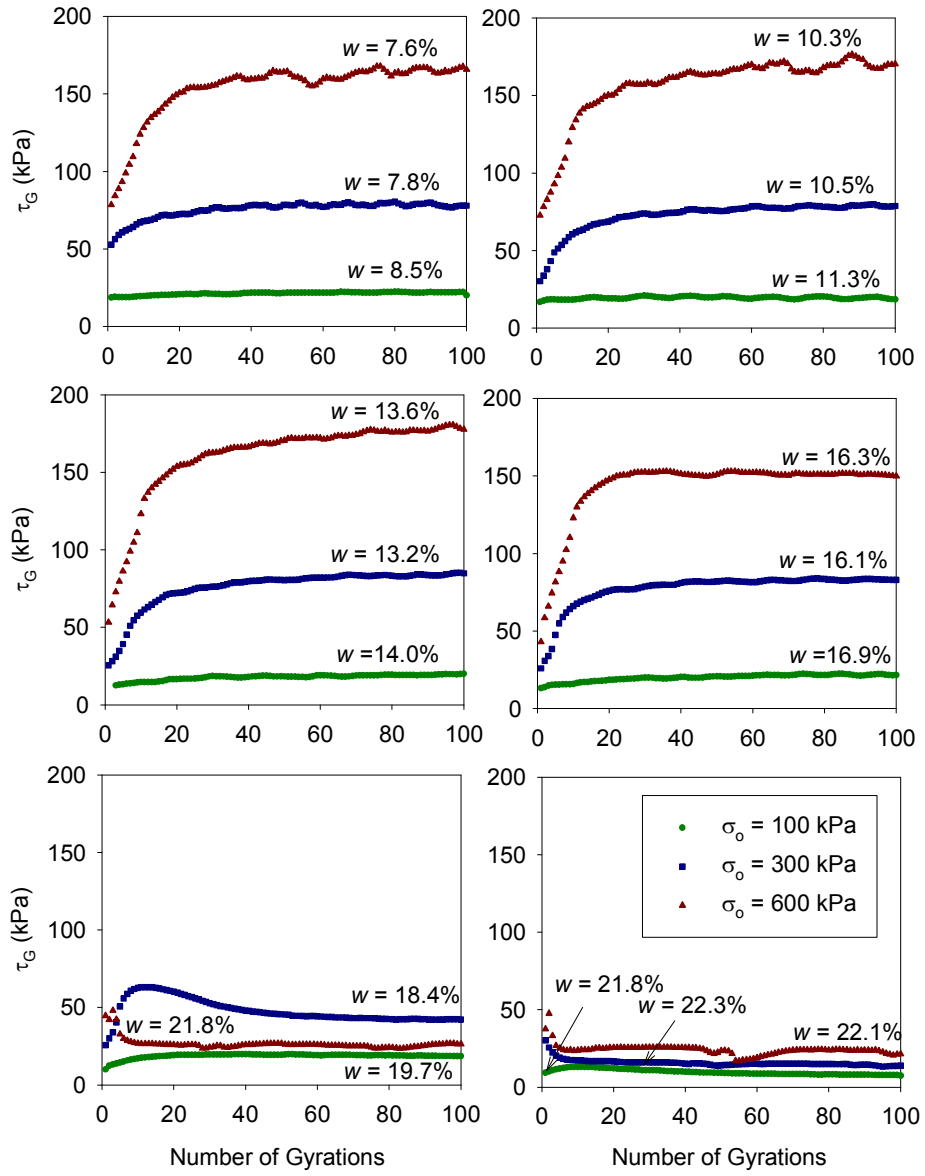
Figure 109. τ_G versus number of gyrations for loess (USCS: ML)
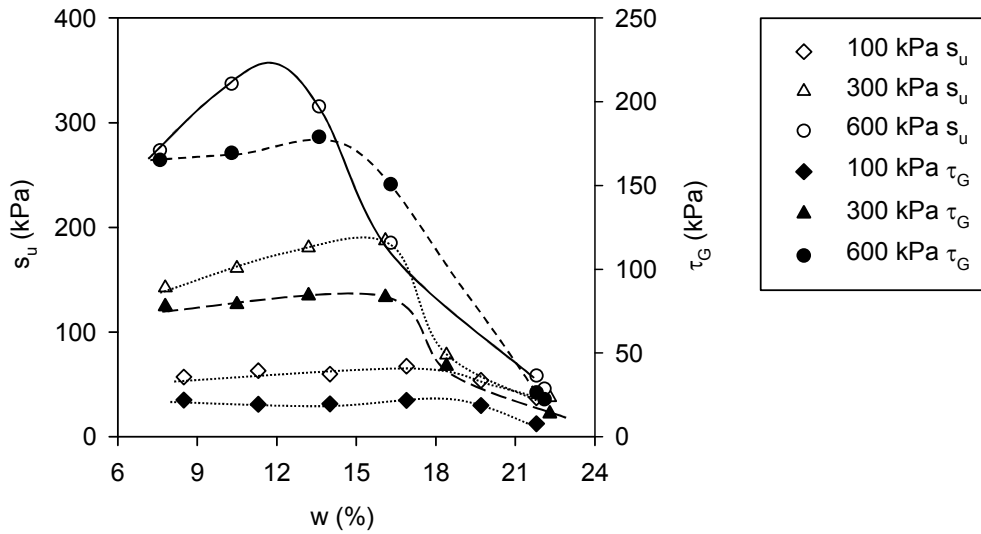
Figure 110. s_u and τ_G versus moisture content for gyratory compacted specimens after 100 gyrations at σ_o = 100, 300, and 600 kPa for loess (USCS: ML)
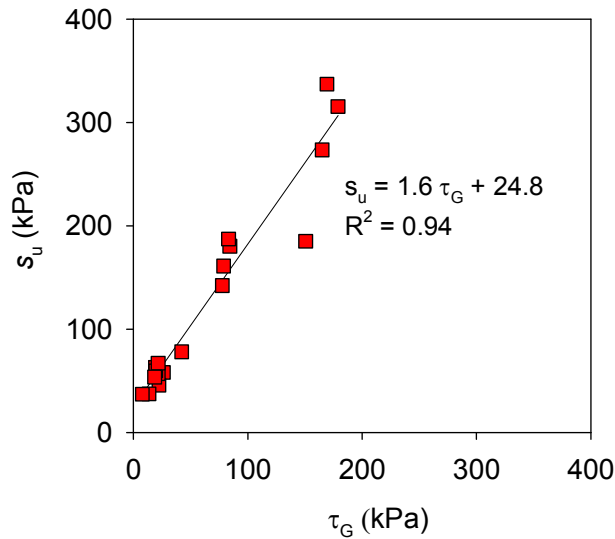
Figure 111. Relationship between s_u and τ_G for loess (USCS: ML)

Relationship between PDA Shear Resistance and Resilient Modulus

Resilient modulus (M_r) tests and unconsolidated-undrained triaxial compression (UU) tests were performed on gyratory compacted specimens with the height to diameter ratio of H/D = 1:1 and H/D = 2:1. The H/D = 1:1 specimens were directly produced from the gyratory

compactor, while the H/D = 2:1 specimens were trimmed from the gyrator samples using a tube sample to reduce the diameter. TH 60 non-granular material was prepared at the optimum moisture content based on the standard Proctor test (w_{opt}=18%). The mean M_r value was calculated from fifteen different loading sequences. The Witczak and Uzan (1988) model which was mentioned in the research method chapter was used in the interpretation of the results.

Model coefficients k_1, k_2, k_3 and R^2 values from the tests are summarized in Table 18. Plots of σ_d versus M_r for the samples tested are provided in Figure 112. Comparison between M_r results obtained at different testing sequence for the H/D = 1:1 and 2:1 samples is presented in Figure 113. With exception of samples compacted at σ_o = 300 kPa, the results show that H/D = 1:1 and 2:1 samples sizes produce similar or slightly lower M_r values. τ_G measurements for M_r test specimens are shown in Figure 114. Figure 115 shows τ_G-s_u and τ_G-M_r regression relationships for H/D = 1:1 and 2:1 samples. τ_G-s_u results obtained for loess show similar trends as loess material and there was no influence of sample size on the relationship. The τ_G-M_r relationship showed separate trends for H/D = 1:1 and 2:1 samples. Although the data is limited, the correlations show promise in terms of using the PDA τ_G measurements which are relatively less time consuming to obtain than s_u or M_r testing.

Table 18. Comparison of M_r for 2:1 and 1:1 height to diameter ratio specimens – TH-60 soil 306 (USCS: CL)

Gyratory pressure (kPa)	Sample size H×D (mm)	w (%)	γ_d (kN/m³)	Average[*] M_r (MPa) [range[**] in MPa]	Model coefficients	τ_G (kPa)	s_u (kPa)	s_u @ ε=1% (kPa)	s_u @ ε=5% (kPa)	ε_f (%)
600	142.7× 72.4	19.8	17.2	19.9 [11.3 to 43.6]	k_1=83.5 k_2=0.64 k_3=-0.67 R^2=0.72	27.4	91.1	27.6	62.1	17.8
	151.7× 149.9	17.5	17.9	20.7 [15.7 to 35.5]	k_1=114.6 k_2=0.62 k_3=-0.43 R^2=0.88	44.6	148.9	34.5	110.3	11.7
300	148.6× 72.4	18.0	17.6	29.9 [18.6 to 48.4]	k_1=167.3 k_2=0.19 k_3=-0.49 R^2=0.88	30.9	130.0	34.5	93.1	14.6
	153.1× 149.9	17.2	17.7	21.1 [15.5 to 28.7]	k_1=139.2 k_2=0.36 k_3=-0.32 R^2=0.80	33.7	137.6	44.8	120.7	11.2
100	142.5× 71.9	21.8	16.3	12.7 [7.1 to 26.6]	k_1=45.2 k_2=0.39 k_3=-0.81 R^2=0.93	9.1	56.3	25.9	44.8	20.2
	160.4× 149.9	20.3	16.5	15.2 [10.6 to 25.8]	k_1=80.0 k_2=0.40 k_3=-0.52 R^2=0.95	13.6	66.1	20.7	60.3	14.1

[*]Average of M_r determined from 15 load sequences; [**]range of M_r values from the 15 load sequences
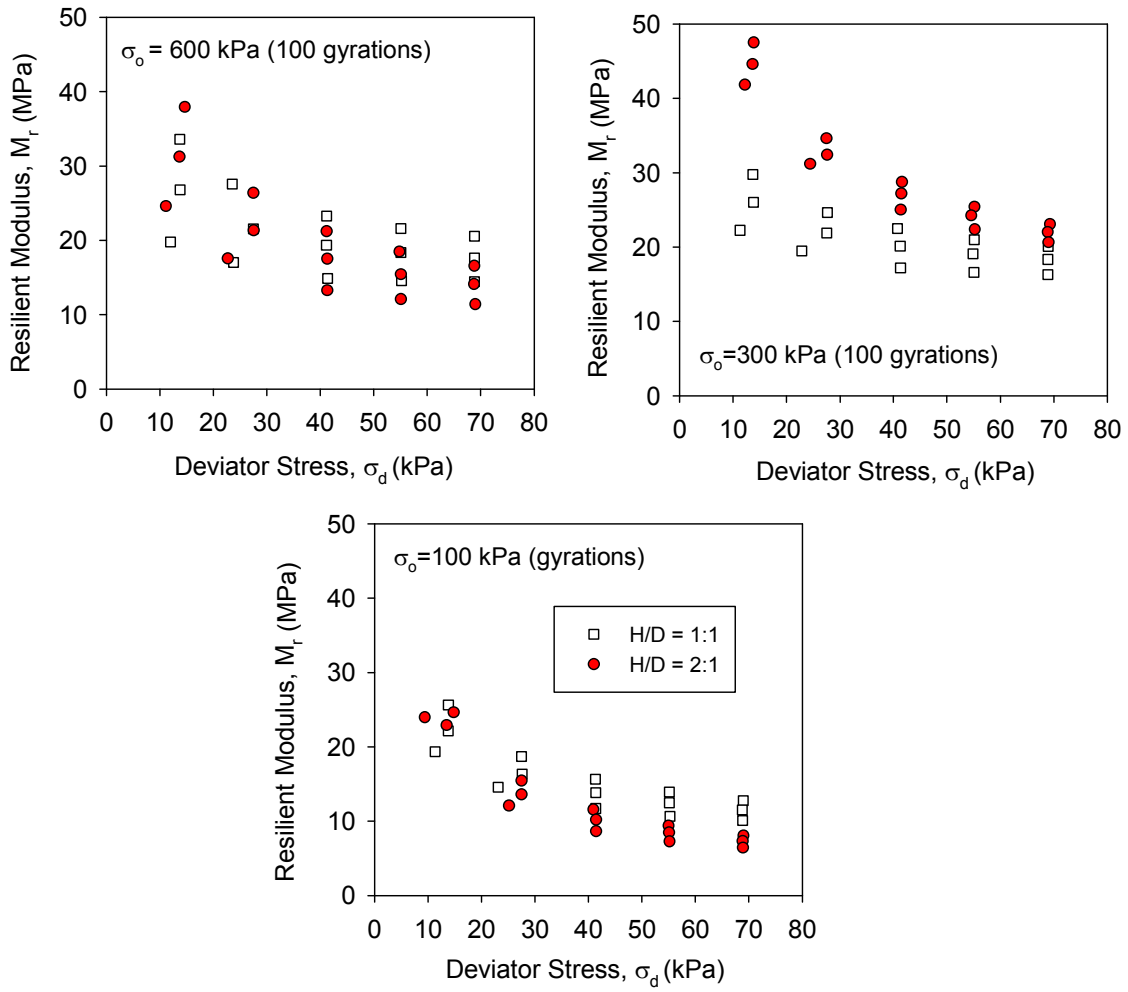
Figure 112. Effect of height to diameter ratio (H/D = 1 and 2) on M$_r$ of gyratory compacted specimens at σ$_o$ = 100, 300 and 600 kPa at 100 gyrations –TH-60 soil 306 (USCS: CL)
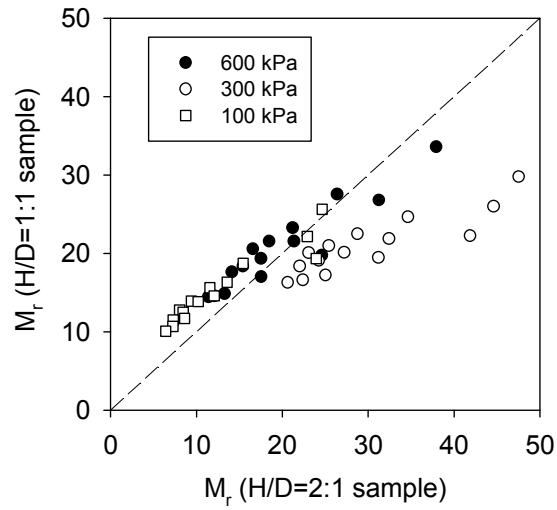
Figure 113. Relationship between H/D = 2:1 and 1:1 M_r results on gyratory compacted specimens – TH60 soil 306 (USCS: CL)
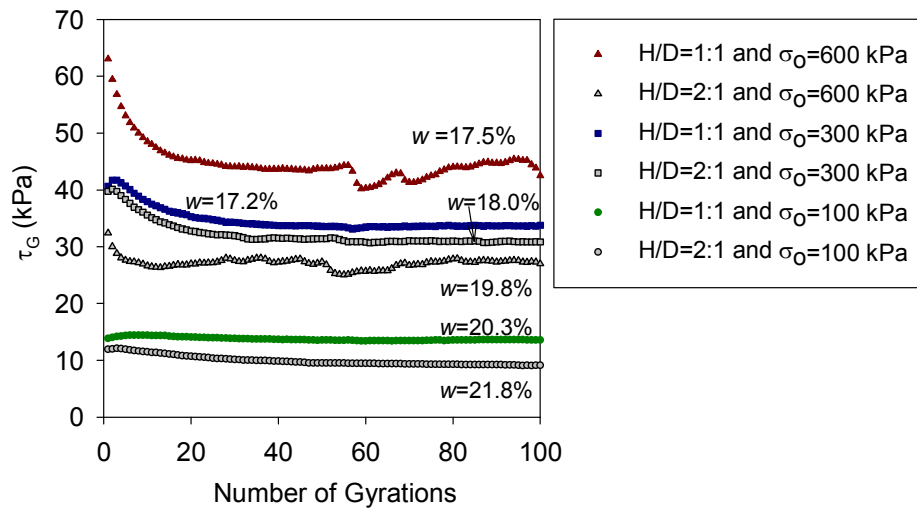
Figure 114. τ_G versus number of gyrations for σ_o = 100, 300, and 600 compacted specimens TH60 soil 306 (USCS: CL)
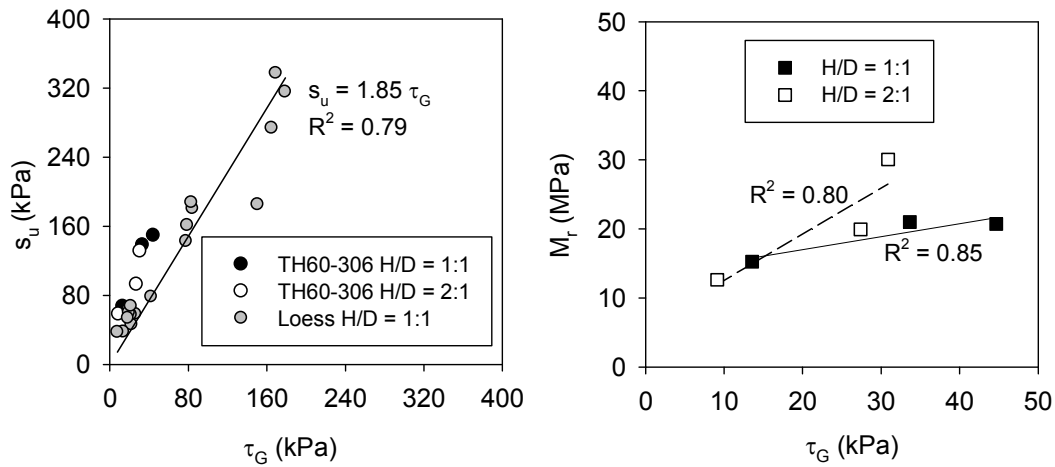
Figure 115. Correlation between s_u, M_r and τ_G for samples with H/D = 1 and 2 – TH 60 soil 306 (USCS: CL)

Establish Field Target Values for Quality Assurance

Field E_{LWD} target value determination study consists of performing LWD test with 200 mm diameter loading plate on uncompacted material. The idea was that with multiple hammer drops the soil would compact and the E_{LWD} value would reach an asymptote thus establishing a field target value. Results are presented in Figure 116 for field tests at TH 60 in non-granular soil. Results indicated that with increasing number of drops E_{LWD} increases and d_{LWD} decrease to approach an asymptotic value. Moisture contents for each tested point are provided and were in the range of 9.5 to 12.4%. E_{LWD} values ranged from about 6 MPa to 16 MPa. No trend was observed in the E_{LWD} or d_{LWD} values with moisture content.
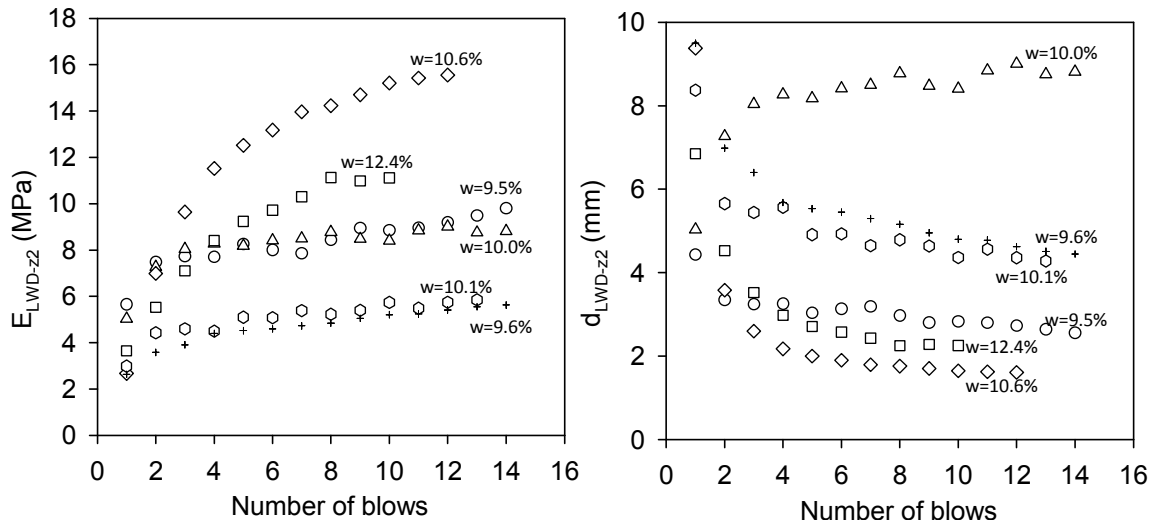
Figure 116. Results from in situ LWD tests showing E_{LWD} increase and d_{LWD} decrease with number of blows at locations with different in situ moisture contents – TH60

Linking Laboratory LWD-TVs to In situ LWD Measurements

The approach of developing w-γ_d-E_{LWD}/DPI contours described above is useful in determining target E_{LWD} or d_{LWD} values for a specified moisture range and target minimum density in situ. Gyratory compacted specimens of TH60 non-granular soil 306 were prepared and tested using 100-mm diameter plate and 150-mm diameter plate Zorn LWD, and DCP under "stiff" boundary conditions. PDA shear resistance was measured during gyratory compaction process for all the samples. Contours of $E_{LWD-Z1.5}$, $E_{LWD-Z1.0}$, s_u (determined from DPI-s_u relationships) and τ_G are presented in Figure 117, Figure 118 and Figure 119. Multiple regression models for the "stiff" boundary condition tests are presented on the contour plots.

Regression relationships between τ_G and LWD/DCP test measurements are presented in Figure 120. The regression relationships show strong correlations with R^2 values > 0.7. The τ_G and s_u predicted from DPI showed encouraging trend in the data.

Comparison between $E_{LWD-Z1.5}$ and $E_{LWD-Z1.0}$ measurements is presented in Figure 121. A line

based on Terzaghi's theoretical relationships (see Figure 86) is also shown in Figure 121. Results indicate that the best fit regression line for the measurements is in close agreement with Terzaghi's theoretical relationship.

Figure 122 shows w-γ_d relationship and E_{LWD} contours obtained from the "stiff" boundary model for TH60 soil 306 (w_{opt} = 17.3%, USCS: CL) in comparison with in situ w-γ_d at E_{LWD} test locations from TH 60 site with similar material characteristics (w_{opt} = 17.3%, USCS: CL). E_{LWD-Z2} and d_{LWD-Z2} values for in situ w-γ_d values were predicted from the laboratory-determined $E_{LWD-Z1.5}$ using Terzaghi's theoretical relationship. The predicted values are compared with actual in situ measurement values in Figure 122. Only two in situ test measurements that are in the range of moisture and density of laboratory samples are within the range of laboratory test measurements.

Multiple regression model with rigid boundary conditions developed for TH60 soils combining 301, 303, and 305 materials (average w_{opt} = 14.0%) are used to compare in situ w-γ_d measurements at E_{LWD} test locations from TH60 test site (average w_{opt} = 13.8%) in Figure 123. The in situ test measurements showed were predicted from the laboratory-determined E_{LWD-Z1} using Terzaghi's theoretical relationship (see Figure 121). The predicted values are compared with actual in situ measurement values in Figure 123. The regression relationships indicate positive relationships and predicted E_{LWD-Z2} values are about 0.6 times the actual in situ E_{LWD-Z2} measurements.

$E_{LWD-z1} = -2358+147.4w+140.9\gamma_d-8.2w\gamma_d-0.6w^2$

$R^2 = 0.91$, n = 21

$E_{LWD-z1.5} = -1442.3+90.9w+86.5\gamma_d-4.9w\gamma_d-0.5w^2$

$R^2 = 0.93$, n = 22
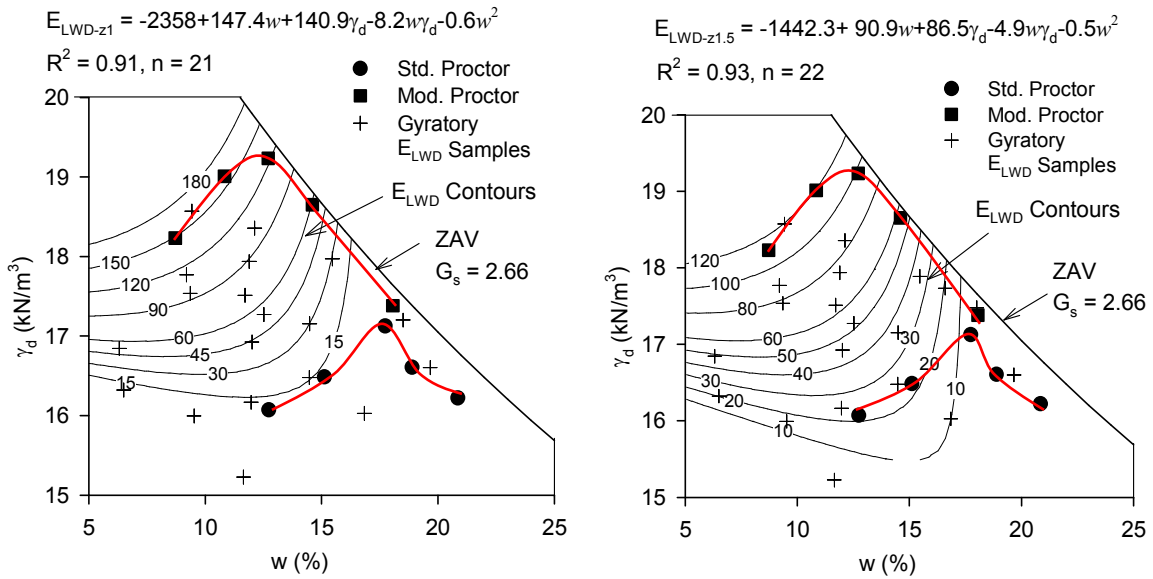
Figure 117. E_{LWD-Z1} and $E_{LWD-Z1.5}$ contours in relationship with moisture and dry unit weight with stiff boundary conditions – TH60 soil 306 material (USCS: CL)

$DPI = 104.5-9.5w-2.3\gamma_d+0.4w^2$

$R^2 = 0.97$, n = 17

$s_u = 643.3+23.2w-90\gamma_d-1.1w^2+3.1\gamma_d^2$

$R^2 = 0.97$, n = 17
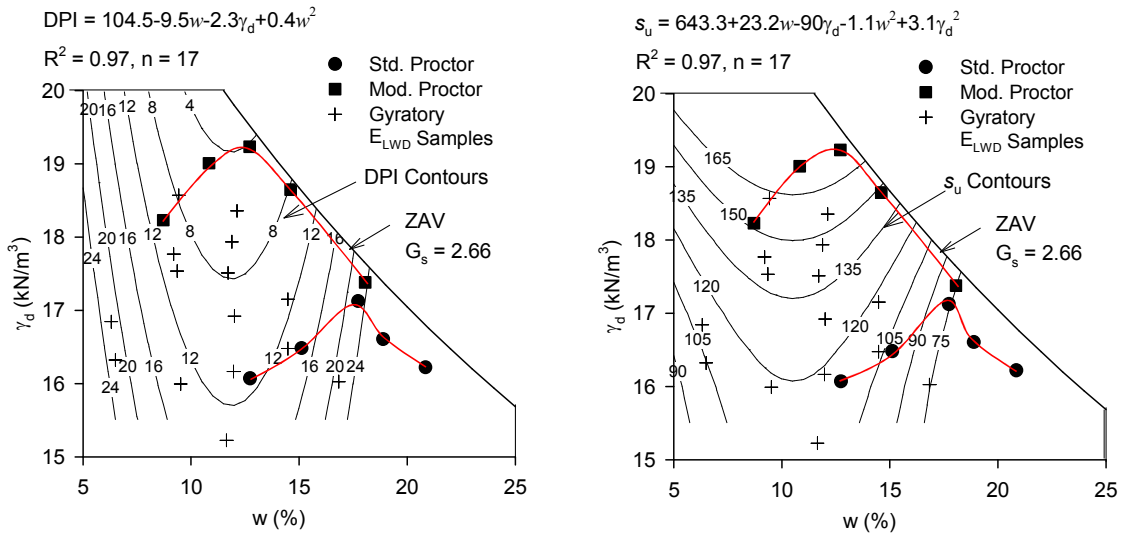
Figure 118. DPI and s_u contours in relationship with moisture and dry unit weight with stiff boundary conditions – TH60 soil 306 material (USCS: CL)

$$\tau = -2301.5 + 127.2w + 148\gamma_d - 8.1w\gamma_d$$

$R^2 = 0.97$, n = 24
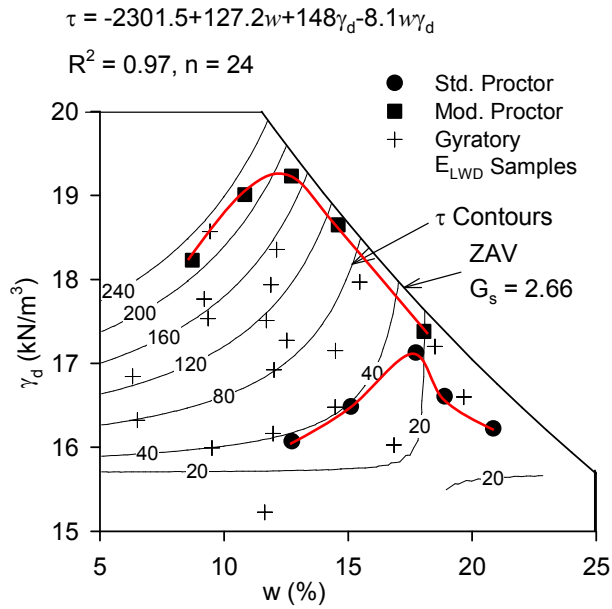
Figure 119. τ_G **contours in relationship with moisture and dry unit weight with stiff boundary test – TH60 soil 306 material (USCS: CL)**
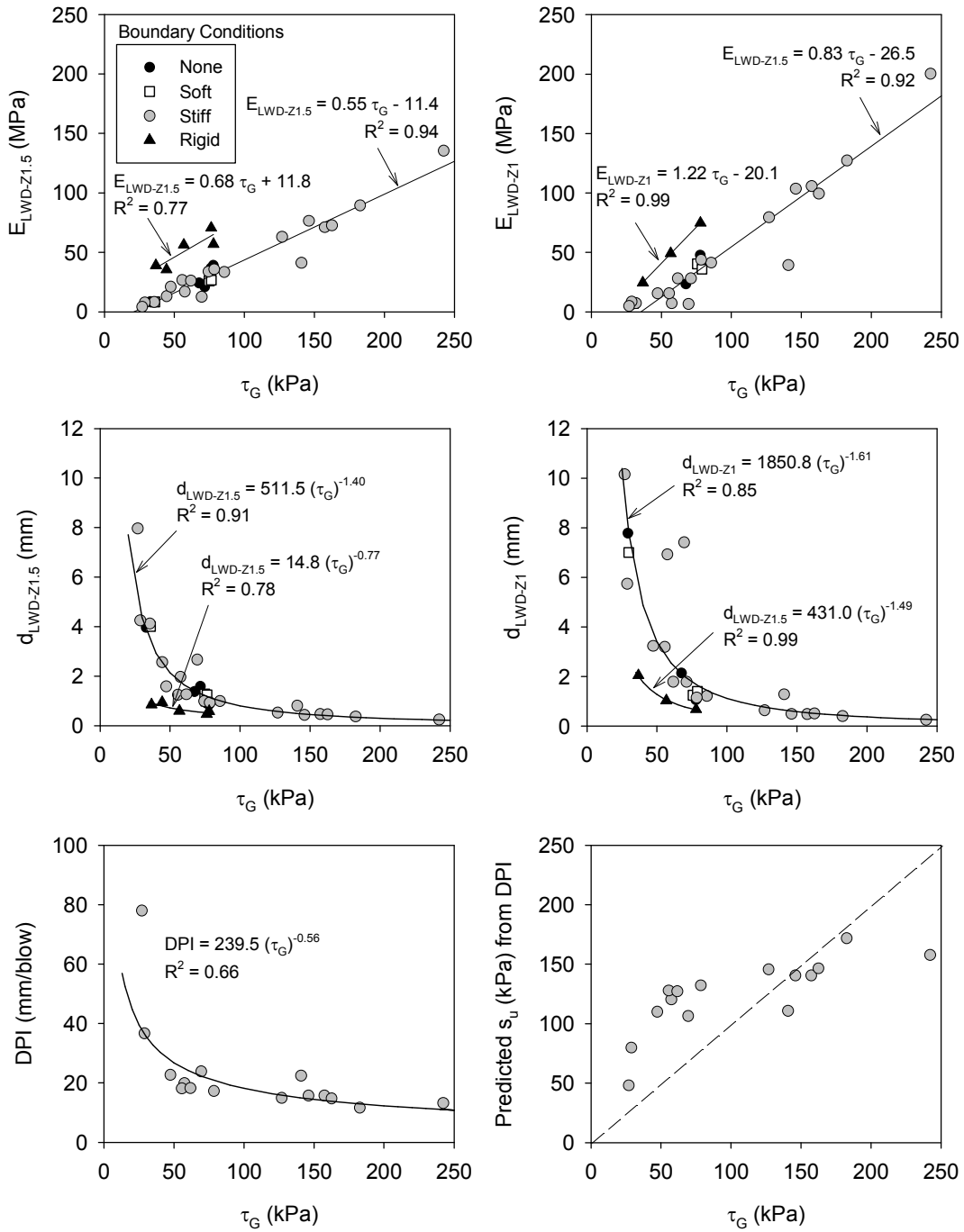
Figure 120. Correlations between τ_G and LWD/DPI measurements with different boundary conditions – TH60 soil 306 material (USCS: CL) (from White et al. 2009)
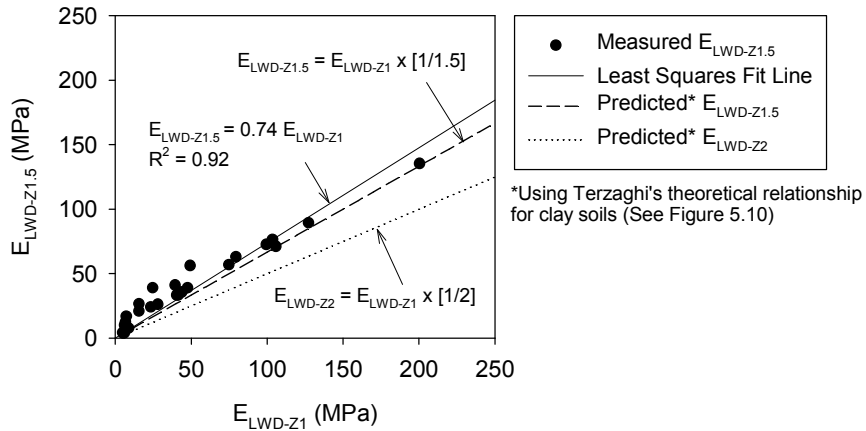
Figure 121. Relationships between laboratory E_{LWD-Z1} and E_{LWD-Z2} measurements in comparison with Terzaghi's theoretical relationships – TH60 soil 306 material (USCS: CL) (from White et al. 2009)
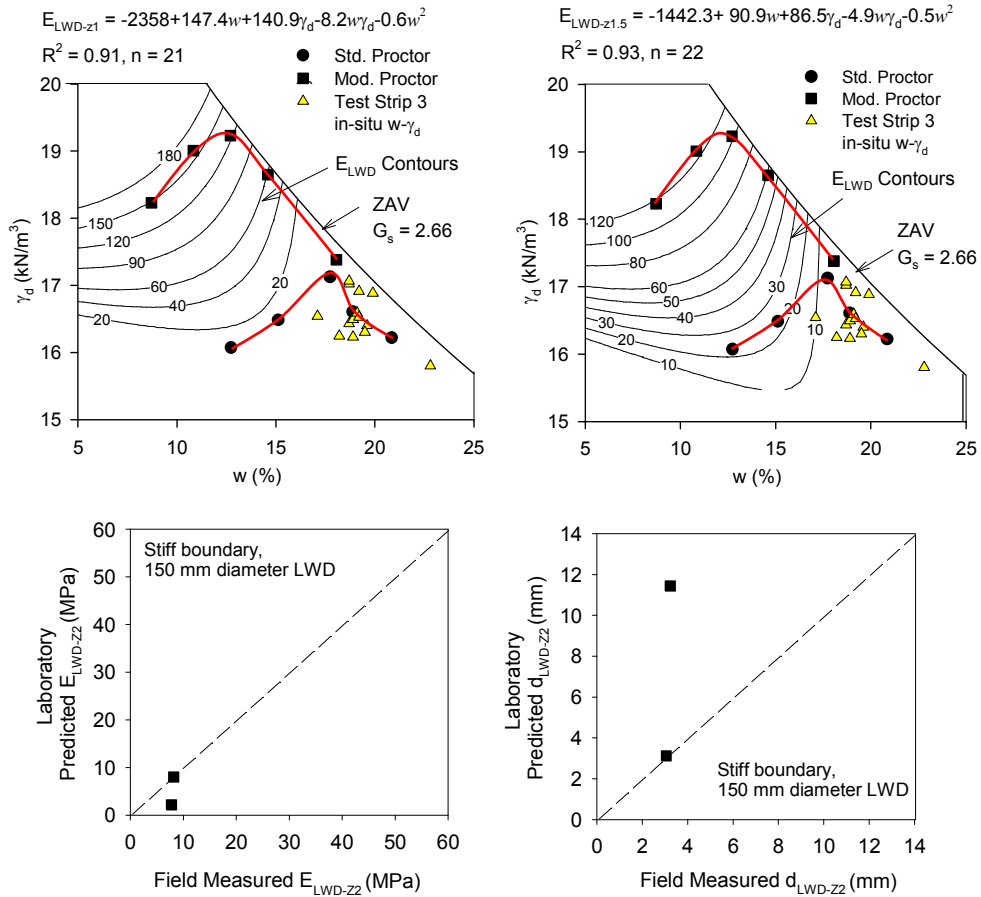
Figure 122. Comparison between in situ LWD measurements and laboratory predicted LWD target values (TH60 soil 306 "stiff" boundary model) (from White et al. 2009)
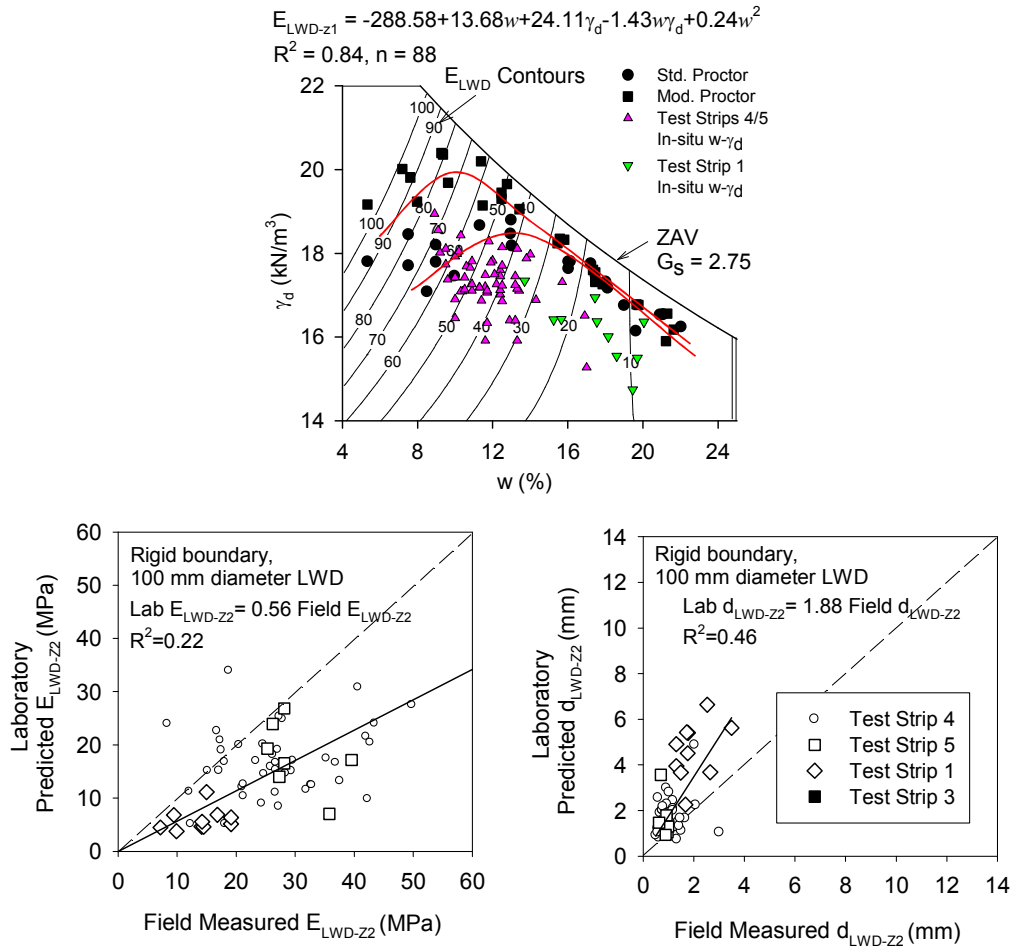
Figure 123. Comparison between in situ LWD measurements and laboratory predicted LWD target values (TH60 soil 301, 302, 303 combined rigid boundary model) (from White et al. 2009)

CHAPTER 6. CONCLUSIONS AND RECOMMENDATIONS

The objectives of this study were to evaluate the use of mechanistic-based compaction measurement devices such as light weight deflectometer (LWD), falling weight deflectometer (FWD), plate load test (PLT), Briaud compaction device (BCD), and dynamic cone penetrometer (DCP) for measuring the stiffness/strength of the compacted material; and to gain a better understanding of the factors that affect these devices; and to evaluate correlations between the measurements of these devices. A final objective for this study was to develop an approach for target value determination for QC/QA using the LWD. Data were collected from laboratory tests and from tests conducted at six field locations.

Some of the key findings obtained from this research are:

- Influence of plate diameter and plate contact stress on E_{LWD}
    - Limited data showed good correlations between different plate diameters, but need more data to ensure statistically significant.
- Various factors affect correlations between LWD, FWD, PLT and BCD:
    - Differences in applied contact stresses,
    - Differences in deflection measurement method,
    - Differences in measurement influence depths,
    - Assumption of constant contact stress for LWD vs. measured stress for FWD/BCD/PLT,
    - Measurement errors associated with each device.
- The estimated $E_{equivalent}$ provide relative good correlations with measured ELWD using the approach adopted in this research ($R^2 = 0.5$ to 0.7). However, the approach has limitations.
- The relationships between the PDA τ_G values and other soil engineering parameters (e.g., E_{LWD}, M_r, s_u) showed good correlation coefficients ($R^2 > 0.7$). A significant advantage with using the PDA devices is that it is less time consuming than other test methods (i.e., E_{LWD}, UU, UC, or M_r tests).

The general recommendations for future study include:

- Obtain LWD measurements with different device configurations for a wide-variety of soils.
- Different approaches for estimating Eequivalent need to considered and compared to obtain the better correlation relationships.
- A new mold which can better simulate the actual field boundary condition needs to develop for conducting the target value determination study in the laboratory,
- τ_G from PDA provide encouraging results in relating to the engineering properties of the compacted material. Future studies should focus on linking τ_G to field measurements.

REFERENCES

AASHTO. (1999). *Standard method of test for determining the resilient modulus of soils and aggregate materials T-307*, American Association of State Highway and Transportation Officials, Washington, D.C.

ASTM. (1983). "Test method for compaction and shear properties of bituminous mixtures by means of the U.S. Corps of Engineers gyratory testing machine." *Annual book of ASTM Standards, ASTM D3387,* West Conshohocken, PA.

ASTM. (1993). "Standard test method for repetitive static plate load tests of soils and flexible pavement components, for use in evaluation and design of airport and highway pavements." *Annual book of ASTM Standards, ASTM D1195,* West Conshohocken, PA.

ASTM. (2000). "Test method for laboratory compaction characteristics of soils using standard effort." *Annual book of ASTM Standards, ASTM D698,* West Conshohocken, PA.

ASTM. (2000). "Test method for laboratory compaction characteristics of soils using modified effort." *Annual book of ASTM Standards, ASTM D1557,* West Conshohocken, PA.

ASTM. (2000). "Standard classification of soils for engineering purposes (Unified Soil Classification System)." *Annual book of ASTM Standards, ASTM D2487,* West Conshohocken, PA.

ASTM. (2003). "Standard test method for unconsolidated-undrained triaxial compression test on cohesive soils." *Annual Book of ASTM Standards, ASTM D2850,* West Conshohocken, PA.

ASTM. (2003). "Standard test method for use of the dynamic cone penetrometer in shallow pavement applications." *Annual Book of ASTM Standards, ASTM D6951,* West Conshohocken, PA.

ASTM. (2005). "Test method for density of soil and soil aggregate inplace by nuclear methods (shallow depth)." *Annual Book of ASTM Standards, ASTM D2922,* West Conshohocken, PA.

ASTM. (2005). "Test methods for liquid limit, plastic limit, and plasticity index of soils." *Annual Book of ASTM Standards, ASTM D4318,* West Conshohocken, PA.

ASTM. (2006). "Test method for unconfined compressive strength of cohesive soil." *Annual Book of ASTM Standards, ASTM D2166,* West Conshohocken, PA.

Bahia, H. U., and Paye, B.C. (2004). "Using gyratory compactor to measure mechanical stability of asphalt mixtures." Final Report, WisDOT, Madison, WI.

Briaud, J., Li, Y., and Rhee, K. (2006). "BCD: a soil modulus device for compaction control." *Journal of Geotechnical and Geoenvironmental Engineering*, Vol.132, No. 1, pp. 108-115.

Burnham, T., (1996). *Application of the Dynamic Cone Penetrometer to Mn/DOT's Pavement Assessment Procedures*, Revised Draft Report, Office of Minnesota Road Research.

Chaddock, B. C. J., and Brown., A., (1995). "In situ Test for Road Foundation Assessment," *Proc., Unbound Aggregate in Roads – UNBAR 4.* A. Dawson, and B. Jones, Eds., Nottingham, U.K.

Chen, D., Lin, D., Liau, P. and Bilyeu, J. (2005). "A Correlation between Dynamic Cone Penetrometer Values and Pavement Layer Moduli." *Geotechnical Testing Journal*, ASTM International, Vol. 28, No.1, p. 42-49

Coyle, H. M., and West, E. C. (1956). *Laboratory compaction of a silty clay to simulate field density curves*, MS Thesis, Massachusetts Institute of Technology, MA.

Fleming, P. R., Lambert, J. P., Frost, M. W. and Rogers, C. D. "In situ assessment of stiffness modulus for highway foundations during construction." *In Proceedings of the 9th International Conference on Asphalt Pavements, Copenhagen, 2002*. International Society for Asphalt Pavements, White Bear Lake, MN, USA, 2002, pp. 1–12 (CD-ROM).

Fleming, P.R., Frost, M.W., and Lambert, J.P., (2007). "Review of Light Weight Deflectometer for Routine In Situ Assessment of Pavement Material Stiffness." *Transportation Research Record. 2004*, Transportation Research Board, Washington D.C., 80-87.

George, K.P., (2003). *Falling Weight Deflectometer for Estimating Subgrade Resilient Moduli*, Final Report FHWA/MS-DOT-RD-03. Mississippi Department of Transportation, Jackson, MS.

Guler, M., Bahia, H. U., Bosscher, P. J., and Plesha, M. E. (1996). "Device for Measuring Shear Resistance of Hot-Mix Asphalt in Gyratory Compactor." *Transportation Research Record: Journal of the Transportation Research Board,* No. 1723, 116-124.

Gupta , S., Kang, D.H., Ranaivoson, A. (2009). *Hydraulic, Mechanical, and Leaching Characteristics of Recylced Materials.* Draft Report submitted Minnesota Department of Transportation, St. Paul, MN.

Harrison, J.A. (1986). "Correlation of CBR and Dynamic Cone Penetrometer Strength Measurement of Soils" Australian Road Research, June 1986, Vol. 16, No.2, pp130-136.

Kelyn, E.G. (1975), "The Use of the Dynamic Cone Penetrometer (DCP)." Report 2/74.

Transvaal Roads Department, Pretoria.

Kim, W., and Labuz, J. (2006). *Resilient modulus and strength of base course with recycled bituminous material,* Final Report MN/RC 2007-05. Minnesota Department of Transportation, St. Paul, MN.

KUAB (2009). *Operation and technical reference manual*: *KUAB 2m-FWD model KUAB 150*, Rättvik, Sweden.

Li, Y. (2004). Use of a BCD for Compaction Control, Department of Civil Engineering, Texas A&M University, Ph.D.

Lin. D., Liau, C., and Lin, J., (2006). "Factors Affecting Portable Falling Weight Deflectometer Measurements," *J. Geotech. Geoenviron. Eng.,* Vol. 132, No.6, 804-808.

Livneh, M., Ishai, I., and Livneh, N., (1995). "Effect of the Vertical Confinement on Dynamic Cone Penetrometer Strength Values in Pavement and Subgrade Evaluations," TRR 1473, pp. 1-8.

Livneh, M., and I. Ishai. Pavement and Material Evaluation by a Dynamic Cone Penetrometer (1987), *Proc., Sixth International Conference on the Structural Design of Asphalt Pavement,* Vol. 1, Ann Arbor, Michigan, pp. 665-674.

McElvaney, J., and Djatnika, I. (1991). "Strength evaluation of lime-stabilized pavement foundations using the dynamic cone penetrometer." *Australian Road Research*, 21(1), 40-52.

McRae, J. L. (1965). *Gyratory testing machine technical manual for bituminous mixtures, soils, and base course materials,* Engineering Developments Company, Inc., Vicksburg, MA.

Mooney, M.A., and Miller, P.K., (2009). "Analysis of Lightweight Deflectometer Test Based on In Situ Stress and Strain Response." *J. Geotech. Geoenviron. Eng.,* Vol. 135, pp. 199-207.

Odemark (1949). "Investigations as to the Elastic Properties of Soils and Design of Pavements according to the Theory of Elasticity," *Statens Väginstitut, Mitteilung* No.77, Stockholm, Sweden.

Pressure Distribution Analyzer, (2007). *Operating manual, Test Quip LLC*, Barnes, WI

Powell, W. D., Potter, J. F., Mayhew, H. C., and Nunn, M. E., (1984). "The Structural Design of Bituminous Roads." *TRRL Report LR 1132*, pp.62.

Puppala, A.J., (2008). "Estimating Stiffness of Subgrade and Unbound Materials for Pavement Design," *NCHRP Project 20-5, Synthesis Topic 38-09*, Transportation Research Board.

Rhee, K. (2008). PhD Dissertation, Texas A&M University, College Station, TX.

Siekmeier, J. A., Young, D., and Beberg, D. (2000). "Comparison of the Dynamic Cone Penetrometer with Other Tests during Subgrade and Granular Base Characterization in Minnesota." *Nondestructive testing of pavements and backcalculation of moduli: ASTM STP 1375*, S. D. Tayabji and E. O. Lukanen, eds., Vol. 3, ASTM, Philadelphia.

Sridharan, A., Gandhi, and Suresh, S., (1990). "Stiffness Coefficients of Layered Soil Systems." *J. Geotech. Eng.,* Vol. 116, pp.604-624.

Terzaghi, K., 1955, "Evaluation of Coefficient of Subgrade Reaction," *Geotechnique*, Vol.5, No.4, pp.297-326.

Ullidtz, Per. (1987). *Pavement Analysis*. Vol. 19. Amsterdam: Elsevier Science.

Vennapusa, P.K., and White, D.J., (2009). "Comparison of Light Weight Deflectometer Measurements for Pavement Foundation Materials." *Geotechnical Testing Journal*, Vol. 32, No.3, West Conshohocken, PA, p. 239-251.

Webster, S.L., Grau, R.H., and Williams, R.P., (1992). "Description and Application of Dual Mass Dynamic Cone Penetrometer," U.S. Army Engineer Waterways Experiment Station, Instruction Report, No. GL-92-3.

Weidinger, D.M., Ge, L., (2009). "Laboratory Evaluation of the Briaud Compaction Device." *Journal of Geotechnical and Geoenvironmental Engineering*. Vol. 135, No. 10, pp.1543-1546.

White, D. J., Vennapusa, P., Zhang, J. Gieselman, H. and Morris, M. (2009). *Implementation of Intelligent Compaction Performance Based Specifications in Minnesota.* Final Report, EERC 09-02, Earthworks Engineering Research Center, Iowa State University, Ames, IA.

Zorn, G. (2000). *Operating manual: Light drop-weight tester ZFG2000,* Zorn Stendal, Germany.

ACKNOWLEDGEMENTS

APPENDIX I: FIELD TEST DATA

DCP and CBR plot from Geosynthetic Reinforcement Study
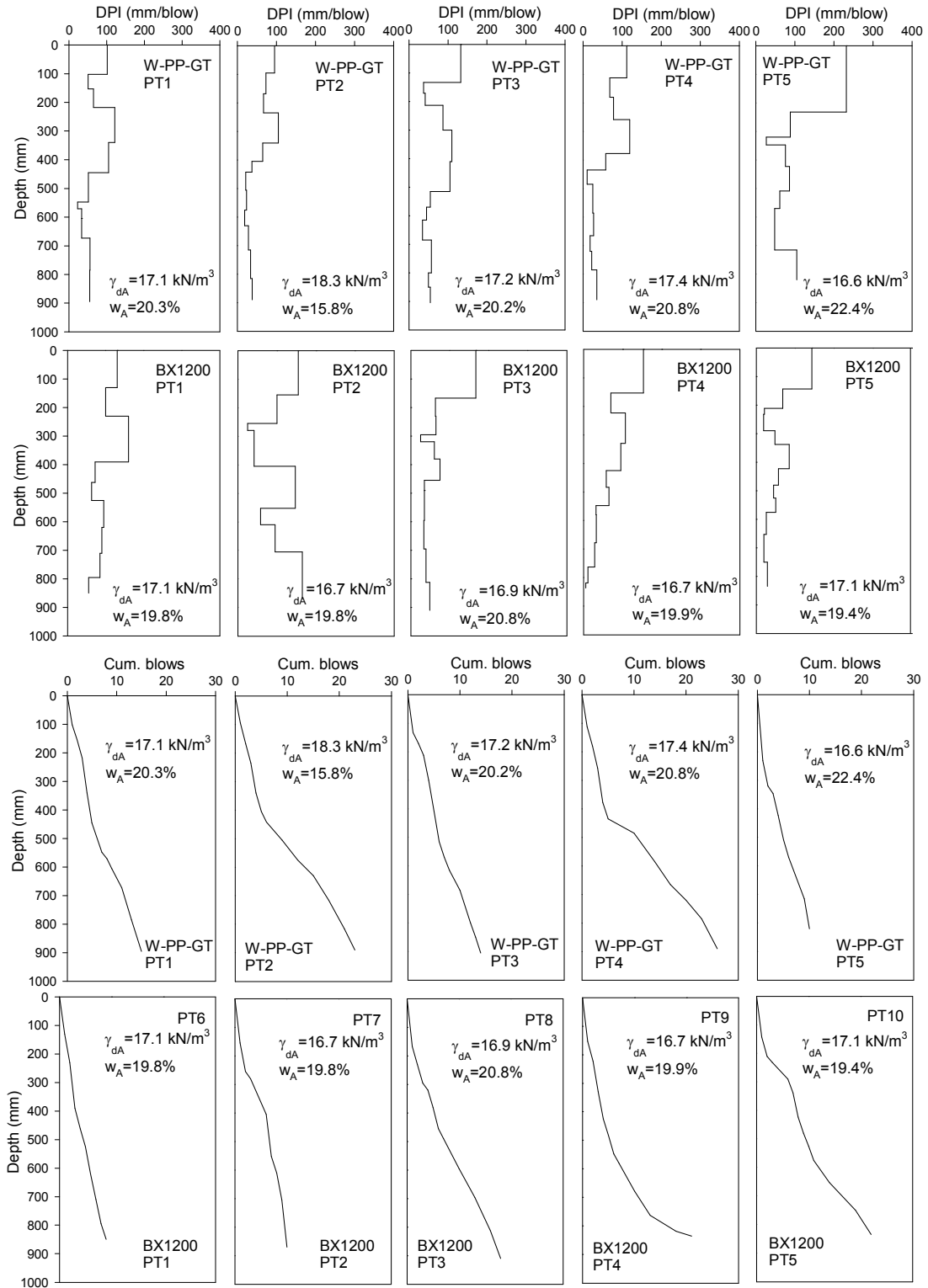
Figure 124. DCP profiles for W-PP-GT and BX1200 sections
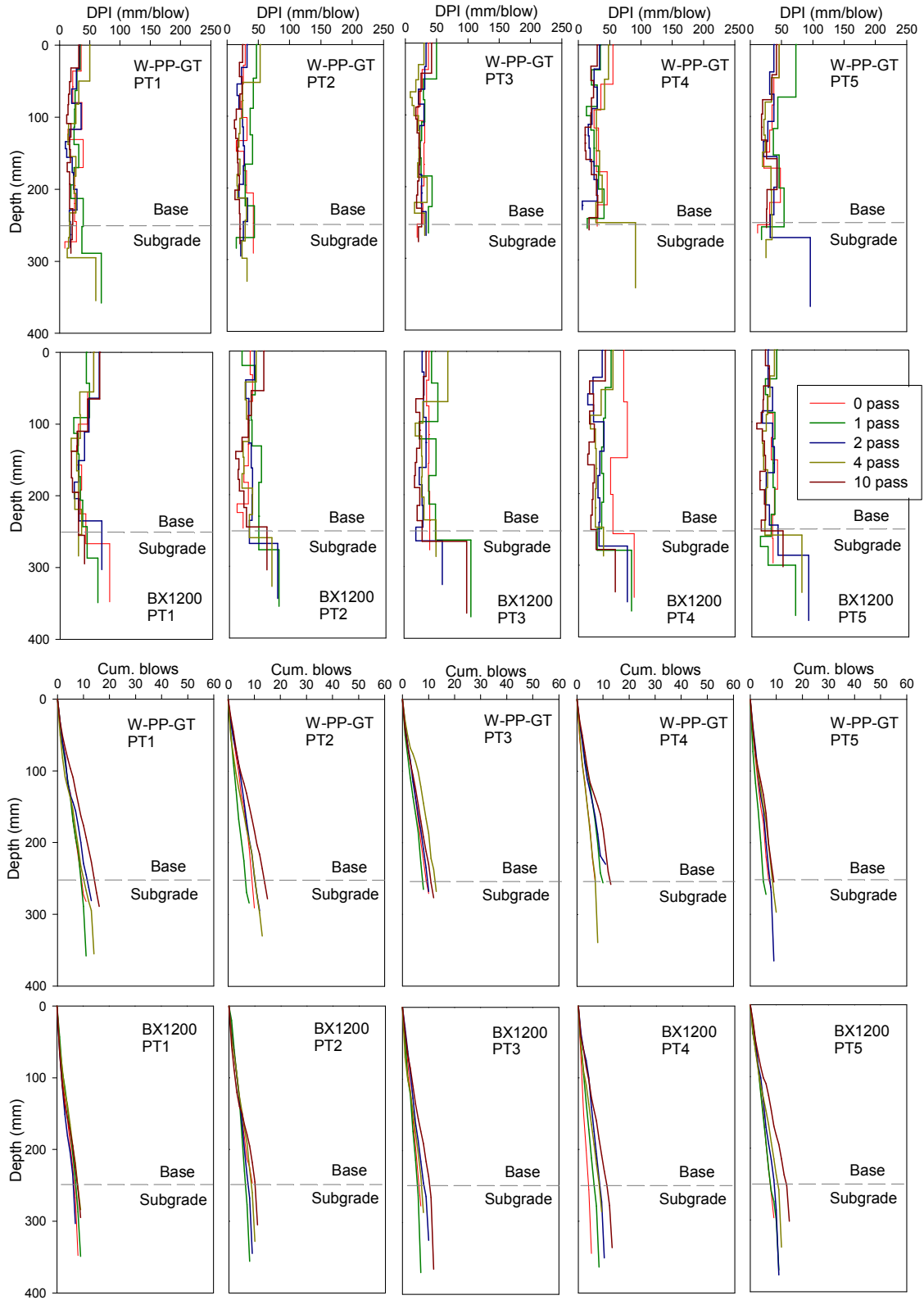
Figure 125. DCP profiles for W-PP-GT and BX1200 sections – subbase layer 1
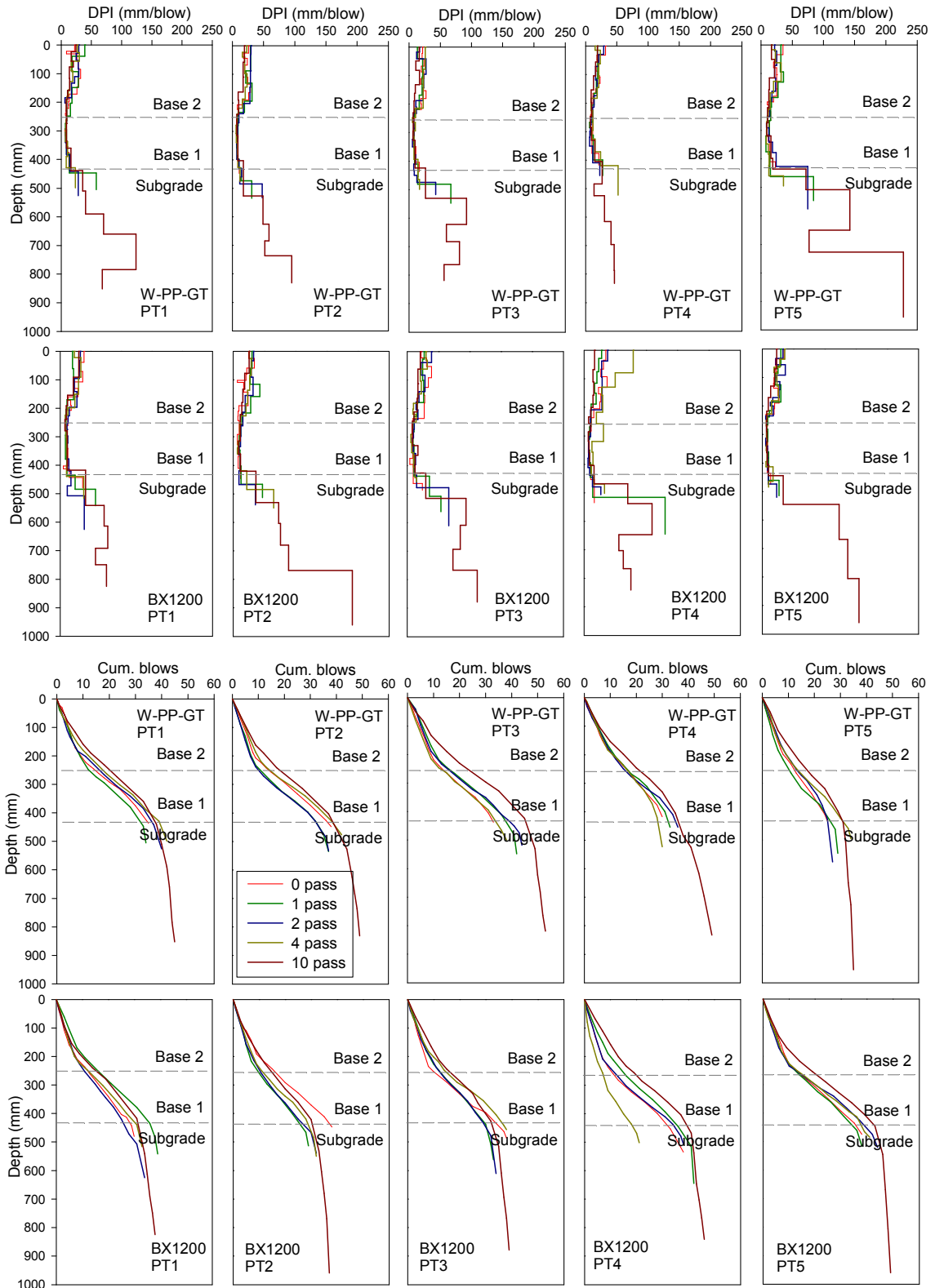
Figure 126. DCP profiles for W-PP-GT and BX1200 section – subbase layer 2
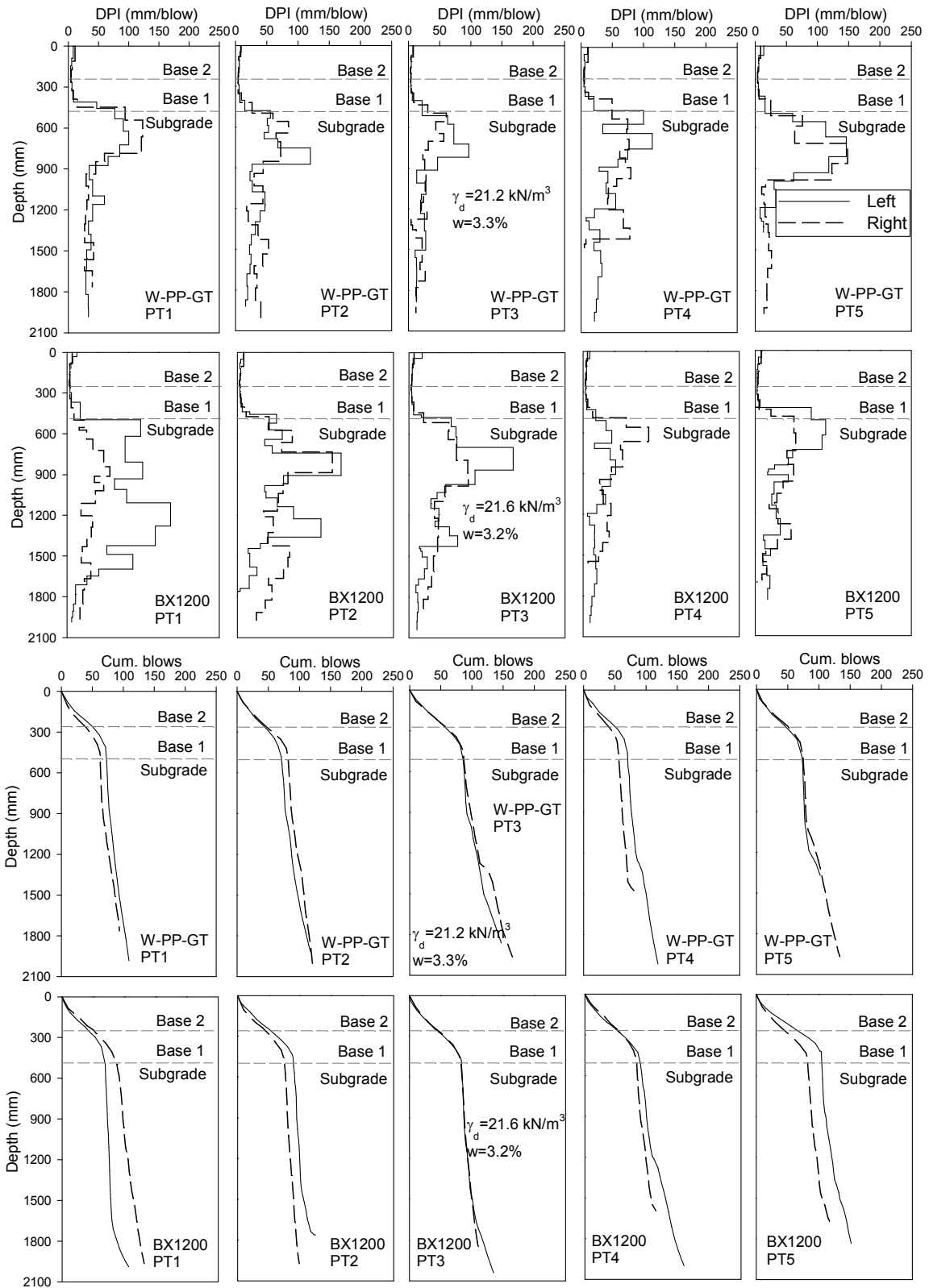
Figure 127. DCP profiles for W-PP-GT and BX1200 sections – final full depth test
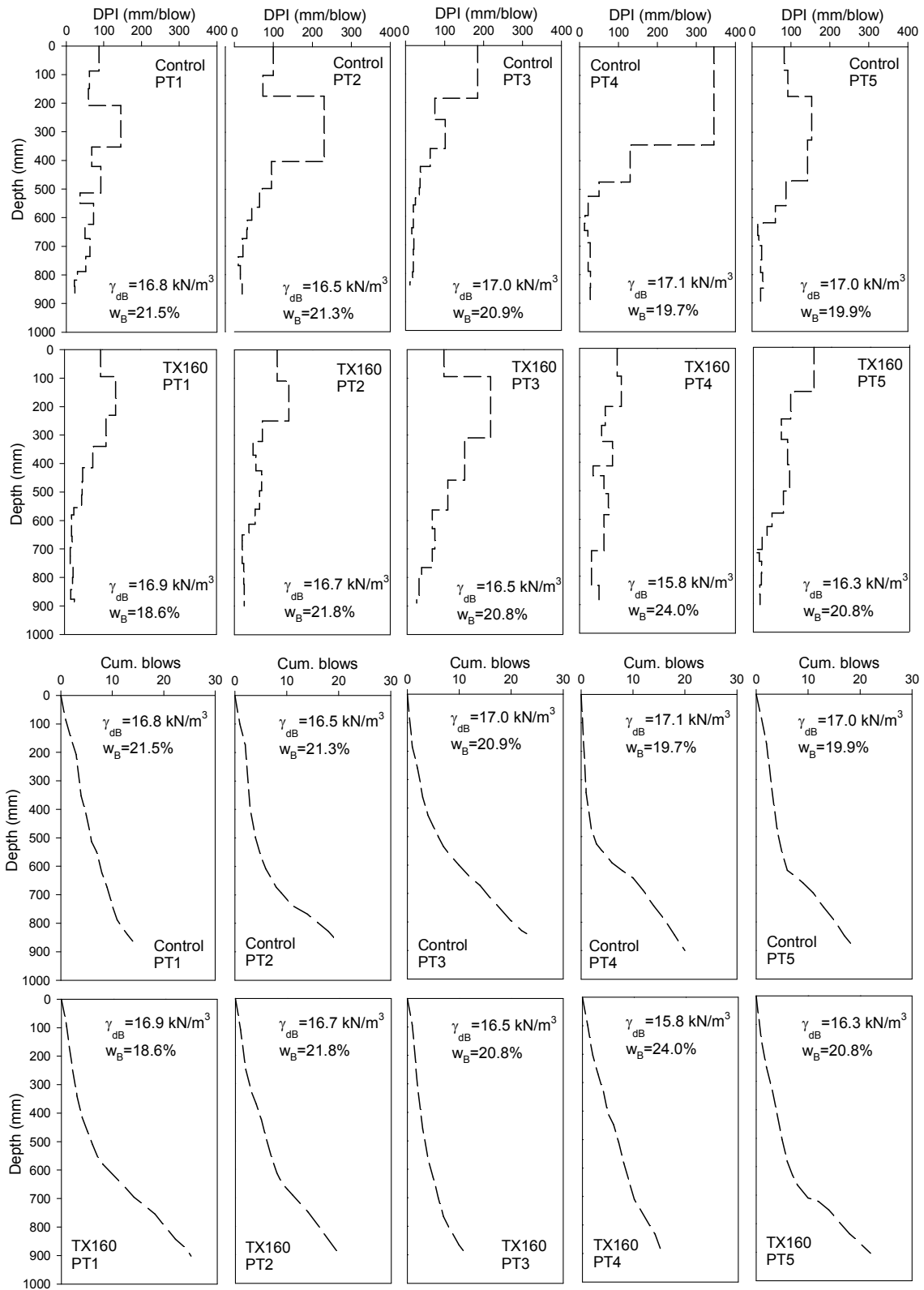
Figure 128. DCP profiles for control and TX160 sections
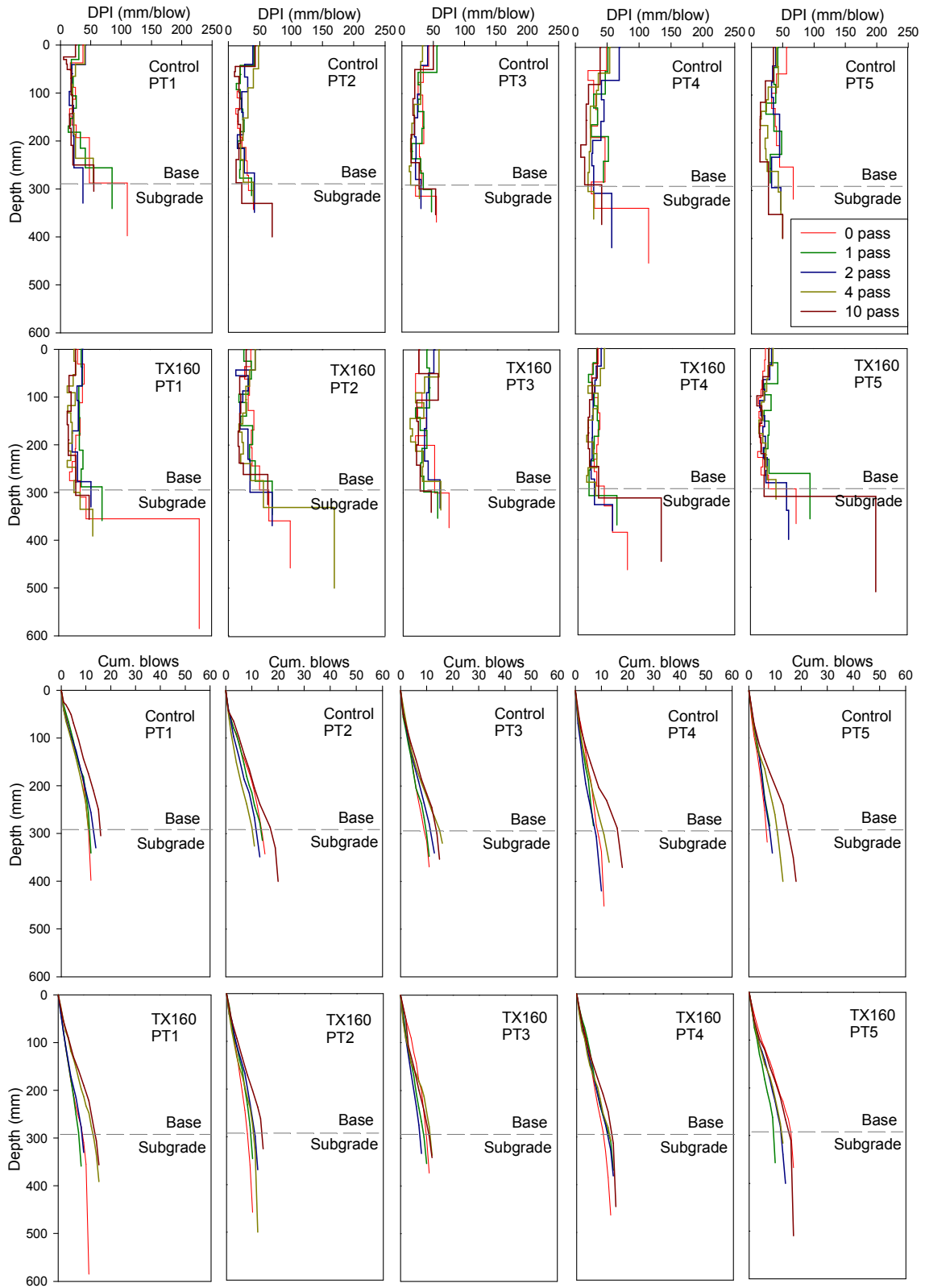
Figure 129. DCP profiles for control and TX160 sections – subbase layer 1
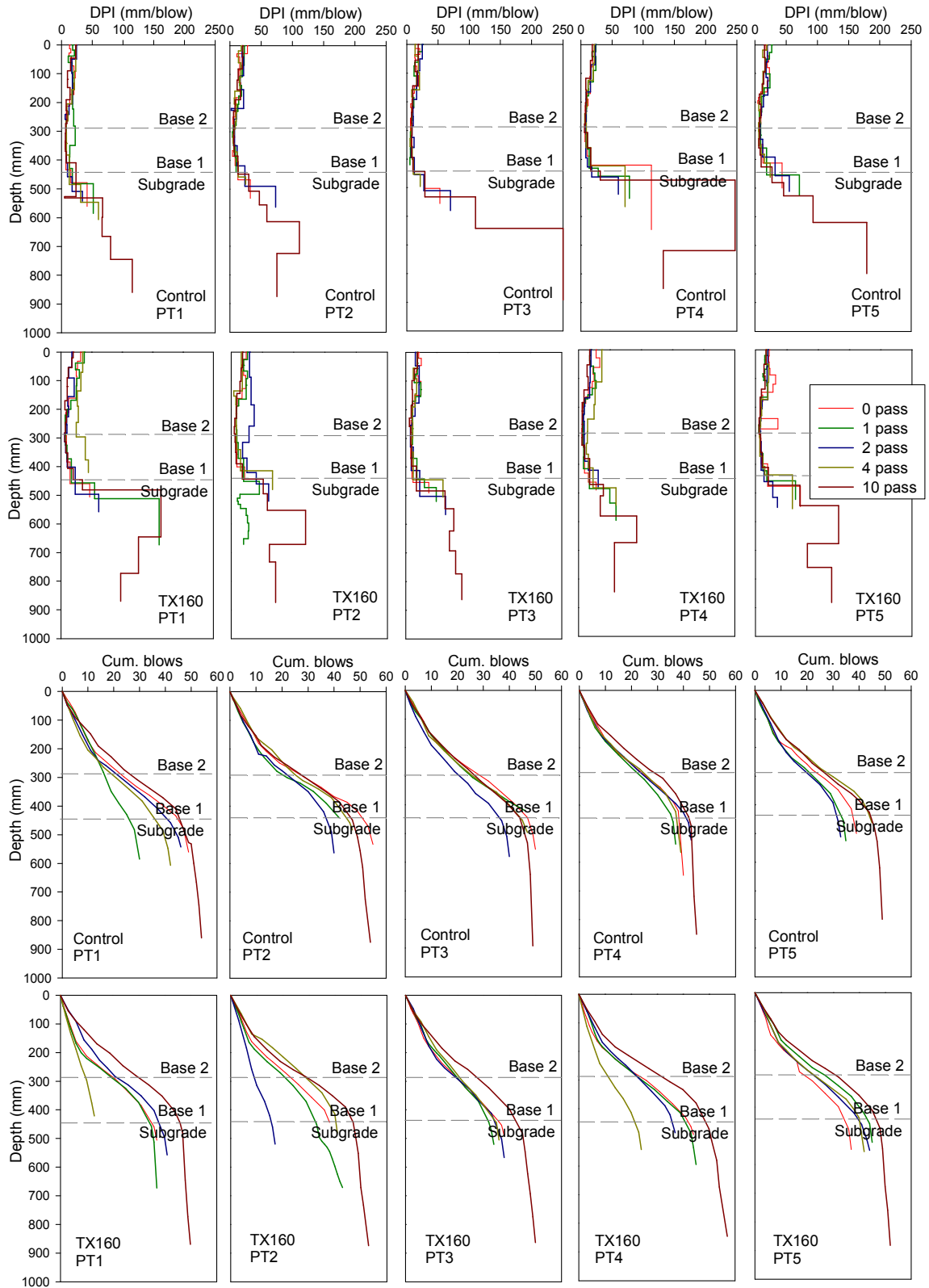
Figure 130. DCP profiles for control and TX160 sections – subbase layer 2
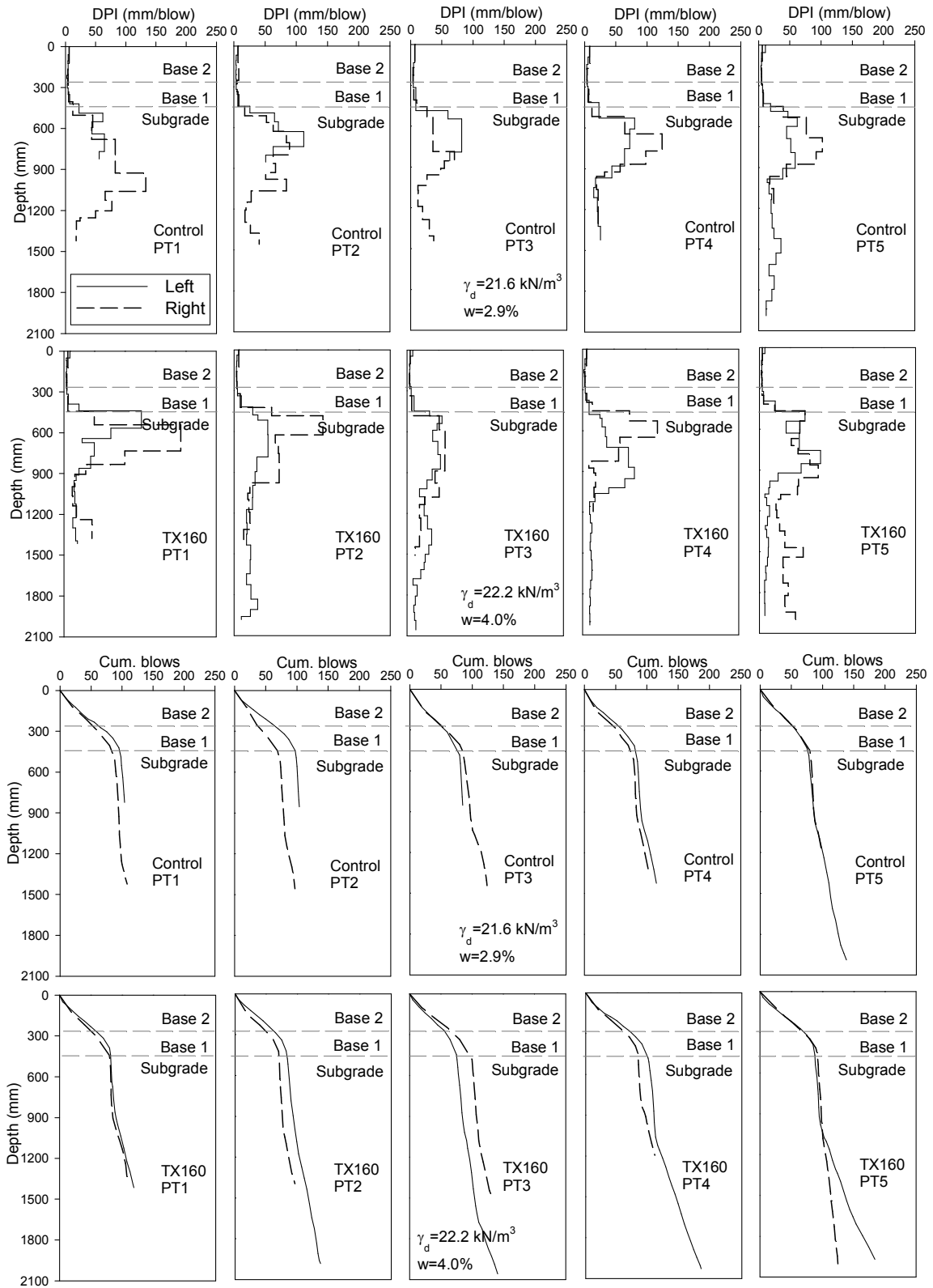
Figure 131. DCP profiles for control and TX160 sections – final full depth test
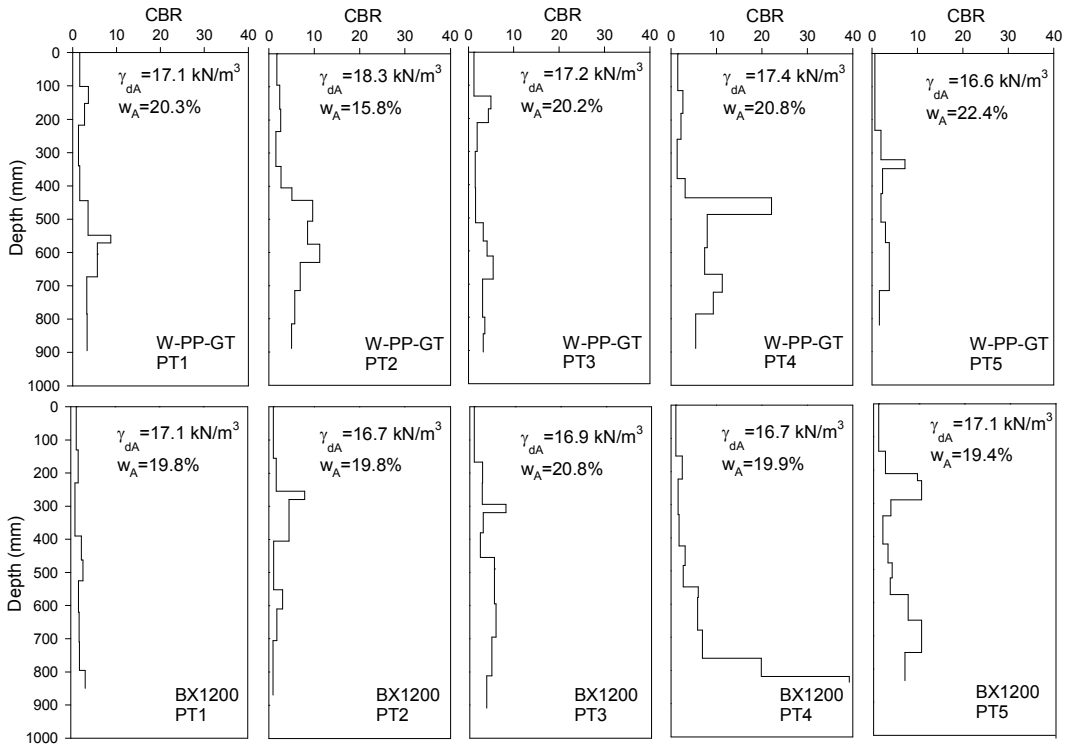
Figure 132. CBR profiles for subgrade layer for W-PP-GT and BX1200 sections
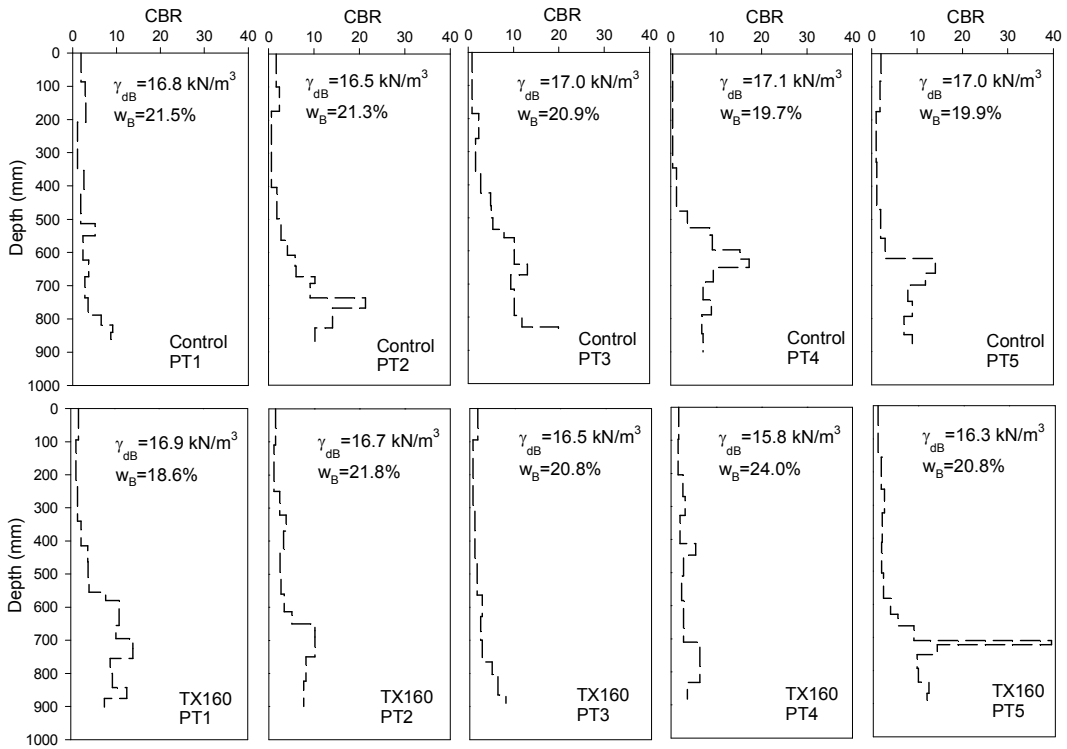
Figure 133. CBR profiles for subgrade layer for control and TX160 sections
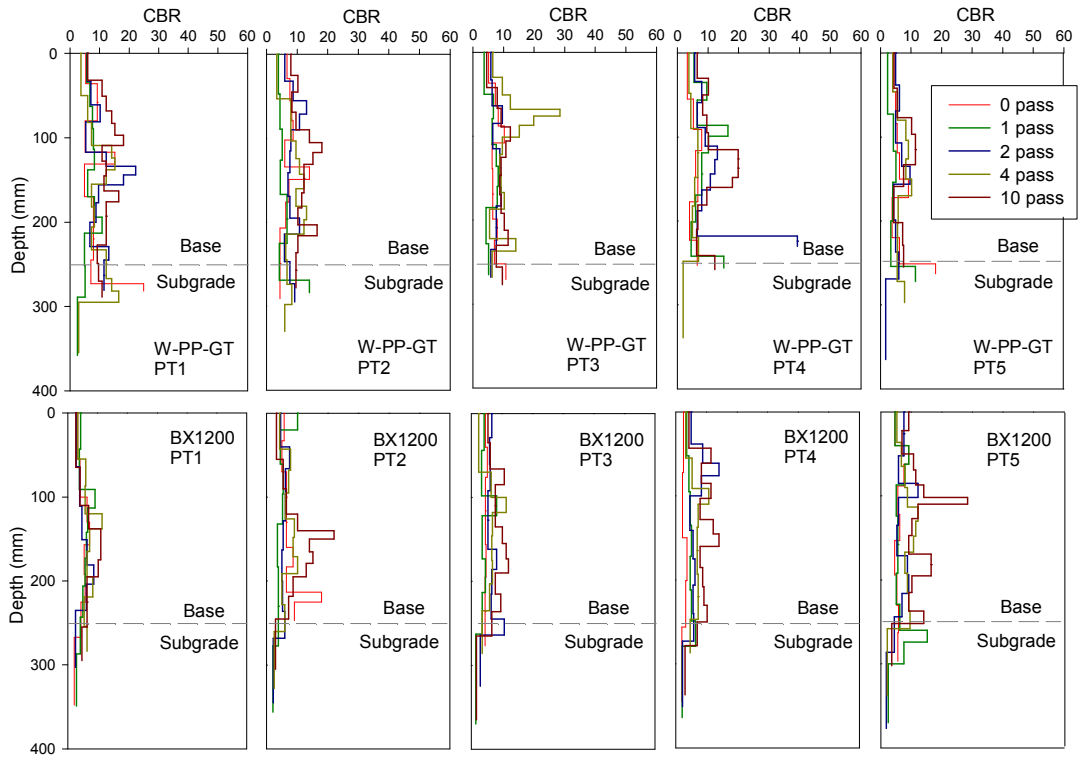
Figure 134. CBR profiles for W-PP-GT and BX1200 sections – subbase layer 1
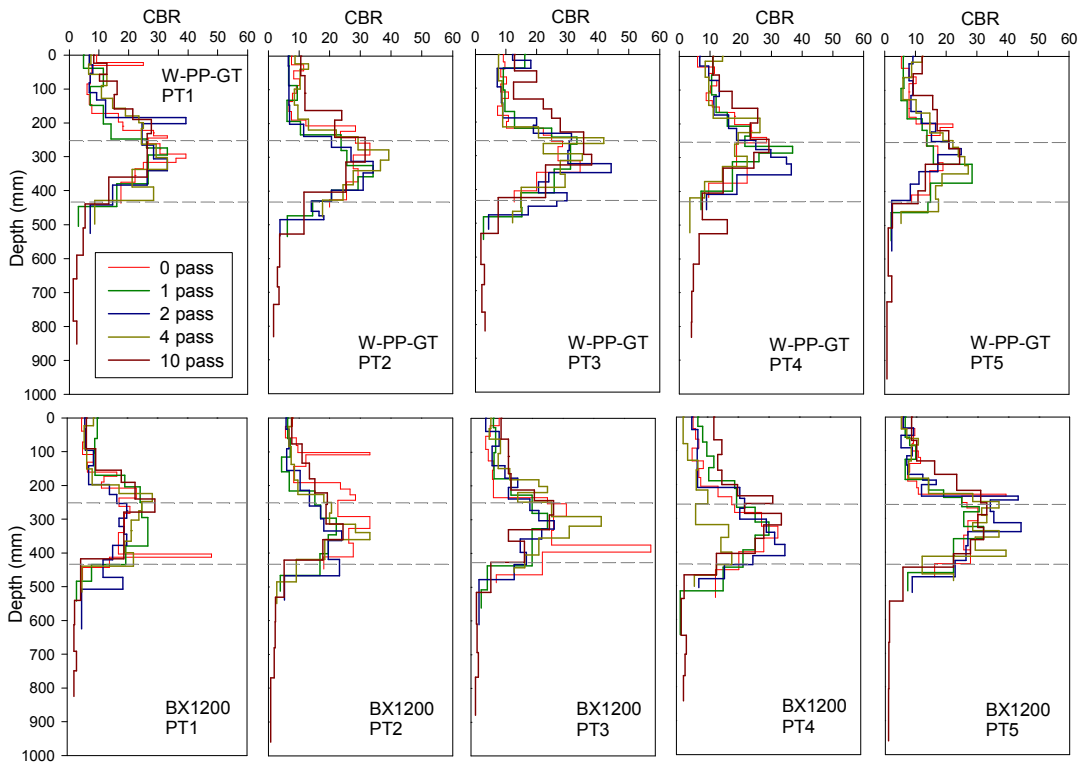
Figure 135. CBR profiles for W-PP-GT and BX1200 sections – subbase layer 2
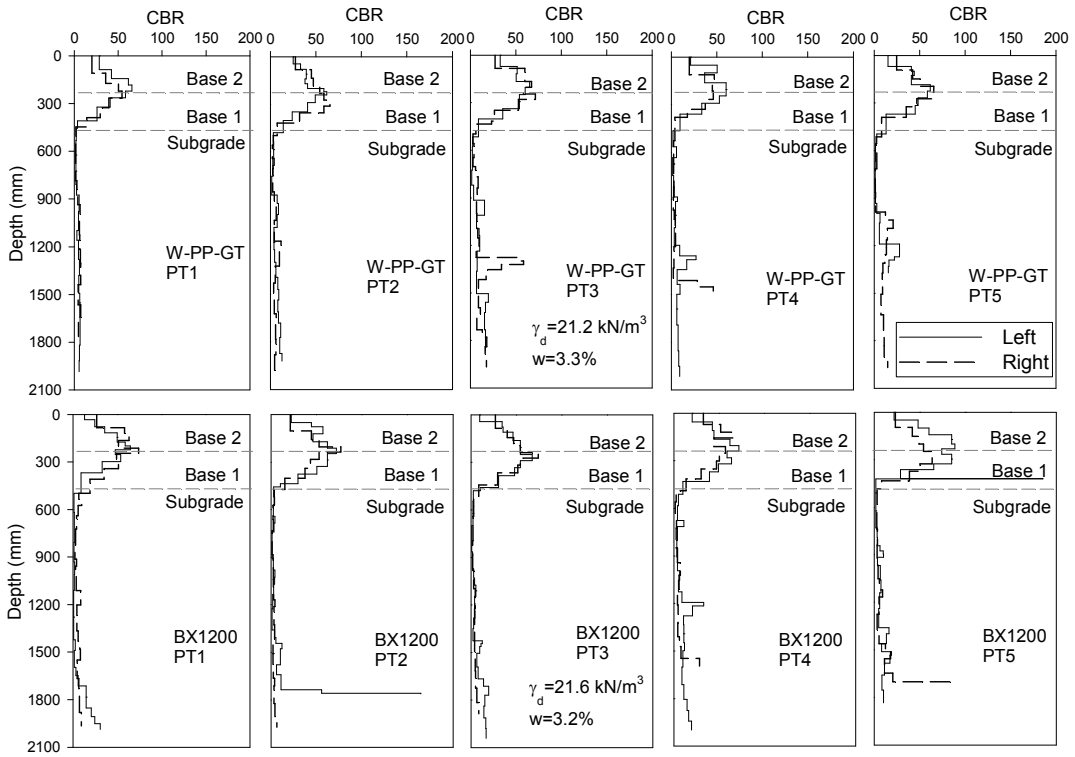
Figure 136. CBR profiles for W-PP-GT and BX1200 sections – final full depth test
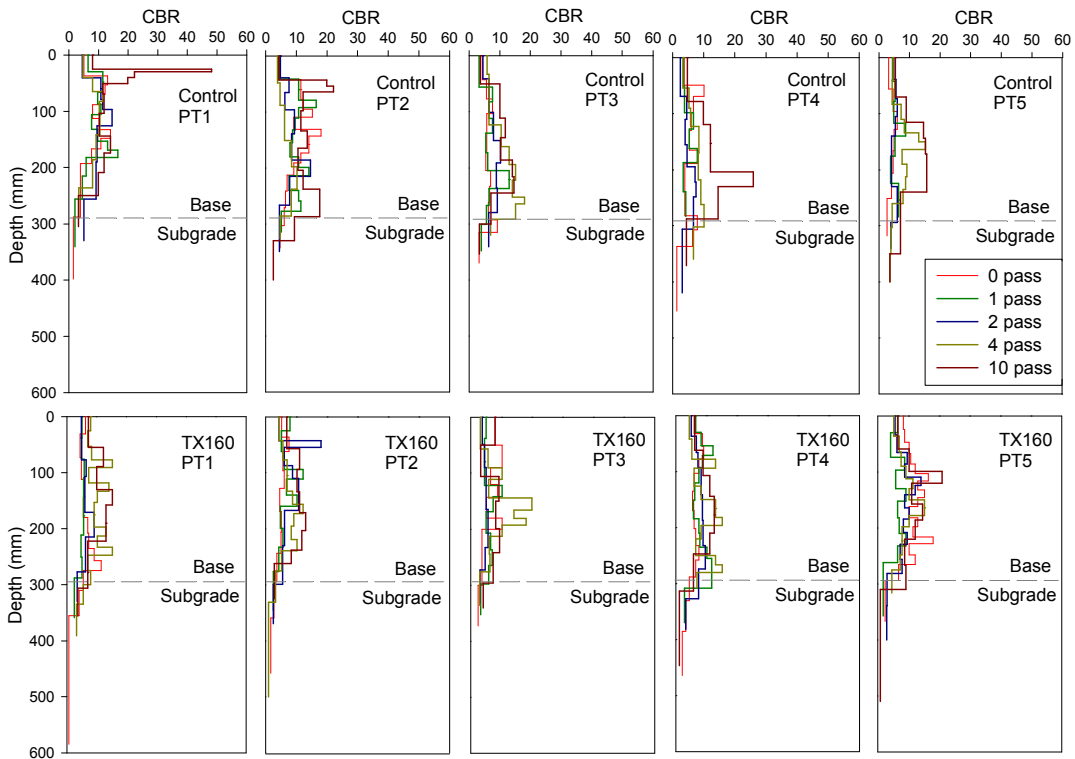
Figure 137. CBR profiles for control and TX160 sections – subbase layer 1
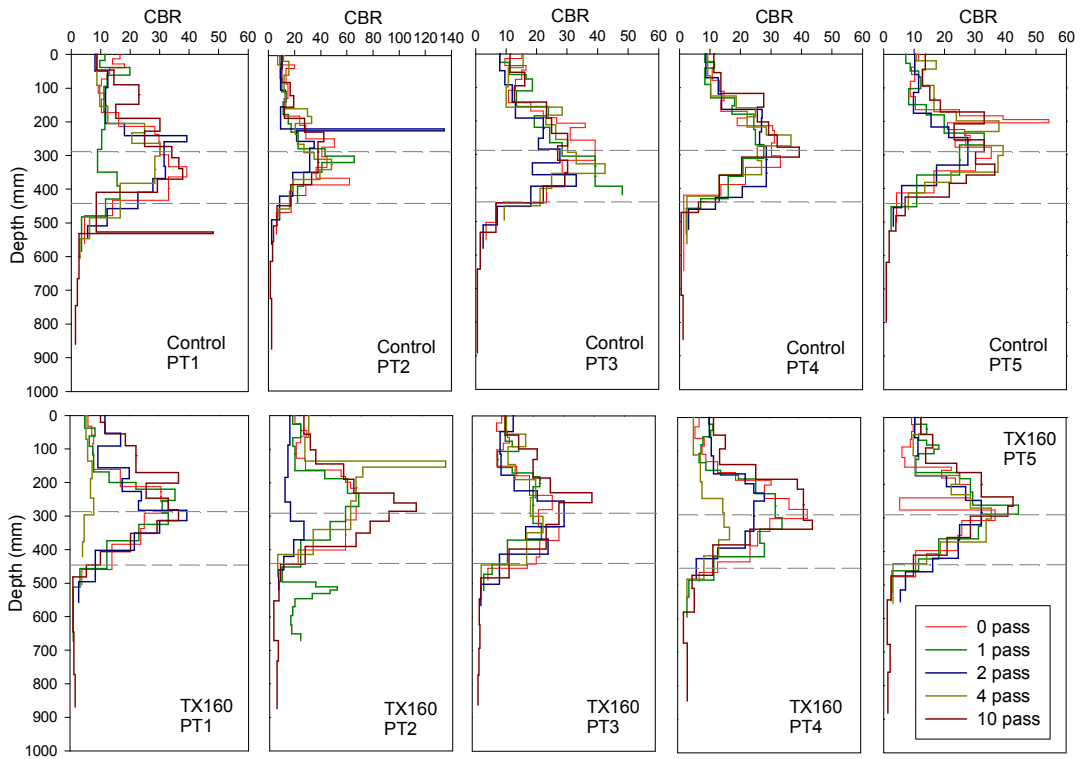
Figure 138. CBR profiles for control and TX160 sections – subbase layer 2
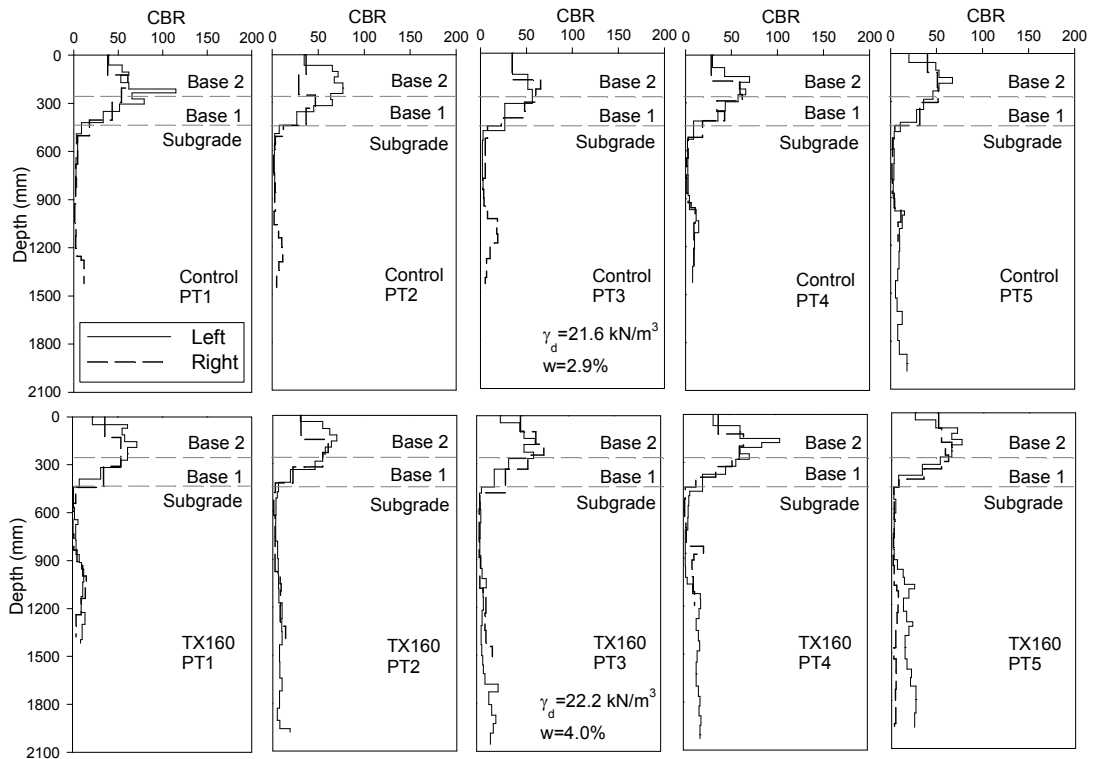
Figure 139. CBR profiles for control and TX160 sections – final full depth test

Table 19. Summary of DCP testing on subgrade

Section	Point	Material	Depth Range (mm)	DPI	CBR
W-PP-GT	1	Subgrade	0 – 571	71.4	2.5
W-PP-GT	2	Subgrade	0 – 442	73.7	2.4
W-PP-GT	3	Subgrade	0 – 615	76.9	2.3
W-PP-GT	4	Subgrade	0 – 435	87.0	2.0
W-PP-GT	5	Subgrade	0 – 570	95.0	1.8
BX1200	1	Subgrade	0 – 620	103.3	1.6
BX1200	2	Subgrade	0 – 552	78.9	2.2
BX1200	3	Subgrade	0 – 490	70.0	2.5
BX1200	4	Subgrade	0 – 580	82.9	2.1
BX1200	5	Subgrade	0 – 575	52.3	3.6
Control	1	Subgrade	0 – 623	77.9	2.2
Control	2	Subgrade	0 – 641	91.6	1.9
Control	3	Subgrade	0 – 535	76.4	2.3
Control	4	Subgrade	0 – 592	98.7	1.7
Control	5	Subgrade	0 – 633	90.4	1.9
TX160	1	Subgrade	0 – 580	72.5	2.4
TX160	2	Subgrade	0 – 613	76.6	2.3
TX160	3	Subgrade	0 – 628	125.6	1.3
TX160	4	Subgrade	0 – 584	73.0	2.4
TX160	5	Subgrade	0 – 582	97.0	1.7

Table 20. Summary of DCP testing on subbase 1

Section	Point	Material	Depth Range (mm)	DPI	CBR
W-PP-GT	1	Subbase 1	0 – 193	17.5	11.8
W-PP-GT	2	Subbase 1	0 – 203	18.5	11.2
W-PP-GT	3	Subbase 1	0 – 212	23.6	8.5
W-PP-GT	4	Subbase 1	0 – 210	19.1	10.7
W-PP-GT	5	Subbase 1	0 – 202	28.9	6.8
BX1200	1	Subbase 1	0 – 225	32.1	6.0
BX1200	2	Subbase 1	0 – 218	24.2	8.2
BX1200	3	Subbase 1	0 – 215	23.9	8.4
BX1200	4	Subbase 1	0 – 208	23.1	8.7
BX1200	5	Subbase 1	0 – 215	17.9	11.5
Control	1	Subbase 1	0 – 209	16.1	13.0
Control	2	Subbase 1	0 – 204	18.5	11.1
Control	3	Subbase 1	0 – 216	21.6	9.3
Control	4	Subbase 1	0 – 204	22.7	8.9
Control	5	Subbase 1	0 – 240	18.5	11.1
TX160	1	Subbase 1	0 – 222	18.5	11.1
TX160	2	Subbase 1	0 – 203	20.3	10.0
TX160	3	Subbase 1	0 – 199	28.4	6.9
TX160	4	Subbase 1	0 – 210	21.0	9.6
TX160	5	Subbase 1	0 – 220	18.3	11.2

Table 21. Summary of DCP testing on TB-A after trafficking subbase 2

Section	Point	Material	Depth Range (mm)	DPI	CBR
W-PP-GT	1L	Subbase[1]	0 – 409	5.8	41.1
		Subgrade	409 – 875	77.7	2.2
W-PP-GT	1R	Subbase[1]	0 – 389	6.7	34.6
		Subgrade	448 – 846	99.5	1.7
W-PP-GT	2L	Subbase[1]	0 – 404	6.1	38.4
		Subgrade	480 – 874	65.7	2.7
W-PP-GT	2R	Subbase[1]	0 – 419	5.3	45.1
		Subgrade	499 – 854	71.0	2.5
W-PP-GT	3L	Subbase[1]	0 – 403	5.0	48.4
		Subgrade	515 – 821	76.5	2.3
W-PP-GT	3R	Subbase[1]	0 – 416	5.0	48.0
		Subgrade	497 – 767	45.0	4.1
W-PP-GT	4L	Subbase[1]	0 – 361	5.6	42.8
		Subgrade	466 – 824	71.6	2.4
W-PP-GT	4R	Subbase[1]	0 – 331	6.6	35.2
		Subgrade	529 – 887	71.6	2.4
W-PP-GT	5L	Subbase[1]	0 – 369	5.7	41.8
		Subgrade	496 – 933	109.3	1.5
W-PP-GT	5R	Subbase[1]	0 – 389	5.6	42.8
		Subgrade	513 – 864	87.8	1.9
BX1200	1L	Subbase[1]	0 – 367	5.8	40.6
		Subgrade	497 – 932	108.8	1.5
BX1200	1R	Subbase[1]	0 – 408	5.1	47.1
		Subgrade	574 – 958	48.0	3.8
BX1200	2L	Subbase[1]	0 – 375	4.7	51.8
		Subgrade	437 – 907	67.1	2.6
BX1200	2R	Subbase[1]	0 – 401	5.7	41.3
		Subgrade	574 – 885	103.7	1.6
BX1200	3L	Subbase[1]	0 – 383	5.3	44.9
		Subgrade	478 – 865	96.8	1.7
BX1200	3R	Subbase[1]	0 – 365	5.2	45.9
		Subgrade	641 – 982	85.3	2.0
BX1200	4L	Subbase[1]	0 – 429	5.0	47.6
		Subgrade	511 – 906	39.5	4.8
BX1200	4R	Subbase[1]	0 – 413	5.3	45.2
		Subgrade	490 – 851	72.2	2.4
BX1200	5L	Subbase[1]	0 – 363	3.8	65.1
		Subgrade	421 – 844	84.6	2.0
BX1200	5R	Subbase[1]	0 – 434	5.4	43.9
		Subgrade	484 – 963	59.9	3.0

[1] Subbase includes subbase 1 and subbase 2 as included in depth ranges.

Table 22. Summary of DCP testing on TB-B after trafficking subbase 2

Section	Point	Material	Depth Range (mm)	DPI	CBR
Control	1L	Subbase[1]	0 – 421	4.4	55.1
		Subgrade	489 – 824	55.8	3.2
Control	1R	Subbase[1]	0 – 405	5.1	47.5
		Subgrade	503 – 927	60.6	2.9
Control	2L	Subbase[1]	0 – 442	4.6	53.4
		Subgrade	493 – 855	51.7	3.5
Control	2R	Subbase[1]	0 – 443	6.4	36.4
		Subgrade	512 – 930	69.7	2.5
Control	3L	Subbase[1]	0 – 485	6.1	38.8
		Subgrade	485 – 854	73.8	2.4
Control	3R	Subbase[1]	0 – 407	5.1	47.2
		Subgrade	534 – 957	42.3	4.4
Control	4L	Subbase[1]	0 – 414	5.2	46.3
		Subgrade	528 – 967	62.7	2.8
Control	4R	Subbase[1]	0 – 410	5.9	40.3
		Subgrade	516 – 924	81.6	2.1
Control	5L	Subbase[1]	0 – 430	5.7	41.3
		Subgrade	488 – 907	52.4	3.5
Control	5R	Subbase[1]	0 – 450	5.6	42.2
		Subgrade	529 – 876	86.8	2.0
TX160	1L	Subbase[1]	0 – 389	4.9	49.7
		Subgrade	439 – 911	52.4	3.5
TX160	1R	Subbase[1]	0 – 442	5.5	43.0
		Subgrade	542 – 906	91.0	1.9
TX160	2L	Subbase[1]	0 – 338	4.5	54.1
		Subgrade	516 – 896	47.5	3.9
TX160	2R	Subbase[1]	0 – 423	6.0	38.9
		Subgrade	483 – 978	82.5	2.1
TX160	3L	Subbase[1]	0 – 335	5.2	46.5
		Subgrade	484 – 875	48.9	3.7
TX160	3R	Subbase[1]	0 – 482	4.8	50.2
		Subgrade	482 – 888	58.0	3.1
TX160	4L	Subbase[1]	0 – 376	4.2	58.9
		Subgrade	572 – 952	54.3	3.3
TX160	4R	Subbase[1]	0 – 392	4.9	49.2
		Subgrade	454 – 825	74.2	2.3
TX160	5L	Subbase[1]	0 – 391	4.6	52.9
		Subgrade	468 – 920	64.6	2.7
TX160	5R	Subbase[1]	0 – 416	4.6	52.6
		Subgrade	465 - 956	70.1	2.5

[1] Subbase includes subbase 1 and subbase 2 as included in depth ranges.

Raw Data from the Influence of Layered Soil Profiles on Surface Modulus Study

Soft soil over stiff soil – Data from Ohio Bridge Approach Project Site

Table 23. Raw data for the correlation between $E_{equivalent}$ and E_{LWD-Z2} – Ohio Site

PT#	Sum (I_Z)	Sum (CBR×I_Z)	$CBR_{equi.}$ [Sum (CBR×I_Z)/ Sum (I_Z)]	$E_{equi.}$	E_{LWD-Z2}
1	12.5	229.0	18.3	113.0	61.9
2	0.03	0.005	0.2	5.9	5.9
3	4.2	69.2	16.6	106.3	17.7
4	7.5	133.0	17.7	110.6	38.1
5	7.9	123.7	15.6	102.0	51.4
6	6.8	101.3	14.9	98.9	52.3
7	14.9	462.5	31.1	158.7	85.7
8	10.6	423.7	40.0	186.2	73.5
9	2.1	7.3	3.5	39.5	8.9
10	5.9	106.7	18.2	112.5	36.1
11	9.3	154.7	16.6	106.3	59.7
12	11.1	221.3	20.0	119.5	68.2
13	3.2	34.6	10.9	80.9	47.3
14	7.2	164.1	22.9	130.3	61.4
15	0.6	5.3	8.8	70.8	8.0
16	16.0	354.8	22.2	127.7	19.6
17	5.9	106.2	17.9	111.3	21.2
18	8.8	164.2	18.7	114.5	27.7
19	13.7	381.6	27.9	148.1	29.5
20	4.6	60.6	13.1	91.3	13.9
21	3.3	18.0	5.4	51.8	8.5
22	0.5	1.1	2.1	28.7	7.5
23	7.5	179.9	23.9	133.9	29.6
24	7.0	183.3	26.3	142.5	28.1
25	5.6	166.1	29.6	153.8	39.8
26	4.1	65.0	15.7	102.5	22.9
27	0.8	1.9	2.5	31.6	7.7
28	3.5	36.5	10.5	79.0	18.6
29	7.6	170.6	22.5	129.1	35.0
30	6.3	89.3	14.1	95.6	26.8
31	2.8	30.9	11.1	81.9	20.4

Stiff soil over soft soil – Data from Hormel PCC Project Site

Table 24. Raw data for the correlation between E$_{equivalent}$ and E$_{LWD-Z2}$ – Dubuque Site

PT#	Sum (I$_Z$)	Sum (CBR×I$_Z$)	CBR$_{equi.}$ [Sum (CBR×I$_Z$)/ Sum (I$_Z$)]	E$_{equi.}$	E$_{LWD-Z2}$
1	25.7	1407.0	54.8	227.9	40.2
2	11.5	238.6	20.7	122.3	20.0
3	22.6	989.0	43.8	197.6	24.6
4	10.1	172.2	17.0	107.9	14.7
5	23.1	1176.5	51.0	217.6	25.6
6	4.2	24.7	5.9	54.6	13.7
7	7.7	122.5	15.8	103.0	16.2
8	5.7	54.2	9.5	74.1	13.3
9	12.6	272.0	21.6	125.5	21.2
10	9.2	443.7	48.1	209.6	30.6
11	5.2	83.9	16.1	104.0	17.6
12	10.2	312.8	30.7	157.2	25.2
13	18.1	905.9	49.9	214.8	85.1
14	7.6	130.8	17.1	108.3	15.0
15	8.7	240.2	27.5	146.7	19.3
16	12.5	526.3	42.1	192.6	46.9
17	11.1	294.1	26.6	143.4	37.0
18	10.9	355.4	32.7	163.7	32.3
19	14.1	523.8	37.2	177.8	36.6
20	13.1	294.3	22.5	129.0	17.7
21	17.8	546.0	30.6	157.1	30.0
22	13.6	345.7	25.5	139.6	18.9
23	14.9	418.7	28.1	148.6	19.7
24	17.0	551.5	32.5	163.3	27.2
25	17.1	527.8	30.8	157.7	23.7
26	11.3	220.4	19.4	117.4	19.1
27	16.7	517.7	31.0	158.3	37.2
28	23.9	1242.6	52.1	220.6	50.1
29	8.1	109.8	13.5	93.2	17.1
30	9.7	179.1	18.5	113.7	21.0
31	7.0	92.9	13.3	92.3	13.3
32	8.2	120.3	14.7	98.3	13.0
33	2.7	10.8	4.0	42.9	9.3
34	3.9	26.9	6.8	60.2	12.6
35	16.9	666.0	39.4	184.5	45.6
36	10.0	397.1	39.9	186.0	40.4
37	7.4	86.9	11.7	84.8	16.3
38	9.3	153.6	16.5	105.7	19.6
39	7.0	154.4	22.0	127.2	20.2
40	12.9	336.5	26.1	141.7	18.9
41	4.4	27.9	6.4	57.5	8.3
42	8.5	127.2	15.1	99.7	18.7

PT#	Sum (I_Z)	Sum (CBR×I_Z)	CBR$_{equi.}$ [Sum (CBR×I_Z)/ Sum (I_Z)]	E$_{equi.}$	E$_{LWD-Z2}$
43	5.6	59.1	10.6	79.7	13.8
44	6.8	84.1	12.3	87.8	9.1
45	12.2	242.9	19.9	119.1	32.4
46	2.7	10.9	4.1	43.1	12.8
47	2.5	9.6	3.9	41.8	7.7
48	3.3	17.2	5.2	50.6	7.2
49	12.0	312.7	26.1	141.7	17.0
50	10.1	177.4	17.6	110.0	17.0
51	9.7	175.8	18.1	112.1	12.3
52	16.3	650.9	40.0	186.3	30.5
53	25.0	1118.4	44.7	200.0	27.0
54	20.1	844.6	42.1	192.7	43.4
55	15.3	425.5	27.9	147.8	36.9
56	10.8	187.8	17.4	109.3	27.2
57	9.4	145.4	15.4	101.2	33.8
58	14.2	319.0	22.4	128.6	45.4
59	12.3	269.4	22.0	127.0	26.1
60	12.2	263.9	21.6	125.7	27.1
61	13.6	338.1	24.9	137.5	34.7
62	9.7	168.6	17.4	109.2	15.4
63	7.0	84.5	12.1	86.7	20.6
64	7.7	118.1	15.4	101.2	22.7
65	6.7	89.5	13.3	92.0	21.6
66	10.3	189.8	18.4	113.4	23.3
67	19.4	786.0	40.6	188.0	50.9
68	12.4	288.0	23.2	131.4	21.1
69	11.5	240.6	21.0	123.4	32.7
70	11.5	258.3	22.5	129.1	30.3
71	9.1	125.4	13.8	94.4	23.6
72	8.3	110.4	13.3	92.3	22.4
73	5.3	45.1	8.6	69.6	13.6
74	4.5	31.2	7.0	61.1	11.4
75	4.2	27.1	6.5	58.2	13.3
76	3.5	20.4	5.8	54.1	17.5
77	11.4	295.3	25.8	140.9	39.2
78	23.0	890.7	38.8	182.7	53.9
79	21.0	764.6	36.4	175.4	59.4
80	22.2	814.3	36.6	176.2	70.2
81	23.2	913.9	39.4	184.6	74.2
82	20.0	779.3	38.9	183.1	58.3
83	19.3	756.6	39.3	184.3	56.5
84	11.6	271.1	23.4	132.4	47.6

Intermediate case – Data from West Virginia Project Site

Table 25. Raw data for the correlation between E$_{equivalent}$ and E$_{LWD-Z2}$ – West Virginia

PT#	Sum (I$_Z$)	Sum (CBR×I$_Z$)	CBR$_{equi.}$ [Sum (CBR×I$_Z$)/ Sum (I$_Z$)]	E$_{equi.}$	E$_{LWD-Z2}$
1	1.7	4.6	2.7	33.2	5.0
2	1.7	5.2	3.0	35.4	5.7
3	1.6	4.7	3.0	35.5	4.7
4	1.5	5.1	3.4	38.6	3.5
5	0.7	1.8	2.6	32.1	2.7
6	1.1	1.6	1.6	23.4	4.3
7	1.0	2.7	2.7	33.3	4.0
8	1.2	3.8	3.1	36.4	4.3
9	1.1	3.6	3.2	37.2	4.5
10	1.5	6.9	4.5	46.0	4.3
11	5.1	43.4	8.5	69.2	15.9
12	5.1	39.9	7.8	65.2	22.0
13	4.8	35.4	7.3	62.8	15.9
14	3.4	18.2	5.4	51.8	13.5
15	3.6	21.7	6.0	55.4	9.7
16	3.3	15.8	4.8	48.2	13.1
17	4.3	30.4	7.0	61.1	11.8
18	3.4	16.3	4.8	48.1	16.6
19	1.8	4.7	2.6	32.5	10.6
20	4.3	27.7	6.4	57.8	15.8
21	4.9	34.4	7.0	60.9	15.7
22	3.4	17.7	5.2	50.6	17.5
23	3.9	23.5	6.1	55.8	14.8
24	5.3	46.8	8.9	71.2	10.5
25	2.4	10.1	4.2	44.0	8.5
26	3.8	20.9	5.5	52.6	13.0
27	3.8	23.2	6.0	55.6	16.3
28	3.0	13.9	4.6	46.7	14.2
29	3.1	13.7	4.3	45.0	14.9
30	4.6	30.9	6.7	59.6	16.0
31	5.9	59.3	10.1	77.2	16.9
32	5.8	51.1	8.8	70.5	15.2
33	5.0	36.8	7.4	63.4	14.2
34	5.5	61.0	11.1	82.0	10.9
35	4.1	23.7	5.8	54.4	8.7
36	2.8	12.9	4.6	46.5	12.1
37	4.1	24.1	5.8	54.4	11.4
38	4.5	29.0	6.4	57.8	11.1
39	4.8	36.7	7.6	64.6	14.8
40	5.1	38.3	7.5	63.8	15.5
41	5.3	47.7	9.0	71.9	19.8
42	5.2	43.4	8.4	68.5	15.8

PT#	Sum (I_Z)	Sum (CBR×I_Z)	CBR$_{equi.}$ [Sum (CBR×I_Z)/ Sum (I_Z)]	$E_{equi.}$	E_{LWD-Z2}
43	7.1	92.4	12.9	90.5	15.4
44	3.5	17.9	5.1	50.0	10.9
45	4.4	30.1	6.8	59.9	10.0
46	3.9	24.6	6.3	57.2	13.5
47	4.6	31.5	6.9	60.3	12.3
48	3.5	21.8	6.3	57.2	12.9
49	3.9	25.2	6.4	57.7	16.3
50	5.5	45.1	8.2	67.8	13.8
51	7.4	89.7	12.0	86.4	20.8
52	7.4	83.5	11.4	83.3	15.7
53	5.6	48.6	8.7	70.4	15.2
54	6.7	78.4	11.7	84.7	10.9
55	4.5	34.6	7.6	64.6	9.0
56	3.1	18.3	5.9	54.6	12.3
57	4.6	42.7	9.2	72.9	18.8
58	5.4	44.3	8.2	67.4	12.4
59	5.8	52.7	9.1	72.1	16.7
60	7.4	90.5	12.2	87.2	15.5
61	7.9	126.7	16.1	104.1	23.9
62	6.6	81.5	12.3	87.5	31.0
63	6.8	78.7	11.5	84.1	30.9
64	6.9	85.3	12.4	88.2	25.0
65	6.0	58.9	9.9	76.1	26.5
66	5.2	52.7	10.2	77.8	25.9
67	5.8	85.7	14.7	98.2	27.9
68	4.9	50.6	10.4	78.9	27.3
69	5.0	47.2	9.4	73.8	26.2
70	6.5	78.9	12.1	86.6	26.3
71	3.1	34.7	11.2	82.7	20.4
72	3.4	36.3	10.7	80.2	26.3
73	2.9	46.5	15.8	102.9	28.6
74	3.0	44.8	15.2	100.2	21.3
75	3.2	26.8	8.4	68.7	18.9
76	2.7	36.2	13.2	91.6	26.0
77	2.7	23.8	8.7	70.4	23.3
78	2.7	26.2	9.9	76.1	23.0
79	4.0	47.5	11.9	85.7	25.6
80	3.7	46.0	12.5	88.6	23.6
81	5.0	58.4	11.8	85.3	22.4
82	3.5	37.2	10.8	80.5	24.4
83	4.9	79.3	16.2	104.5	25.6
84	3.9	52.7	13.7	93.8	22.2
85	4.3	47.8	11.2	82.6	23.6
86	3.7	38.1	10.3	78.1	20.8
87	3.1	28.4	9.2	72.9	25.2
88	3.8	41.2	10.9	80.9	22.9

PT#	Sum (I_Z)	Sum ($CBR \times I_Z$)	$CBR_{equi.}$ [Sum ($CBR \times I_Z$)/ Sum (I_Z)]	$E_{equi.}$	E_{LWD-Z2}
89	3.3	37.9	11.4	83.3	23.3
90	5.7	70.1	12.4	88.0	22.3
91	5.0	69.5	13.9	94.6	30.9
92	2.5	62.9	14.1	95.5	26.6
93	2.4	39.0	15.9	103.4	22.8
94	4.2	52.7	12.6	89.1	20.7
95	4.3	56.2	13.0	90.9	19.0
96	3.6	43.5	12.1	86.9	20.1
97	3.7	39.5	10.8	80.7	22.0
98	4.6	58.0	12.7	89.6	24.0
99	2.6	16.3	6.2	56.4	26.4
100	4.8	65.7	13.7	93.9	22.3
101	4.7	63.9	13.7	94.0	26.6
102	2.8	40.3	14.6	97.7	27.5
103	3.6	67.7	18.8	115.1	25.9
104	3.0	47.8	15.9	103.3	22.6
105	2.7	35.8	13.2	91.5	16.0
106	2.0	25.5	12.6	88.8	24.7
107	2.5	30.2	12.0	86.3	23.7
108	2.9	38.4	13.2	91.6	25.9
109	3.2	53.1	16.5	105.9	26.8
110	2.8	46.1	16.6	106.2	24.9
111	1.9	5.0	2.6	32.8	4.6
112	1.4	4.7	3.3	37.4	4.0
113	1.1	4.7	4.3	45.0	4.2
114	0.5	3.3	6.4	57.5	4.6
115	1.6	4.6	3.0	35.5	4.6
116	1.5	5.1	3.3	38.1	6.0
117	1.4	3.9	2.8	33.7	3.9
118	1.1	2.1	1.9	26.7	4.1
119	1.6	3.5	2.3	29.7	5.3
120	1.1	4.4	3.8	41.4	4.2
121	5.8	57.4	9.9	76.3	20.0
122	6.8	73.3	10.9	80.9	21.0
123	3.8	22.1	5.9	54.5	20.1
124	4.1	26.4	6.5	58.2	16.6
125	3.0	13.3	4.4	45.3	14.8
126	4.3	25.2	5.9	54.8	16.6
127	4.2	23.4	5.6	53.1	15.8
128	3.5	27.2	7.8	65.7	17.4
129	5.2	36.9	7.0	61.3	24.4
130	7.7	87.4	11.3	83.2	16.0
131	6.2	60.4	9.7	75.3	17.0
132	6.3	63.5	10.0	76.9	16.1
133	4.2	27.9	6.6	59.0	17.1
134	3.2	15.3	4.8	48.3	15.5
135	3.7	20.0	5.4	52.0	12.9

PT#	Sum (I_Z)	Sum (CBR×I_Z)	CBR$_{equi.}$ [Sum (CBR×I_Z)/ Sum (I_Z)]	E$_{equi.}$	E$_{LWD-Z2}$
136	3.9	20.1	5.2	50.6	14.5
137	4.8	34.2	7.2	62.2	10.1
138	4.0	23.0	5.8	53.9	11.0
139	5.6	45.8	8.2	67.8	17.1
140	4.5	29.6	6.6	59.0	14.8
141	4.4	42.3	9.7	75.1	14.7
142	3.8	27.8	7.3	63.0	15.5
143	2.8	19.1	6.8	59.9	16.3
144	2.8	12.3	4.4	45.7	13.8
145	3.3	17.6	5.3	51.1	13.1
146	3.2	18.3	5.7	53.3	13.4
147	4.0	36.0	9.0	72.0	11.4
148	2.5	10.9	4.4	45.1	11.5
149	3.9	26.9	7.0	60.9	15.4
150	5.9	50.2	8.6	69.4	14.2
151	4.3	35.9	8.4	68.4	13.5
152	2.8	16.0	5.6	53.1	18.6
153	3.1	30.0	9.7	75.3	14.8
154	3.2	18.8	5.9	54.9	15.1
155	4.9	36.8	7.5	64.0	14.1
156	6.7	64.1	9.6	74.9	14.5
157	4.7	32.3	6.9	60.5	12.4
158	4.4	38.0	8.7	70.3	10.7
159	5.3	46.5	8.9	71.0	15.6
160	5.8	50.9	8.8	70.8	15.2
161	6.7	125.7	18.9	115.2	13.7
162	5.1	68.9	13.6	93.6	19.2
163	3.0	25.6	8.6	69.8	17.5
164	2.5	26.3	10.5	79.4	15.4
165	2.6	25.9	10.0	76.6	14.8
166	3.5	35.7	10.3	78.3	14.0
167	3.2	30.6	9.5	74.5	13.4
168	2.7	19.0	7.0	61.0	13.3
169	2.9	26.5	9.1	72.1	16.6
170	3.4	38.8	11.4	83.5	14.2
171	8.0	125.0	15.6	102.0	30.7
172	4.8	92.2	19.3	116.7	20.9
173	6.7	118.5	17.6	110.2	29.5
174	5.6	83.4	15.0	99.4	28.9
175	6.6	109.6	16.7	106.6	25.4
176	4.9	60.7	12.3	87.6	23.2
177	6.1	87.4	14.3	96.6	25.4
178	5.8	69.4	12.0	86.1	28.0
179	5.6	74.1	13.3	92.2	24.2
180	6.3	77.8	12.4	87.9	27.5
181	4.6	59.0	12.7	89.6	27.5
182	4.5	67.7	15.2	100.4	26.3

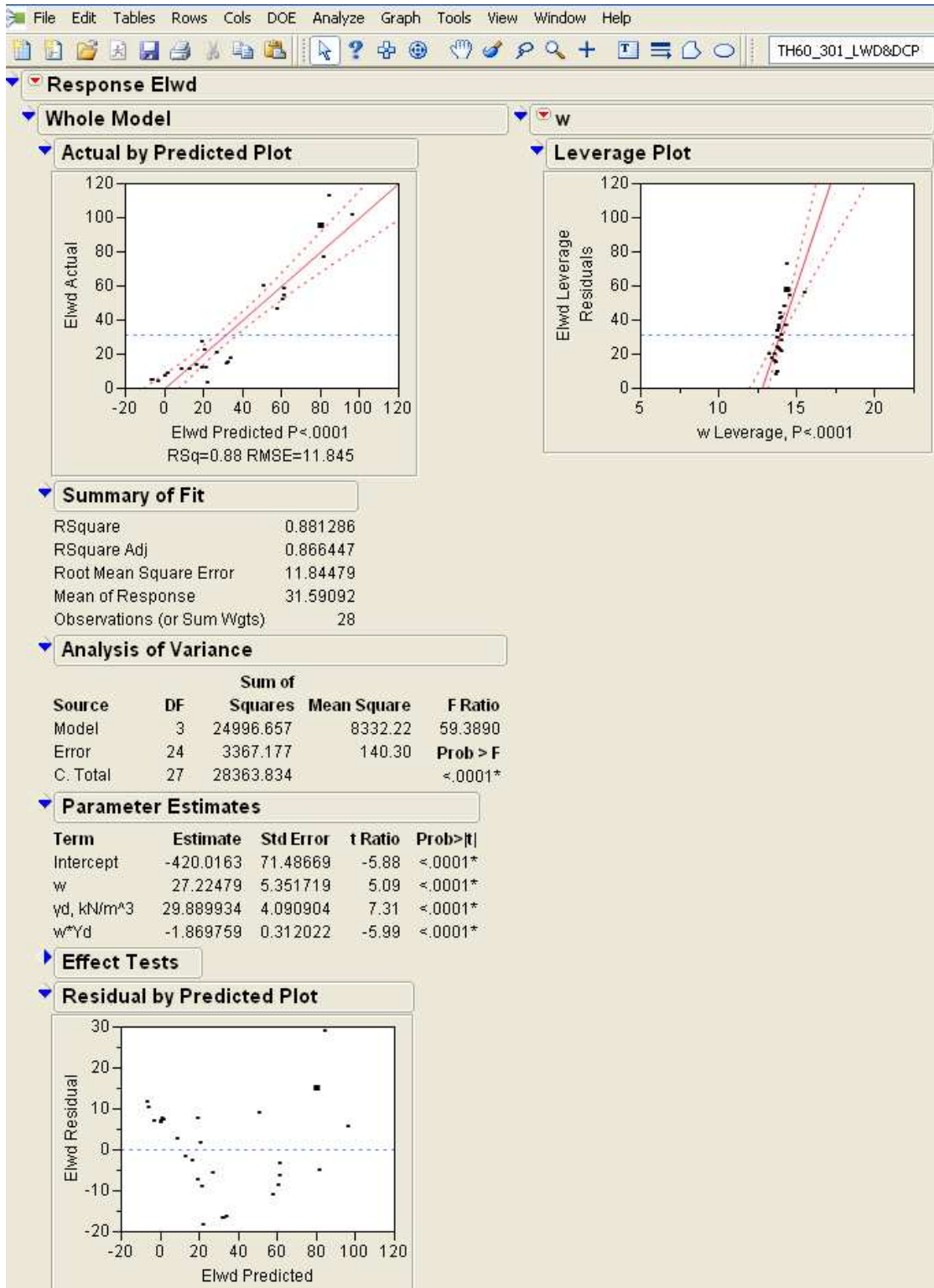| PT#	Sum (I_Z)	Sum (CBR×I_Z)	CBR$_{equi.}$ [Sum (CBR×I_Z)/ Sum (I_Z)]	E$_{equi.}$	E$_{LWD-Z2}$
183	4.9	83.6	17.1	108.0	32.4
184	4.7	61.0	12.9	90.4	37.9
185	4.9	57.5	11.8	85.4	33.0
186	4.7	51.8	11.1	81.9	23.9
187	5.8	66.5	11.4	83.3	23.2
188	8.0	104.8	13.2	91.5	25.2
189	6.7	86.4	12.9	90.1	33.1
190	7.9	125.2	15.8	102.7	29.5
191	3.1	46.8	14.9	99.1	33.8
192	3.1	70.8	22.6	129.3	27.4
193	3.4	46.4	13.5	93.0	34.5
194	3.0	50.0	16.8	107.1	29.0
195	2.6	32.6	12.7	89.3	31.7
196	3.3	55.9	16.8	106.8	25.0
197	1.7	10.8	6.5	58.3	24.7
198	2.7	36.5	13.6	93.4	24.0
199	3.0	47.7	15.7	102.6	29.5
200	2.9	45.2	15.8	103.0	27.4
201	2.3	34.5	15.1	100.0	26.5
202	4.7	92.5	19.7	118.3	29.3
203	3.4	63.5	18.8	115.1	28.6
204	3.1	53.5	17.5	109.6	29.5
205	4.6	83.4	17.9	111.5	27.1
206	2.1	12.8	6.0	55.6	24.1
207	2.8	67.3	24.4	135.7	22.5
208	2.9	42.7	14.6	97.9	21.5
209	1.7	14.7	8.7	70.4	26.5
210	3.0	48.6	16.4	105.2	25.6
211	4.0	75.2	18.9	115.2	30.5
212	4.1	72.3	17.5	109.7	32.2
213	3.2	55.5	17.3	109.0	30.2
214	2.9	56.3	19.2	116.4	28.1
215	3.6	66.2	18.3	112.9	28.0
216	4.7	85.7	18.3	113.0	28.0
217	3.4	67.2	19.5	117.7	23.1
218	3.2	56.6	17.7	110.4	26.0
219	3.4	68.2	20.2	120.4	29.0
220	3.7	73.2	20.0	119.6	23.5

APPENDIX II: STATISTICAL MODELS

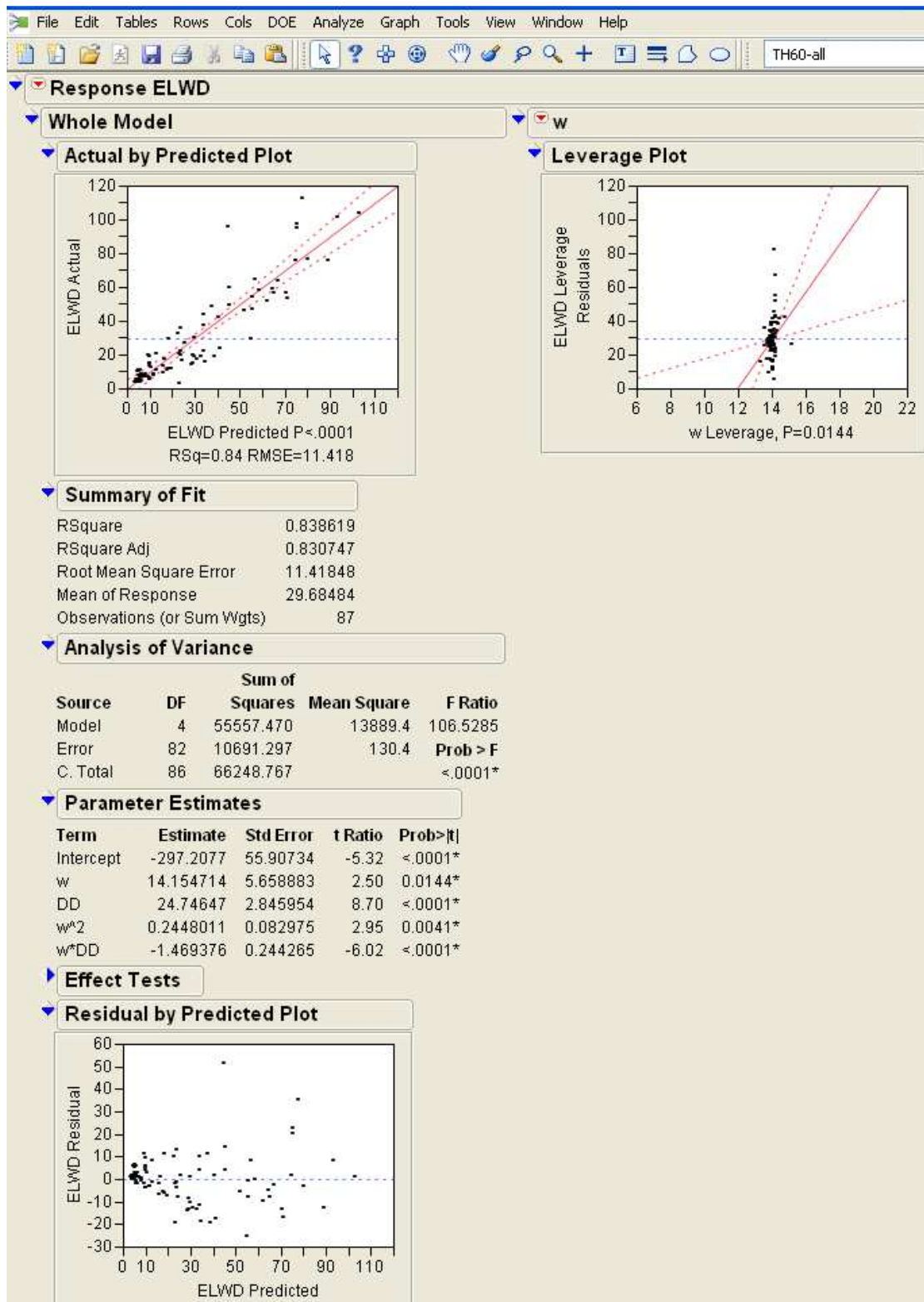**E$_{LWD-Z1}$ contours in relationship with *w* and γ$_d$ – US10 granular material**
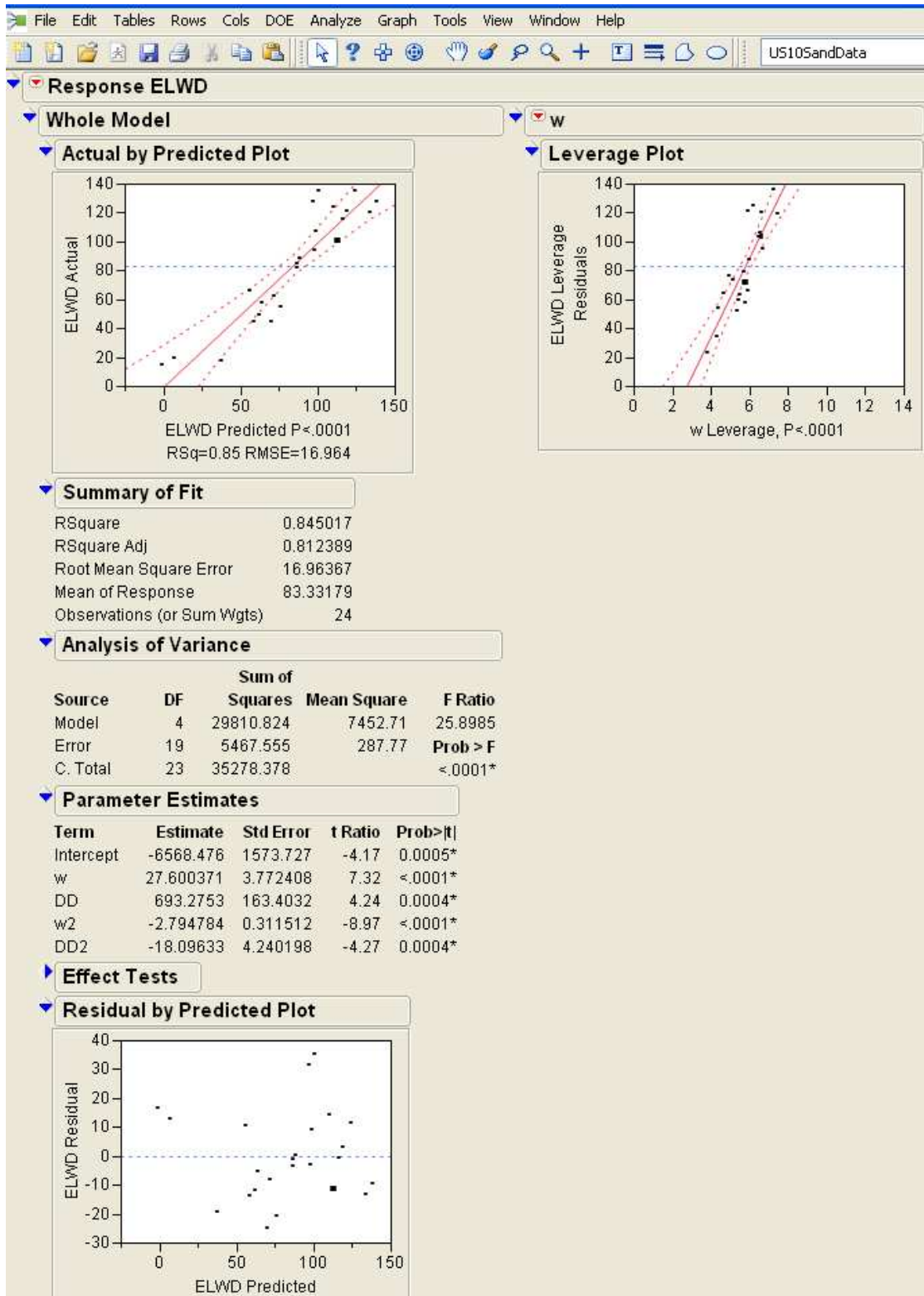
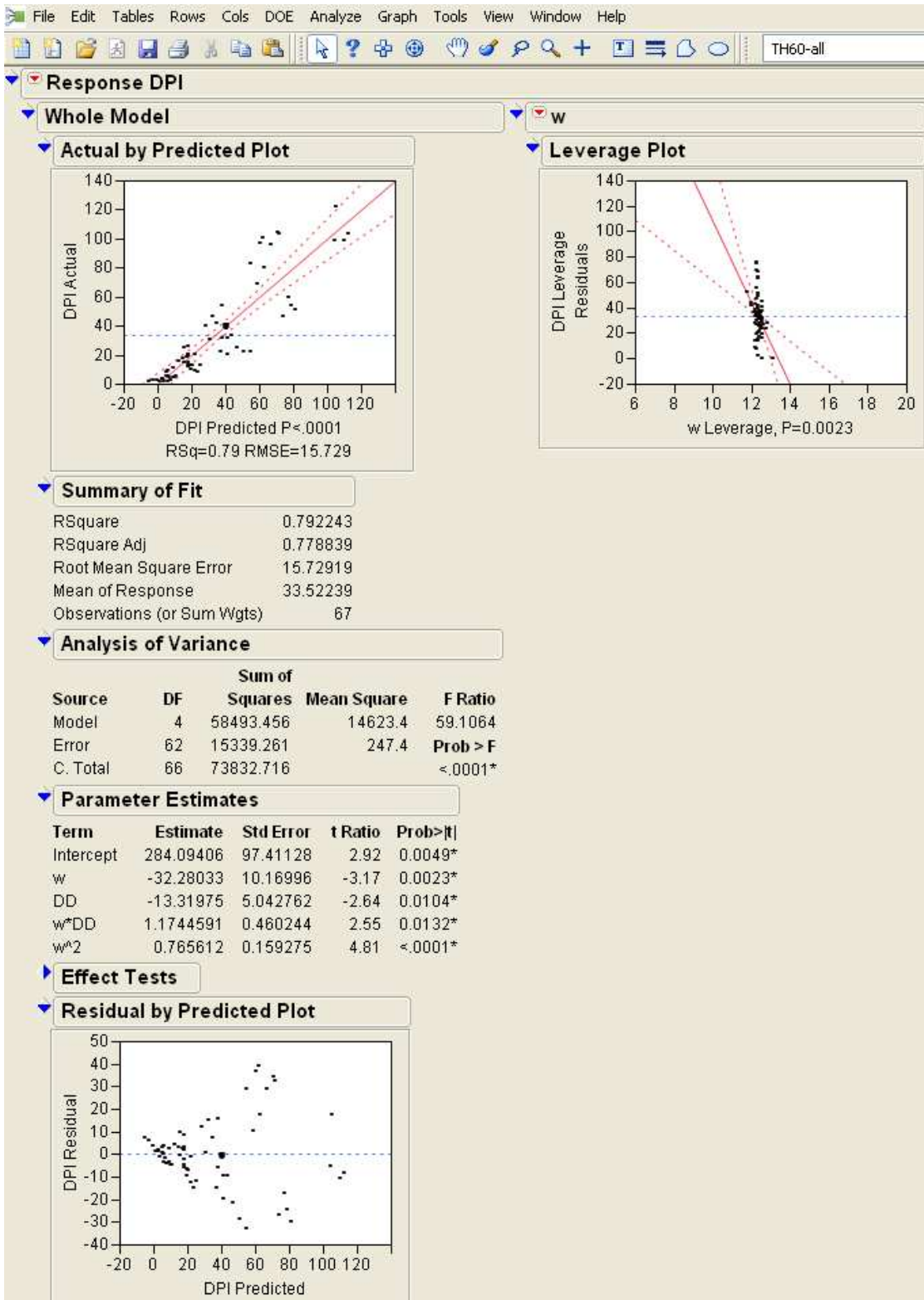**E$_{LWD-Z1}$ contours in relationship with *w* and γ$_d$ – TH36 silty clay material**

E$_{\text{LWD-Z1}}$ contours in relationship with *w* and γ$_d$ – TH60 soil 301 material

File   Edit   Tables   Rows   Cols   DOE   Analyze   Graph   Tools   View   Window   Help

TH60_301_LWD&DCP

Response Elwd

Whole Model

w

Actual by Predicted Plot

Elwd Actual (y-axis: 0 to 120)
Elwd Predicted P<.0001
RSq=0.88 RMSE=11.845

Leverage Plot

Elwd Leverage Residuals (y-axis: 0 to 120)
w Leverage, P<.0001

Summary of Fit

RSquare	0.881286
RSquare Adj	0.866447
Root Mean Square Error	11.84479
Mean of Response	31.59092
Observations (or Sum Wgts)	28

Analysis of Variance

Source	DF	Sum of Squares	Mean Square	F Ratio
Model	3	24996.657	8332.22	59.3890
Error	24	3367.177	140.30	Prob > F
C. Total	27	28363.834		<.0001*

Parameter Estimates

Term	Estimate	Std Error	t Ratio	Prob>|t|
Intercept	-420.0163	71.48669	-5.88	<.0001*
w	27.22479	5.351719	5.09	<.0001*
γd, kN/m^3	29.889934	4.090904	7.31	<.0001*
w*Yd	-1.869759	0.312022	-5.99	<.0001*

Effect Tests

Residual by Predicted Plot

Elwd Residual (y-axis: -20 to 30)
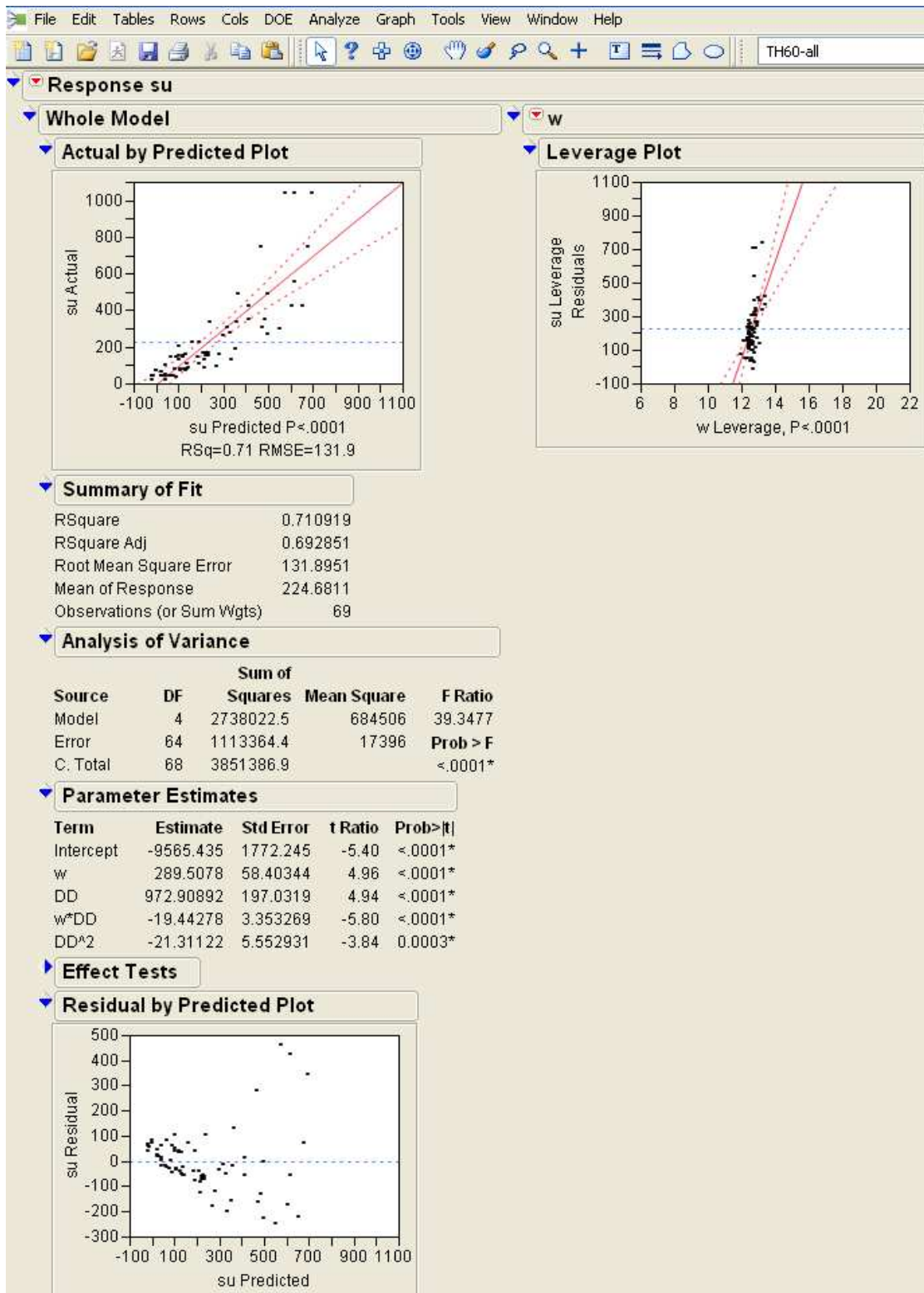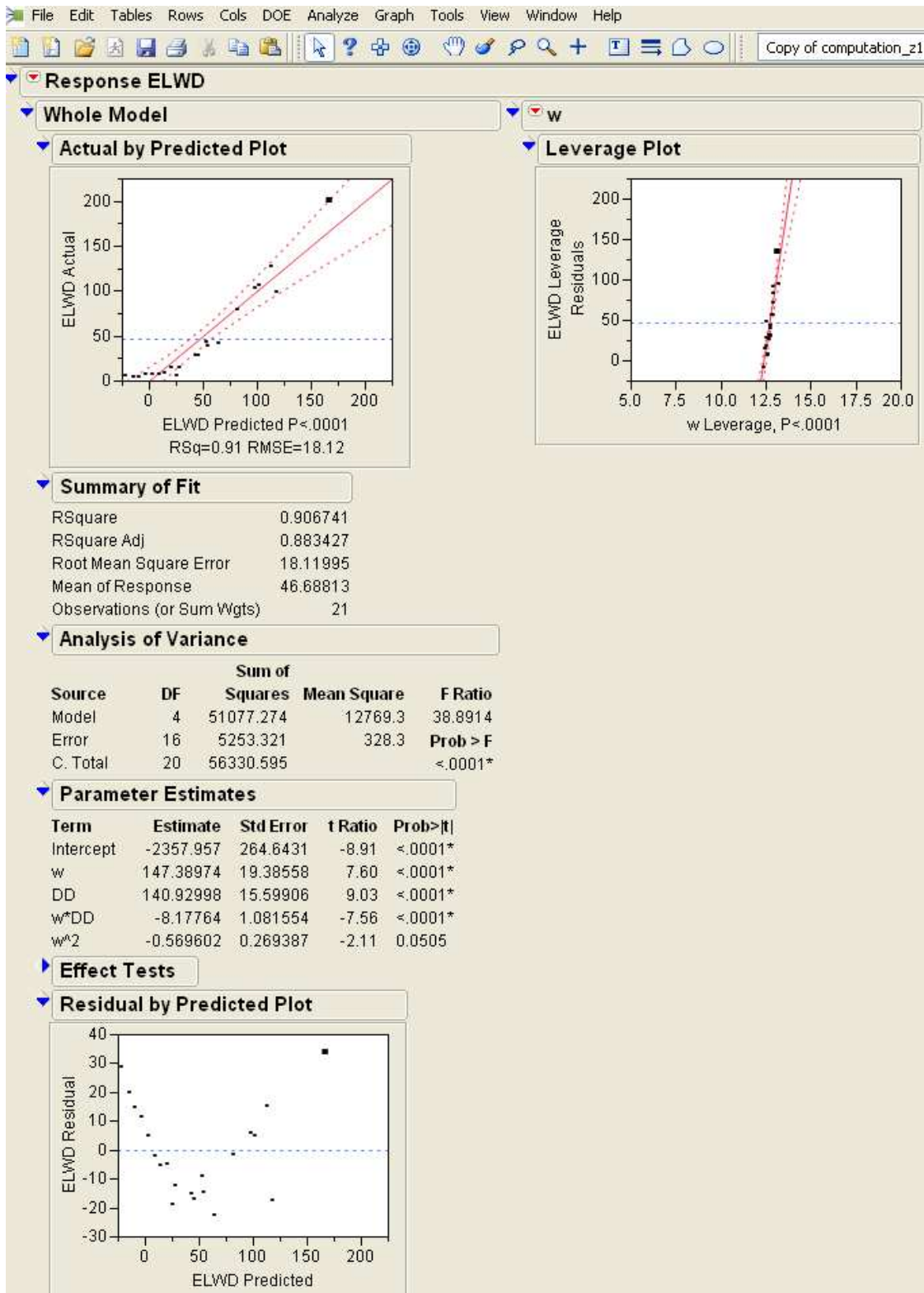Elwd Predicted

E$_{LWD-Z1}$ contours in relationship with *w* and γ$_d$ – TH60 (301, 303, and 305 combined)

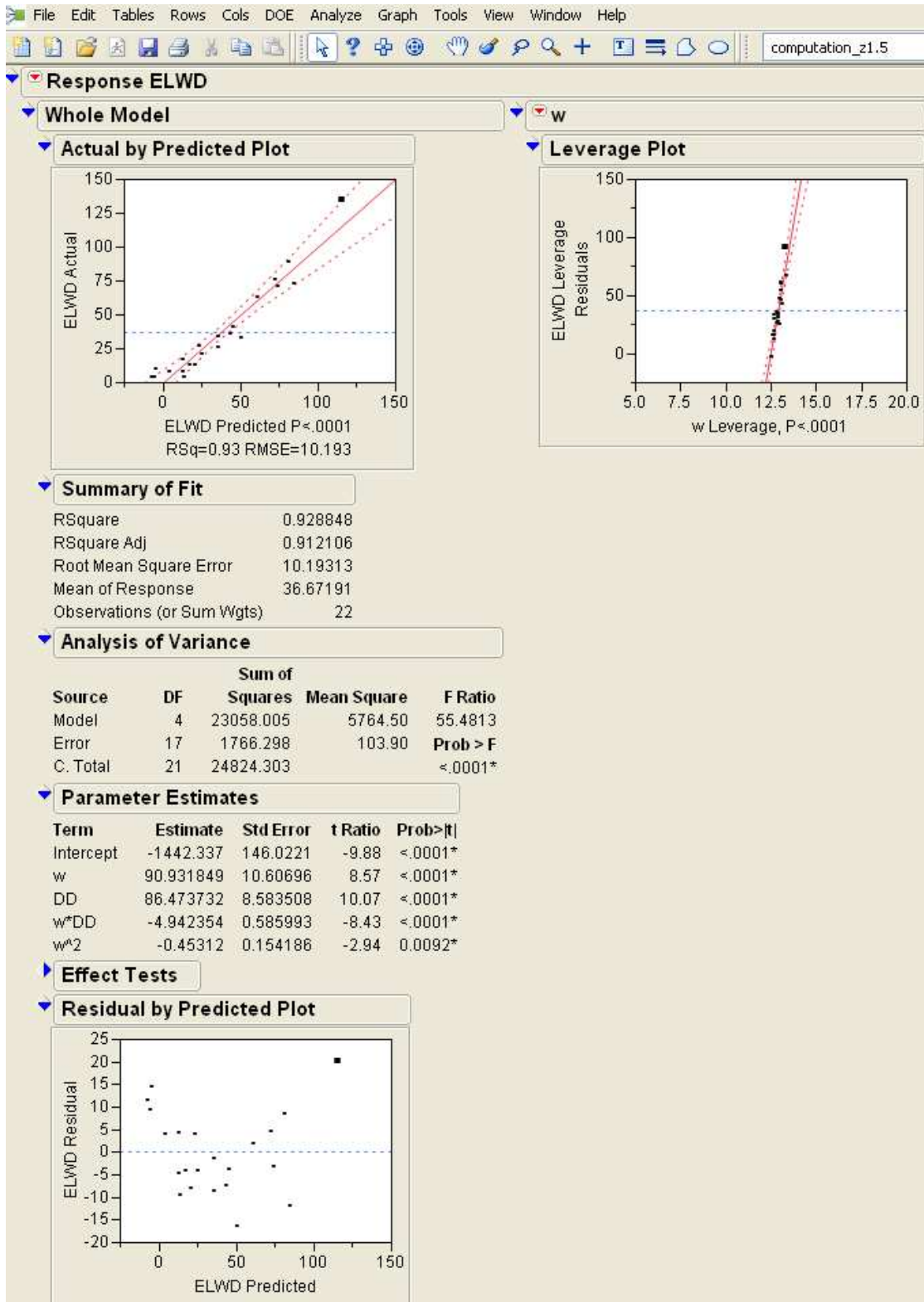**DPI contours in relationship with *w* and γ_d – TH60 (301, 303, and 305 combined)**
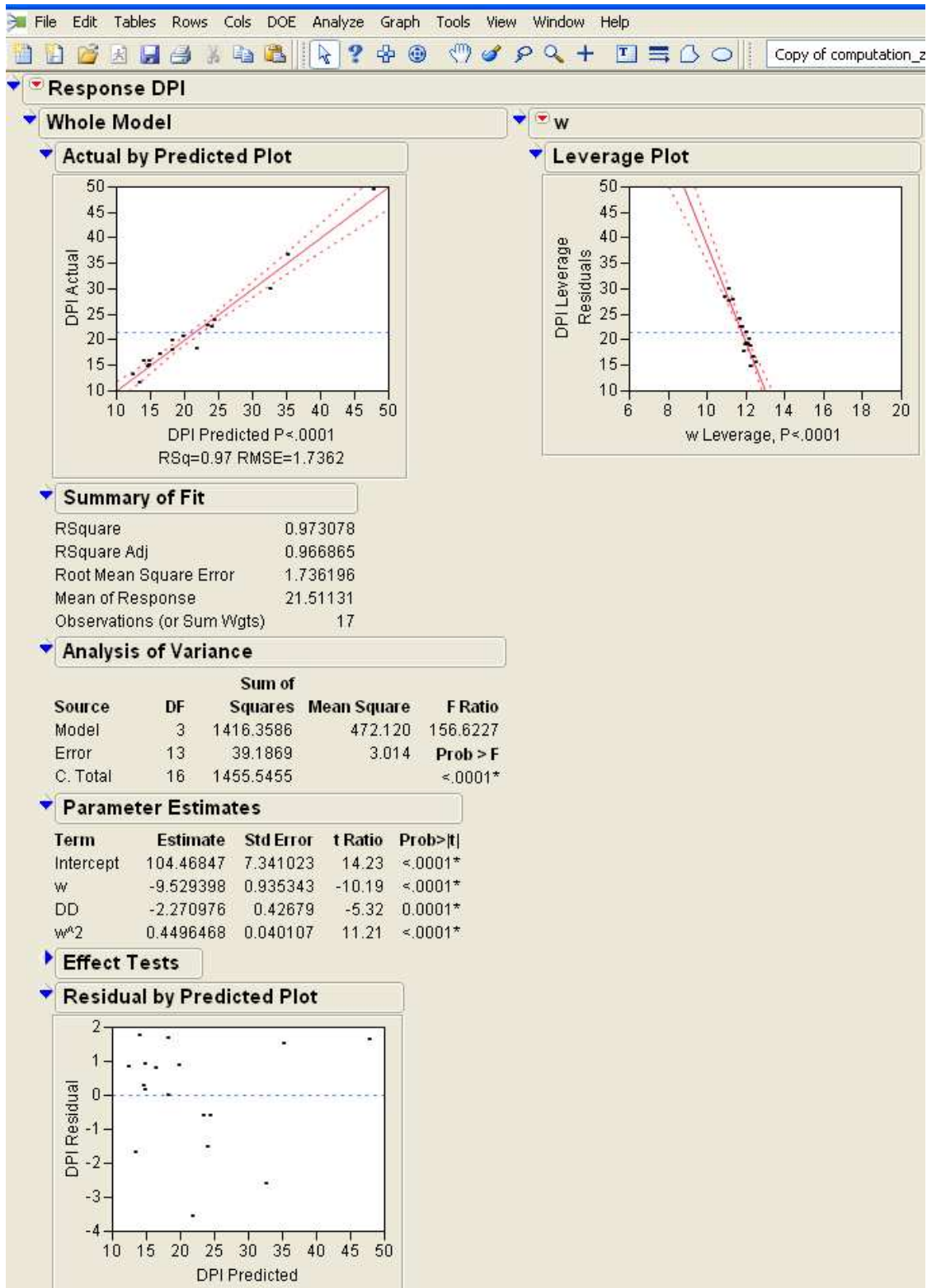
s_u contours in relationship with w and γ_d – TH60 (301, 303, and 305 combined)

E$_{LWD-Z1}$ contours in relationship with *w* and γ$_d$ with stiff boundary – TH60 soil 306
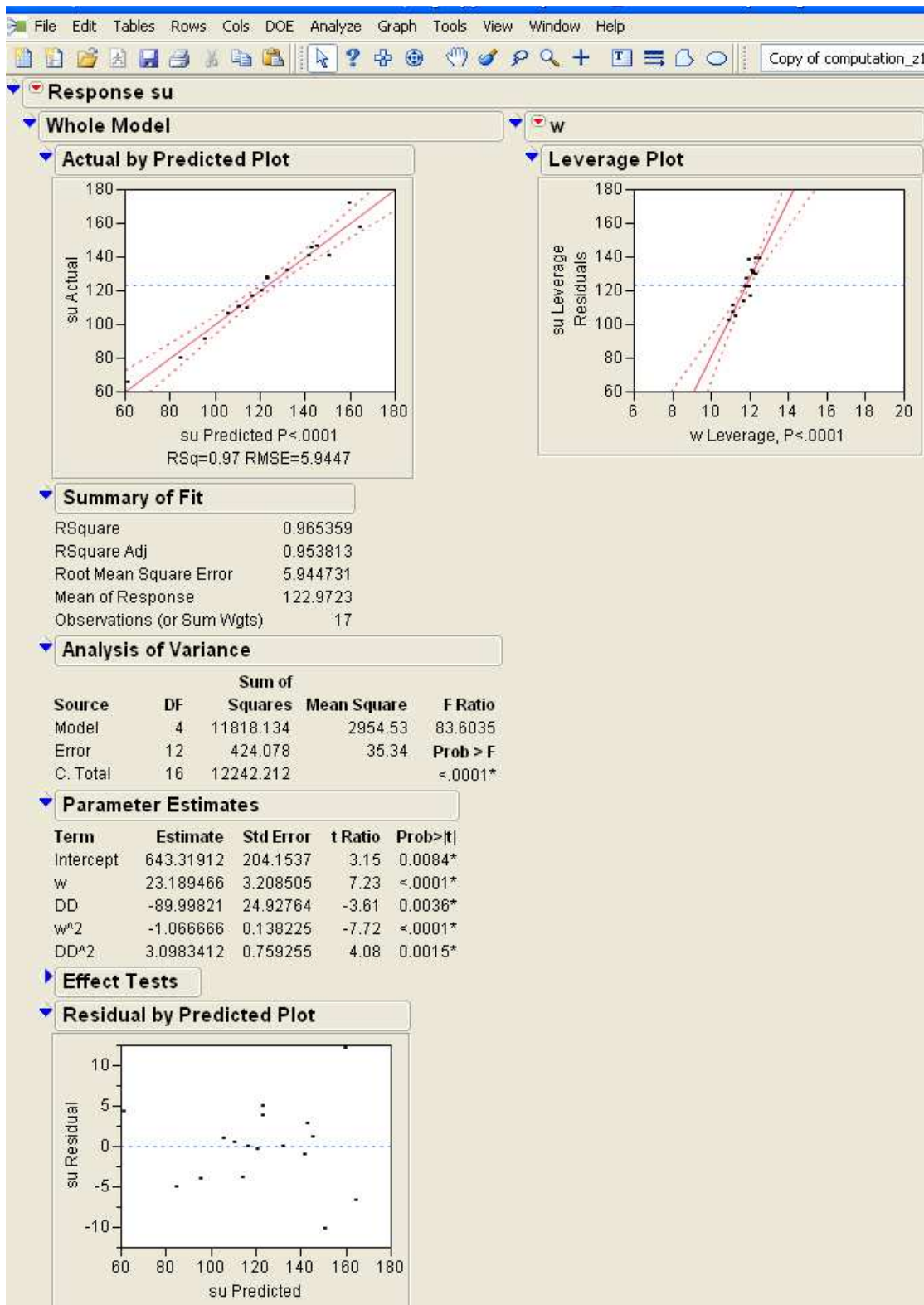
E$_{LWD-Z1.5}$ contours in relationship with *w* and γ$_d$ with stiff boundary – TH60 soil 306

DPI contours in relationship with *w* and γ$_d$ with stiff boundary – TH60 soil 306

s_u contours in relationship with w and γ_d with stiff boundary – TH60 soil 306

τ$_G$ contours in relationship with *w* and γ$_d$ with stiff boundary – TH60 soil 306